THESIS

HYDROCARBON SEALING CAPACITY OF PALEOSOLS, WASATCH FORMATION, RIFLE, COLORADO

Submitted by

Jarrad G. Berg

Geosciences Department

In partial fulfillment of the requirements

For the Degree of Masters of Science

Colorado State University

Fort Collins, CO

Summer 2005

COLORADO STATE UNIVERSITY

DECEMBER 17, 2004

WE HEREBY RECOMMEND THAT THE THESIS PREPARED UNDER OUR SUPERVISION BY JARRAD G. BERG ENTITLED HYDROCARBON SEALING CAPACITY OF PALEOSOLS, WASATCH FORMATION, RIFLE, COLORADO BE ACCEPTED AS FULLFILLING IN PART REQUIREMENTS FOR THE DEGREE OF MASTERS OF SCIENCE.

Committee on Graduate Work

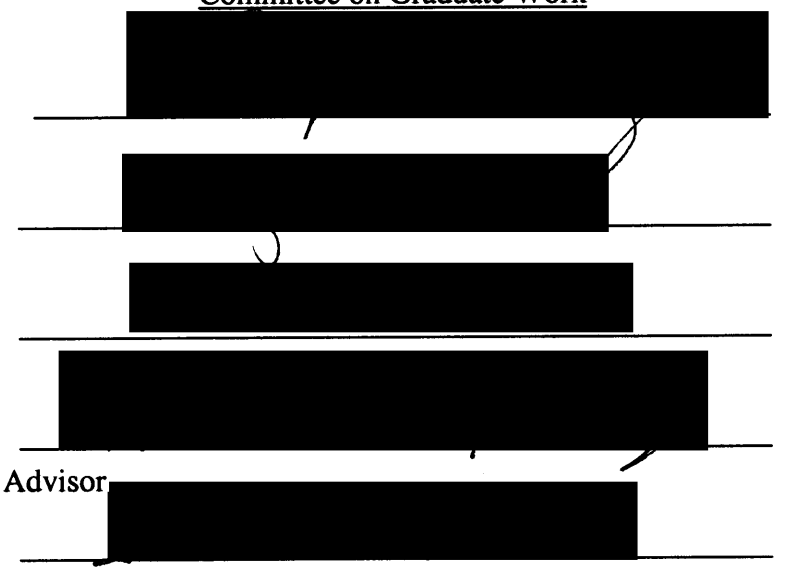

Advisor

Department Head/Director

ABSTRACT OF THESIS

HYDROCARBON SEALING CAPACITY OF PALEOSOLS, WASATCH FORMATION, RIFLE, COLORADO

Hydrocarbon reservoirs require a seal to keep the hydrocarbons from migrating out of the reservoir. Therefore, recognition of seal rocks and determination of seal properties are extremely important for exploration. Seal rocks are commonly fine-grained shale and mudstone. Previous seal rock studies have mostly been limited to marine shales. Other fine-grained rocks that may provide seals for hydrocarbon deposits include paleosols. Two floodplain paleosol packages in the Eocene Wasatch Formation were sampled to determine how paleosol characteristics, clay matrix and quartz grain content, and stratigraphic position affect sealing capacity. Outcrops sampled are located in the Piceance basin approximately 2 miles northwest of Rifle, CO in Hubbard Gulch. The Wasatch is divided into three members, the Atwell Gulch, the Shire, and the Molina, in ascending stratigraphic order. Vertisol packages in the low net-to-gross Shire Member deposits are the main focus of this project.

Mercury injection capillary pressure analysis was used to evaluate the sealing capacity of 80 samples from two paleosol packages, five lithofacies, and four microfacies. Capillary pressure curves constructed from mercury injection data were used to compare sealing capacity at 10% mercury saturation. Sealing capacity values range from 467 to 7667 psia. No significant differences in sealing capacity were found between the upper and lower paleosol packages, or among lithofacies. Microfacies, defined primarily on the basis of quartz grain size, show an inverse relationship with sealing capacity. For all samples analyzed as seals correlation analysis suggests that high sealing capacity correlates with high matrix and low grain content, smaller pore-throat diameters, relatively low TOC and relatively high grain density. In general good seals have one class of pore throats and minimal variation in pore-throat size distribution. Visibly good seals exhibit multicolor mottling, angular to subangular peds, slickensides, and paleo-root structures; all features common in well-developed paleosols.

Because of the nature of outcrop exposure, lateral variations with respect to distance from contemporaneous paleo-channels were not determined. Samples collected directly above or below paleo-channels consistently exhibit poor sealing capacity, while samples further away from the paleo-channels vertically tend to have higher sealing capacity. Using available data it was not possible to determine the cause of the relationship between sealing capacity and paleosol development. The textures visible in the present day paleosols may be primary (depositional), or secondary (from soil forming and or diagenetic processes).

Jarrad G. Berg
Geoscience Department
Colorado State University
Fort Collins, CO 80523
Summer 2005

ACKNOLEDGEMENTS

I would like to thank Chevron Corporation, the American Association of Petroleum Geologists, and the Earth Resources department at CSU for providing the funding that made this project possible. I would also like to thank Dr. Frank Ethridge for accepting me as a graduate student, providing constant guidance on this project, and giving me the opportunity to learn from his knowledge and past experiences. I thank Dr. Sally Sutton and Dr. Eugene Kelly for providing assistance and guidance through out the whole project. I greatly appreciate Dr. William Almon (Chevron Corporation) and Dr. William Dawson (Chevron Corporation) who contributed to this research with knowledge and guidance.

Others were involved with the completion of the project and are greatly appreciated. Sage Betts provided assistance with fieldwork. John Neasham completed all the MICP analyses and prepared samples for porosity and permeability tests. Steve Blecker taught me how to perform the Total Organic Carbon measurements and allowed me to use the Soils Laboratory at CSU. Charles Bohn helped prepare samples in the lab for analysis. Bellatrix Castelblanco and Andre Obligado provided a starting point for this project with their studies previous to mine.

Thank you to all of the friends I met while attending CSU. You have made the whole graduate school experience very enjoyable and a worthwhile event.

Finally, a very special thank you goes to my wife, Andrea, for providing help in the field as well as supporting me with the decision to return to graduate school. Without her constant support, I would not have been able to finish this project.

TABLE OF CONTENTS

List of Figures

List of Tables

Chapter 1. Introduction

1.1 Purpose

Hydrocarbon accumulations require four components in order to develop: source beds, a reservoir, correct timing of migration of the hydrocarbons, and a seal. Without a seal the hydrocarbons would migrate out of the reservoir. Seals are, therefore, a very important part of hydrocarbon accumulations. Recognition of seal rocks and determination of seal properties for a trap are imperative. Understanding the properties of the seal and the spatial distribution of the seal can aid in evaluating the risk of a potential accumulation.

1.2 Hypothesis

The hypothesis for this project is that paleosols with higher sealing capacities as determined from MICP analyses will have lower percentages of quartz grains and a smaller average quartz grain size. These paleosols will also have higher clay contents, determined from thin sections and XRF data. This study will evaluate the lateral variability of the sealing capacity of paleosols, relative to themselves, that developed on flood plain deposits of the Eocene Wasatch Formation near Rifle, Colorado.

1.3 Study Area

The study area consisted of the Wasatch Formation outcrops in the Piceance Basin in western Colorado, northwest of the town of Rifle (Figure 1.1). The study area is restricted to a ridge about 1000 meters in length with excellent exposure. All of the samples came from two separate paleosol packages; one at an elevation of 5,720 feet and the other located at 5,740 feet. The sampling locations are noted in the small blue box located in the subset map in Figure 1.1.

The Paleocene to Eocene Wasatch sits unconformably above the Hunter Canyon Formation and is overlain by the Green River Formation (Figure 1.2). The Shire Member of the Wasatch Formation was studied for this project.

1.4 Seal Background

Hydrocarbon seals are commonly fine-grained rocks that are impermeable to fluid flow, such as shale and mudstones. Paleosols typically fall into the mudstone category of sedimentary rocks due to their average grain size. Paleosols are composed of weathered rocks. The unweathered rock is called parent material. Depending on the location, the parent material could be igneous, metamorphic, or sedimentary. The paleosols in this study are mudstones that formed on overbank deposits during flooding events in a fluvial depositional system. Mudstones are found extensively throughout the sedimentary rock record, and past research has indicated that mudstones constitute two-thirds of the sedimentary rock record (Schieber, 1999). Because of their fine-grained texture, which makes them hard to classify and compare, studies of these rocks lags behind studies of sandstones and carbonates.

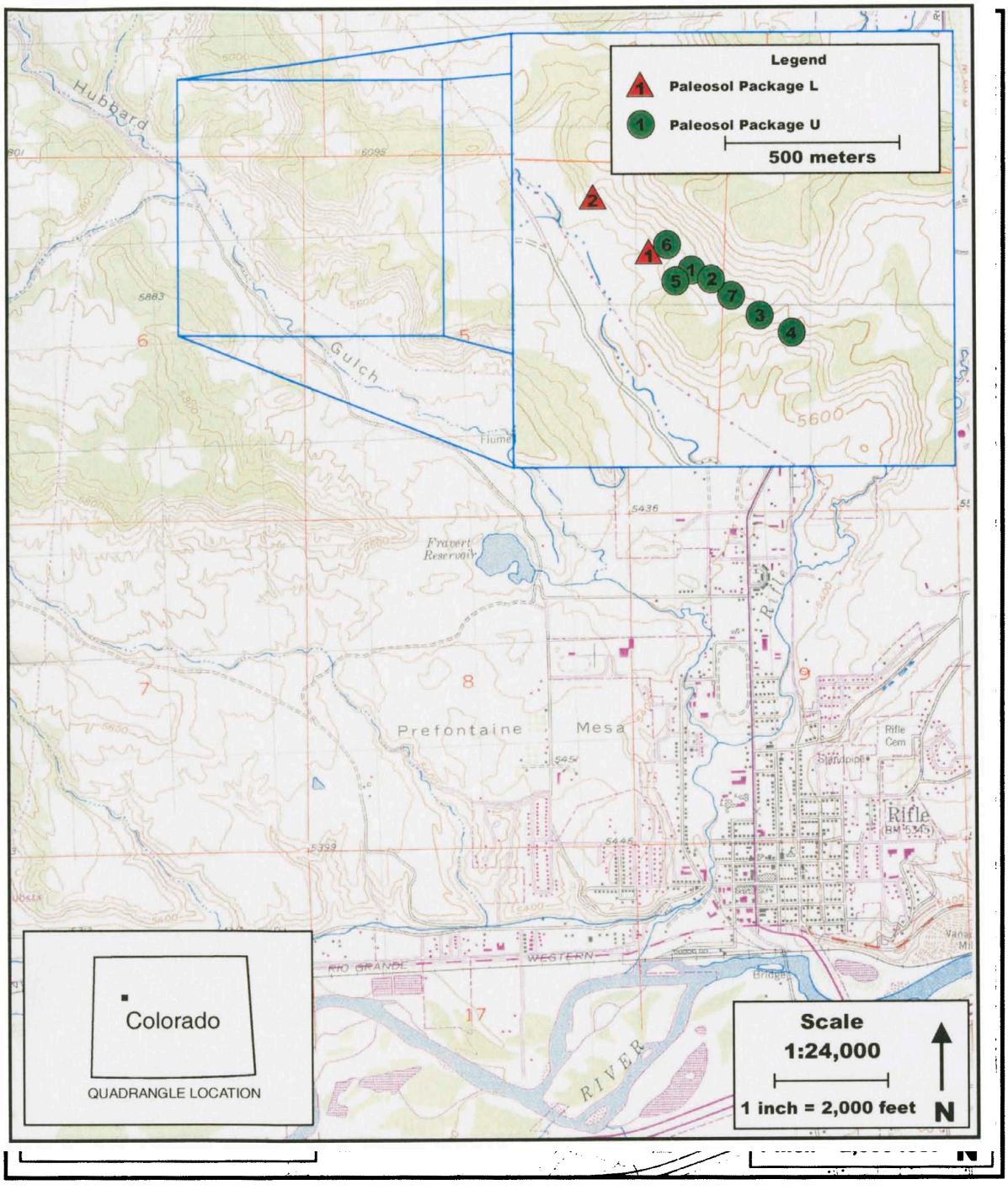

Figure 1.1 Map of study area with sample locations indicated.

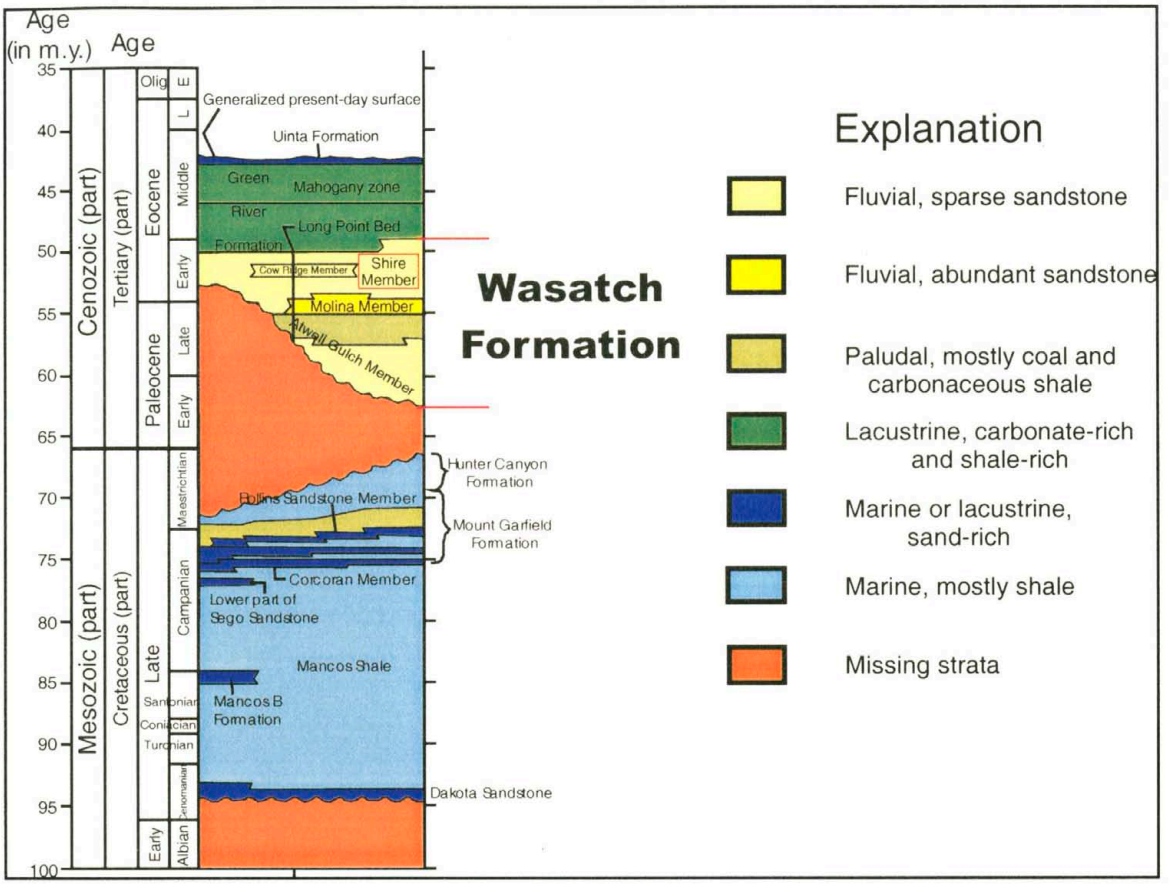

Figure 1.2 General stratigraphic column of the Piceance Basin with red lines indicating the Wasatch Formation. The member used for the study, the Shire Member, is outlined with a red box, while the whole Wasatch Formation is outlined with red lines. Modified from Johnson,1989.

Downy (1984), Jennings (1987), Schowalter (1979), and Vavra et al. (1992) provide reviews of how capillary pressure can affect hydrocarbon entrapment and techniques used in exploration and development of reservoirs with the main focus on mercury injection capillary pressure (MICP) analysis. Downy (1984) uses the term seal to refer to a layered lithologic unit capable of impeding hydrocarbon movement. He goes on to state that the quality of a seal is determined by the minimum pressure required to displace water from pores or fractures in the seal.

When fluids migrate through the pore system in the subsurface the distribution and movement of the fluid is determined by capillary size. Capillary in this sense means

the action or condition by which a fluid is drawn into small openings, such as very small pores, by surface tension (Bates and Jackson, 1984). Capillary phenomena are well seen in systems where the fluids are immiscible, such as oil and water (Almon and Thomas, 1991). The surface between the two fluids is affected by interfacial tension. Interfacial tension causes a pressure difference between the two fluids, called capillary pressure. Within a hydrocarbon reservoir there is a third component that plays into the capillary pressure, the rock surface in the pore throats. The attraction of the fluids to the rock surface is called wettability (Almon and Thomas, 1991). The relationship of theses pore system parameters can be seen in Figure 1.3.

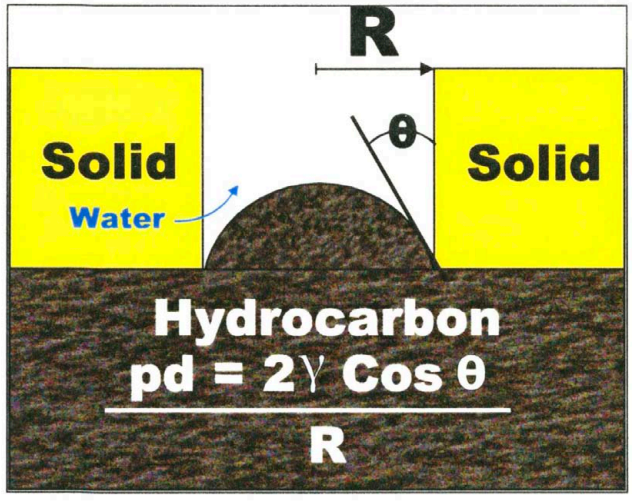

WHERE pd=displacement pressure

γ =Oil-water interfacial tension

Θ=Contact angle of oil and water against the solid

R=Radius of the pore throat

Figure 1.3 The hydrocarbon-water displacement of a pore system. Redrawn from Almon and Thomas, 1991.

The displacement pressure can be measured in the laboratory by injecting a non-wetting fluid into a cleaned and dried sample under increasing pressure. In almost all cases, mercury is used as the non-wetting fluid. The capillary pressure is measured as the mercury increasingly saturates the sample under pressure (Almon and Thomas, 1991). A typical device used to make these measurements is seen in Figure 1.4.

Jennings (1987) discusses one of the problems of using MICP to study seals. He indicates that capillary pressure tests are normally completed on 1 ½ inch long by 1 inch diameter plug used for routine core analysis. As with other formation analysis completed on a hydrocarbon well, the MICP analysis can be performed on well cuttings or chips but core is preferred. The cuttings or chips provide inaccurate MICP results due to the large surface-area to volume ratio (Jennings, 1987).

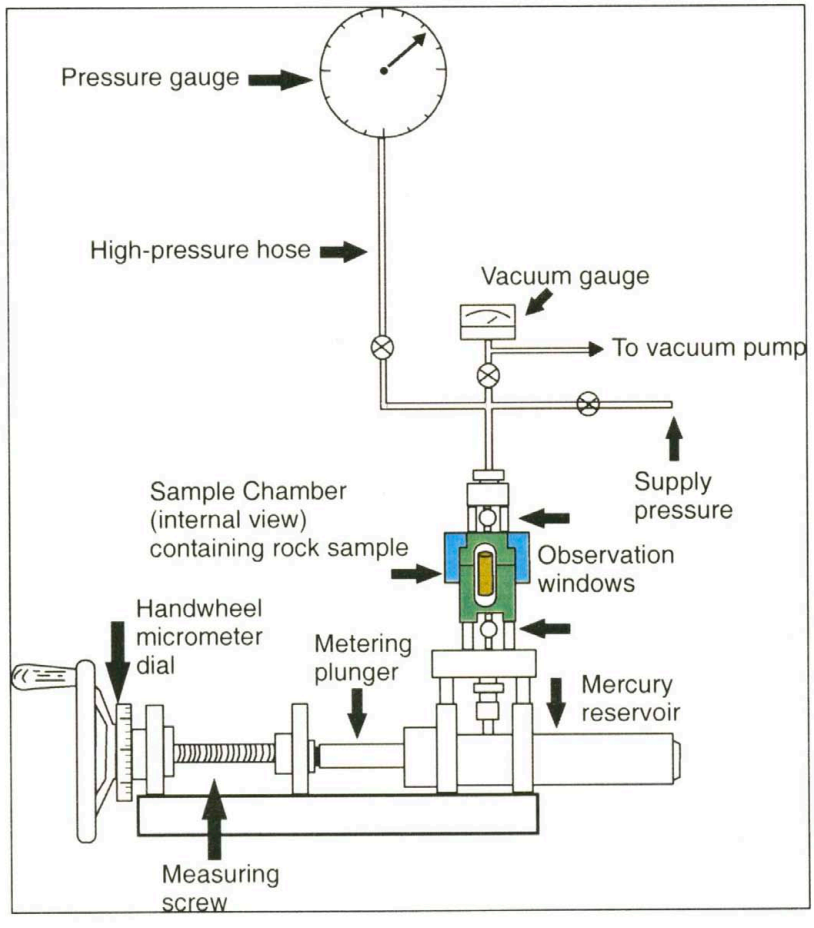

Figure 1.4 Device for obtaining mercury injection capillary data. Redrawn from Jennings, 1987.

Downey (1984) mentions the point of trying to use "micro" data from a single core to characterize an entire "macro" sealing surface. The probability that the "micro" properties of the core are invariant over the entire seal is very small. However, these assumptions about seals over a large area are made on a daily basis using MICP data and other data available.

Jennings (1987) states that in evaluating reservoir rock, at least two samples must be obtained to reflect the true overall character of the reservoir; one sample from the most effective foot and one sample from the least effective foot. Doing this helps the reservoir qualities to be bracketed. This same technique may work for evaluating sealing properties as well. He also notes that large scale fractures, which have major impacts on sealing capacities, cannot be measured from MICP analysis. On the other hand, micro-fractures can be analyzed using MICP analysis.

Schowalter (1979) recognized that the pressure required to form a continuous filament of mercury across the largest interconnected pores of a rock is an important variable in seal assessment. He found that this pressure, which he defined as displacement pressure, usually occurs between mercury saturations of 4.5 and 17%. The pressure at 10% mercury saturation is a good approximation to use for comparison of the different samples of sandstones, shales, and chalks that were used in his study. For this paper, the value of 10% mercury saturation will also be used to compare the sealing capacities of the paleosol samples that were obtained.

Capillary pressure data cannot be used alone for evaluation and interpretation of the seal properties. Capillary pressure of a seal is only one component of seal characteristics. Other components, such as thickness, lateral extent, and fracture systems

also play a role in the sealing capacity of the rock. MICP data must be integrated into geological, geophysical, or engineering programs to provide the most help.

Previous work on seals has been mainly confined to marine shales (Sutton et al., 2004, Almon et al., 2001, Kaldi and Atkinson, 1997, Boult et al., 1997, Jiao and Surdam, 1997, and numerous others). Few researchers have examined other fine grained rocks, such as paleosols, as seals.

In the central Sumatra Basin of Indonesia, a thick regionally extensive paleosol covers the Basin and has focused the migration of hydrocarbons towards the eastern margin of the Basin. The paleosol is well developed and sealing capacity correlates with total clay content and position within the soil horizon. C horizons provide the best sealing capacities, while B horizons exhibit slightly less sealing capabilities (Almon and Dawson, 2000).

In the Powder River Basin of Wyoming, paleosols are the seals for several hydrocarbon reservoirs found in the Muddy Sandstone. The paleosol forms both the top and lateral seal for the overpressured compartments. The sealing capacity characteristics were created by pedogenic processes and were enhanced by burial diagenesis (Jiao and Surdam, 1994)

In the Cooper Basin of west-central Australia, paleosols and floodplain mudstones of the Nappamerri Group are the regional seals for a large hydrocarbon reservoir. The paleosols are highly bioturbated and have very strong soil structure features. Root traces and siderite nodules are also present in the paleosols (Dragomirescu et al., 2001).

1.5 Paleosol Background

All scientists who work on paleosols do not agree on the definition of what constitutes a paleosol. Early workers defined paleosols as a soil that formed on a landscape of the past (Ruhe, 1965; Yaalon, 1971; as in Birkeland, 1999). Some scientists believe that the environmental conditions, both today and during the time of soil formation, determine whether or not an ancient soil can be called a paleosol. Birkeland (1999) classifies paleosols as soils that were buried, regardless of whether original environmental conditions were different than present day environmental conditions. Holliday (2004) proposes that the term paleosol be applied only to soils that are lithified. For this paper, a combination of Birkeland and Holliday's definitions will be used. Paleosols are defined as soils that formed from rocks that were exposed to the environment, buried, and have been relithified. The paleosols of the Wasatch are lithified and the present day environmental conditions may be quite different than those during the time of deposition.

Three main characteristic features used to recognize paleosols include traces of life, soil horizons, and soil structure (Retallack, 2001). Root traces are evidence that plants once grew in the material. Root traces can be distinguished from other fossil traces, because most root traces taper and branch downward, and are very irregular in width (Retallack, 2001). Root traces do have their limitations as identifiers of paleosols as they have not been found in paleosols older than the Silurian, which is when the first vascular land plants appeared (Retallack, 2001).

The patterns of the root traces may also provide information of the history of the paleosol, such as former drainage, vegetation types, and indurated parts of the paleosol.

The root patterns can also indicate features of the paleosol that occurred before burial, as the roots would grown around hard parts of the soils, such as pebbles and nodules (Retallack, 2001).

Ancient soil horizons are also evident in the rock record by gradational changes in texture, color, and/or mineral content. The ancient soil horizons are highly variable depending on the conditions under which the soil formed and was later buried. Even in highly altered paleosols, the top of the uppermost horizon is usually truncated sharply, and the boundaries in the lower horizons are more gradational (Retallack, 2001). Exceptions can occur, such as slow sedimentation on the top, allowing plants to grow, erasing the sharp contact on the uppermost horizon, and sharp horizon contacts within the paleosol, usually associated with unweathered parent material in sedimentary rocks. Paleosols may appear massive and structureless in the field, but laboratory data, such as petrographic or geochemical, may provide evidence that reveals horizons that were undetectable (Retallack, 2001).

Soil structure is also visible in the rock record and is quite distinct from characteristics seen in other geologic material. Soil structures include the formation of pedons (natural aggregates of soil), cutans (modified surface within a soil), glaebules or mottles (segregations of materials distinct from other parts of the soil), and microfabric (Retallack, 2001).

Pedons or peds are formed during soil development and modern ones can usually be crushed by hand. All different shapes and sizes can form, each one reflecting particular kinds of soil and environments (Retallack, 2001). Compaction and alteration after burial can make the identification of peds in paleosols difficult. The pattern of

cracking and breaking of the paleosols from the outcrop may be paleosol structure or features of burial or modern weathering. Care must be taken to identify peds in the field (Retallack, 2001).

Cutans are the modified surfaces of peds, and they vary greatly in composition, which is how they are classified. Cutans in soil are formed in one of three ways: 1) the washing down of material into cracks between the peds, 2) alteration inward from a surface, and 3) differential shear forces within the soil. Cutans can also occur during diagenesis and metamorphism, but those thought to be original can be important guides to chemical conditions in the original soil. One such example is the presence of noncalcareous, nonclayey, ferruginous cutans indicating acidic and highly oxidizing conditions that would be found in well-drained, sandy soils of humid climates (Retallack, 2001).

Glaebules and mottling are abundant in many soils and paleosols, but are not limited to these materials. Marine rocks, cooling volcanic tuffs, and deposits around springs are also known to contain glaebules and mottling (Retallack, 2001). Care must be taken when using mottling or glaebules to determine if a unit is a paleosol, as they could be pre-pedogenetic, pedogenetic, or diagenetic (Retallack, 2001).

Some microscopic structures are also a characteristic of soils and paleosols. One of the more distinctive structures is the appearance of the fine-grained part of the paleosol in thin section, called plasmic fabric (Retallack, 2001). As a soil develops the increase in abundance of cutans, which obscure original sedimentary, metamorphic, or igneous textures, is expressed by the development of sepic plasmic fabric or "bright clay" fabric. Bright clay is highly oriented and has a high birefringence under crossed nicols with the

microscope. On the other hand, weakly oriented clay appears dull and is termed asepic plasmic fabric. Sepic and asepic plasmic fabrics can be divided even further (see Brewer, 1976). The degree of development of bright clay fabric is due in part to the time available for soil formation and also in part to the intensity of the soil forming processes. In order to view the types of bright clay fabrics, thin sections must be ground more carefully and must be thinner than the standard 0.03 mm. This allows enough light to penetrate the clayey soil matrix (Retallack, 2001).

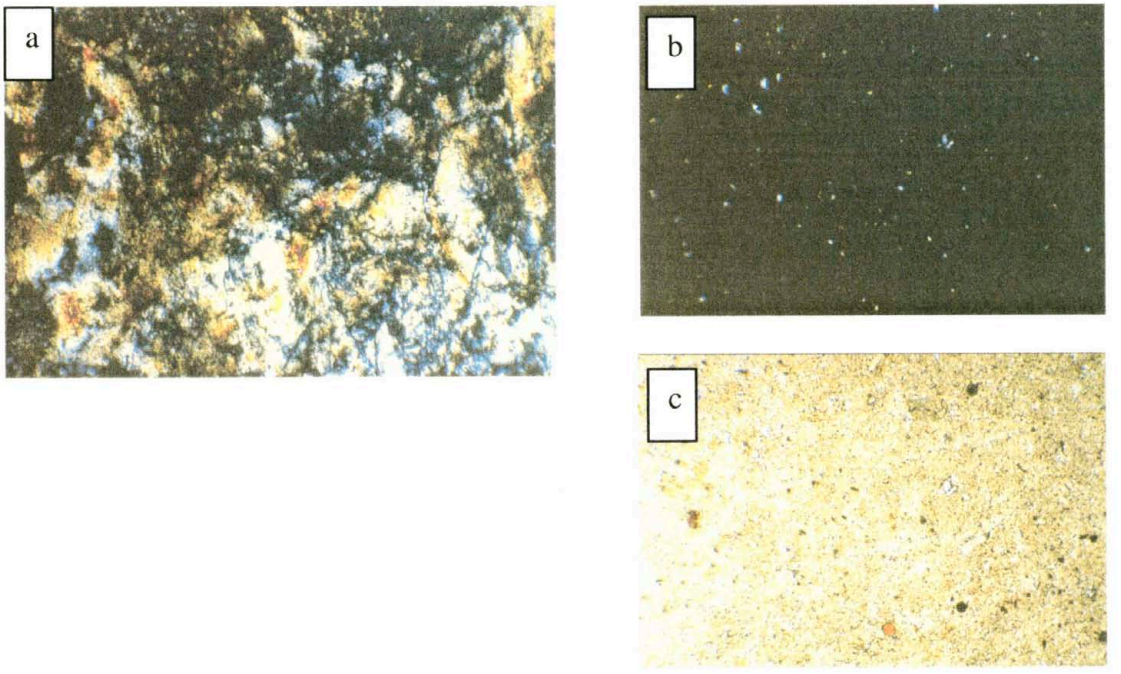

Figure 1.5 Sepic plasmic microfabric (a) and asepic microfabric (b and c). Field of view is 1.4 mm wide for a and 0.8 mm for b and c. Photos b and c are the same photos with b having crossed nicols. Dark color is due to randomness of clay orientation. Photos from Retallack, 1997.

Root traces, soil horizons, and soil structures are not necessarily seen in all paleosols, but provide a starting point for the recognition of paleosols in the rock record. One must keep in mind that some or all of these features may be disrupted or destroyed during compaction and burial diagenesis, making the recognition of the paleosol difficult.

Chapter 2. Geologic Setting

2.1 Tectonic History

The Wasatch Formation was deposited in the Piceance Basin, a small northwest-southeast trending Cretaceous-Paleocene basin located in western Colorado, and created by Laramide tectonism (Johnson, 1989) (Figure 2.1).

During the Sevier Orogeny (Late Jurassic through Late Cretaceous) a large basin, called the Rocky Mountain foreland basin, was created by the eastward thrusting of Mesozoic and Paleozoic rocks (Cole and Cumella, 2003). The foreland basin underwent rapid subsidence during the Cretaceous, which caused major marine flooding. This flooding caused several thousand feet of marine sediments, the Mancos Shale, to be deposited in the area.

During the Late Cretaceous Campanian, pulses of mountain building along the Sevier Orogenic Belt caused influxes of clastic sediments and pushed the shoreline of the Cretaceous Epeiric seaway further to the east. The Mesaverde Group of strata are composed of sediments deposited during transgressive and regressive cycles at the base, overlain by marginal-marine and coastal plain sediments deposited when the shoreline was further to the east. (Johnson, 1989).

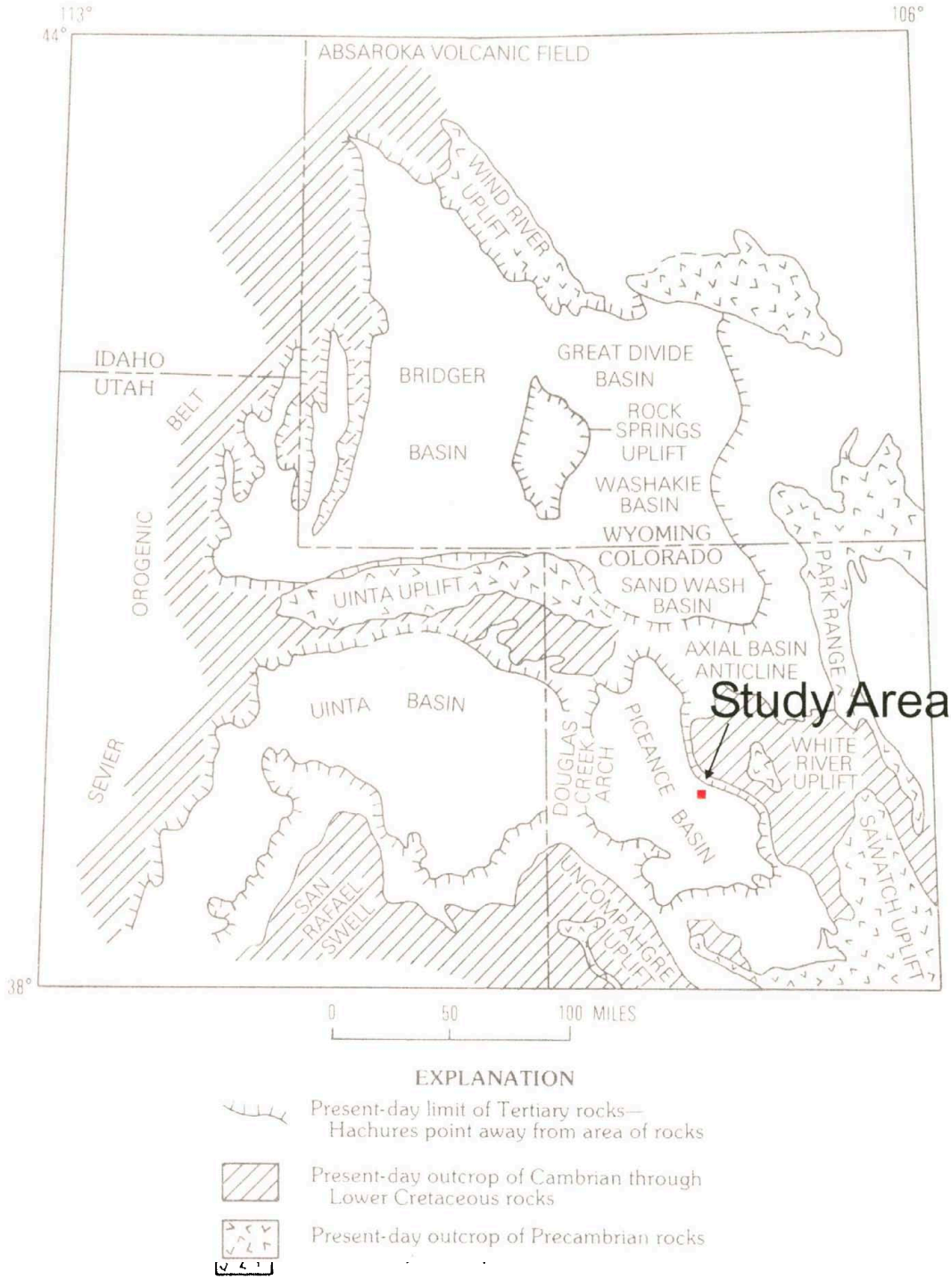

Figure 2.1 Location of the Piceance Basin with uplifts and surrounding basins labeled. study area is located with a red box. From Johnson, 1989.

The Laramide Orogeny began in the Late Cretaceous Campanian and overlapped the final thrusting events on the Sevier Orogenic Belt. The orogeny produced uplifts that rearranged drainage patterns, provided new sources of sediments, and separated the larger Rocky Mountain Basin into several small basins including the Piceance Basin (Johnson and Flores, 2003).

Before the end of the Cretaceous, a major period of regional uplift affected the rising Laramide uplifts and the basins that were created by the Laramide uplifts. The large unconformity that was caused by this major uplift period separates the Mesaverde Group from the younger Tertiary Wasatch Formation throughout the basin (Johnson, 1989).

The Piceance Basin is bounded on the northwest by the Uinta Uplift, on the north and northeast by the Axial Basin Anticline, on the east by the White River Uplift and Elk Mountains, on the southeast by the Sawatch Uplift, on the south by the San Juan Volcanic Field, on the south and southwest by the Uncompahgre Uplift, and on the west by the Douglas Creek Arch, Gunnison Uplift, and West Elk Mountains (Johnson, 1989) and (Cole and Cumella, 2003) (Figure 2.1 and 2.2).

The highland features that surround the basin were created at different times and controlled the drainage and provided sediments to the fluvial and lacustrine systems that were located in the basin (Lorenz and Nadon, 2002). The basin is highly asymmetrical and has gently dipping western and southwestern edges and a sharply upturned eastern edge. This eastern edge is commonly referred to as the Grand Hogback. The Hogback is believed to be underlain by a deep-seated west-thrusting reverse or thrust fault (Johnson, 1989).

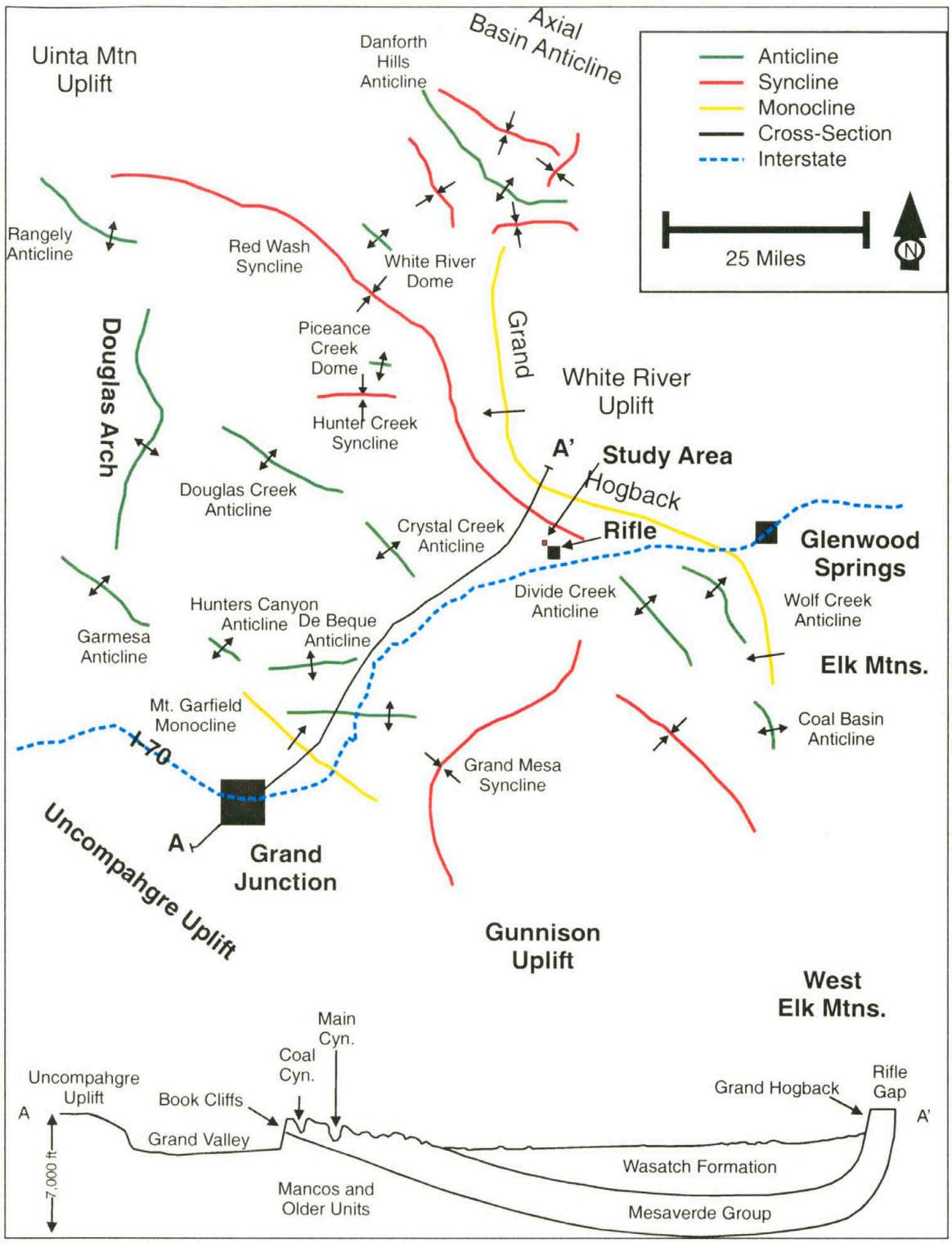

Figure 2.2 Plan-view and cross-section along A-A' of the Piceance Basin. Study area is located with a red box. Modified from Cole and Cumella, 2003

Multiple major southeast-plunging anticlinal structures are found throughout the basin and are believed to be related to the eastern terminus of the Uinta Uplift. These structures are also thought to be underlain by major southwest thrusting, high angle thrust, or reverse faults related to the more major thrust fault along the southern boundary of the Uinta Uplift. Several minor east and southeast trending anticlines are also present in the Piceance Basin. These minor anticlines may have formed as a result of reactivation of older faults during the Laramide Orogeny (Johnson, 1989).

The Basin is structurally deepest along the Red Wash Syncline (See Figure 2.2) (Cole and Cumella, 2003). The Wasatch Formation is nearly horizontal, essentially parallel to the overlying Anvil Points Member of the Green River Formation (Shroba and Scott, 1997).

2.2 Stratigraphy

The Wasatch Formation was deposited on a major regional unconformity (see Figure 1.2). The strata below the unconformity, commonly referred to as the Mesaverde Group, are composed of sediments deposited during marine transgression and regression cycles, and fluvial deposits from a coastal plain (Johnson, 1989). Below the Mesaverde Group are marine rocks, the Mancos Shale, and rocks deposited on a coastal plain, the Dakota Formation. The rocks deposited on top of the Wasatch Formation, mainly the Green River and Uinta Formations, are lacustrine.

The Wasatch Formation is currently divided into 3 different members, in ascending stratigraphic order, the Atwell Gulch, Molina and Shire (Lorenz and Nadon, 2002) (Figure 2.3). A newly proposed fourth member, the Doodlebug Gulch, (Shroba

and Scott, 1997), incorporates about 14 fluvial sandstone intervals greater than 1 m thick and 13 intervening mudstone intervals that were previously included in the overlying lacustrine Green River Formation. This newly proposed member is about 370 m thick. The member focused on for this project is the Shire Member.

Donnell (1969) describes the Atwell Gulch Member as a series of drab brown and gray shales and sandstones with several thin, discontinuous interbeds of coal and carbonaceous shale. Shroba and Scott (1997) describe it as a unit with two parts: (1)a nonmarine volcaniclastic-rich upper part that consists of abundant multicolored fine-grained clastic intervals that include thick claystone, mudstone, and siltstone interbedded with less abundant thinner intervals of coarse-grained volcaniclastic beds of fluvial sandstones and abundant conglomerates and (2) a largely nonvolcanic lower part that

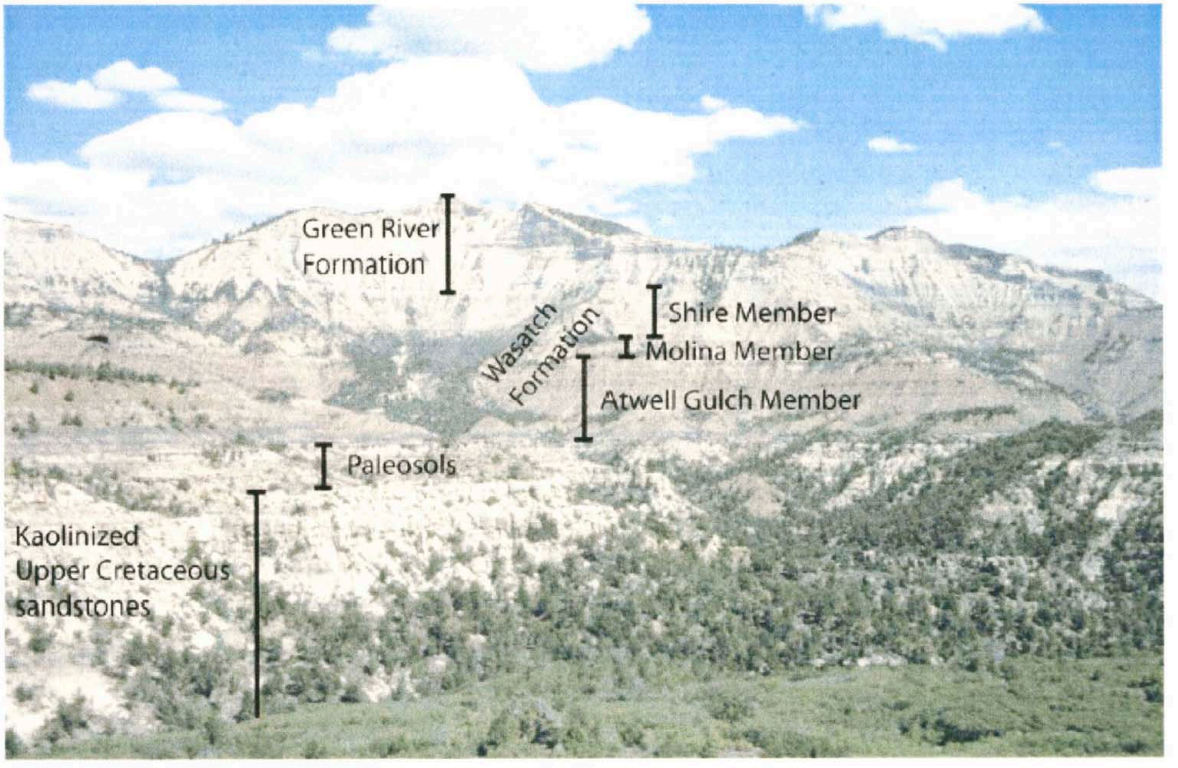

Figure 2.3 Photograph showing the three members of the Wasatch Formation and other formations above and below. The paleosols located below the Wasatch are believed to Paleocene in age. Photograph was taken towards the northeast from Garfield Mesa, which is located about 35 miles to the west of the study area. From Johnson and Flores (2003).

consists predominantly of multicolored fine-grained clastic intervals that include thick claystone, mudstone and siltstone interbedded with less abundant thinner intervals of coarse-grained clastic beds of fluvial sandstones and sparse conglomerates. The Atwell Gulch Member ranges in thickness from 170 to 270 meters.

Donnell (1969) describes the Molina Member as mostly consisting of sandstone with thin interbeds of multicolored claystones and siltstones. Shroba and Scott (1997) further describe the Molina as a nonmarine, predominantly multicolored, fine-grained clastic intervals consisting of thick claystone, mudstone, and siltstone interbedded with less abundant, coarse-grained, clastic intervals of thin fluvial sandstone. The Molina Member ranges from 105-160 m in thickness.

Donnell describes the Shire Member as a unit with multicolored claystones and siltstones, mainly purple, lavender, and red with minor amounts of lenticular brown sandstones. Shroba and Scott (1997) describe the Shire Member as nonmarine, predominantly multicolored, fine-grained clastic intervals of thick claystone, mudstone, and siltstone interbedded with sparse intervals of minor coarse-grained clastic beds of thin fluvial sandstone. The Shire Member is about 1,550 m thick in the area that Shroba and Scott focused on.

There is some disagreement over the total thickness of the Wasatch Formation. Lorenz and Nadon (2002) indicate that the Wasatch Formation varies from about 600 – 1,200 m thick; while Donnell (1969) states that the formation ranges from 380 – 1,960 m thick. Shroba and Scott (1997) indicate that based on drill hole data and map relations, about 2,275 m of the formation is exposed, including their proposed Doodlebug Gulch

Member. The addition of the units from the overlying Green River Formation adds about 370 m of thickness to the total amount exposed from Shroba and Scott (1997) Without this 370 m added, Shroba and Scott's (1997). Wasatch Formation thickness is reduced to about 1,905 m. This number is close to Donnell's thickness of 1,960 m. More work on these members may clarify the thickness of the Wasatch Formation across the basin.

Lorenz and Nadon (2002) studied the Molina Member of the Wasatch Formation near the study area and noted that the Molina is an anomalously sandy unit in the overall muddy stratigraphy of the Wasatch. They also mention that the members that underlie and overlie the Molina Member consist of more than 60% mudstone. The sandstones in these units are lenticular, distinctly different from the tabular sandstone bodies in the Molina. The abrupt change from tabular sandstones to lenticular sandstones indicates the top and base of the Molina Member, which in turn indicates the base of the Shire Member. Shroba and Scott (1997) indicate that the Molina Member is distinguished from the Shire by the presence of about 20% sandstone beds that are more resistant than those of the Shire due to a stronger calcareous cement. Figure 2.4 shows the multicolored paleosols and lenticular shaped sandstone bodies of the Shire Member that Donnell (1969), Shroba and Scott (1997), and Lorenz and Nadon (2002) describe in their papers.

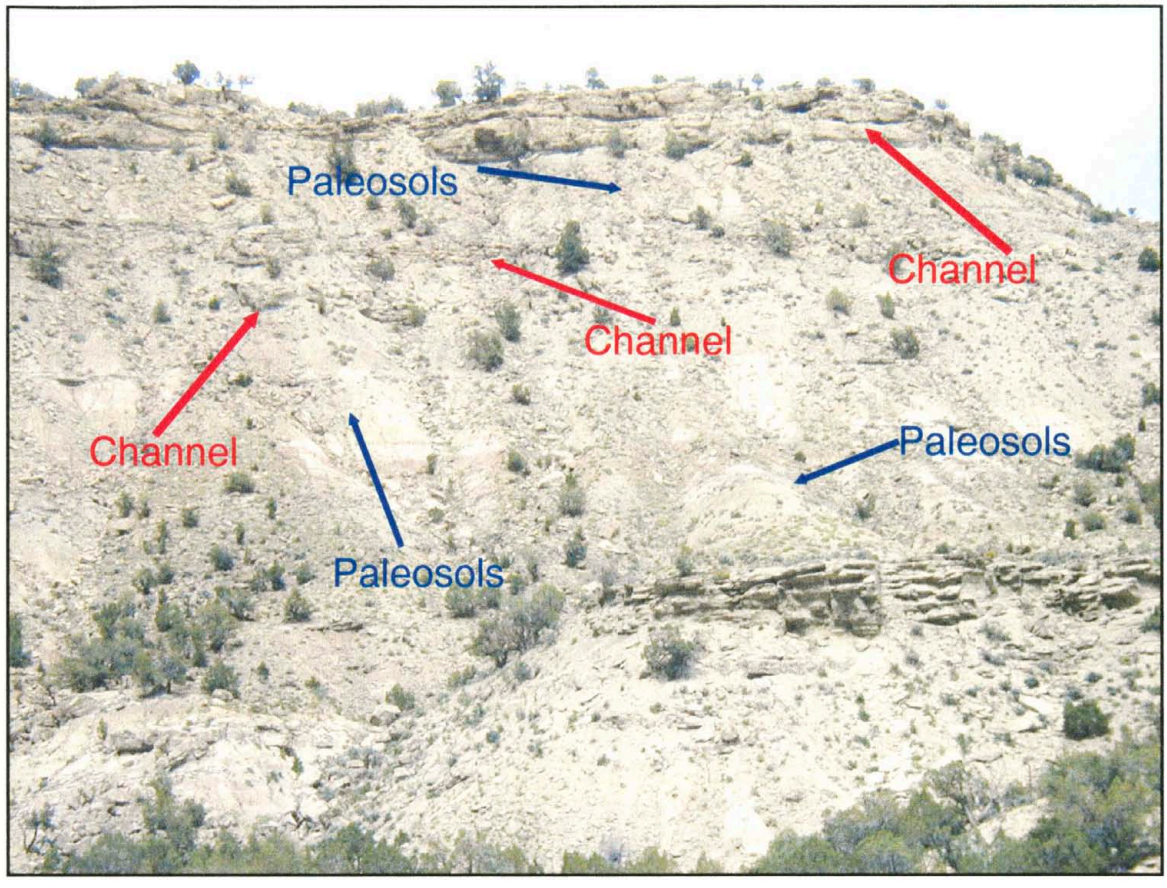

Figure 2.4 Paleosols and lenticular sandstone bodies from the Shire Member in the study area.

Ali Al-Anboori (2003) worked on the sandstones of the Shire Member in the same field area as this study. His research was designed to improve the understanding of the architecture of the sandstones and to test the hypothesis that low net-to-gross reservoirs are the product of high sinuosity river systems. He describes the Shire Member as consisting of isolated, stacked ribbon sandstones scoured and incised into thick floodplain mudstones and siltstones (paleosols), with occasional thick sheet-like sandstones with gravel bars at their base. Most of the work was related to the architecture of the sandstones, but some descriptions of the paleosols were included.

Ali Al-Anboori recognized paleosols on the basis of pedogenic features such as slickensides, colored horizons, roots, and mottles. The paleosols range from weakly to well-developed and are between 0.5 m to 3 m thick. The fine grain size and dominance of soil features suggest the paleosols were floodplain or overbank deposits, and that the sandstones were produced by braided or straight channel systems rather than high-sinuosity channel systems (Ali Al-Anboori, 2003).

Lyons (2000) also worked on the sandstones of the Shire Member near Parachute, CO, located about 15 miles southwest of the study area for this project. The main goal of this effort was to determine the relationship between channel avulsion and aggradation height by studying the geometry of the channel belt sandstone bodies. He describes the Shire Member as being composed of isolated ribbon sand bodies within finer-grained, floodplain mudstones. He also mentions that strong color banding of the floodplain mudstones is suggestive of paleosol development. Paleosols of meter-scale thickness are amalgamated into distinct horizons of greater or lesser maturity. These larger scale bands are on the order of 50 meters thick.

Chapter 3. Methodology

3.1 Field Methods

The rocks studied were sampled from an outcrop of the Wasatch Formation in the Piceance Basin in western Colorado. The ridge containing the rocks is on Bureau of Land Management land along a county road in Hubbard Gulch, approximately 2 miles northwest of the town of Rifle. The outcrop is located in the center of the Rifle 1:24,000 Quadrangle, with latitude-longitude coordinates of approximately 39° 34' N, 107°49' W.

The general trend of the outcrop is north-west to south-east and it has multiple ridges and drainage channels that can be seen on the topographic map (Figure 1.1). The outcrop (Figure 3.1) contains multiple layers of paleosols that are easily recognized by the color changes seen in the outcrop. Discontinuous, lenticular shaped sand bodies can be found throughout the outcrop, with a relatively thick sandstone channel capping the top of the ridge.

The sampling locations were determined by using a random stratified sampling plan, which if done properly, reduces the number of samples required to determine variability within the sampled population. It defines the areas of greatest interest and provides for reduction in the number of samples in other areas. The areas of interest were locations in the outcrop where changes in color and lithology were observed. These areas were likely to have varying concentrations of elements or differences in sealing capacity related to the observable macroscopic differences in the outcrop.

Figure 3.1 Photomosaic of whole outcrop. Field of view is ~ 1000 m long.

Two different paleosol packages were sampled for this project, Paleosol Package U (PPU) and Paleosol Package L (PPL). Two locations were sampled for the PPL because they were the only visibly correlative locations for that paleosol package. The PPU had very good exposure and was correlative across the outcrop, but many areas were too steep to be safely accessed, 7 different locations were sampled.

The Wasatch Formation section was photographed, described, measured, and sampled in July 2003. A return trip was made in August 2003 and a final follow up trip in October 2004. A total of 85 samples were collected; 20 were obtained from the lower paleosol and the remaining 65 were obtained from the upper paleosol. Of the 65 samples from the upper paleosol, five were collected from channel sands and were not evaluated as seals.

Samples at all locations were collected by using a rock hammer and pickaxe. The pickaxe was used to remove the weathered rock material from the surface. The sampling depth ranged from 10 cm to 100 cm from the weathered surface. Figure 3.2 shows a sampling position with the weathered material removed.

Once unweathered rock material was exposed, a close-up photograph was taken at each location and samples were collected (Figure 3.3). The samples collected, 3 to 5 fist-sized samples at each position, were placed into sample bags which were then labeled with a marker indicating the sample number. Before being placed in the bag, the orientation of each sample as taken from the outcrop was marked with an arrow in the "up" direction so that thin sections could be constructed that were perpendicular to bedding or soil horizon development.

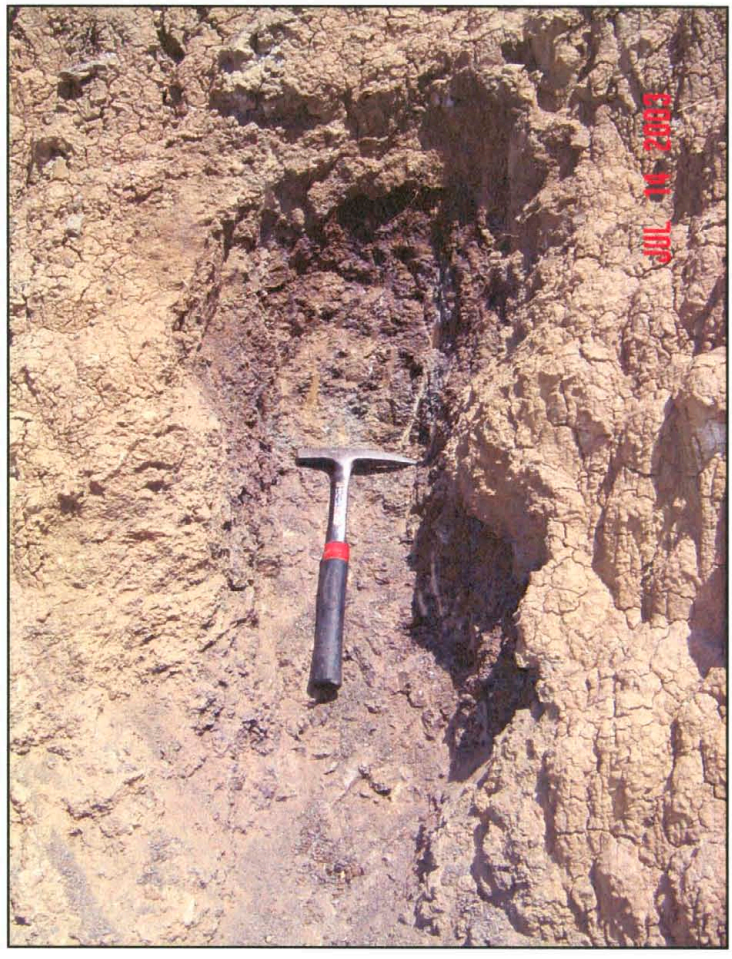

Figure 3.2 Sampling location with weathered material removed. Hammer is 38 cm long.

Figure 3.3 Close up of sample location before collection of sample. Marker is13.8 cm long.

Each sample location was described in a field book and the following characteristics were recorded: location, elevation from handheld GPS unit, and trend of the outcrop (Table 3.1)

Table 3.1 Sampling locations with recorded data

Sampling Location	Number of Samples	UTM Northing (meters)	UTM Easting (meters)	Elevation (feet)	Trend
B1	10	4382836	258512	5669	252°
B2	10	4382906	258462	5692	291°
L1	11	4382819	258594	5750	290°
L2	1	4382823	258610	5767	270°
L3	12	4382663	258804	5770	275°
L4	9	4382654	258940	5820	312°
L5	18	4382816	258572	5757	170°
L6	1	4382918	258525	5767	253°
L7	13	4382738	258669	5757	310°

Other data obtained at the outcrop include: reaction to acid, presence of paleoroots, pedogenic structure size and shape, depth to unweathered material, rock type, and both weathered and unweathered color using a Munsell Rock Color Chart. Once all samples were collected and placed in a sealed bag, a photograph was taken that showed the point of the outcrop where the sample was collected (Figure 3.4). This photograph was used to reference sample locations once field work was completed.

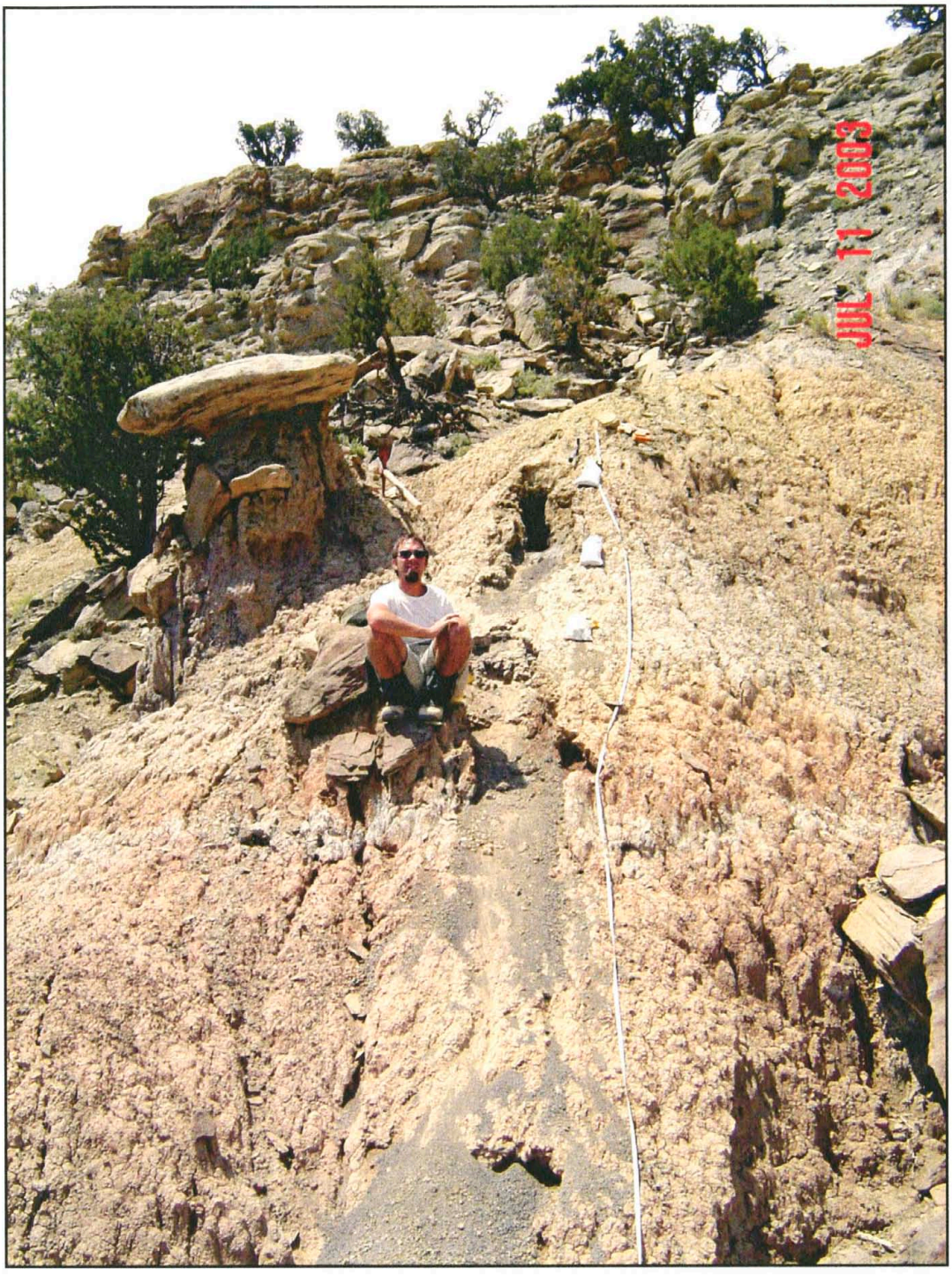

Figure 3.4 Samples collected at a location at their respective positions stratigraphically in the outcrop.

3.2 Mercury Injection Capillary Pressure Analysis

Mercury injection capillary pressure (MICP) analysis was used to measure the sealing capacity of each paleosol mudstone sample. All of the paleosol samples were used for MICP analysis, which was performed by John Neasham at PoroTechnologies.

MICP data is collected by measuring the percentage of rock pore volume that is saturated by the non-wetting fluid (mercury) as it is incrementally injected into a clean and dry sample. Sufficient time is given at each increment to allow for equilibrium. The mercury is non-wetting and therefore does not adhere to the pore walls. This ensures an accurate measurement of the mercury that has been injected into the sample. The displacement pressure (Pd) is the pressure at which mercury first enters a sample after closure, which is described below (Vavra et al., 1992).

The data were corrected for closure, which is the point where mercury stops filling the surface irregularities of the sample and actually enters the pores (Vavra et al., 1992). Closure points were picked for each sample following the procedure of Almon (personal communication). The procedure is as follows. First, the raw data for cumulative intruded mercury and its corresponding pressure were entered into a spread sheet. Then, the log (base10) value for each pressure value in the spreadsheet was calculated. Next, columns were created for the change in pressure and change in mercury saturation at each step (Δ1 P and Δ1 S). The 1st derivative was calculated by dividing Δ1 P by Δ1S. Then, the second change of pressure (Δ2P) was calculated from Δ1P at each step. A graph was created using the 1st derivative of the cumulative pressure, the actual cumulative pressure and Δ2P. The closure point was picked from the cumulative mercury saturation curve at the point where the 1st derivative and the Δ2P curves deviate.

(Figure 3.5). Table 3.2 is a portion of a spreadsheet used to calculate the data used to plot the three curves seen in Figure 3.5.

Table 3.2 Data used to plot curves in Figure 3.5

Measured Pressure (psia)	Log (base10) of Pressure	Cumulative Intruded Mercury (mL/gm)	Δ1P	Δ1 Sat	1st Derivative
1.6 (a)	0.20411998	0 (c)	-	-	-
1.82 (b)	0.26007139	0 (d)	0.0559514 (e)	0 (f)	0 (g)
1.96	0.29225607	0.0001	0.0321847	0.0001	0.003107068
2.15	0.33243846	0.0001	0.0401824	0	0
2.36	0.372912	0.0002	0.0404735	0.0001	0.00247075
2.59	0.41329976	0.0002	0.0403878	0	0
2.83	0.45178644	0.0002	0.0384867	0	0
3.09	0.48995848	0.0002	0.038172	0	0
3.38	0.5289167	0.0004	0.0389582	0.0002	0.005133705
3.69	0.56702637	0.0005	0.0381097	0.0001	0.002624006

Measured pressure and cumulative intruded mercury columns were raw entered data. Log of pressure column was calculated from measured pressure. (e) was calculated from (b)-(a) and (f) was calculated from (d)-(c). (g) was derived from (f)/(e). The calculations were carried throughout the spreadsheet.

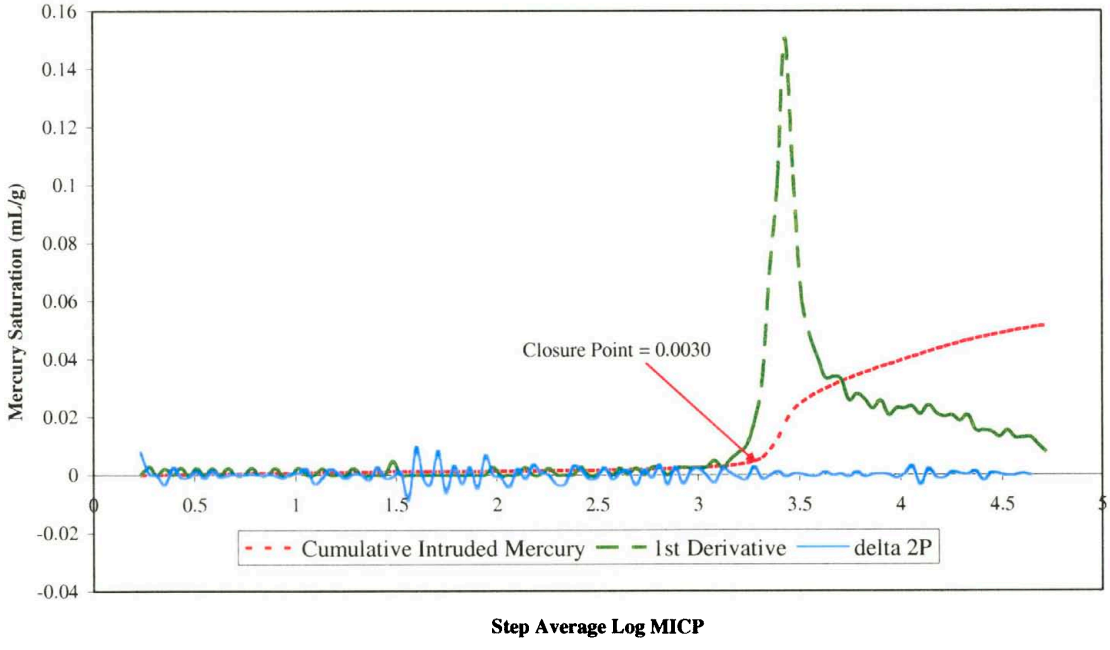

Figure 3.5 Closure is picked where the 1st derivative and the Δ2P curves deviate, corresponding to a saturation of 0.0030 on the cumulative intruded mercury saturation curve.

After the data is corrected for closure, an injection curve is plotted with mercury saturation on the x-axis and mercury injection pressure on the y-axis (Figure 3.6a). The injection pressure at 10% mercury saturation was picked for each sample. This value is used as a measure of the sealing capacity of each sample, and is the value used to compare sealing capacities from the different paleosols.

The pore throat diameter filled at each pressure increase can be calculated using the equation: $D_i = \frac{0.145038\,\sigma\,(-4\cos\Theta)}{P_i}$ Where D_i is the diameter of the cylindrical pore throat, σ is the interfacial tension of the mercury/air system, Θ is the air/mercury/solid contact angle, and P_i is the pressure in psia. In the air/mercury system, the interfacial tension is 480 dynes/cm and the contact angle is 140° (Obligado, 2002).

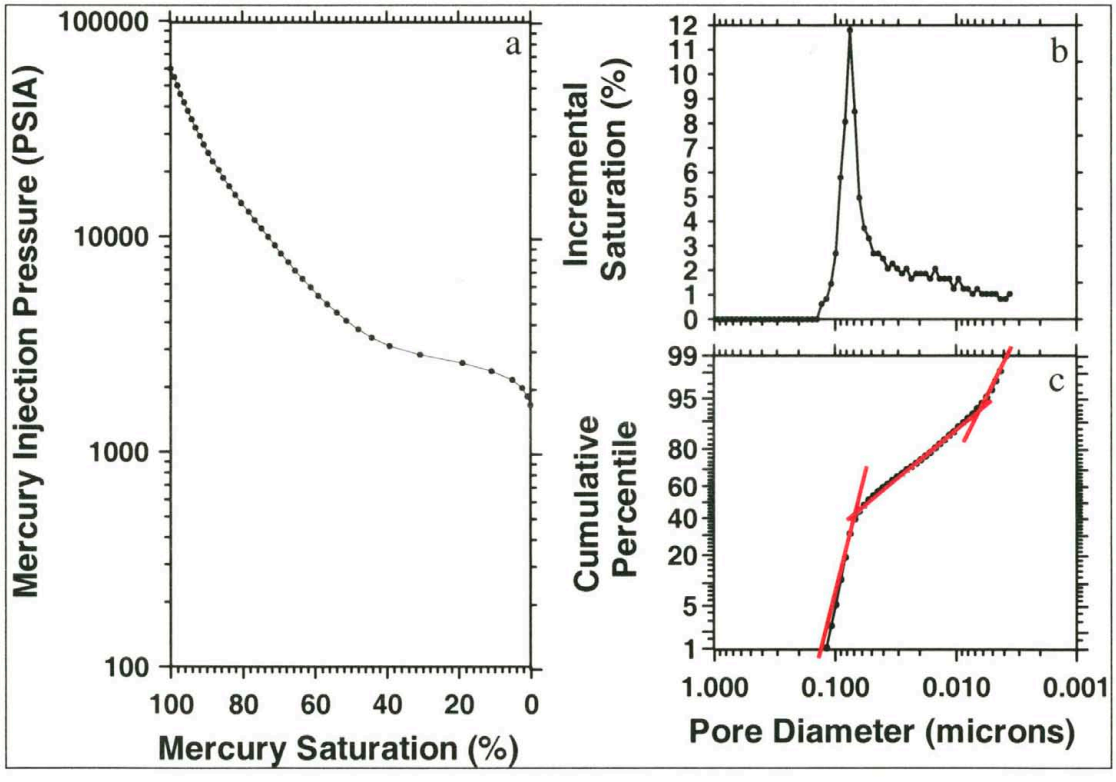

Figure 3.6 (a) Example plot showing mercury injection curve and the injection pressure at 10% saturation. (b and c) Pore diameter distributions with respect to incremental and cumulative pore volume. From the cumulative curve (c), three modal classes of pore throat diameters are evident in this sample (1, 2 and 3) by the red lines.

Plots of the pore throat diameter versus the cumulative and incremental percent pore volume can give valuable information about the pore throat size distribution for each shale sample (Figure 3.6b and 3.6c) (Pittman, 1992). The example cumulative pore throat diameter distribution curve shows three modal classes of pore throat diameters for this particular sample.

3.3 Porosity and Permeability

Porosity and permeability measurements were obtained for each of the 80 paleosol samples. Two different methods were used to obtain the data. One method involved calculating the porosity and permeability measurements from the MICP data. The other method involved direct measurement of porosity and permeability.

To prep the sample for porosity and permeability measurements, a core plug was obtained from the sample using liquid nitrogen for the drill bit coolant and lubricant. The plugs were then dried in a convection oven that was set at 180°F. Once stable weights were obtained, the plugs were placed into airtight containers and allowed to cool to room temperature before dry weight measurements were recorded (Devier, Personal Communication).

Grain volume measurements were made using a small volume helium porosimeter, using Boyle's Law principle of gas expansion. Boyle's Law states that $p*V=c$, where p is pressure, V is volume, and c is a constant. The apparent grain density was calculated from the dry weight and grain volume measurement. Pore volume measurements were obtained from the plugs by mounting them in a rubber-sleeved,

hydrostatically loaded overburden cell. Using helium gas, pore volume was measured using Boyle's Law. For samples that could not be plugged, Archimedes bulk volume measurements were made. Archimedes principle of bulk volume states that the volume of fluid displaced by a solid is equal to the volume of the solid. In this case, the samples were submerged in toluene to make the Archimedes bulk volume measurement (Devier, Personal Communication).

With all of the above calculations made, porosity was calculated using the measured grain volume and pore volume data for the plugged samples. Porosity values for the unpluggable samples were calculated using the measured grain value and Archimedes bulk volume measurements. Apparent grain density was also calculated from dry weight and grain volume measurements (Devier, Personal Communication).

Permeability measurements were performed only on the samples that were able to be plugged. For these samples, a steady state permeability was measured after pore volume measurement. Nitrogen was passed through the sample at a known rate and the pressure on each side of the sample was measured. Steady state flow was achieved when a constant pressure drop was recorded on each side of the sample. Permeability was then calculated using Darcy's Law (Figure 3.7) for linear gaseous flow (Devier, Personal Communication).

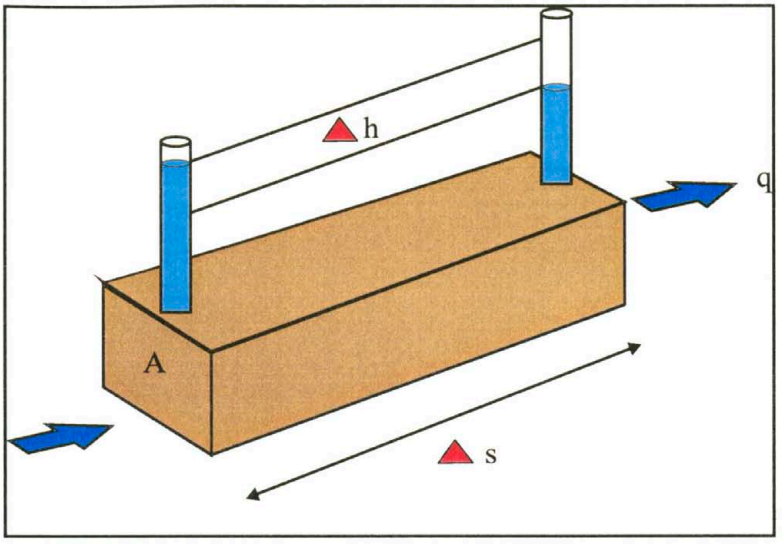

Darcy's Law

$$v = \frac{q}{A} = ki \qquad i = \frac{\Delta h}{\Delta s}$$

Where q = flow rate
A = cross-sectional area
i = hydraulic gradient
v = flow velocity
k = coefficient of permeability

Figure 3.7 Basic concept of Darcy's Law used to calculate permeability.

3.4 Geochemical Analysis

Total Organic Carbon

The total organic carbon (TOC) was measured for each sample by the author. The sample was first crushed into pencil eraser sized pieces using a 2 lb. Eastwing crack hammer on a steel plate. The pieces were placed inside a stainless steel vial and inserted into a SPEX 8000 mixer/mill and allowed to run for 5 minutes. The finished product was a homogenous fine powder. Next, between 5 and 10 grams of the each sample was washed with 10% hydrochloric acid (HCl), causing the inorganic carbon in $CaCO_3$ and $CaMg(Co_3)_2$ to be dissolved, and then rinsed with distilled water. This process of washing and rinsing continued for each sample until a reaction between the sample and HCl was not detected. The rinsed sample was then placed into a 100° C drying oven for 24 hours. Once dried, the inorganic carbon free sample was placed into a glass vial for later use.

The percent organic carbon in each sample was determined using a LECO (model

CHN-1000) analyzer, in the Soils Laboratory at Colorado State University. Approximately 0.2 grams of sample were placed into a small teardrop shaped piece of tinfoil and placed into the LECO and combusted at about 900° C in an oxygenated atmosphere. The analyzer measures the amount of hydrogen, carbon, and nitrogen in the gas given off from combustion.

X-Ray Fluorescence

X-ray fluorescence is a procedure in which samples are irradiated with X-rays produced by a high-intensity X-ray tube. The elements in the sample become excited and emit their own characteristic fluorescent X-rays, the wavelengths of which are used to identify the elements. Their concentrations are determined by comparing intensities of characteristic X-ray peaks produced by the sample to those produced by reference standards (Obligado, 2002).

A total of 57 samples were sent to XRAL Laboratories for bulk chemistry analysis of major and trace elements by X-ray fluorescence. The samples chosen from each location spanned a range of sealing capacities from high to low.

At XRAL Laboratories, each of the unwashed powdered samples was pulverized using a chromium steel mill to a size of #200 mesh. The samples were analyzed using XRAL Laboratories XRF77 Whole and Trace Analysis.

3.5 Thin-Section Petrography

Thin sections (85) were prepared at Petrographic International, Inc. Both paleosols and sandstones were injected with blue epoxy and cut perpendicular to bedding.

The thin sections were analyzed petrographically by the author in order to determine rock composition (mineralogy, matrix, and cementation) and degree of bioturbation. Microscopic structures were not analyzed in the thin sections; however, "bright clay" fabrics were noticed in some of the slides (Figure 3.8).

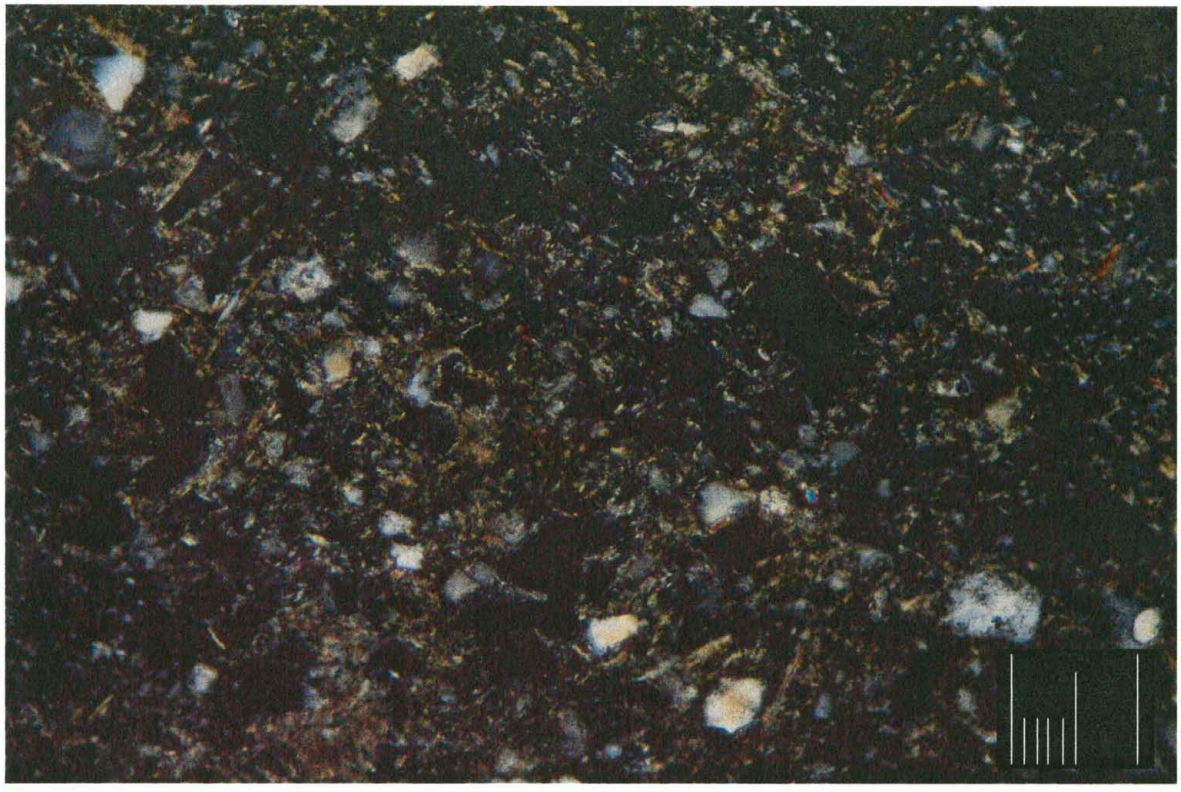

Figure 3.8 Photomicrograph of "bright clay" fabric from the study area. Notice the high birefringence around the yellow and gray quartz grains. Scale is 0.1 mm long.

Compositional analysis of the samples was obtained using a method that involves moving the mechanical stage on the microscope a measured distance and recording what is directly beneath the cross-hairs in the eyepiece. A total of 250 points were counted over the whole slide, and the mineral counts were then converted to percentages.

The silt grain size of each sample was determined by measuring the apparent long axis of 30 randomly selected quartz grains. These measurements were averaged and converted to the phi scale, in which increasing phi values correspond to decreasing grain

size. The standard deviation of the grain size measurements was used as a measure of sorting. The roundness of each grain measured was determined qualitatively using a grain size comparison chart from www.carbonaterocks.com. The grains were assigned a number from 1 to 5, with 1 being angular and 5 being well rounded.

Preferred orientation of organic matter and preferred orientation of matrix was analyzed in the thin sections, but does not apply, as none of the samples exhibited any signs of preferred orientation of organic matter or matrix.

The degree of bioturbation was determined using a qualitative scale based on the percentage of sedimentary structures disturbed by biogenic sources such as roots or organisms. The scale ranges from 0 to 6, where 0 denotes no bioturbation, while 6 represents a completely bioturbated sample lacking any trace of original bedding (Pemberton et al, 1992). The seven categories are: 0 - Unbioturbated; all original sedimentary structures preserved. 1- Very slightly bioturbated (1 - 5 % disruption of original bedding). 2 - Slightly bioturbated; discrete, isolated, trace fossils (5-30% of original bedding disrupted). 3. Moderately bioturbated; burrows overlapping locally (30-60% of original bedding disturbed). 4 - Highly bioturbated; last remnants of bedding discernable, burrow overlap (60-90% of original bedding disturbed). 5 - Intensely bioturbated; bedding is completely disturbed, but burrows are still discrete in places and the fabric is not mixed (90-99% of original bedding disturbed). 6 - Completely bioturbated; bedding is almost or absolutely homogenized, (100% of original bedding disturbed) (Drosser and Bottjer, 1986 and Reineck, 1967; in Pemberton et al, 1992).

Chapter 4. Outcrop Results

4.1 Review of Sampling Locations

A total of 9 different locations (see Figure 1.1 and Table 3.1) were sampled to collect data for this project. Of these 9 locations, 2 were sampled for the paleosols stratigraphically lower in the section (Paleosol Package L, PPL). These samples are identified with a letter "B". The remaining 7 locations were stratigraphically higher in the section (Paleosol Package U, PPU). These samples are identified with a letter "L".

4.2 Paleosol Package L (PPL)

Location B1

Location information for sampling point B1 is found in Table 4.1. The steepness of the outcrop at this location required that the sample locations be moved in a stepwise fashion along the face of the outcrop (Figure 4.1).

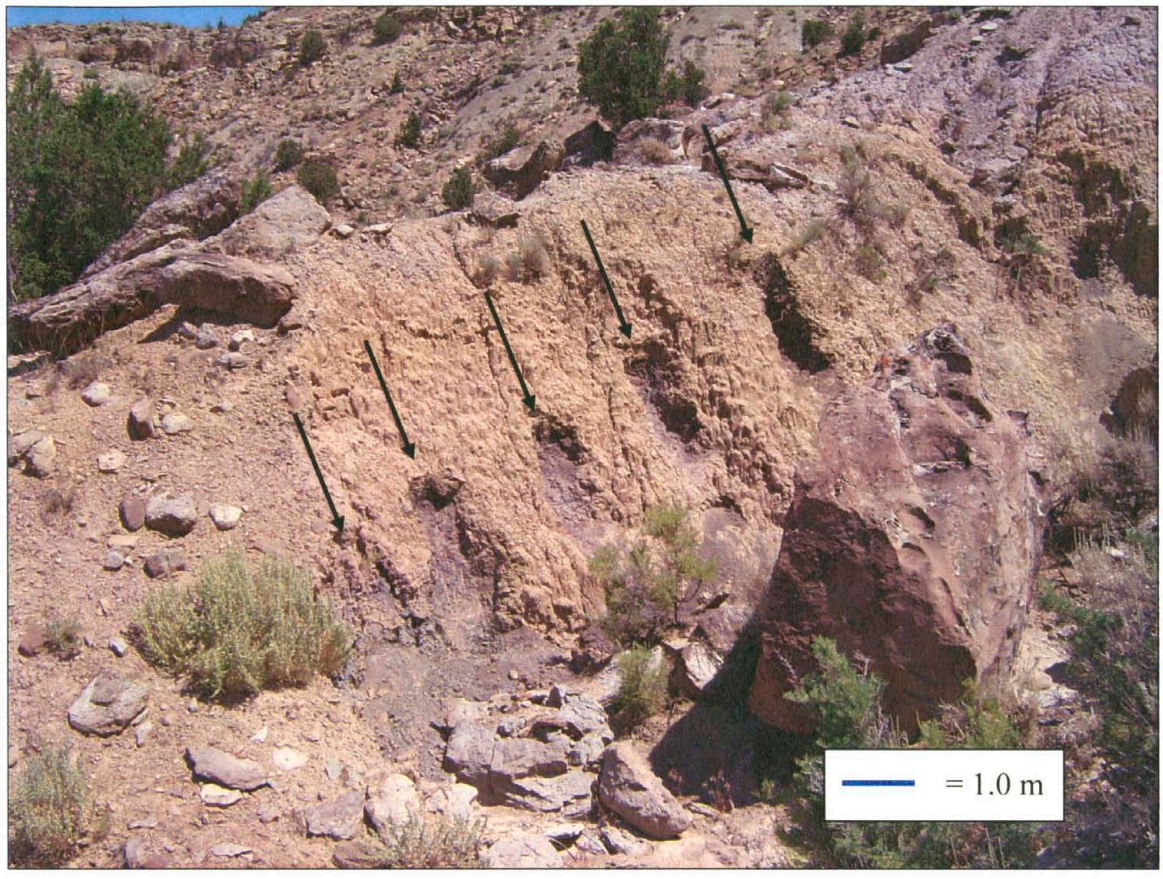

Figure 4.1 Sampling location of B1. Arrows indicate the stepwise placement of sampling locations due to steepness of outcrop. The beds are orientated horizontally in the photograph.

A total of 10 samples were obtained at this location. The outcrop weathered to a grayish-orange color and fresh surfaces ranged from dark gray to grayish purple. Mottling was developed in all samples. Mottling is segregation of materials with very irregular shapes and diffuse boundaries (Retallack, 1997). Sampling depths range from 0.15 m to 0.40 m to avoid obviously weathered material. Pedogenic structures were noted at all 10 sampling points at this location. Root traces were noted in five of the samples, and only one of the samples reacted to HCl acid in the field. White calcareous flakes were noted in two of the samples. The time of formation of the flakes could not be determined

Table 4.1 Sampling details for location B1

UTM	4382836N	258512E	Elevation	5669 ft	Trend	252°	Dip	0°	
Sample #	Strat. Loc. (m)	Depth to Sam. (m)	Weathered Color	Fresh Color	Peds	Roots	Acid	Mottling	Comments
B1-1	0.35	0.15	10YR 7/4	N4	Y	N	N	Y	
B1-2	0.80	0.40	10YR 7/4	5P 2/2	Y	Y	N	Y	
B1-3	1.00	0.30	10YR 7/4	5RP 2/2	Y	Y	N	Y	
B1-4	1.10	0.20	10YR 7/4	5RP 4/2	Y	Y	N	Y	White flakes noted
B1-5	1.30	0.30	10YR 7/4	5RP 2/2	Y	Y	N	Y	
B1-6	1.70	0.25	10YR 7/4	5RP 2/2	Y	Y	N	Y	
B1-7	2.20	0.40	10YR 7/4	5RP 2/2	Y	N	N	Y	
B1-8	2.40	0.20	10YR 7/4	5P 4/2	Y	N	N	Y	White flakes noted
B1-9	2.60	0.40	10YR 7/4	5RP 2/2	Y	N	N	Y	
B1-10	3.10	0.40	10YR 7/4	5RP 4/2	Y	Y	Y	Y	

Location B2

Location information for sampling point B2 is found in Table 4.2. Two different pits (Figure 4.2) were dug to obtain the ten samples collected at this location.

This outcrop weathered to a grayish orange and contained fresh surfaces of dark gray to grayish purple. Mottling was noted in most samples. All ten samples at this location exhibited peds that ranged from angular to subrounded. Five samples reacted to acid while four samples were noted as having paleoroots. Samples were obtained at depths of 0.15 m to 0.25 m to avoid obviously weathered material. Five of the collected samples contained white calcareous flakes, while three samples had rounded nodules (0.5cm-2cm) in them. The nodules were not calcareous in all cases. No determination could be made if the flakes and nodules were a product of soil formation or due to modern weathering events.

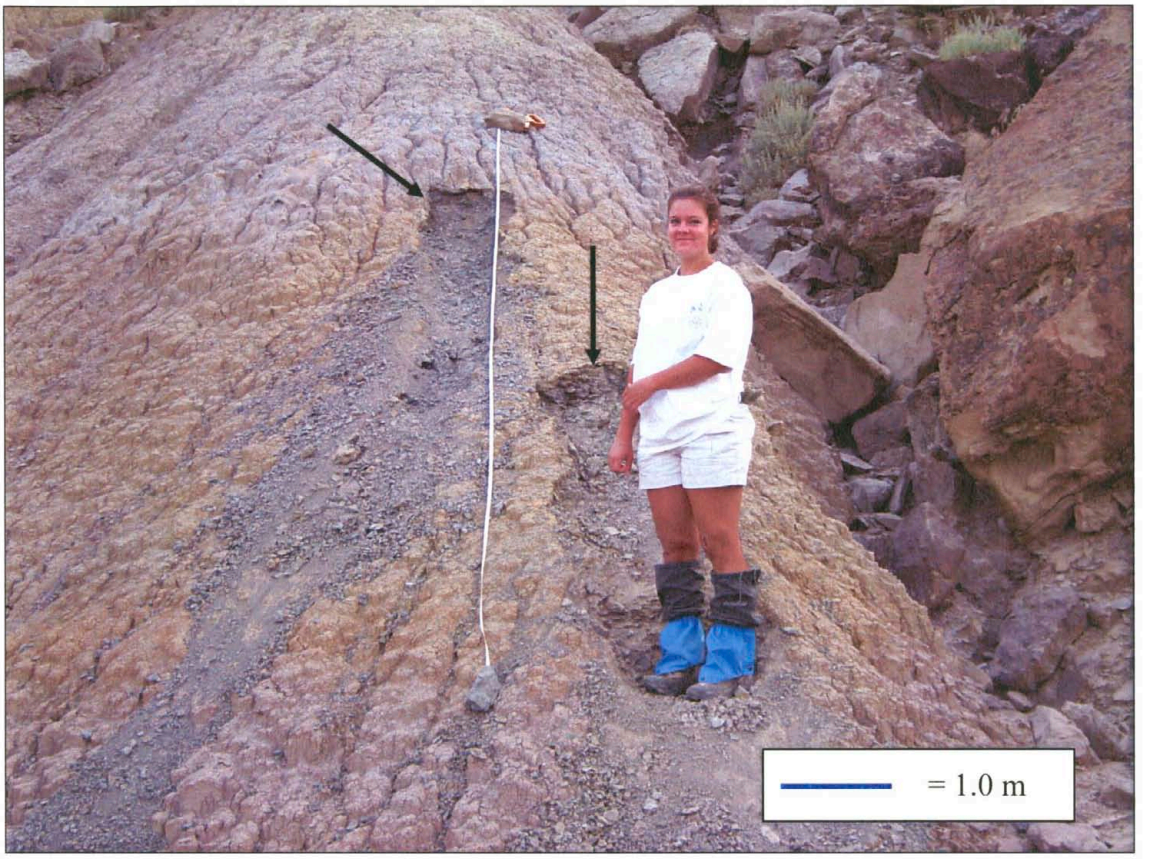

Figure 4.2 Sampling location of B2. Arrows indicate sampling pits.

Table 4.2 Sampling details for location B2

UTM	4382906N	258462E	Elevation	5692 ft	Trend	291°	Dip	0°	
Sample #	Strat. Loc. (m)	Depth to Sam. (m)	Weathered Color	Fresh Color	Peds	Roots	Acid	Mottling	Comments
B2-1	0.20	0.25	10YR 7/4	5P 2/2	Y	Y	N	Y	White calc. flakes
B2-2	0.60	0.15	10YR 7/4	5P 4/2	Y	Y	Y	Y	White calc. flakes
B2-3	1.10	0.15	10YR 7/4	N4	Y	N	N	Y	White calc. flakes
B2-4	1.50	0.20	10YR 7/4	N4	Y	N	N	Y	White calc. nodules
B2-5	2.00	0.25	10YR 7/4	N3	Y	N	N	Y	
B2-6	2.30	0.20	10YR 7/4	N5	Y	N	Y	Y	White calc. nodules
B2-7	2.80	0.25	10YR 7/4	N5	Y	N	N	Y	White non-calc. Nodules
B2-8	3.40	0.15	10YR 7/4	N5	Y	N	Y	Y	
B2-9	4.10	0.20	10YR 7/4	N4	Y	Y	Y	Y	White calc. flakes
B2-10	4.50	0.20	10YR 8/2	N5	Y	Y	Y	Y	White calc. flakes

4.3 Paleosol Package U (PPU)

Location L1

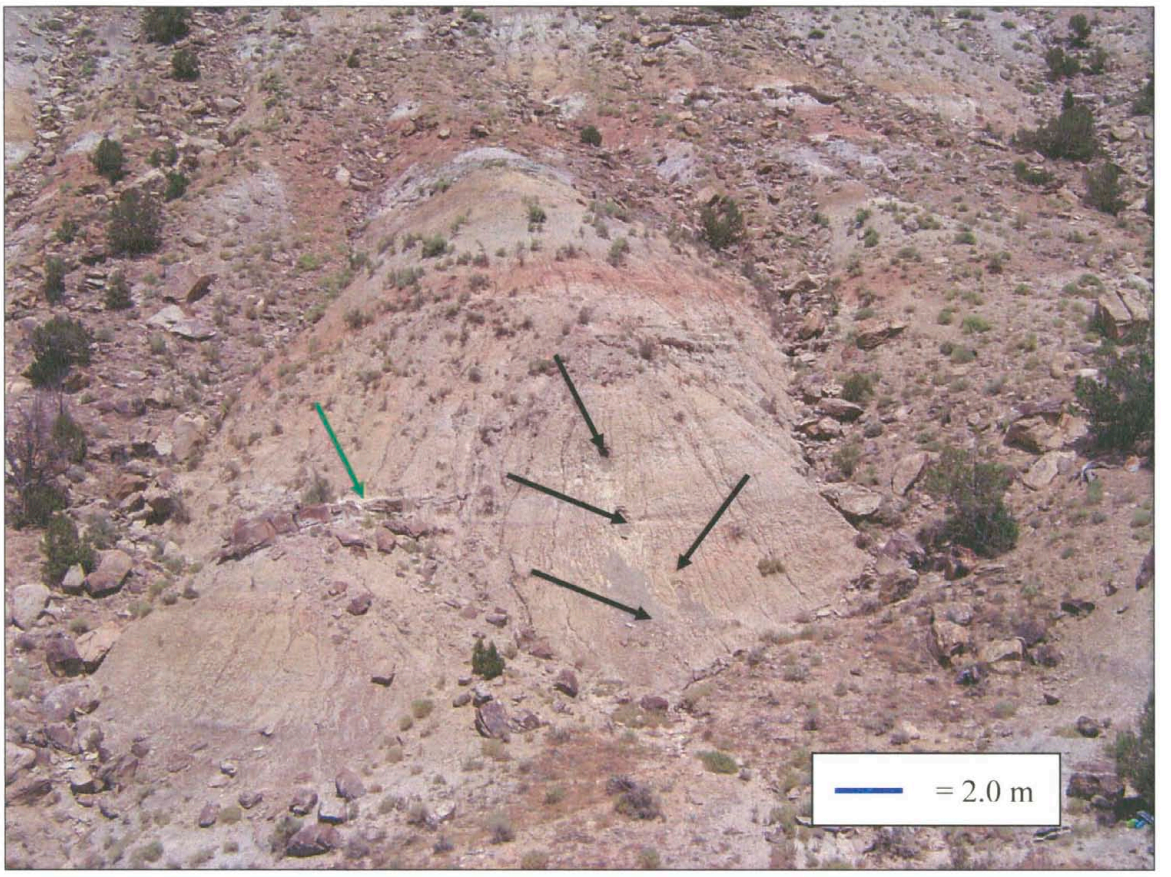

Figure 4.3 Sampling location for L1. Arrows indicate some sample locations (black are paleosol samples and green is sandstone sample).

Location information for sampling point L1 is found in Table 4.3. A total of 11 samples were collected from this location on two separate occasions. The second trip was to collect additional samples in some of the thicker paleosol units. Of the 11 samples collected, one was a sandstone from a lenticular channel (green arrow in Figure 4.3). The outcrop weathers to a pink color with fresh surfaces exhibiting a light gray color. The sandstone is massive, well indurated, calcareous, well sorted, and fine grained. No fossils or other sedimentary structures were noted. This sample was not evaluated as a seal.

The paleosols at this location weather to a grayish orange to yellowish gray, fresh surfaces were yellowish and grayish browns to dusky blue in color. Nine of the ten samples exhibited peds that were angular to subangular in shape. Mottling was noted in all of the samples with peds. The sample without peds broke into very small pieces, which may be due to paleosol structure or effects of modern weathering. Seven samples reacted to acid while only two samples exhibited paleoroot structures. To avoid obviously weathered material, sampling depths at this location ranged from 0.10 m to 0.50 m. No calcareous flakes or nodules were noted at this location.

Table 4.3 Sampling details for location L1

UTM	4382819N	258594E	**Elevation**	5750 ft.	**Trend**	290°	**Dip**	0°	
Sample #	**Strat. Loc. (m)**	**Depth to Sam. (m)**	**Weathered Color**	**Fresh Color**	**Peds**	**Roots**	**Acid**	**Mottling**	**Comments**
L1-1	6.00	0.10	NA	NA	N	N	Y	N	Sandstone
L1-2	1.50	0.38	5Y 7/2	10YR 4/2	Y	N	Y	Y	
L1-3	1.70	0.45	10YR 6/2	5YR 3/2	Y	Y	Y	Y	
L1-4	3.90	0.40	10YR 6/2	5YR 3/2	Y	N	Y	Y	
L1-5	4.00	0.40	10YR 6/2	5YR 3/2	Y	N	Y	Y	
L1-6	4.10	0.40	10YR 6/2	5YR 3/2	Y	N	N	Y	
L1-7	7.00	0.38	10YR 8/2	5Y 6/1	Y	N	N	Y	
L1-8	1.00	0.30	5Y 7/2	10YR 4/2	Y	N	Y	Y	
L1-9	2.70	0.40	5Y 7/2	5PB 3/2	Y	N	Y	Y	
L1-10	6.40	0.40	5Y 7/2	5YR 3/2	Y	Y	N	Y	
L1-11	10.2	0.50	5Y 7/2	5Y 4/1	N	N	N	N	Very small pieces

Location L2

Figure 4.4 Sampling location L2. Person is 1.6 m tall for scale. Channel is outlined in red.

Location information for sampling point L2 is found in Table 4.4. Only one sample was obtained from this location. As seen in Figure 4.4, a sandstone channel was present (outlined in red). The surface of the outcrop weathered to a grayish brown color and was yellowish gray on a fresh surface. The sandstone at this location contained slightly more clay than the sandstone from location L1. This sandstone is characterized by poorly sorted fine to medium sized sand grains, and climbing ripples (Figure 4.5).

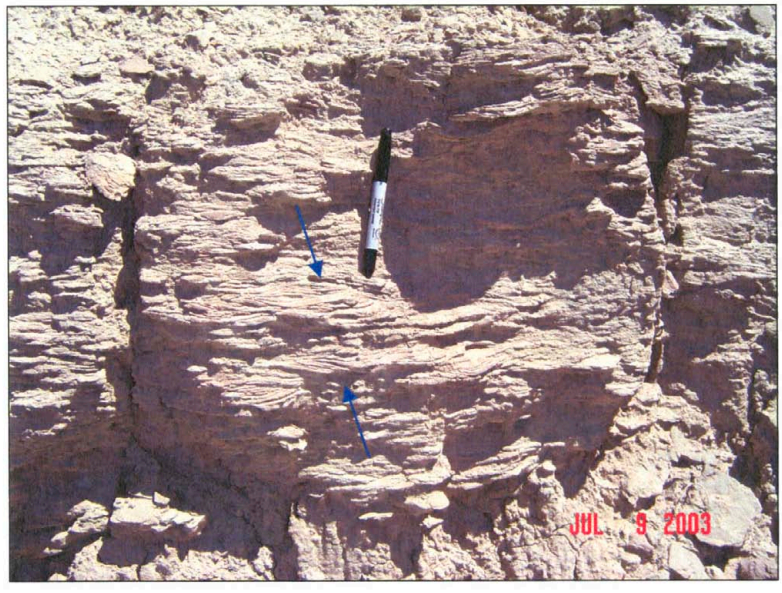

Figure 4.5 Laminations in clay–rich sandstone at location L2. Marker is 13.8 cm long. Climbing ripples noted by blue arrows.

Table 4.4 Sampling details for location L2

UTM	4382823N	258610E	Elevation	5767 ft.	Trend	270°	Dip	0°	
Sample #	Strat. Loc. (m)	Depth to Sam. (m)	Weathered Color	Fresh Color	Peds	Roots	Acid	Mottling	Comments
L2-1	NA	0.10	5Y 7/2	5YR 4/1	N	N	Y	N	Sandstone

Location L3

Location information for sampling point L3 is found in Table 4.5. Twelve samples were collected at this location; 11 paleosol and 1 clay-rich sandstone. The sandstone sample was not analyzed as a seal. The sandstone weathered yellowish gray in color and was olive gray when a fresh surface was exposed.

The sandstone is characterized by poorly sorted, fine to medium size quartz grains, with laminations of clay. The sandstone was not laterally extensive; however, it appears to correlate with a sandstone from sampling location L7 which is about 120m further east.

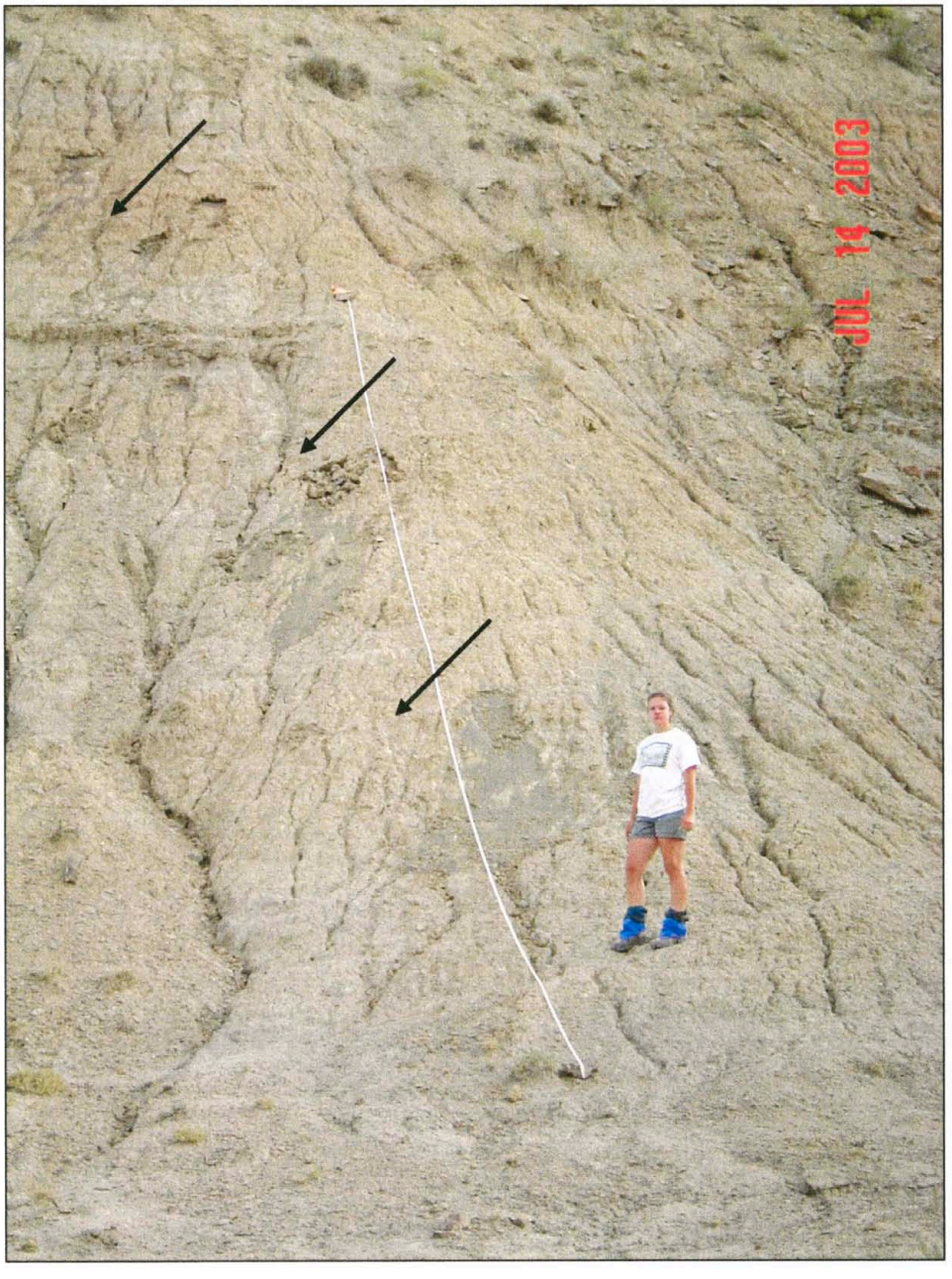

Figure 4.6 Sampling location L3. Arrows indicate some of the sampling points at this location. Person is 1.6 m tall for scale.

Table 4.5 Sampling details for location L3

UTM	4382663N	258804E	Elevation	5770 ft.	Trend	275°	Dip	0°	
Sample #	Strat. Loc. (m)	Depth to Sam. (m)	Weathered Color	Fresh Color	Peds	Roots	Acid	Mottling	Comments
L3-1	6.50	0.75	5Y 7/2	N4	Y	N	N	Y	
L3-2	9.50	0.40	5Y 7/2	5YR 4/1	Y	N	Y	Y	
L3-3	15.0	0.15	5Y 8/4	5Y 6/1	N	N	Y	N	Sandstone/shale
L3-4	17.9	0.15	10YR 6/2	5YR 4/1	Y	Y	Y	Y	
L3-5	20.3	0.25	10YR 7/4	10YR 5/4	Y	Y	N	Y	Wt. fib. calc. min. b/w peds
L3-6	24.6	0.38	5Y 7/2	5GY 7/2	Y	N	N	Y	Wt. fib. calc. min. b/w peds
L3-7	2.40	0.40	5Y 7/2	5Y 4/1	Y	N	N	Y	
L3-8	4.30	0.40	5Y 7/2	10YR 4/2	Y	N	N	Y	
L3-9	5.60	0.50	5Y 7/2	N5	Y	N	Y	Y	Clear non-calc. mineral obs.
L3-10	7.70	0.50	5Y 7/2	10YR 2/2	N	N	N	N	
L3-11	8.50	0.50	5Y 7/2	10YR 4/2	N	N	Y	Y	Very small chips
L3-12	12.7	0.50	5Y 7/2	5Y 5/6	N	N	Y	Y	Small chips

The paleosols at this location weathered to a yellowish gray to grayish orange. Fresh surfaces exhibited shades of gray and brown. Mottling was noted in 10 of the 12 samples that were collected. Four of the samples did not exhibit pedogenic structures. One sample was a sandstone, two samples were removed from the outcrop in pieces too small (<2 cm) to determine pedogenic structures, and the remaining sample did not have any characteristics of ped formation. Peds noted in the other eight samples were angular to subangular and were 8-10 cm in diameter. Six of the samples reacted to acid, while only two were noted as having paleo-root structures. Depth from obviously weathered material ranged from 0.15 m to 0.75 m at this location.

Two of the samples collected exhibited white calcareous fibrous-looking material between the pedons. One of the samples had a clear, non-calcareous deposit on the fresh surfaces. The cause of these features is unknown.

Location L4

Location information for sampling point L4 is found in Table 4.6. A total of 9 samples were collected at this location, and the weathered outcrop color was yellowish gray. Fresh surfaces exhibited shades of gray, grayish red and grayish blue. Mottling was noted in all samples collected. All of the samples exhibited angular to subrounded pedogenic structures that ranged from 1 to 8 cm in diameter. Only four of the samples reacted to acid, and two samples were noted as having paleoroot structures. Sampling depths at this location ranged from 0.15 to 0.40 m to avoid obviously weathered material. One sample revealed small round nodules (2-3mm) on fresh, exposed surfaces.

Table 4.6 Sampling details for location L4

UTM	4382654N	258940E	Elevation	5820 ft.	Trend	312°	Dip	0°	
Sample #	Strat. Loc. (m)	Depth to Sam. (m)	Weathered Color	Fresh Color	Peds	Roots	Acid	Mottling	Comments
L4-1	2.40	0.20	5Y 7/2	5GY 6/1	Y	N	Y	Y	Small(2-3mm) nodules
L4-2	4.50	0.25	5Y 7/2	5G 6/1	Y	N	N	Y	
L4-3	6.20	0.15	5Y 6/4	N7	Y	N	N	Y	
L4-4	7.40	0.15	5Y 7/2	5Y 6/1	Y	N	N	Y	White layer
L4-5	7.80	0.15	5Y 6/4	5GY 6/1	Y	N	N	Y	Above layer
L4-6	8.10	0.15	5Y 6/4	5G 8/1	Y	N	N	Y	Top of layer
L4-7	11.5	0.23	5Y 6/4	5PB 5/2	Y	N	Y	Y	
L4-8	15.3	0.40	10YR 6/2	10R 4/2	Y	Y	Y	Y	
L4-9	18.0	0.38	5Y 7/2	5GY 6/1	Y	Y	Y	Y	

Figure 4.7 Sampling location L4. Arrows indicates white horizon referenced in text. Person is 1.8 m tall for scale.

A faint, white colored layer or horizon was also noted at L4 (see Figure 4.7 and Figure 4.8). Samples were taken right below the horizon, in the horizon, and right above the horizon. All three of the samples exhibited the same characteristics in the field; pedogenic structures, no presence of paleoroot structures, and no reaction to acid. The horizon was more easily seen at a distance from the outcrop than up-close.

Figure 4.8 White horizon at location L4. Three samples were obtained. Marker is 13.8 cm long.

Location L5

Location information for sampling point L5 is found in Table 4.7. The outcrop was sampled on two separate occasions; one event sampled the whole outcrop, while the second event sampled two paleosols that were each approximately 1.5 m thick. These paleosols were sampled to determine how the sealing capacity varies between paleosols. The lower paleosol was bounded by a slight change in topography at the base and a sharp color change at the top. The upper paleosol was bounded by a sharp color change from

gray to brown at the base and a thin, purplish, slightly more resistant layer on the top (see Figure 4.9).

A total of 18 samples were collected at this location, the weathered outcrop color was yellowish to olive gray. Fresh surfaces exhibited shades of gray. No mottling was noted in any of the samples collected over the whole outcrop. All of the samples exhibited pedogenic structures that were angular in shape and ranged from 1 to 8 cm in diameter. Eight of the samples reacted to acid, four samples exhibited paleoroot structures. Obvious unweathered sample depths at this location ranged from 0.30 to 0.50 m.

Table 4.7 Sampling details for location L5

UTM	4382816N	258572E	Elevation	5757 ft.	Trend	170°	Dip	0°	
Sample #	**Strat. Loc. (m)**	**Depth to Sam. (m)**	**Weathered Color**	**Fresh Color**	**Peds**	**Roots**	**Acid**	**Mottling**	**Comments**
L5-1	2.10	0.38	5Y 6/1	5Y 6/1	Y	N	N	Y	
L5-8	4.60	0.40	5Y 6/1	5Y 2/1	Y	N	N	Y	
L5-2	5.00	0.30	5Y 6/1	N5	Y	N	N	Y	
L5-9	5.10	0.35	5Y 6/1	5Y 2/1	Y	N	N	Y	
L5-10	5.30	0.50	5Y 6/1	5Y 2/1	Y	N	N	Y	
L5-11	5.60	0.50	5Y 6/1	5Y 2/1	Y	N	N	Y	
L5-12	5.80	0.40	5Y 6/1	5Y 2/1	Y	N	N	Y	
L5-13	6.50	0.35	5Y 7/2	5Y 4/1	Y	N	Y	Y	
L5-14	6.80	0.35	5Y 7/2	5Y 4/1	Y	Y	N	Y	
L5-15	7.10	0.38	5Y 7/2	5Y 2/1	Y	Y	Y	Y	
L5-16	7.30	0.35	5Y 7/2	5Y 2/1	Y	Y	Y	Y	
L5-3	7.50	0.40	5Y 6/1	5Y 6/1	Y	N	Y	Y	
L5-17	7.60	0.30	5Y 7/2	5Y 2/1	Y	N	Y	Y	
L5-18	7.90	0.35	5Y 7/2	5Y 3/2	Y	N	Y	Y	
L5-4	8.20	0.35	5Y 5/2	5Y 4/1	Y	N	Y	Y	Weath. grains look purple
L5-5	10.10	0.35	5Y 7/2	N4	Y	N	Y	Y	
L5-6	12.50	0.40	5Y 7/2	N5	Y	N	N	Y	
L5-7	14.50	0.40	5Y 7/2	N5	Y	Y	N	Y	SS piece on top of hill

Note: Sample numbers 1-7 are from the whole outcrop and samples 8-18 were sampled in the two paleosols.

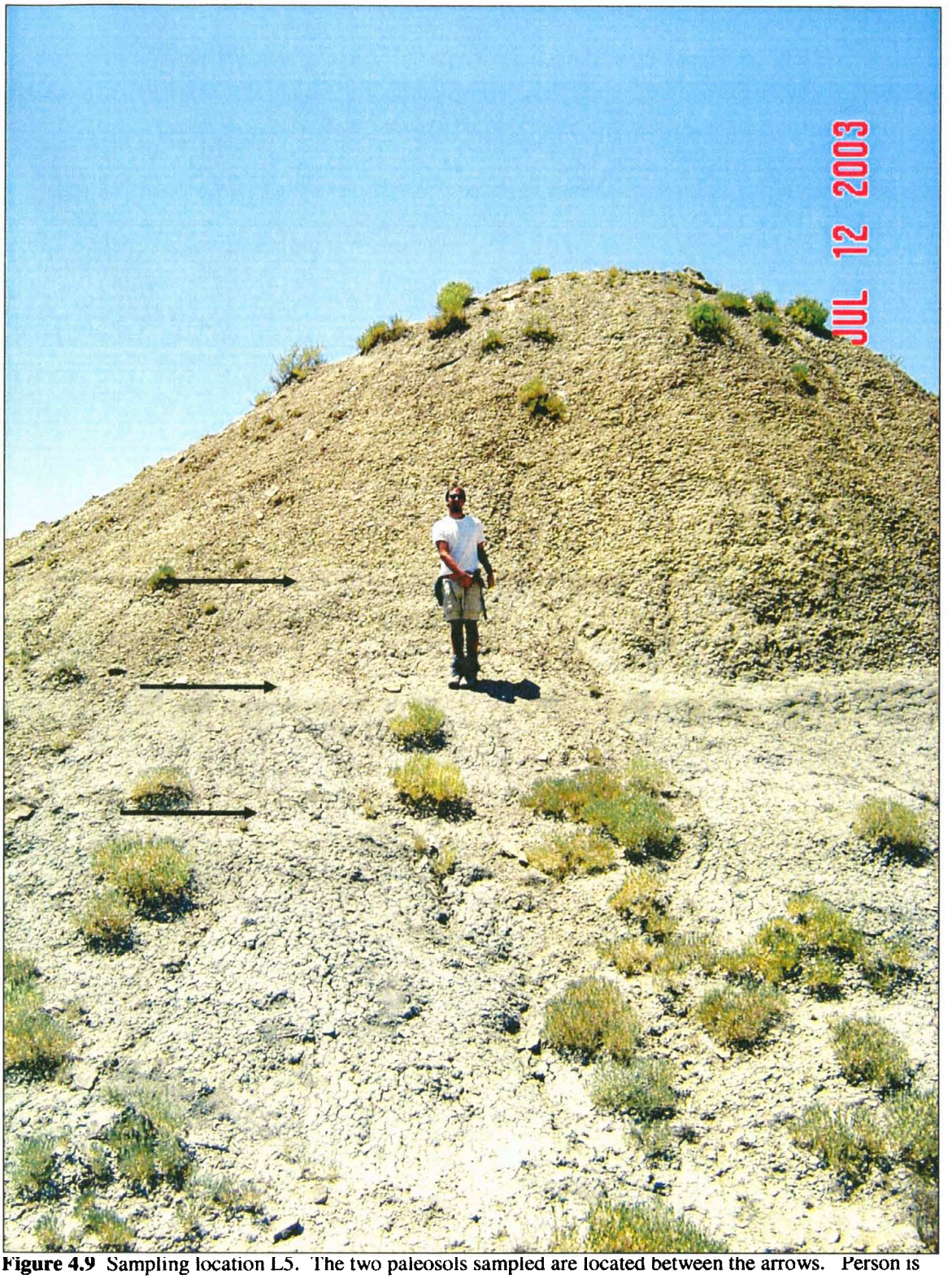

Figure 4.9 Sampling location L5. The two paleosols sampled are located between the arrows. Person is 1.8 m tall for scale.

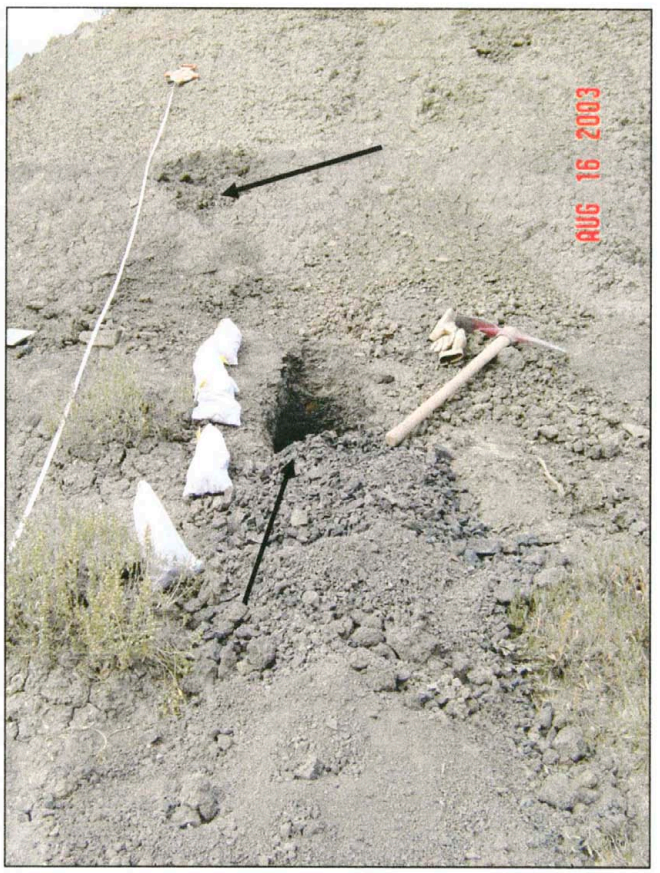

Figure 4.10 Sampling location L5. Arrows indicate some of the sample points for the upper and lower paleosols. Pick is 105 cm long.

Location L6

Location information for sampling point L6 is found in Table 4.8. A total of 11 samples were collected at this location on two separate trips. Only one of the samples was analyzed because the other 10 samples taken from the outcrop were too small in size. It is unclear whether the small size was due to paleosol structure or modern weathering. A return trip to the sample location to attempt to excavate to unweathered material proved unsuccessful, except for one sample.

Table 4.8 Sampling details for location L6

UTM	4382918N	258525E	Elevation	5767 ft.	Trend	253°	Dip	0°	
Sample #	**Strat. Loc. (m)**	**Depth to Sam. (m)**	**Weathered Color**	**Fresh Color**	**Peds**	**Roots**	**Acid**	**Mottling**	**Comments**
L6-11	4.00	1.00	5Y 7/2	5Y 7/2	Y	N	Y	N	

Once the surface of the weathered outcrop was broken and any depth into the outcrop was reached, the material above the proposed sample location, under the weathered material, collapsed preventing any further deepening of the sample location (Figure 4.12). Further removal of the weathered material just repeated the process and no progress could be made.

The weathered outcrop color was yellowish to olive gray, and fresh surfaces exhibited shades of purple, orange, brown, and gray. Mottling was noted in seven of the samples, and gray paleoroot structures (Figure 4.13) were also observed in one of the samples. Four of the samples reacted to acid. Sampling depths ranged from 0.30 to 0.50 m for the first attempt and 1.0 m during the second trip to avoid obviously weathered material.

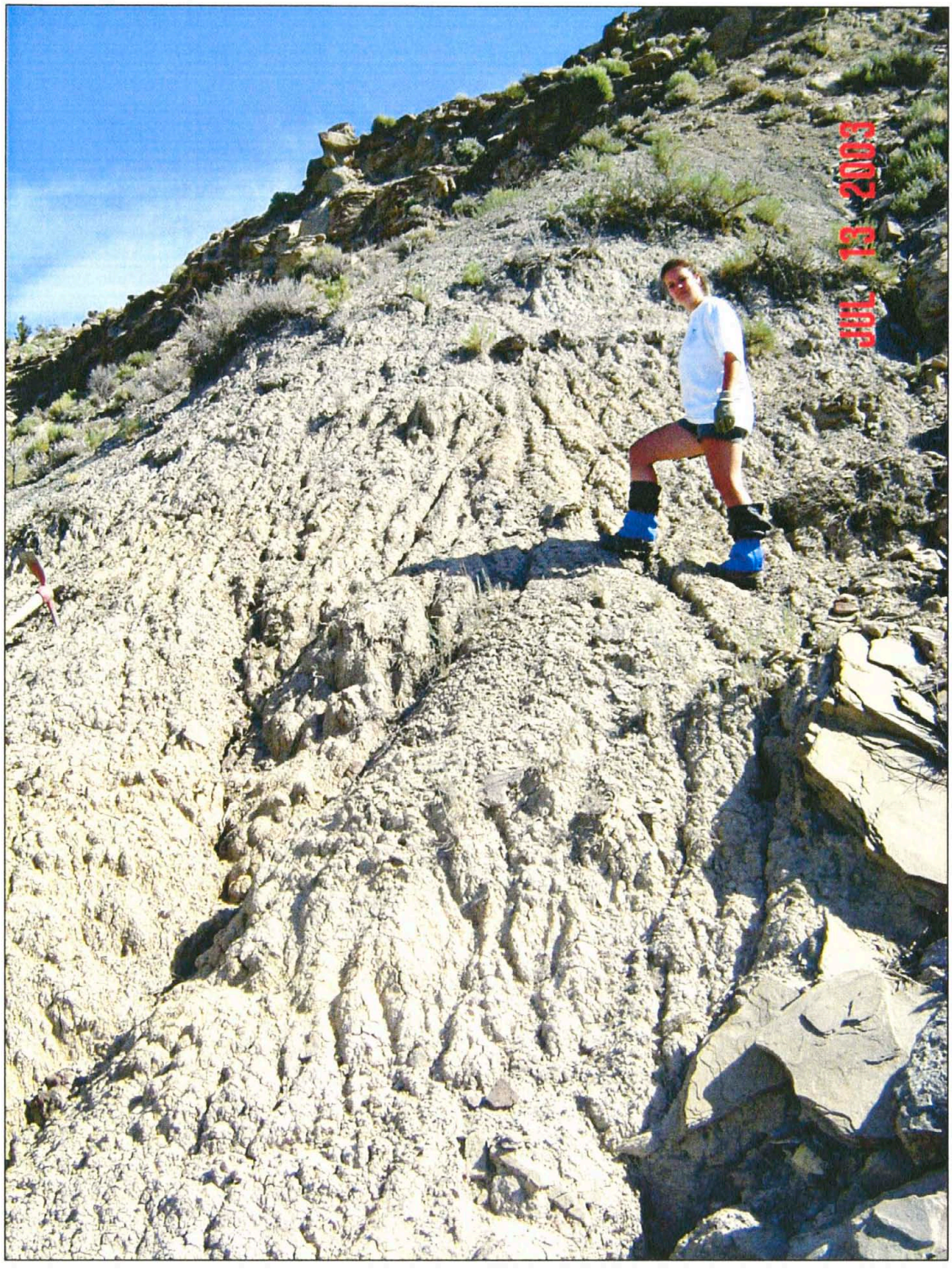

Figure 4.11 Sampling location L6. Person is 1.6 m tall for scale.

Figure 4.12 Sample location U6. Samples were obtained but were unable to be analyzed due to the very small grain size. Notice the caving of underlying material. Pick is 105 cm long.

Figure 4.13 Paleoroot structures observed at location U6 indicated by the arrows. The white marks are from the pick and hammer used to excavate the location. Hammer is 38 cm long.

Location L7

Figure 4.14 Location L7 with samples near sample position.

Location information for sampling point L7 is found in Table 4.9. A total of 13 samples were collected at this location, two of the samples were determined to be shaly sandstones and were not analyzed as seals. The outcrop weathers yellowish gray to reddish brown in color. Fresh surfaces exhibited shades of red, gray, and brown. Eleven

samples had orange colored mottling that was noted in the field. All of the samples, except for the two sandstone samples, exhibited pedogenic structures that were angular in shape and ranged from 3 to 5 cm in diameter. Five of the samples reacted to acid, four samples were noted as having paleoroot structures. Samples were collected at depths of 0.10 to 0.40 m to avoid obviously weathered material.

The clay-rich sandstones at this location exhibited thin, shale laminations. Also, one of the sandstones, sample 13, appears to visually correlate with a shaly sandstone sample from location L3. No analyses, other than thin sections, were completed on the sandstones.

Table 4.9 Sampling details for location L7

UTM	4382738N	258669E	Elevation	5757 ft.	Trend	310°	Dip	0°	
Sample #	**Strat. Loc. (m)**	**Depth to Sam. (m)**	**Weathered Color**	**Fresh Color**	**Peds**	**Roots**	**Acid**	**Mottling**	**Comments**
L7-1	0.50	0.30	5Y 7/2	N4	Y	Y	N	Y	
L7-2	1.00	0.30	5Y 7/2	10R 4/2	Y	N	N	Y	
L7-3	1.70	0.40	5Y 7/2	5YR 5/2	Y	N	N	Y	
L7-4	2.50	0.30	5Y 7/2	5Y 6/1	Y	Y	N	Y	
L7-5	3.00	0.25	5Y 7/2	N6	Y	Y	Y	Y	
L7-6	3.70	0.25	5Y 7/2	5Y 6/1	Y	N	Y	Y	
L7-7	4.30	0.38	5Y 8/1	N6	Y	N	Y	Y	
L7-8	4.60	0.10	10R 4/6	N7	N	N	Y	N	Few laminations, forms ridge
L7-9	7.00	0.40	5Y 7/2	N7	Y	N	N	Y	
L7-10	7.40	0.40	5Y 8/1	N6	Y	N	N	Y	
L7-11	9.40	0.35	5Y 7/2	N7	Y	N	N	Y	
L7-12	9.90	0.40	5Y 8/1	10YR 4/2	Y	Y	N	Y	
L7-13	10.5	0.20	5Y 7/2	5Y 6/1	N	N	Y	N	Laminations, same as L3-3?

Chapter 5. Data Analysis

5.1 Mercury Injection Capillary Pressure Data

Results from Mercury Injection Capillary Pressure (MICP) analysis for the PPL, PPU, and all samples are shown in Table 5.1. Statistically, the PPL and PPU are not significantly different, with a p-value of 0.133, not assuming equal variances. A more detailed table showing the MICP data from all of the individual samples is located in Appendix A. MICP curves are shown in Appendix B.

Table 5.1 Selected MICP for upper and lower paleosols

Paleosol	#of samples	Med. Pore Apr. Dia. (microns)				Closure (psia)				10% Saturation (psia)			
		Min	Max	Avg	Std. Dev.	Min	Max	Avg	Std. Dev	Min	Max	Avg	Std. Dev.
PPL	20	0.017	0.033	0.024	0.0052	275	4184	1977	1070	1967	6722	3916	1549
PPU	60	0.003	0.117	0.040	0.0245	241	6650	2342	1456	467	7667	3282	1734
All Samples	80	0.003	0.117	0.036	0.0224	241	6650	2251	1372	467	7667	3441	1703

The PPL from the Wasatch Formation has 10% mercury saturation pressures that range from 1,967 psia to 6,722 psia, with an average pressure of 3,916 psia, and a standard deviation of 1,549 psia. Of the 20 samples, two groups of ten samples each (locations B1 and B2), one group (B1) had a average 10% mercury saturation of 2,793 psia and standard deviation of 733 psia while the other group's average (B2) was 5,040 psia and standard deviation of 1,314. Most of the lower value 10% saturation values are located in location B1. Figure 5.1 shows the distribution of 10% saturation versus stratigraphic position for locations B1 and B2. Similar patterns are seen in the lower part of the profile when the two sampling locations are compared.

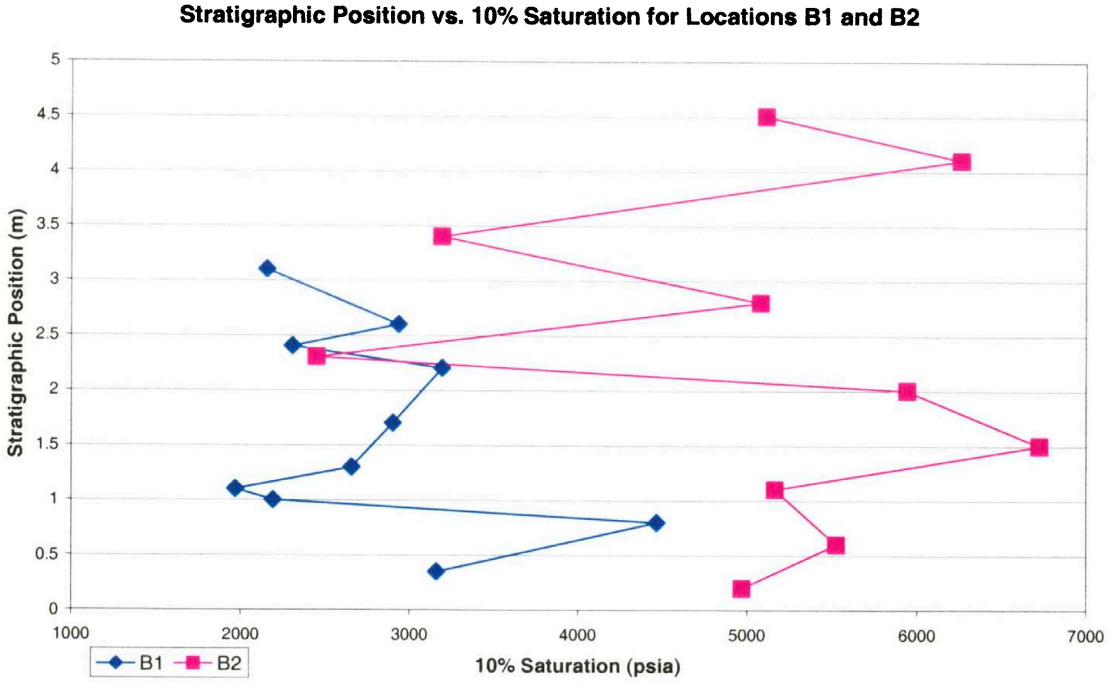

Figure 5.1 Plot of 10% Saturation versus stratigraphic position for sample locations B1 and B2.

The PPL average median pore aperture diameter is 0.024 microns. Location B1 median pore aperture diameter data indicates that the group average is slightly larger, at 0.028 microns, while data from Location B2 shows that group's average is slightly smaller at 0.020 microns. This data supports the fact that lower 10% saturation values have larger pore diameters, which allows the mercury through the system at lower pressures, other factors being equal. Table 5.2 compares the MICP data from each of the sampling locations in the Paleosol Package L.

Table 5.2 Comparison of sample location MICP data from the PPL

Location	# of samples	Average Median Pore Aperture Diameter (microns)	Average 10% Saturation (psia)	Standard Deviation 10% Saturation (psia)
B1	10	0.028	2793	733
B2	10	0.020	5040	1314

Paleosol Package U has 10% mercury saturation pressures that range from 467 psia to 7,667 psia with an average pressure of 3,282 psia, and a standard deviation of 1,734 psia (Figure 5.2). There is a large variation of 10% saturation versus stratigraphic position when all of the locations are compared together.

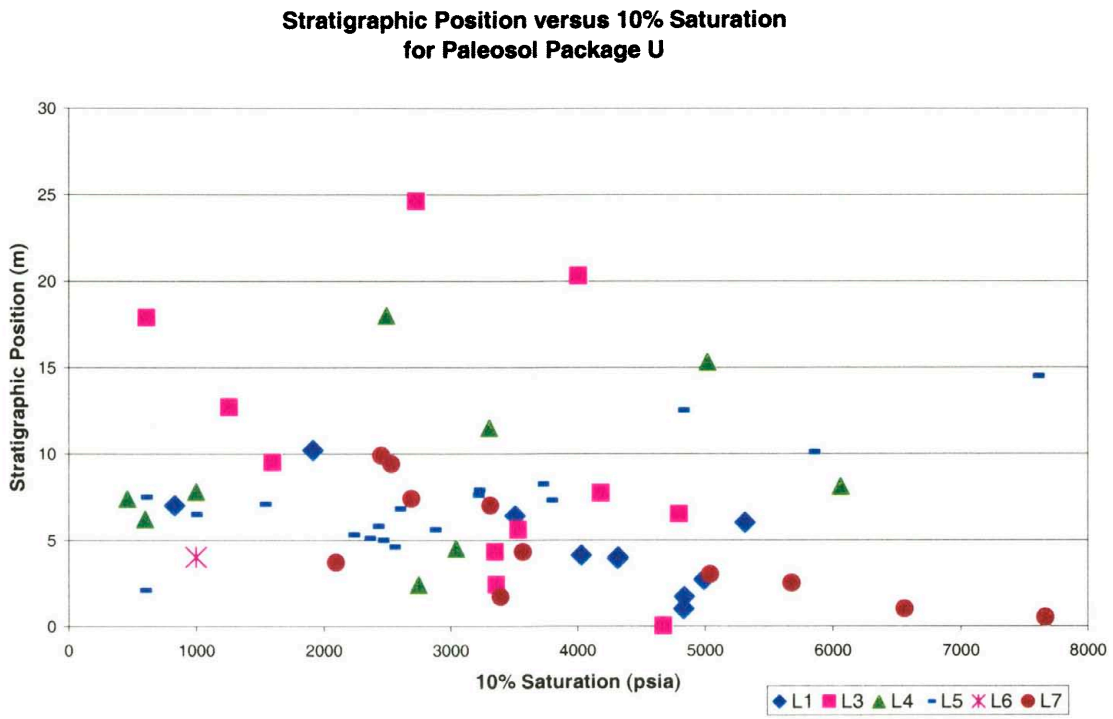

Figure 5.2 Plot of 10% Saturation versus stratigraphic position for PPU sample locations.

A total of 60 samples from 6 different locations (L1, L3, L4, L5, L6, and L7) were collected in the PPU. A suite of samples were collected from two distinct paleosols at Location L5 so that comparisons between two paleosols could be made. The data for the distinct paleosols has also been included in the calculations of overall PPU MICP values. Table 5.3 compares the MICP data from each of the sampling locations in the Paleosol Package U.

Table 5.3 Comparison of sample location MICP data from the PPU

Location	# of samples	Average Median Pore Aperture Diameter (microns)	Average 10% Saturation (psia)	Standard Deviation 10% Saturation (psia)
L7	11	0.027	4094	1863
L1	10	0.031	3895	1446
L3	11	0.034	3105	1402
L4	9	0.047	2754	1921
L5	18	0.050	2944	1775
L6	1	0.086	1003	NA

On the average, locations L1 and L7 had 10% saturation values higher than the average value for the whole PPU. The average pore diameter is negatively related to 10% saturation, meaning as 10% saturation decreases the pore diameter increases. One exception is location L5, which does not follow the relationship. This suggests that there might be some other variable, such as composition or texture, that is controlling the sealing capacity at this location.

Figure 5.3 shows how the sealing capacities vary for each sampling location in both the PPL and PPU. The x-axis is an arbitrary sample location that was assigned to each location so that they could be represented graphically.

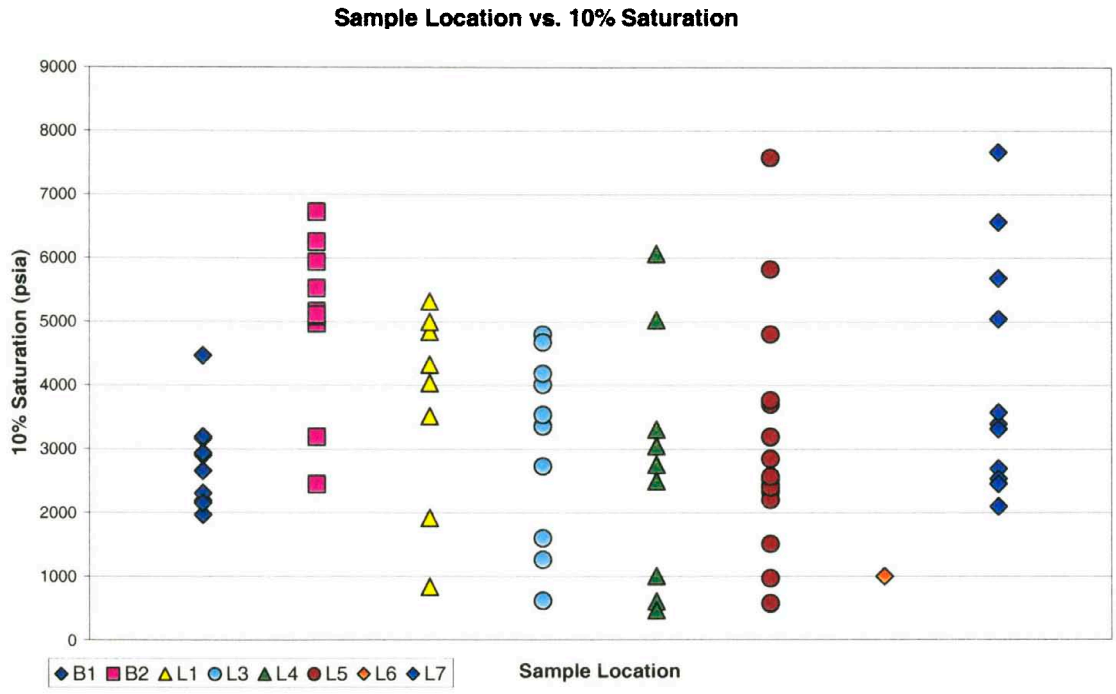

Figure 5.3 Graph of 10% saturation vs. location for both the PPL and PPU.

From Figure 5.3, it is noticeable that there is more variation in sealing capacity within each location than between locations. Location L5 has the highest degree of variability, while Location B1 has the lowest amount of variability.

Location L5 was sampled with a closer sample interval to compare the sealing capacities of two distinct paleosols, A and B, visible in the outcrop. Paleosol A is lower stratigraphically than Paleosol B. The paleosol boundaries were determined by color changes and slope characteristics. Table 5.4 shows some of the MICP data from the two paleosols. Figure 5.4 shows the distribution of 10% saturation values versus the stratigraphic position for each paleosol. All of the MICP data for the paleosols are located in Appendix A.

Table 5.4 Comparison of MICP data from two paleosols at L5

Location	# of samples	Average Median Pore Aperture Diameter (microns)	Average 10% Saturation (psia)	Standard Deviation 10% Saturation (psia)
Paleosol A	5	0.051	2462	245
Paleosol B	6	0.047	2533	1084

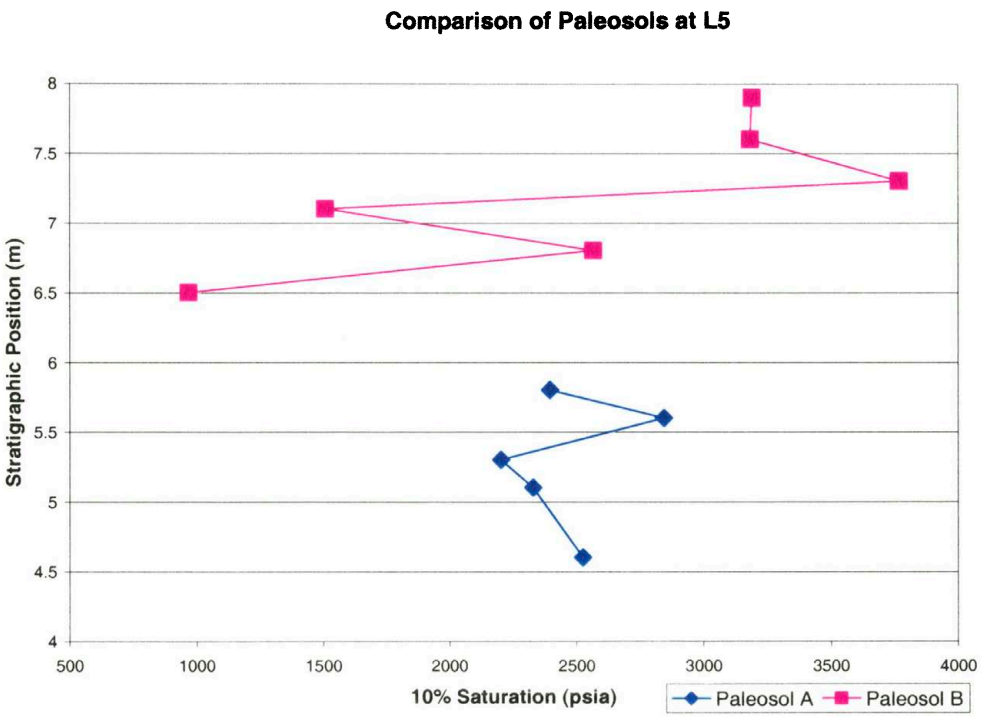

Figure 5.4 10% saturation values versus stratigraphic position for each of the paleosols sampled at Location L5.

MICP data indicates that Paleosol B is the better seal, with an average of 2,533 psia and a standard deviation of 1084 psia. The average pore diameter of Paleosol B is smaller when compared to that of Paleosol A, while Paleosol B has a larger variation of 10% saturation values when compared to Paleosol A.

5.2 Porosity, Permeability and Grain Density Data

Porosity, permeability, and grain density analyses were conducted on each of the samples that were analyzed for MICP test. Table 5.5 contains the porosity and permeability data for the PPL and PPU. Appendix C contains detailed data for each of the samples.

Table 5.5 Sample and MICP porosity, permeability, and grain density data for each paleosol package and all samples.

Wasatch Outcrop Sample #s:		Sample Poro. (%)	MICP Poro. (%)	Sample Air Perm. (md)	MICP Perm. (md)	Sample Grain Den. (g\cc)	Grain Grain Den. (g\cc)
PPL Total n=20	#	**n=20**	**n=80**	**n=9**	**n=80**	**n=20**	**n=80**
	Min	6.1	5.4	0.075	0.001	2.65	2.64
	Max	13.4	9.0	1.445	0.001	2.77	2.70
	Average	10.0	7.4	0.723	0.001	2.70	2.67
	Std Dev	2.1	1.3	0.513	0.000	0.03	0.01
PPU Total n=60	#	**n=57**	**n=80**	**n=20**	**n=80**	**n=57**	**n=80**
	Min	5.1	4.7	0.001	0.000	2.63	2.63
	Max	16.0	11.8	0.188	0.025	2.81	2.72
	Average	11.0	8.7	0.074	0.004	2.71	2.67
	Std Dev	2.3	1.6	0.064	0.005	0.04	0.02
All Samples Total n = 80	#	**n=77**	**n=80**	**n=29**	**n=80**	**n=77**	**n=80**
	Min	5.1	4.7	0.001	0.000	2.63	2.63
	Max	16.0	11.8	1.445	0.025	2.81	2.72
	Average	10.7	8.4	0.282	0.003	2.70	2.67
	Std Dev	2.2	1.6	0.419	0.005	0.03	0.02

All 20 of the samples from the PPL and 57 of the 60 samples from the PPU were tested for porosity using the plug method. Porosity data calculated from MICP data were collected from all 80 samples. Three samples from the PPU were unable to be tested due to the size of the sample provided to the lab. The porosity data show that the PPL has a lower average porosity of 10.0% compared to the PPU porosity average of 11.0 % using the measured porosity data. The averages are slightly lower when using the MICP

calculated data, 7.4% and 8.7% respectively. All of the samples compared together have an average porosity value of 10.7% or 8.4% depending on the data set used.

The permeability data indicate that the PPU has lower permeability when compared to the PPL (0.074 md and 0.723 md, respectively using measured data). The MICP calculated data indicates that the PPL has lower permeability when compared to the PPU (0.001 md and 0.004 md, respectively). The average for all of the samples is 0.282 md (measured) and 0.003 md (calculated). Only 9 of 20 samples from the PPL and 20 of the 60 samples from the PPU were able to be analyzed using the plug method of permeability analysis. All 80 samples were calculated from the MICP data. Of the 20 samples for the PPU, one sample had a permeability value of 22.7 md, which is much higher than the values seen for the rest of the samples. It is clear that this value does not measure the true permeability of the sample, so it has been removed from the data set. The grain densities for both paleosol packages are similar, with the PPL having an average grain density of 2.70 g/cc compared to 2.71 g/cc for the PPU, and all sample grain density average of 2.70 g/cc from measured data. The average for all 3 groups was 2.67 g/cc using the calculated data. All but 3 samples were tested for measured grain density.

5.3 Geochemical Data

Total Organic Carbon

All of the paleosol samples from the Wasatch Formation were analyzed for total organic carbon (TOC). TOC data for both paleosol packages are presented in Table 5.6. Detailed TOC data for each sample is located in Appendix D.

Table 5.6 TOC for samples from both paleosol packages

Paleosol Package		PPL Totals n=20	PPU Totals n=58	All Samples n=78
Total Organic Carbon (%)	Min	0.02	0.09	0.02
	Max	0.27	0.74	0.74
	Average	0.11	0.37	0.30
	Std Dev	0.08	0.18	0.19

Total organic carbon ranges for the PPL are 0.02% to 0.27% with an average of 0.11% and a standard deviation of 0.08%. The PPU TOC minimum and maximum values are 0.09% and 0.74%, respectively, and an average of 0.36% with a standard deviation of 0.18%. Data suggest that, on the average, the PPU has a higher percentage of total organic carbon, although the values are not significantly different from the total sample averages. Figure 5.5 shows how the percentage of total organic carbon changes with respect to stratigraphic position for the PPL locations. In location B1, the TOC percentage decreases until 1.25m, then increases until 3.1 m. The behavior of the TOC percentages is quite different at B2, where TOC increases to 2.75 m, and then decreases to 4.5 m.

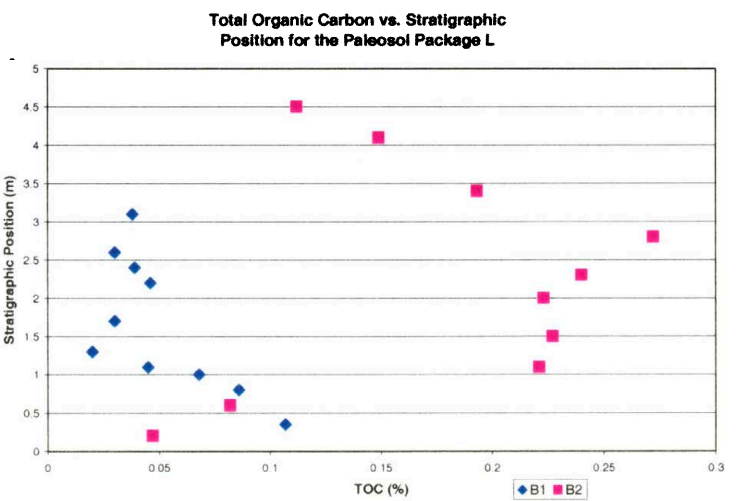

Figure 5.5 Distribution of total organic carbon by percentage in relation to stratigraphic position.

Figure 5.6 shows how the sealing capacity for each sample varies in relation to the percentage of total organic carbon that is present. In general, as sealing capacity increases, the amount of total organic carbon increases.

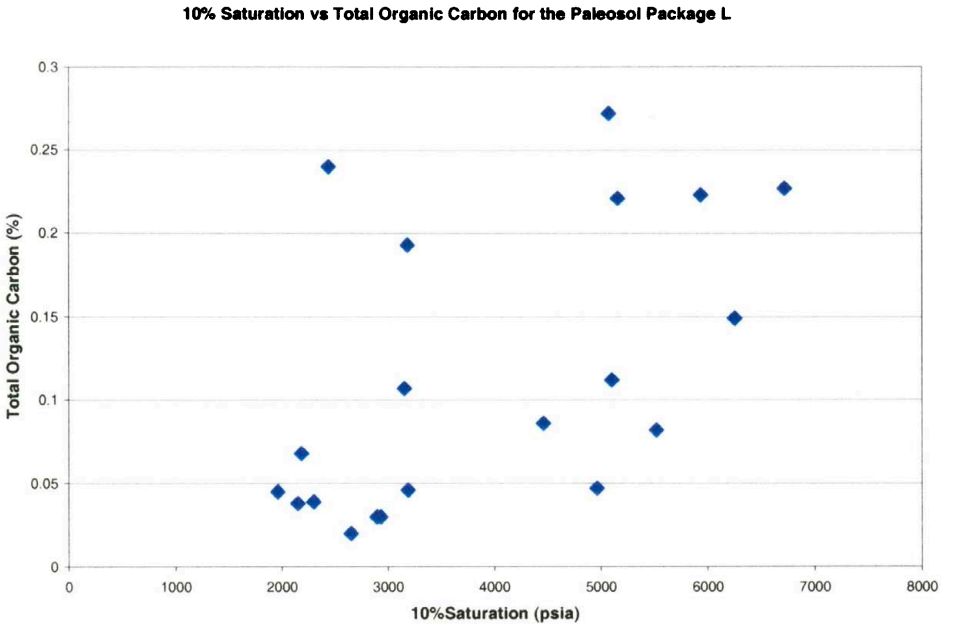

Figure 5.6 Relationship of 10% saturation versus total organic carbon for the PPL.

Figure 5.7 shows how the amount of total organic carbon varies by stratigraphic position for the upper paleosols. All of the sample locations show some degree of variability in TOC percentages, with locations L3, L4, and L5 exhibiting the highest degree of variability. Figure 5.8 indicates how the sealing capacity varies with total organic carbon percentages for the PPU. In general, as sealing capacity increases, the amount of total organic carbon decreases, and the variability of TOC decreases. This relationship is different from what is seen in the lower paleosol, where an increase in sealing capacity corresponds with an increase of TOC.

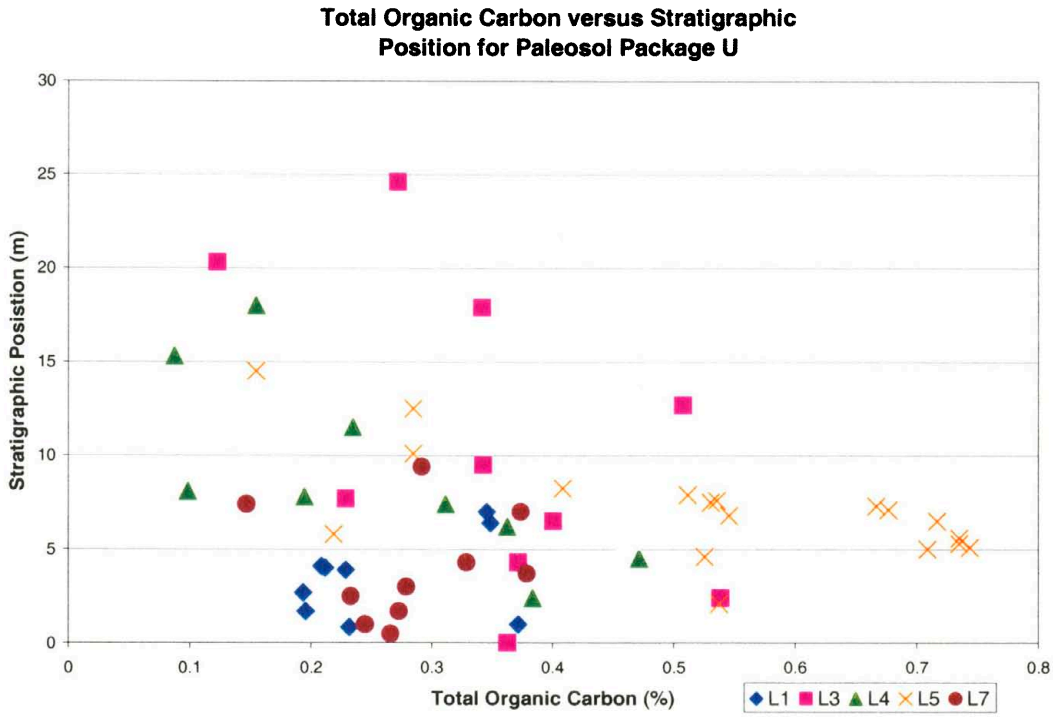

Figure 5.7 Plot of total organic carbon versus stratigraphic position for the PPU.

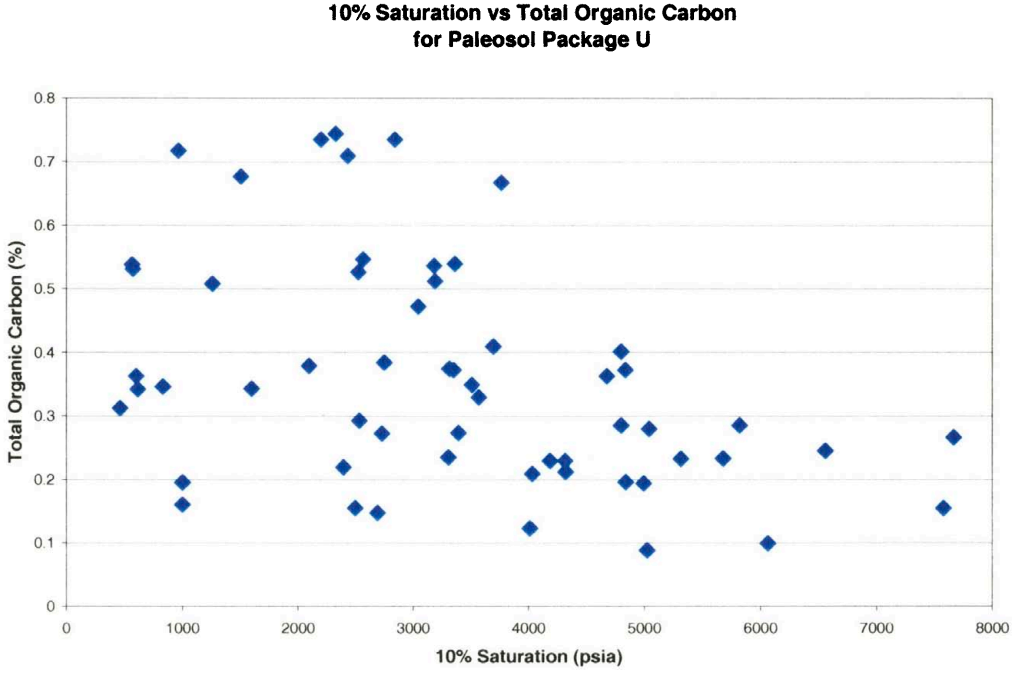

Figure 5.8 Plot of total organic carbon versus 10% saturation for the PPU.

When all of the TOC data is plotted against the sealing capacity (Figure 5.9), the relationship between sealing capacity and percentage of total organic carbon is the same as that for the PPU. As sealing capacity increases, the percentage of total organic carbon decreases, and variability of TOC decreases.

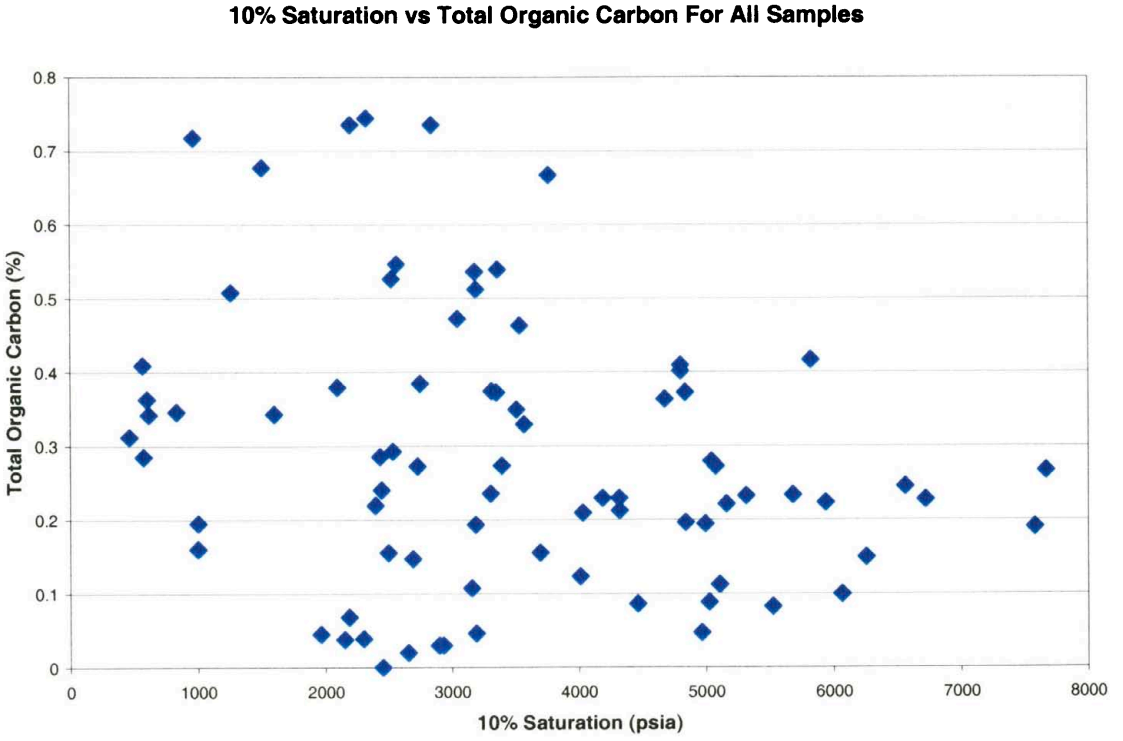

Figure 5.9 Plot of sealing capacity against total organic percentage. The graph indicates that as sealing capacity increases, the TOC percentage decreases, and variability decreases as well.

X-Ray Fluorescence Data

Bulk chemistry data from X-ray fluorescence (XRF) analysis are located in Appendix E, showing major elements measured as % weight oxides and trace elements measured in ppm. Samples were chosen from a range of sealing capacities from each

location. Table 5.7 and 5.8 contain minimums, maximums, averages, and standard deviations for each of the major and trace elements.

Graphs that contain each of the major percentages versus the stratigraphic position for each of the 9 paleosol sampling locations are located in Appendix E. Also in Appendix E are graphs for each of the 9 sampling locations for the trace elemental concentrations versus stratigraphic position.

The XRF data for the PPL and PPU are similar, with not much variation between the concentrations measured for either major or trace elements. The averages for all of the samples combined are not significantly different when compared to the averages for each of the individual paleosol packages. Further evaluation of XRF data has been included in section 5.6 of this chapter.

5.4 Petrographic Data

Results from petrographic analysis of all the Wasatch samples collected are present in Appendix F. This includes composition, grain size and roundness, and degree of bioturbation. Point count analysis (Table 5.9) reveals that the samples from the PPL have an average quartz grain size of 4.8 phi and are, on average, composed of quartz (13%), feldspar (5%), muscovite (<1%), organic matter (2%), and a total average grain percentage of 21%. The average amount of matrix in the PPL is 72%, the average cement is 7%. Pores make up less than 1% of the composition of the samples in this paleosol package. Samples from the PPU consist of, on the average, quartz (13%), feldspar (5%), muscovite (<1%), organic matter (3%), and a total average grain percentage of 21%. The average amount of matrix in the PPU samples is 63%, the average cement is 16%. Pores make up less than 1% of the lower paleosol composition

and the average quartz grain size is 5.2 phi. Compositionally, the two paleosol packages are very similar, with minor differences in the average matrix and cement.

All paleosol sample data together indicate that the overall average quartz grain size is 5.1 phi and the samples are, on average, composed of quartz (13%), feldspar (5%), muscovite (<1%), organic matter (2%), and a total average grain percentage of 21%. The average amount of matrix in all of the samples is 66%, the average cement is 13%. Pore space makes up <1% of the average composition of all of the paleosol samples collected.

The sandstones sampled in the field area have an average grain size of 3.4 phi and consist of quartz (35%), feldspar (9%), micas (<1%), organics (1%), with total average grains of 46%. Only about a quarter of the average sandstone composition was matrix (26%), the average cement was 28%. Based on these percentages and using the classification of Dott from 1964, the sandstones are classified as arkosic wackes.

The point count data shows that when all of the paleosol data are compared to the sandstone data, the paleosols have fewer quartz grains, more matrix in the overall composition of the rocks, and a smaller percentage of cement. The sandstones have a lesser content of organic matter relative to the paleosols.

5.5 Facies Distribution

Within the paleosols, a variety of textural and compositional features are present. For ease of description and interpretation the samples have been categorized into two separate classes of facies. These two classes are lithofacies from outcrop samples and microfacies determined from thin sections.

Table 5.7 Summary of major elemental data (weight % oxides) from XRF analysis

Paleosol Package	Wt. % oxide	SiO_2	Al_2O_3	CaO	MgO	Na_2O	K_2O	Fe_2O_3	MnO	TiO_2	P_2O_5	Cr_2O_3	LOI
	Det. Lim.	**0.01**	**0.01**	**0.01**	**0.01**	**0.01**	**0.01**	**0.01**	**0.01**	**0.01**	**0.01**	**0.01**	**0.01**
PPL n = 15	Min	61.14	12.85	0.14	1.00	0.62	2.30	4.20	0.01	0.54	0.05	0.01	3.80
	Max	74.59	19.22	2.42	1.95	0.93	3.17	6.82	0.06	0.68	0.26	0.02	7.50
	Average	65.96	16.42	1.02	1.56	0.71	2.77	5.37	0.02	0.64	0.15	0.01	5.47
	Std Dev	4.70	2.13	0.84	0.35	0.08	0.31	0.78	0.01	0.05	0.07	0.01	1.13
PPU n = 42	Min	48.21	8.11	0.19	1.24	0.46	1.54	1.68	0.02	0.37	0.07	0.01	4.30
	Max	70.91	18.42	18.85	3.89	1.14	3.44	7.79	1.47	0.79	0.45	0.02	16.90
	Average	60.79	16.12	3.58	2.30	0.81	2.93	5.13	0.07	0.66	0.20	0.01	7.49
	Std Dev	4.15	2.04	2.69	0.44	0.15	0.36	1.16	0.22	0.07	0.08	0.00	1.84
All Samples n = 57	Min	48.21	8.11	0.14	1.00	0.46	1.54	1.68	0.01	0.37	0.05	0.01	3.80
	Max	74.59	19.22	18.85	3.89	1.14	3.44	7.79	1.47	0.79	0.45	0.02	16.90
	Average	62.15	16.20	2.90	2.11	0.78	2.89	5.19	0.06	0.66	0.19	0.01	6.96
	Std Dev	4.84	2.05	2.60	0.53	0.14	0.35	1.07	0.19	0.06	0.08	0.00	1.90

Table 5.8 Summary of trace elemental data (ppm) from XRF analysis

Paleosol Package	ppm	Rb	Sr	Y	Zr	Nb	Ba
	Det. Lim.	**2**	**2**	**2**	**2**	**2**	**20**
PPL n = 15	Min	114	78	30	162	15	354
	Max	177	120	130	277	19	428
	Average	143	100	52	200	17	390
	Std Dev	19	13	23	41	1	19
PPU n = 42	Min	67	87	34	111	8	251
	Max	161	166	87	286	18	668
	Average	135	129	52	184	16	410
	Std Dev	19	20	9	38	2	58
All Samples n = 57	Min	67	78	30	111	8	251
	Max	177	166	130	286	19	668
	Average	137	121	52	188	16	405
	Std Dev	19	23	14	39	2	51

Table 5.9 Point count data for the PPL, PPU, and sandstones from the Wasatch Formation. All grains, matrix, cement, and pore data is in percentages. Bioturbation and roundness numbers are qualitative and the key to the numbers can be found in section 3.4 of this paper or in Appendix F. Grain size data is in phi units.

		GRAINS							MATRIX			CEMENT						Grain Size			
		Quartz	Feld.	Musc.	Rk Frags	Org.	Other grains	TOTAL GRAINS	Fe	Gray	TOTAL MATRIX	All Carb.	Clay	Sid.	TOTAL CEMENT	PORES	Biotur	Grain Size (phi)	Std Dev (phi)	Round. (Qual)	Std Dev
PPL n = 20	Min	3	0	0	0	0	0	8	14	25	55	0	1	0	1	0	3	3.5	0.5	2	0.6
	Max	32	10	2	0	6	1	37	64	54	91	14	8	2	20	2	5	6.2	1.0	3	1.1
	Average	13	5	0	0	2	1	21	35	37	72	1	5	0	7	0	4	4.8	0.7	3	0.8
	Std Dev	9	3	1	0	2	0	9	13	10	10	3	2	1	4	1	1	0.9	0.1	0	0.2
PPU n = 60	Min	2	0	0	0	0	0	6	0	0	4	0	0	0	2	0	1	3.0	0.3	2	0.4
	Max	54	16	1	1	8	2	60	86	63	87	29	16	18	48	6	6	6.3	0.9	3	1.4
	Average	13	5	0	0	3	1	21	33	30	63	6	7	3	16	0	4	5.2	0.6	3	0.7
	Std Dev	12	3	0	0	1	1	14	19	17	19	6	4	4	9	1	1	0.8	0.1	0	0.2
All Paleosol Samples n = 80	Min	2	0	0	0	0	0	6	0	0	4	0	0	0	1	0	1	3.0	0.3	2	0.4
	Max	54	16	2	1	8	2	60	86	63	91	29	16	18	48	6	6	6.3	1.0	3	1.4
	Average	13	5	0	0	2	1	21	34	32	66	5	7	2	13	0	4	5.1	0.6	3	0.7
	Std Dev	11	3	0	0	1	1	13	18	16	18	6	4	4	9	1	0	0.8	0.1	0	0.2
Sandstone Samples n = 5	Min	10	2	0	0	0	0	22	0	3	12	11	0	0	24	0	0	2.7	0.5	3	0.6
	Max	57	14	1	2	2	1	63	50	13	54	16	13	15	34	0	3	4.0	0.6	3	1.3
	Average	35	9	0	1	1	1	46	17	9	26	14	4	11	28	0	2	3.4	0.5	3	1.0
	Std Dev	17	5	0	1	1	1	15	20	4	17	2	5	6	4	0	2	0.5	0.1	0	0.3

The samples were initially divided into 6 lithofacies (Table 5.10). The six lithofacies are, in the order of decreasing sealing capacity, 2.) gray to purple rooted siltstone with minor purple and brown mottling; 4.) gray, calcareous, rooted siltstone with brown and purple mottling; 3.) gray, calcareous, siltstone with brown and purple mottling; 1.) gray siltstone with brown mottling; 5.) gray siltstone with white, calcareous nodules and brown and purple mottling; and 6.)gray, thinly bedded, calcareous shaly sandstone. The sandstone lithofacies was not analyzed as a seal. These lithofacies generally do not occupy either the PPL or the PPU, but are found in both packages at different sampling locations. For example, Lithofacies 1 is not found only at location B1, but also at B2, L1, L3, L4, L5, and L7. The one exception to this is the gray siltstone with white, calcareous nodules and brown and purple mottling lithofacies. This lithofacies occurs only in the PPU and is found at two sampling locations L1 and L3.

Once average quartz grain size data from thin sections was collected, the samples were divided into microfacies depending on the average quartz grain size. Five different microfacies (Table 5.11) were determined and are listed in decreasing quartz grain size: Arkosic Wackes with fine, sand sized quartz grains (not analyzed as a seal); siltstone with very fine, sand sized quartz grains; siltstone with coarse, silt sized quartz grains; siltstone with medium, silt sized quartz grains; and siltstone with fine, silt sized quartz grains. Locations from both the PPU and PPL span the range of microfacies with the exception of the facies not analyzed as a seal. This microfacies is found only in the PPU sampling locations.

Table 5.10 Lithofacies in decreasing sealing capacity. Porosity, 10%saturation, and all compositional data are in percentages. Permeability is in md, pore diameter is in microns, grain size is in phi units and bioturbation is qualitative.

Facies		Porosity	Perm.	Pore Diameter	10% Sat	Grain Size	Std Dev	TOC	Quartz	Feldspar	Muscovite	Organics	Total Matrix	Total Cement	Pores	Bioturbation
2. Gray to purple rooted siltstone with minor brown and purple mottling (n=12)	Min	5.41	22.700	0.017	1967	4.1	0.4	0.02	4	3	0	0	60	3	0	3
	Max	11.80	22.700	0.044	7667	6.1	0.9	0.55	24	10	2	4	84	20	2	5
	Avg	7.64	22.700	0.026	4181	4.8	0.6	0.16	12	6	0	1	69	10	0	4
	Std. Dev	1.63	NA	0.008	2011	0.7	0.2	0.15	7	2	1	1	7	6	1	1
4. Gray calcareous rooted siltstone with brown and purple mottling (n=12)	Min	5.63	0.001	0.017	618	3.0	0.4	0.04	3	0	0	1	14	3	0	2
	Max	10.00	1.445	0.059	6257	6.1	0.9	0.68	51	7	1	7	87	30	2	5
	Avg	8.26	0.496	0.030	3734	4.9	0.6	0.25	17	4	0	3	63	12	0	4
	Std. Dev	1.27	0.654	0.015	1819	1.1	0.1	0.22	16	2	0	2	26	10	1	1
3. Gray calcareous siltstone with brown and purple mottling (n=21)	Min	4.95	0.001	0.017	579	4.0	0.4	0.16	2	2	0	0	4	6	0	1
	Max	10.70	1.185	0.112	6722	6.2	0.9	0.72	49	10	1	7	80	48	1	5
	Average	8.74	0.287	0.039	3356	5.5	0.6	0.34	11	5	0	2	63	18	0	4
	Std. Dev	1.24	0.394	0.025	1567	0.6	0.1	0.15	11	2	0	2	19	11	0	1
1. Gray siltstone with brown mottling (n=31)	Min	4.69	0.001	0.003	467	3.5	0.3	0.03	2	0	0	0	9	1	0	2
	Max	11.80	1.083	0.117	6563	6.3	1.0	0.74	44	16	1	6	91	32	2	5
	Avg	8.46	0.188	0.040	3153	5.0	0.6	0.33	14	5	0	3	66	12	0	4
	Std. Dev	1.90	0.295	0.027	1648	0.8	0.1	0.21	11	3	0	1	17	7	1	1
5. Gray siltstone with white calcareous nodules and brown and purple mottling (n=4)	Min	6.36	NS	0.026	1263	4.4	0.5	0.23	2	2	0	2	72	5	0	6
	Max	9.72	NS	0.041	4679	5.4	0.7	0.51	8	4	0	3	86	14	6	6
	Avg	7.95	NS	0.031	3013	4.9	0.6	0.37	6	3	0	3	76	10	2	6
	Std. Dev	1.60		0.007	1675	0.4	0.1	0.14	3	1	0	0	7	4	3	0
6. Gray thinnly bedded calcareous clayey sandstone (n=5)	Min	NA	NA	NA	NA	2.7	0.5	NA	10	2	0	0	12	24	0	0
	Max	NA	NA	NA	NA	4.0	0.6	NA	57	14	1	2	54	34	0	3
	Avg	NA	NA	NA	NA	3.4	0.5	NA	34	8	0	1	26	28	0	2
	Std. Dev	NA	NA	NA	NA	0.5	0.1	NA	17	5	0	1	17	4	0	2

Table 5.11 Microfacies evaluated as seals listed in decreasing quartz grain size. Microfacies not evaluated as seal at bottom of table. Porosity, 10%saturation, and all compositional data are in percentages. Permeability is in md, pore diameter is in microns, grain size is in phi units and bioturbation is qualitative.

Microfacies		Porosity	Permeability	Pore Diameter	10 %Saturation	Grain Size	Std Dev	TOC	Quartz	Feldspar	Muscovite	Organics	Total Matrix	Total Cement	Pores	Bioturbation
1.Siltstone with very fine sand size qtz. grains (n=6)	Min	5.63	0.052	0.02	1510	3.0	0.52	0.03	3	2	0	1	17	3	0	3
	Max	10.00	1.445	0.06	5525	4.0	0.90	0.68	53	6	0	2	82	26	2	5
	Average	7.52	0.478	0.03	2913	3.5	0.67	0.22	24	4	0	2	60	9	1	4
	Std. Dev	1.98	0.620	0.01	1397	0.3	0.13	0.28	17	1	0	0	23	9	1	1
2.Siltstone with coarse silt size qtz. grains (n=30)	Min	4.69	0.001	0.00	467	4.0	0.31	0.02	4	0	0	0	9	3	0	2
	Max	11.80	0.181	0.12	7578	5.0	1.02	0.54	47	16	2	8	84	48	2	6
	Average	7.56	0.067	0.04	2905	4.5	0.61	0.23	18	7	0	2	58	15	0	4
	Std. Dev	1.64	0.061	0.03	1855	0.3	0.16	0.16	11	3	0	2	19	11	0	1
3.Siltstone with medium silt size qtz. grains (n=35)	Min	6.36	0.001	0.02	837	5.0	0.41	0.11	2	0	0	0	4	1	0	1
	Max	11.80	1.216	0.08	6722	6.0	0.87	0.74	49	8	1	6	91	37	6	6
	Average	9.01	0.234	0.03	3720	5.6	0.59	0.37	8	4	0	3	71	13	0	4
	Std. Dev	1.28	0.341	0.02	1509	0.3	0.11	0.18	8	2	0	1	15	8	1	1
4.Siltstone with fine silt size qtz. grains (n=9)	Min	8.16	0.040	0.02	2332	6.0	0.47	0.19	3	2	0	1	68	4	0	3
	Max	11.60	22.700	0.06	7667	6.3	0.82	0.74	9	6	1	6	87	21	1	5
	Average	9.02	6.117	0.03	4492	6.1	0.57	0.32	5	3	0	3	76	13	0	4
	Std. Dev	1.13	11.065	0.01	1540	0.1	0.11	0.19	2	1	0	2	7	6	0	1
5.Sandstone with fine sand (n=5)	Min	NA	NA	NA	NA	2.7	0.46	NA	10	2	0	0	12	24	0	0
	Max	NA	NA	NA	NA	4.0	0.61	NA	57	14	1	2	54	34	0	3
	Average	NA	NA	NA	NA	3.4	0.52	NA	34	8	0	1	26	28	0	2
	Std. Dev	NA	NA	NA	NA	0.5	0.06	NA	17	5	0	1	17	4	0	2

Lithofacies 1 –Gray Siltstone with Brown and Purple Mottling

These 31 siltstone samples occur at every sampling location in both the PPL and PPU with the exception of location L2, where only one sandstone sample was obtained, and Location L6, where only one sample was also obtained. Average quartz grain size is 5.0 phi, which is coarse to medium sized silt (5.0 phi is the boundary) and average quartz grain roundness is 3 (using the qualitative scale for estimating roundness), which is subrounded.

Lithofacies 1 shows a wide range of compositions, but averages 14% quartz, 5% feldspar, 3% organics and 66% matrix (Table 5.10). Matrix is a significant component of these rocks making up more than half of their total percentage, cement makes up another 13% of the composition. On the average, over 75% of the composition is matrix and cement. Bioturbation ranges from 2 to 5 on the qualitative scale, with an average of 4. This value indicates that 60-90% of the original bedding has been disturbed (Pemberton et al, 1992). Total organic carbon ranges from 0.03 – 0.74 %, with an average of 0.33% which is one of the higher average values of TOC from this data set.

Lithofacies 1 has an average sealing capacity of 3153 psia, with a range of 467 to 6563 psia, and a standard deviation of 1648 (Table 5.10). The average MICP calculated porosity is 8.46%, with a range from 4.69 to 11.80%, and a standard deviation of 1.90%. Figures 5.10 and 5.11 contain photomicrographs and MICP curves for a low sealing capacity sample and a high sealing capacity sample from this lithofacies. Figure 5.10d shows that there are three distinct classes for pore throat diameters, while Figure 5.11d shows one or possibly two pore throat classes.

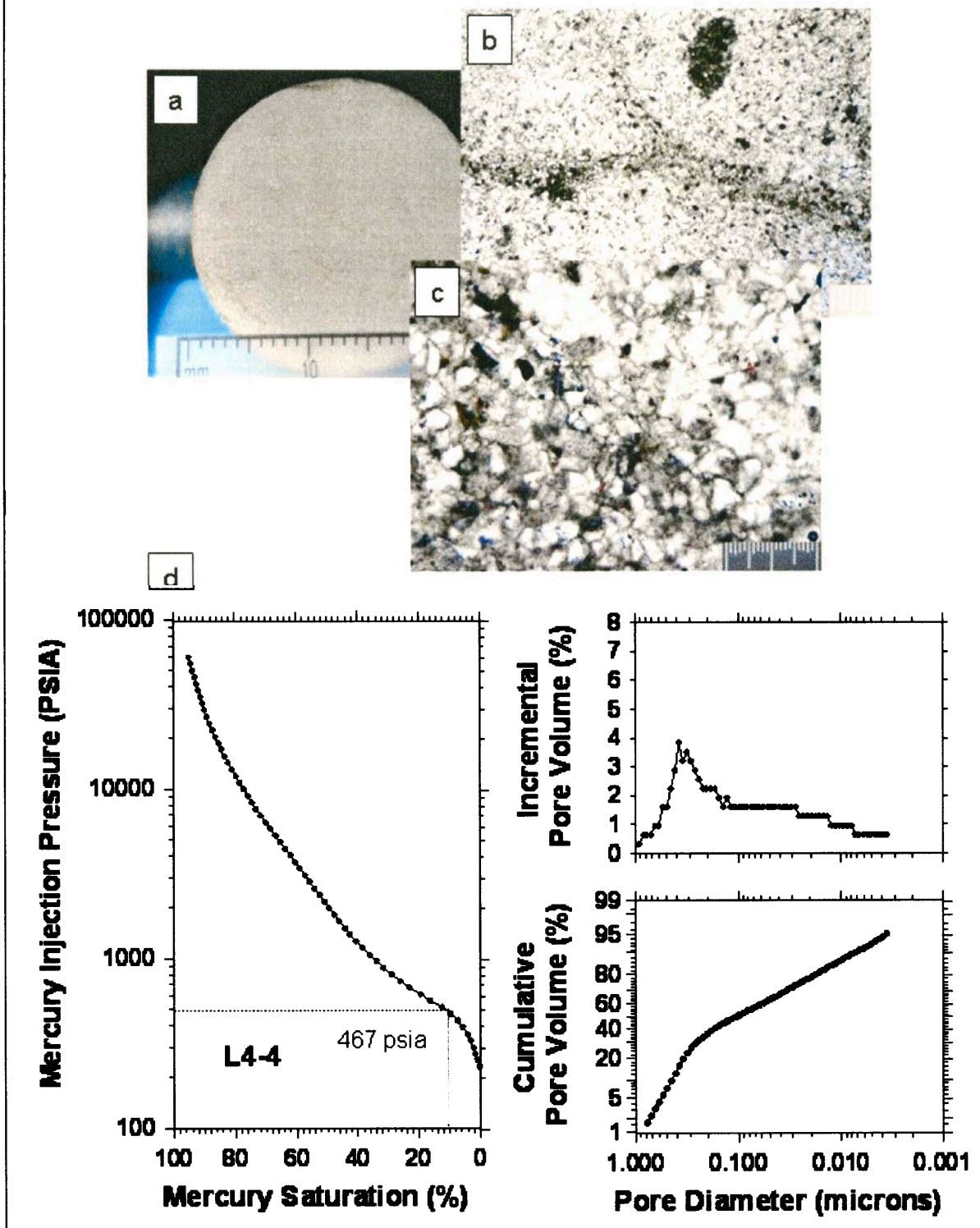

Figure 5.10 Hand sample photograph (a), 1.6X magnification photomicrograph (b), 10X magnification photomicrograph (c), and MICP curves (d) for a low sealing capacity sample for Lithofacies 1. Scale for 1.6X figure is 0.5 mm and 0.2 mm for 10X figure. 10% saturation is 467 psia and there are two modal classes of diameters. (a) courtesy of Poro-Technology.

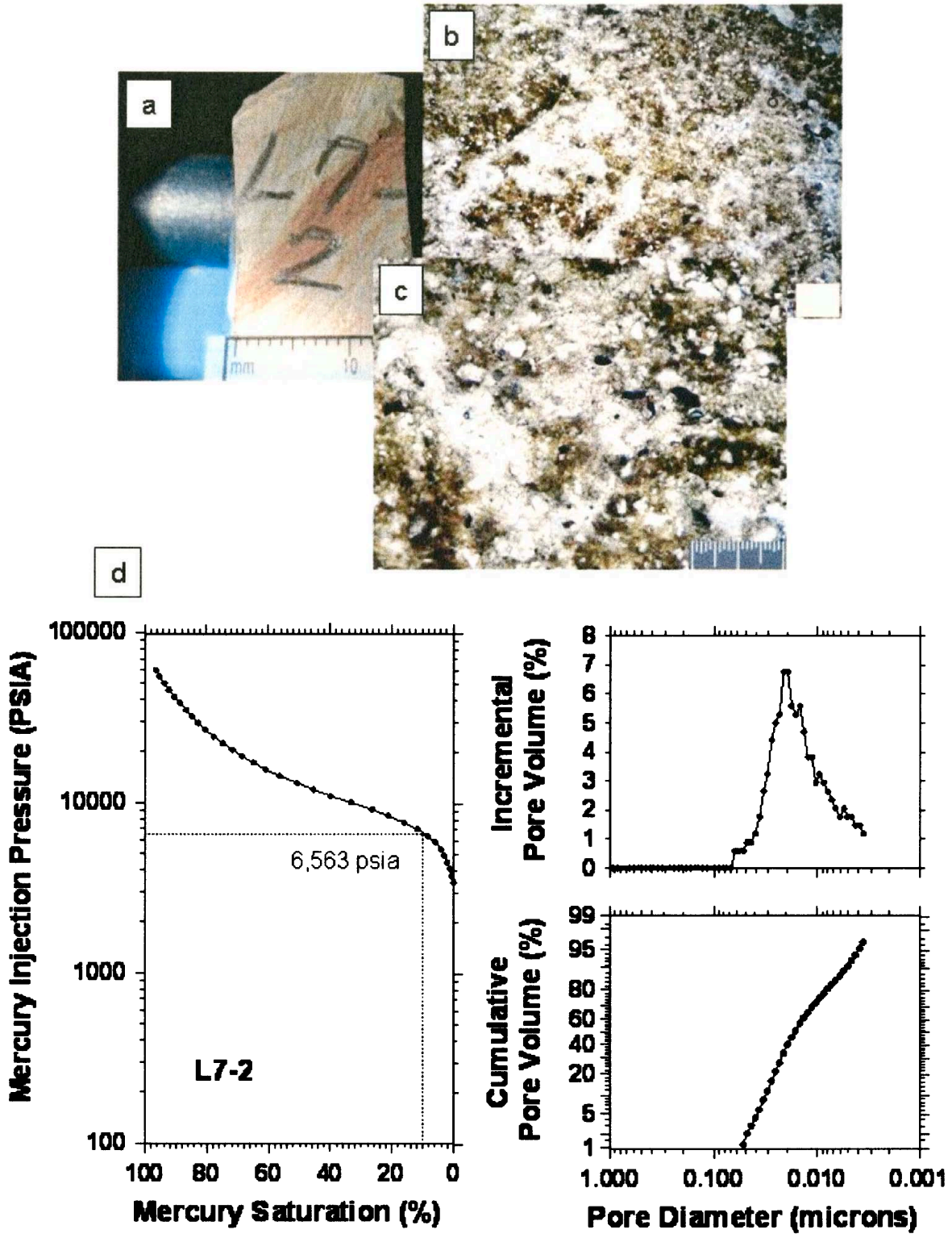

Figure 5.11 Hand sample photograph (a), 1.6X magnification photomicrograph (b), 10X magnification photomicrograph (c), and MICP curves (d) for a high sealing capacity sample for Lithofacies 1. Scale for 1.6X figure is 0.5 mm and 0.2 mm for 10X figure. 10% saturation is 6,563 psia and there are one possibly two modal classes of pore throat diameters. (a) courtesy of Poro-Technology.

Lithofacies 2 –Gray and Purple Rooted Siltstone with Minor Brown and Purple Mottling

These 12 siltstone samples occur at sampling locations B1, L2, L1, L5, and L7. At each location there is not one single stratigraphic position that the facies seems to favor. The average quartz grain size is 4.8 phi, which is coarse silt size. It is near the coarse to medium sized silt boundary of 5.0 phi. The quartz grains measured have an average roundness of 2.8, which is close to the value of 3.0, placing them in the subrounded category using the qualitative scale for estimating roundness.

Lithofacies 2 shows a wide range of compositions, but averages 12% quartz, 6% feldspar, 1% organics, and 69% matrix (Table 5.10). Matrix is a significant component of these rocks. When the cement average (10%) is added to that, almost 80% of the composition is identified. Bioturbation ranges from 3 to 5 on the qualitative scale, with an average of 4. This value indicates that 60-90% of the original bedding has been disturbed (Pemberton et al, 1992). Total organic carbon ranges from 0.02 – 0.55 %, with an average of 0.16%, which is the lowest average value of TOC from the 5 lithofacies analyzed as seals for this project. Lithofacies 2 has an average sealing capacity of 4181 psia, with a range of 1967 to 7667 psia, and a standard deviation of 2011 (Table 5.10). This lithofacies is the best seal of the 5 sealing lithofacies.

The average MICP calculated porosity is 7.64%, with a range from 5.41 to 11.80%, and a standard deviation of 1.63%. This average is the lowest of the facies described here and helps to contribute to the higher sealing capacity by restricting the amount of pore throats thereby restricting fluid migration. Figures 5.12 and 5.13 contain photomicrographs and MICP curves for a low sealing capacity sample and a high sealing

capacity sample from this lithofacies. Both the low and high sealing capacity samples show three classes of pore throats, but the curve for the lower sealing capacity sample (Figure 5.12d) has a larger variation of pore throat diameters.

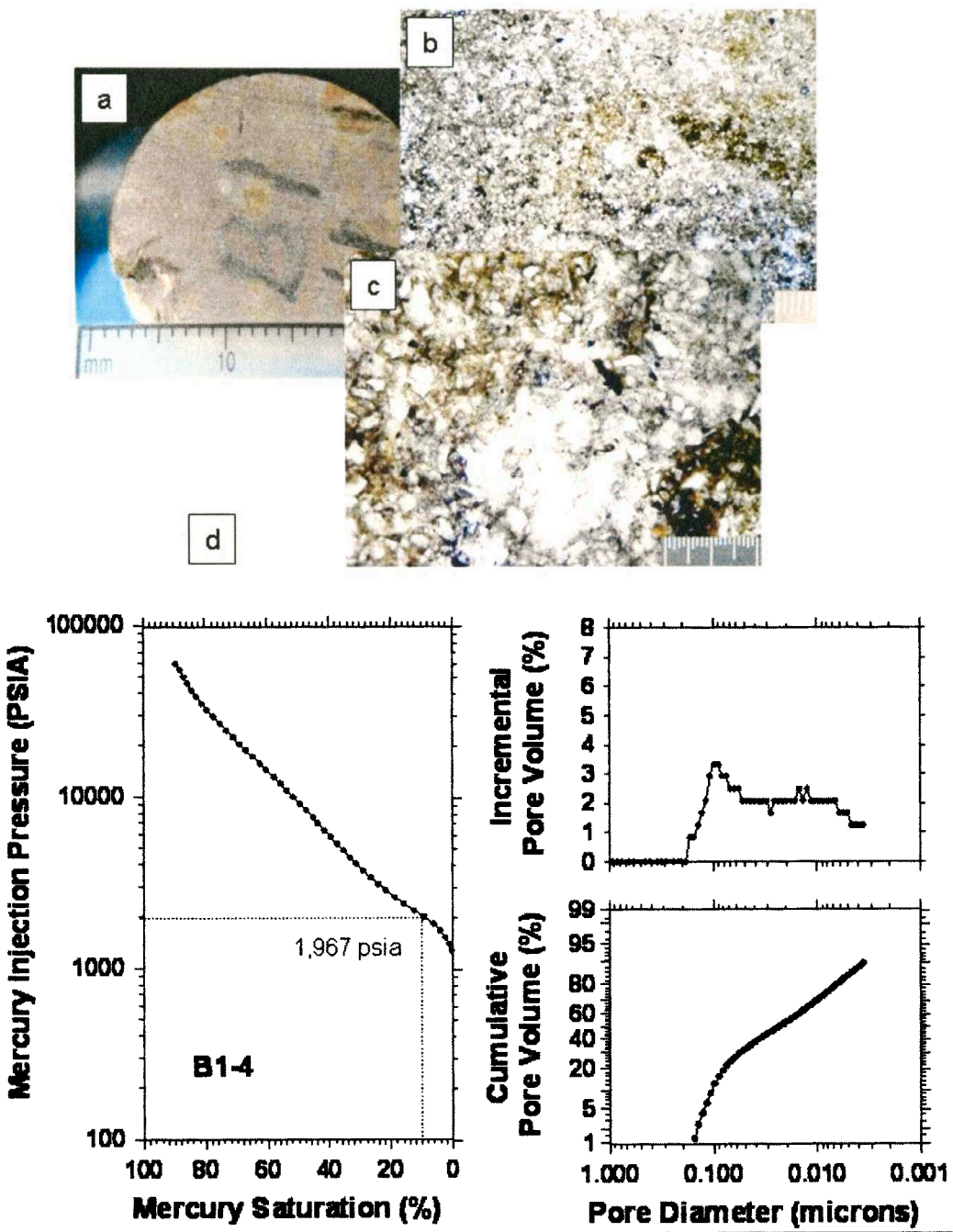

Figure 5.12 Hand sample photograph (a), 1.6X magnification photomicrograph (b), 10X magnification photomicrograph (c), and MICP curves (d) for a low sealing capacity sample for Lithofacies 2. Scale for 1.6X figure is 0.5 mm and 0.2 mm for 10X figure. 10% saturation is 1,967 psia and there are two modal classes of pore throat diameters. (a) courtesy of Poro-Technology.

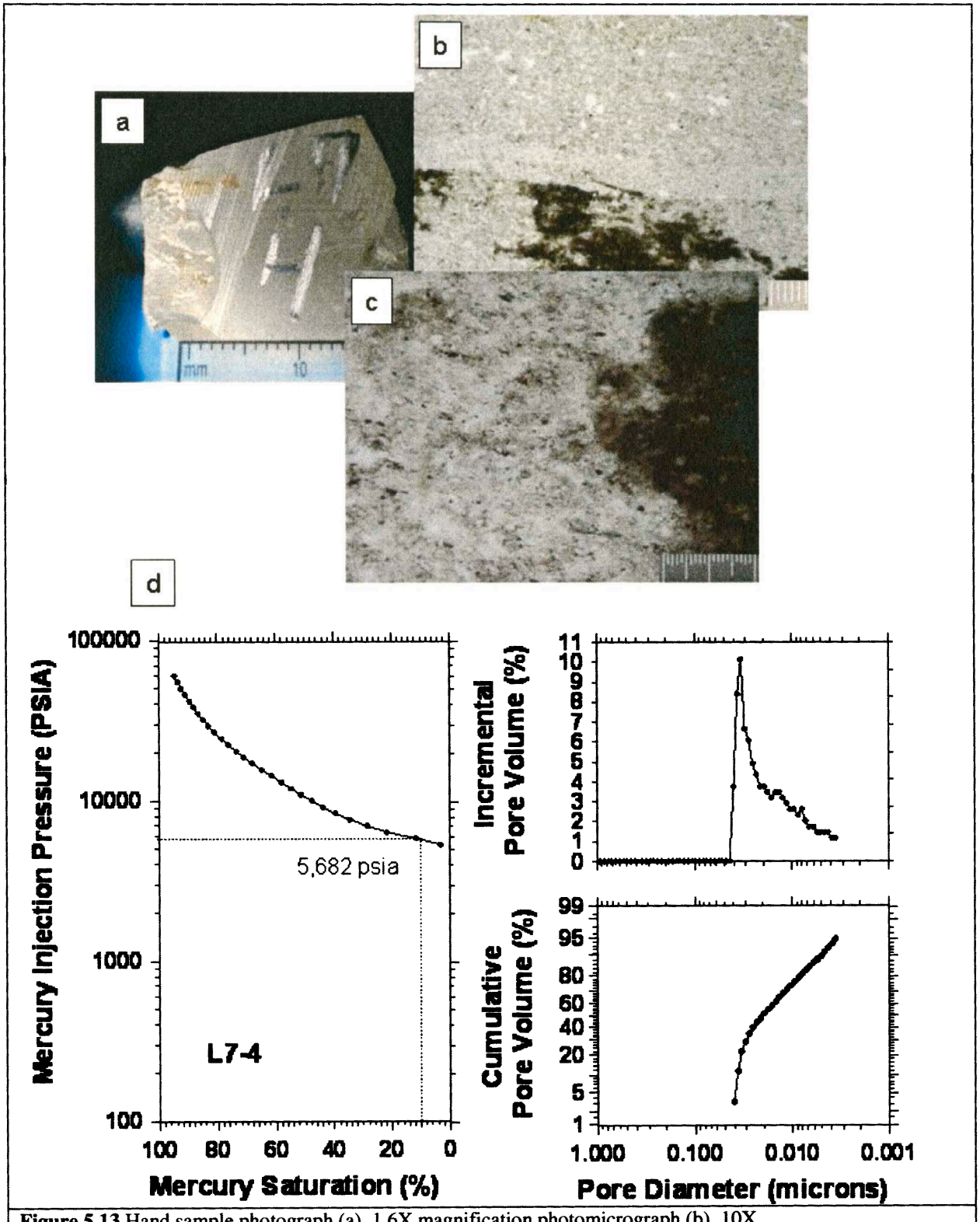

Figure 5.13 Hand sample photograph (a), 1.6X magnification photomicrograph (b), 10X magnification photomicrograph (c), and MICP curves (d) for a high sealing capacity sample for Lithofacies 2. Scale for 1.6X figure is 0.5 mm and 0.2 mm for 10X figure. 10% saturation is 5,682 psia and there are two modal classes of pore throat diameters. (a) courtesy of Poro-Technology.

Lithofacies 3 –Gray, Calcareous Siltstone with Brown and Purple Mottling

These 21 siltstone samples occur at every sampling location in both the PPL and PPU, with the exception of location L2 where only one sandstone sample was obtained, and Location B1. The facies includes location L6, where only one sample was obtained. There does not appear to be any preferred stratigraphic position that the facies fits into. Average quartz grain size is 5.5 phi, which is medium sized silt, they have an average roundness of 3.1 which is subrounded using the qualitative scale for estimating roundness.

Lithofacies 3 shows a wide range of compositions, but averages 11% quartz, 5% feldspar, 2% organics, and 63% matrix (Table 5.10). Matrix is a significant component of these rocks, making up more than half of their total percentage, cement makes up another 18% of the composition. On the average, over 80% of the composition is matrix and cement. Bioturbation ranges from 1 to 5 on the qualitative scale, with an average of 4. This value indicates that 60-90% of the original bedding has been disturbed (Pemberton et al, 1992). Total organic carbon ranges from 0.16 – 0.72 %, with an average of 0.34% which is the second highest average value of TOC from this data set.

Lithofacies 3 has an average sealing capacity of 3356 psia, with a range of 579 to 6722 psia, and a standard deviation of 1567 (Table 5.10). This is the third highest average sealing capacity, which places it 825 psia from the best sealing capacity lithofacies, Lithofacies 2. The average MICP calculated porosity is 8.74 %, with a range from 4.95 to 10.70%, and a standard deviation of 1.24%. This follows the trend of higher porosity equals lower sealing capacity (everything else being equal) that has been seen in these paleosols.

Figures 5.14 and 5.15 contain photomicrographs and MICP curves for a low sealing capacity sample and a high sealing capacity sample from this lithofacies. The high sealing capacity sample exhibits one or two classes of pore throats (Figure 5.15d). The low sealing capacity sample exhibits three distinct classes of pore throat diameters.

Lithofacies 4 –Gray, Calcareous Rooted Siltstone with Brown and Purple Mottling

These 12 siltstone samples occur at every sampling location in both the PPL and PPU with the exception of location L2, where only one sandstone sample was obtained, and Location L6, where only one sample was also obtained. There does not appear to be a stratigraphic position favored by this facies, which is similar to the other lithofacies described to this point. Average quartz grain size is 4.9 phi, which is coarse sized silt grains and they have an average roundness of 3.0, making the quartz grains subrounded using the qualitative scale for estimating roundness.

Lithofacies 4 shows a wide range of compositions, but averages 17% quartz, 4% feldspar, 3% organics, and 63% matrix (Table 5.10). Cement makes up another 12% of the composition. On average, just less than 75% of the composition of the rocks in this lithofacies is composed of matrix and cement. The quartz grain percentage for this lithofacies is the highest average percentage of all of lithofacies. Bioturbation ranges from 2 to 4 on the qualitative scale, with an average of 4. This value indicates that 60-90% of the original bedding has been disturbed (Pemberton et al, 1992). Total organic carbon ranges from 0.04 – 0.68 %, with an average of 0.25%.

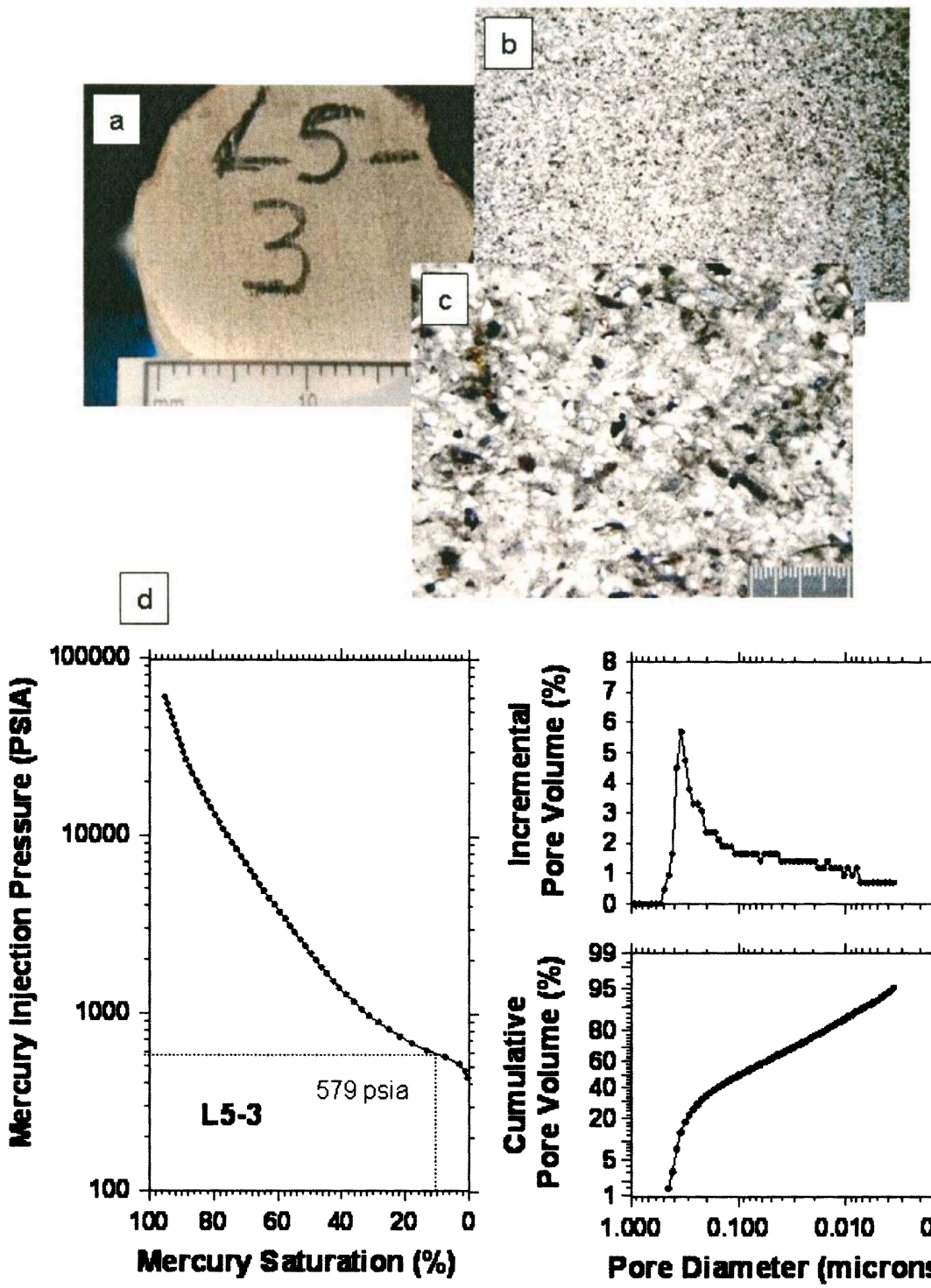

Figure 5.14 Hand sample photograph (a), 1.6X magnification photomicrograph (b), 10X magnification photomicrograph (c), and MICP curves (d) for a low sealing capacity sample for Lithofacies 3. Scale for 1.6X figure is 0.5 mm and 0.2 mm for 10X figure. 10% saturation is 579 psia and there are two modal classes of pore throat diameters. (a) courtesy of Poro-Technology.

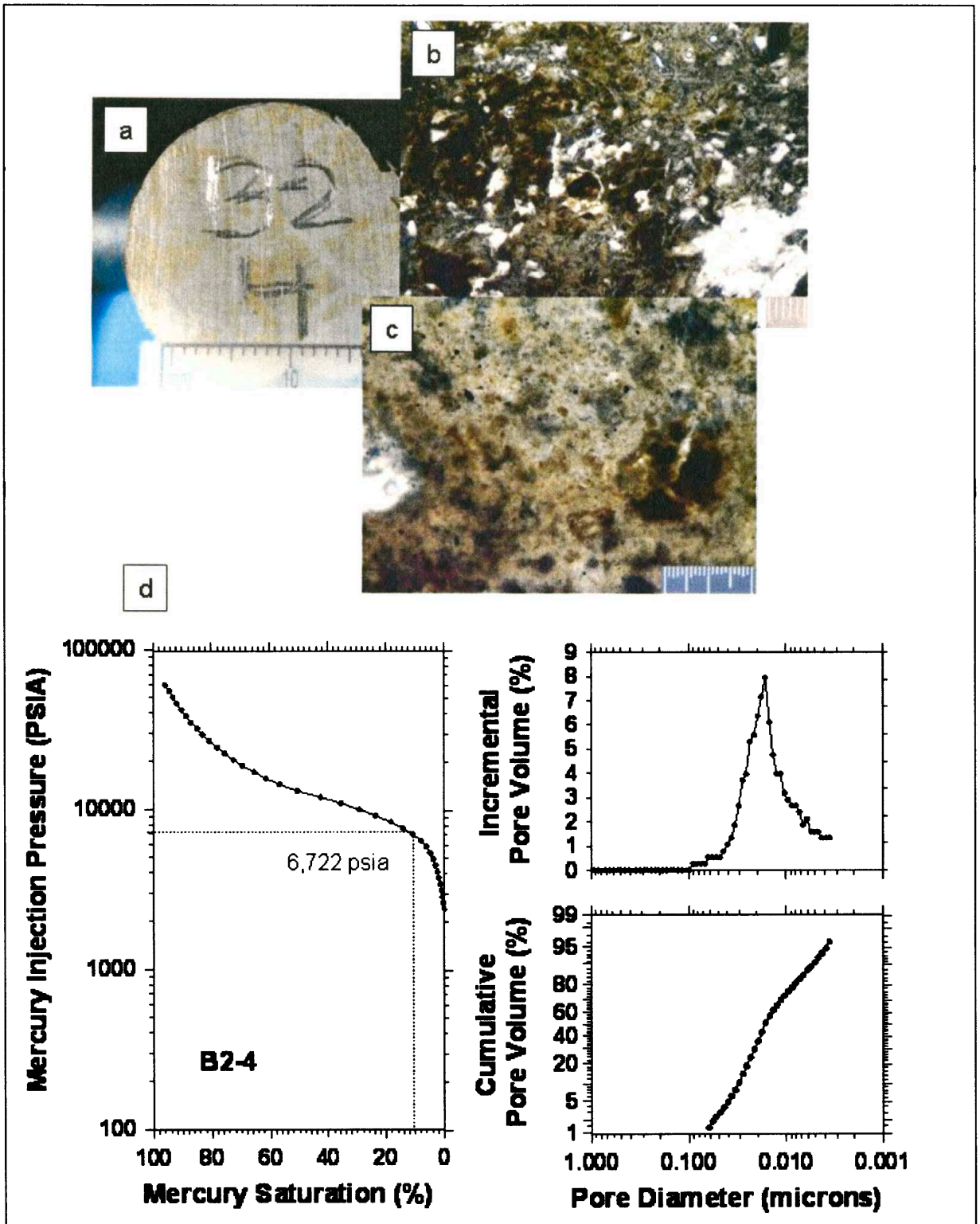

Figure 5.15 Hand sample photograph (a), 1.6X magnification photomicrograph (b), 10X magnification photomicrograph (c), and MICP curves (d) for a high sealing capacity sample for Lithofacies 3. Scale for 1.6X figure is 0.5 mm and 0.2 mm for 10X figure. 10% saturation is 6,722 psia and there are one or two modal classes of pore throat diameters. (a) courtesy of Poro-Technology.

Lithofacies 4 has an average sealing capacity of 3734 psia, with a range of 618 to 6257 psia, and a standard deviation of 1819 (Table 5.10). The average MICP calculated porosity is 8.26 %, with a range from 5.63 to 10.00%, and a standard deviation of 1.27%. Figures 5.16 and 5.17 contain photomicrographs and MICP curves for a low sealing capacity sample and a high sealing capacity sample from this lithofacies. Figures 5.16d and 5.17d show that the better seal has one class of pore throats, while the poor seal has at least two classes of pore throats.

The distinguishing factor for this lithofacies is that paleo-roots were seen in the field during collection of the samples from the outcrop. Compositionally and texturally these rocks are very similar to Lithofacies 2 and 3. The presence of paleoroot structures might have had a negative effect on the sealing capacity of this lithofacies. Mitchell et al (1995) showed that permeability of modern soils could be increased by root systems that create pore space in the soil. They also indicated that the decay of root material provided preferential flow paths for water in modern soils. These paths could have survived burial and compaction and provided a pathway for mercury to travel through, lowering the sealing capacity. It is unclear if the size of the sample used for MICP testing is large enough to affect the analysis.

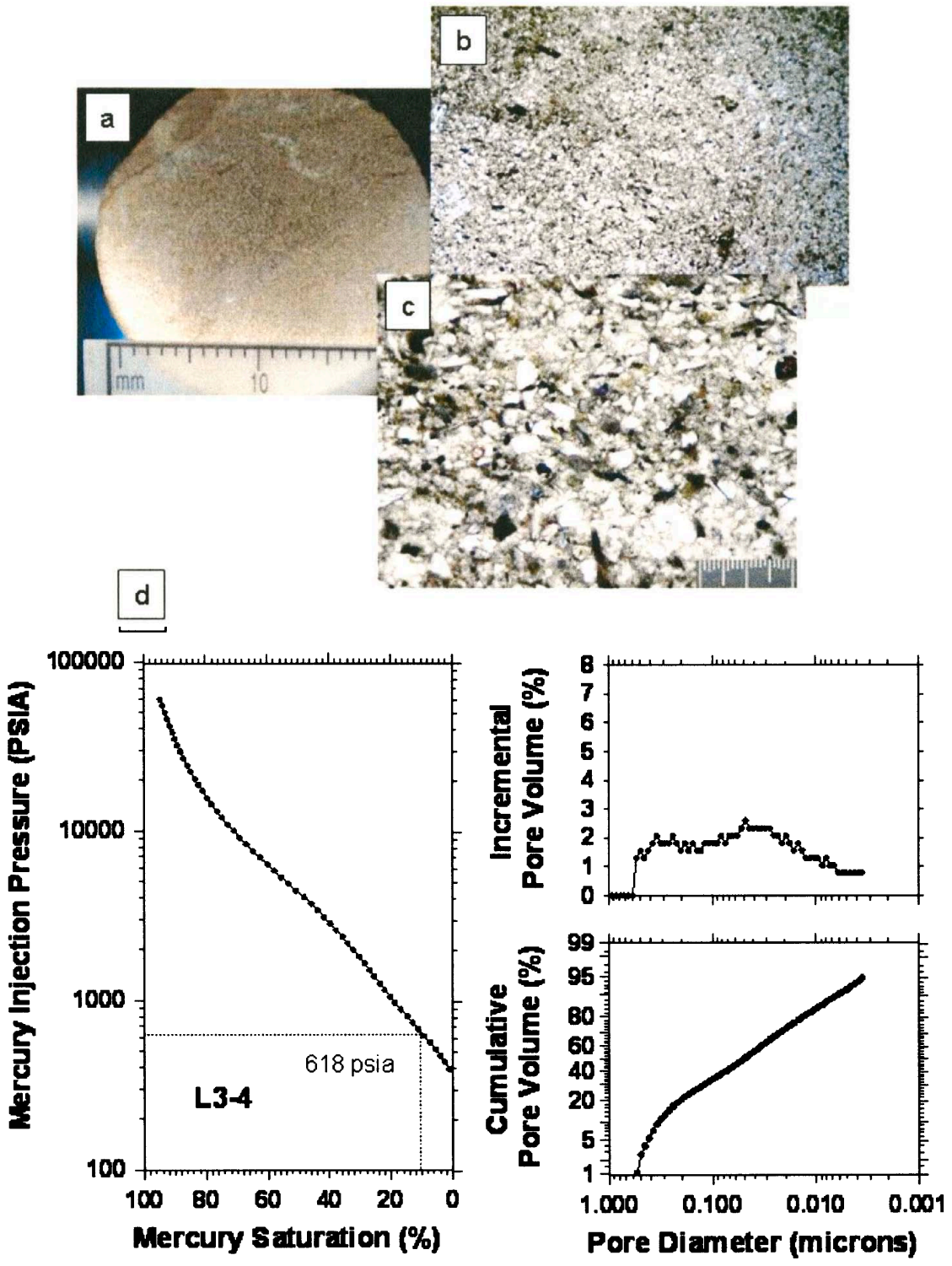

Figure 5.16 Hand sample photograph (a), 1.6X magnification photomicrograph (b), 10X magnification photomicrograph (c), and MICP curves (d) for a low sealing capacity sample for Lithofacies 4. Scale for 1.6X figure is 0.5 mm and 0.2 mm for 10X figure. 10% saturation is 618 psia and there are two modal classes of pore throat diameters. (a) courtesy of Poro-Technology.

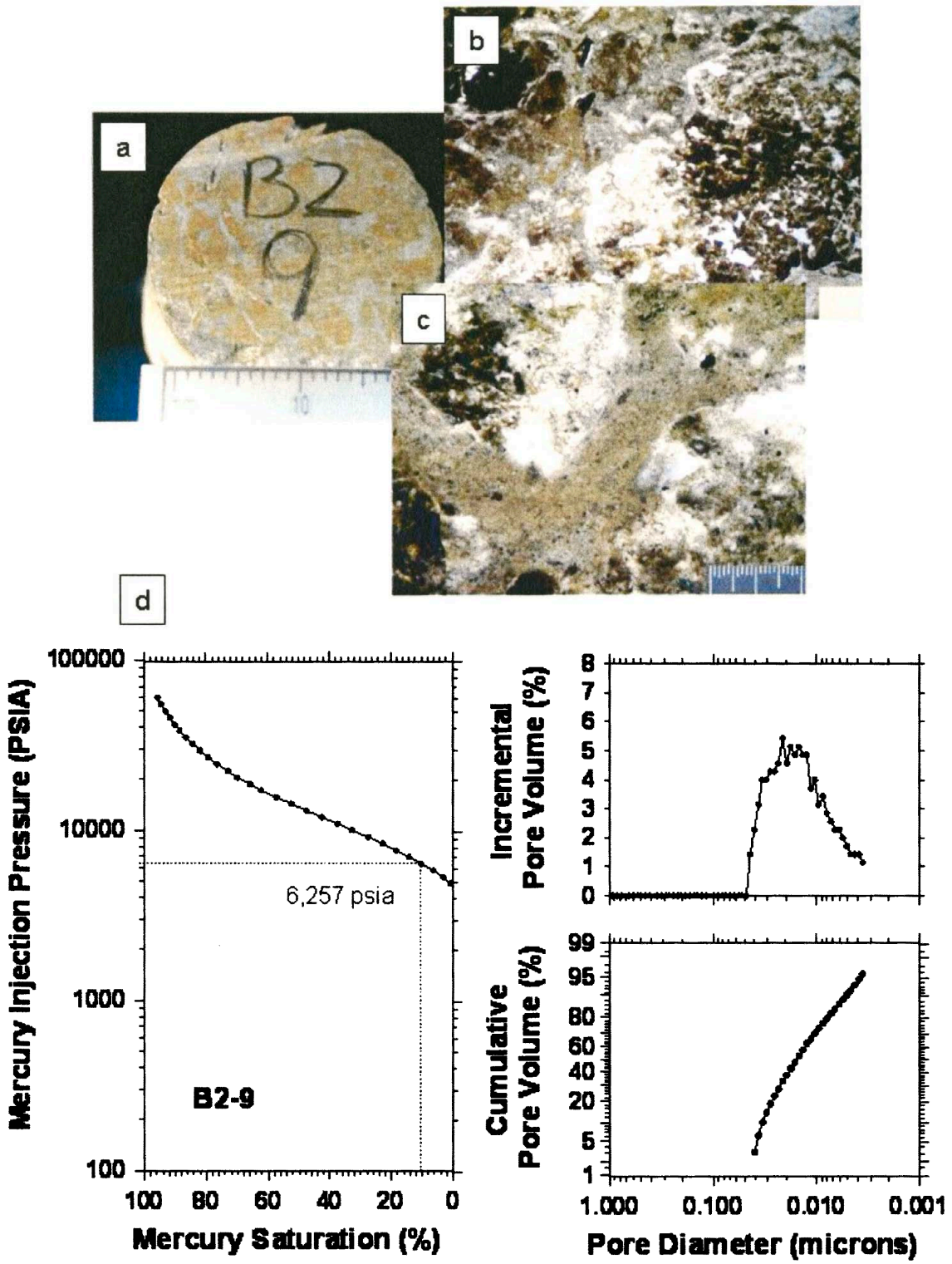

Figure 5.17 Hand sample photograph (a), 1.6X magnification photomicrograph (b), 10X magnification photomicrograph (c), and MICP curves (d) for a high sealing capacity sample for Lithofacies 4. Scale for 1.6X figure is 0.5 mm and 0.2 mm for 10X figure. 10% saturation is 6,257 psia and there is one modal class of pore throat diameters. (a) courtesy of Poro-Technology

Lithofacies 5 –Gray Siltstone with White, Calcareous Nodules and Brown and Purple Mottling

These 4 siltstone samples occur only at 2 sampling locations L1 and L3. A total of 4 samples make up this lithofacies. Unlike the other lithofacies, there appears to be a favored stratigraphic position as these 4 samples were all collected towards the top of their sampled location. Average quartz grain size is 5.4 phi, medium sized silt, and they have an average roundness of 3 which is subrounded using the qualitative scale for estimating roundness.

Lithofacies 5 shows a relatively narrow range of compositions. Averages are 6% quartz, 3% feldspar, 3% organics, and 76% matrix (Table 5.10). Matrix is a significant component of these rocks, making up more than three-quarters of their total composition, cement makes up another 9.60% of the composition. On average, over 85% of the composition of the rocks in this lithofacies is composed of matrix and cement. Bioturbation for all four of these samples was 6 on the qualitative scale, indicating that 100% of the original bedding has been disturbed (Pemberton et al, 1992). Total organic carbon ranges from 0.23 – 0.51 %, with an average of 0.37% which is the highest average value of TOC from this data set.

Lithofacies 5 has an average sealing capacity of 3013 psia, with a range of 1263 to 4679 psia, and a standard deviation of 1675 (Table 5.10). This is the lowest average sealing capacity for this set of described lithofacies. The average MICP calculated porosity is 7.95%, with a range from 6.36 to 9.72%, and a standard deviation of 1.60%. Although this is not the lowest average porosity value, there is not much difference in the average porosity values (range 7.64 to 8.74%) for the whole set of lithofacies. Figures

5.18 and 5.19 contain photomicrographs and MICP curves for a low sealing capacity sample and a high sealing capacity sample from this lithofacies. Figures 5.18d and 5.19d show that the poor seal has two modal classes of pore throats, while the better seal has three modal classes of pore throats.

Lithofacies 6 –Gray, Thinly Bedded, Calcareous Sandstone

The 6 sandstone samples that compose this lithofacies were sampled at 5 different locations, L1, L2, L3, and L7; and were not evaluated as seals. The sandstone in the field area makes ridges that are more resistant to weathering than the encasing paleosols. The sandstone bodies are lenticular in shape and are discontinuous. Some of the sandstones are more laterally extensive than others. A sandstone body appears to be visually correlative between two locations (L3 and L7) for a distance of about 100m (see Figure 1.1). Average quartz grain size is 3.4 phi, which is very fine sand size, and they have an average roundness of 3 which is subrounded using the qualitative scale for estimating roundness.

Lithofacies 6 shows a fairly wide range of compositions for such a small sampling population, but averages 34% quartz, 8% feldspar, and 1% organics (Table 5.10). Overall, this lithofacies is composed of 46% grains, 26% matrix, and 28% cement. Bioturbation ranges from 0 to 3 on the qualitative scale, with an average of 2. This value indicates that 5 to 30% of the original bedding has been disturbed (Pemberton et al, 1992). No other data were collected for these samples.

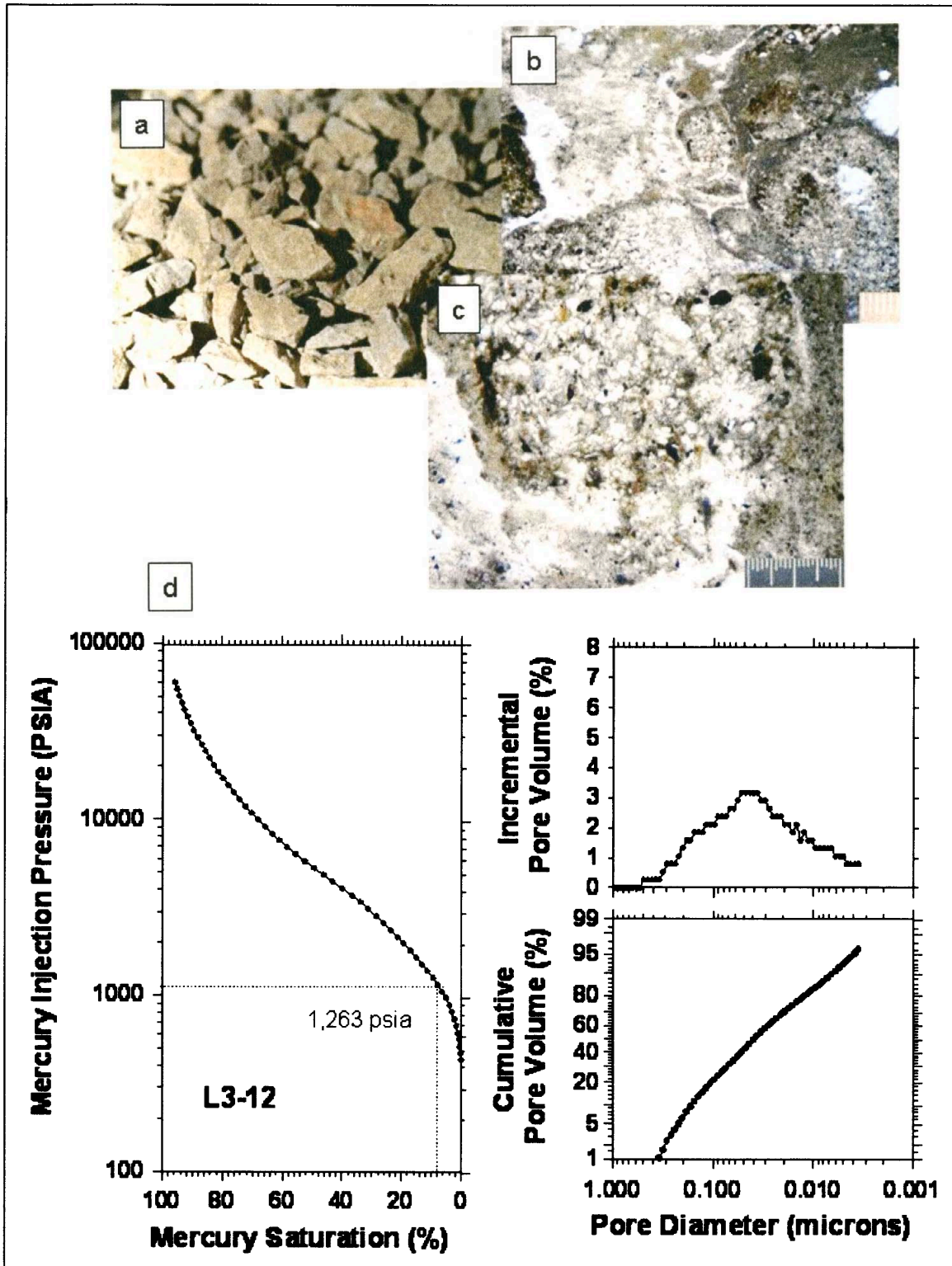

Figure 5.18 Hand sample photograph (a), 1.6X magnification photomicrograph (b), 10X magnification photomicrograph (c), and MICP curves (d) for a low sealing capacity sample for Lithofacies 5. Scale for 1.6X figure is 0.5 mm and 0.2 mm for 10X figure. 10% saturation is 1,263 psia and there is one modal classs of pore throat diameters. (a) courtesy of Poro-Technology.

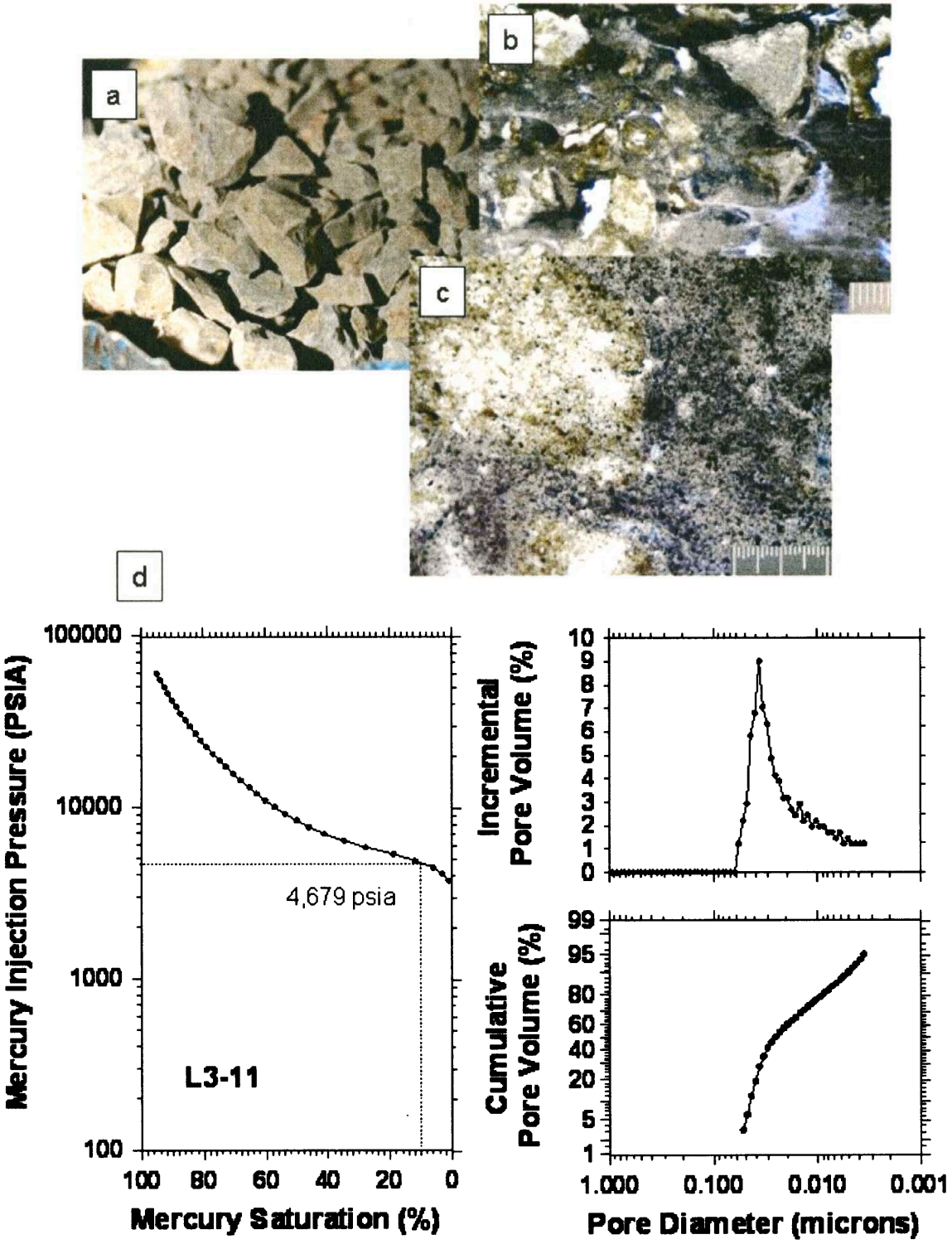

Figure 5.19 Hand sample photograph (a), 1.6X magnification photomicrograph (b), 10X magnification photomicrograph (c), and MICP curves (d) for a high sealing capacity sample for Lithofacies 5. Scale for 1.6X figure is 0.5 mm and 0.2 mm for 10X figure. 10% saturation is 4,679 psia and there are two modal classes of pore throat diameters. (a) courtesy of Poro-Technology.

Microfacies 1 –Siltstone with Very Fine, Sand Size Quartz Grains

The 6 samples of siltstones in this microfacies occur at locations B1, B2, L4, and L5. Four of the samples come from the PPL, with three of the four samples coming from B1. It is interesting to note that the three samples from this paleosol are the top three stratigraphically at that location. The samples from L2, as well as the sample from L4, come from the bottom of the paleosol stratigraphically, while the L5 sample was collected near the middle of the section. This microfacies has an average quartz grain size of 3.5 phi, and an average roundness of 3 phi, which is subrounded using the qualitative scale for estimating roundness.

This facies exhibits the second poorest sealing capacity of the microfacies, with a range of 1510 psia to 5525 psia, an average of 2913 psia, and a standard deviation of 1397 psia. Figures 5.20 and 5.21 contain photomicrographs and MICP curves for a low sealing capacity sample and a high sealing capacity sample from this microfacies. The poor seal (Figure 5.20d) exhibits three modal classes of pore throats, while the better seal shows one class of pore throats.

Microfacies 1 shows a wide range of compositions, but averages 24% quartz, 4% feldspar, 2% organics and 60% matrix (Table 5.11). Cement makes up another 9% of the composition. Bioturbation ranges from 3 to 5 on the qualitative scale, with an average of 4. This value indicates that 60-90% of the original bedding has been disturbed (Pemberton et al, 1992). Total organic carbon ranges from 0.03 – 0.68 %, with an average of 0.22% which is the lowest amount of TOC from the microfacies in this project.

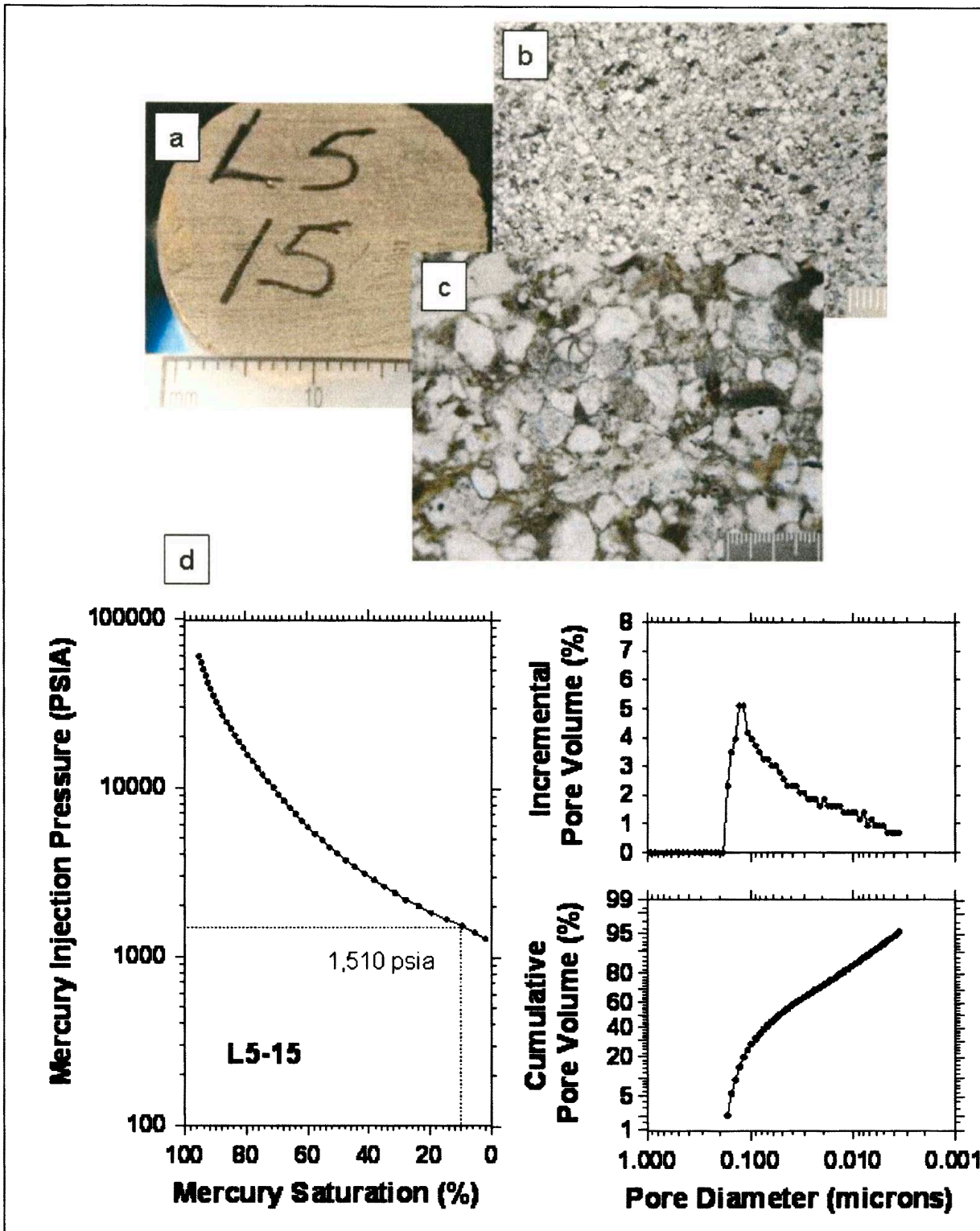

Figure 5.20 Hand sample photograph (a), 1.6X magnification photomicrograph (b), 10X magnification photomicrograph (c), and MICP curves (d) for a low sealing capacity sample for Microfacies 1. Scale for 1.6X figure is 0.5 mm and 0.2 mm for 10X figure. 10% saturation is 1,510 psia and there are two modal classes of pore throat diameters. (a) courtesy of Poro-Technology.

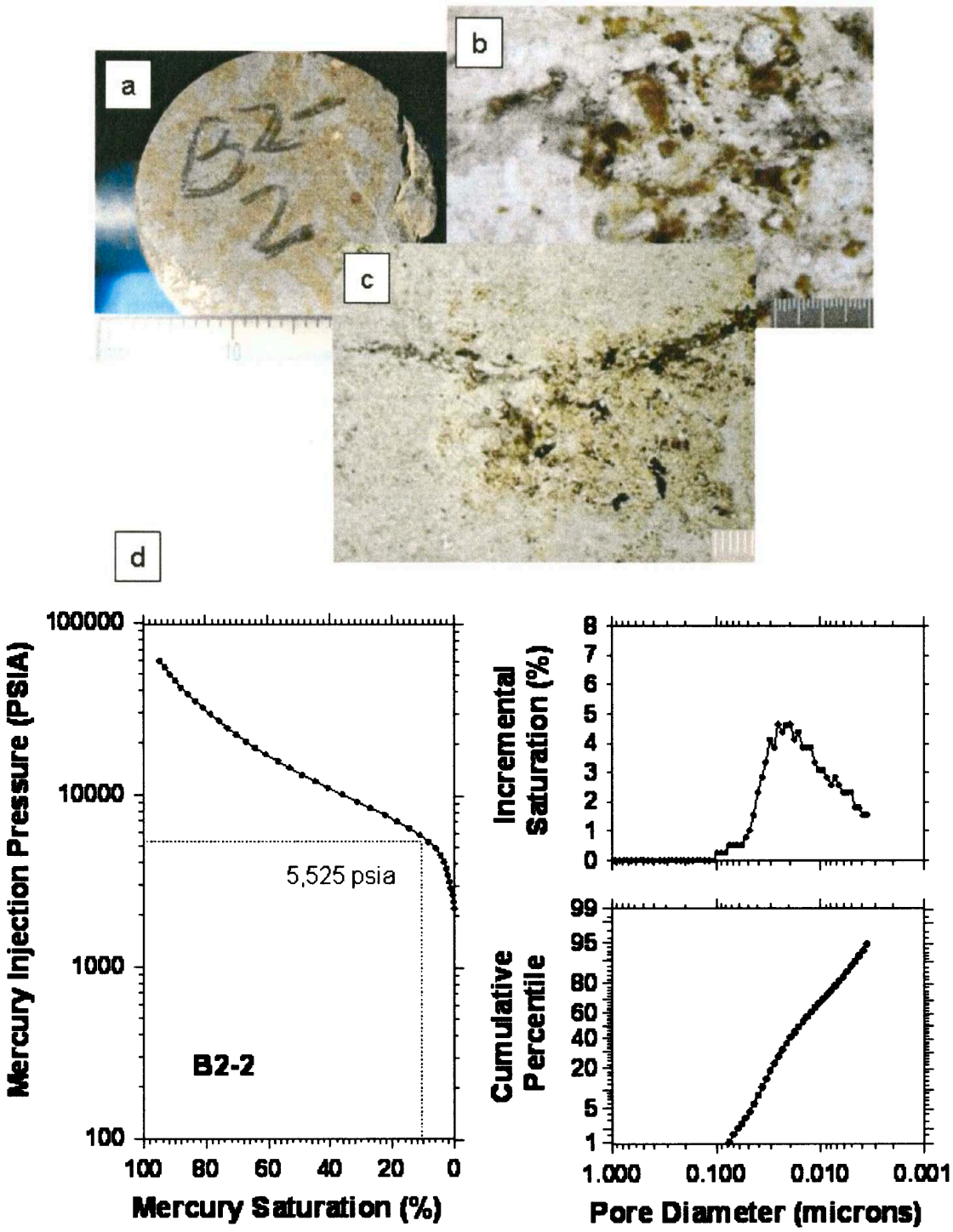

Figure 5.21 Hand sample photograph (a), 1.6X magnification photomicrograph (b), 10X magnification photomicrograph (c), and MICP curves (d) for a high sealing capacity sample for Microfacies 1. Scale for 1.6X figure is 0.5 mm and 0.2 mm for 10X figure. 10% saturation is 5,5525 psia and there is one modal class of pore throat diameters. (a) courtesy of Poro-Technology.

This microfacies has the same average quartz grain size as Microfacies 5, which was not analyzed as seal. Although both facies exhibit similar average quartz grain sizes (3.5 phi and 3.4 phi), there are differences that make this facies a valid, separate facies. The first of these differences is the average percentage of matrix for each facies. Microfacies 1 has an average matrix content of 60% compared to 26% for Microfacies 5 (Figure 5.22)

There is one sample from Microfacies 1 that plots in the group of samples from Microfacies 5. This sample did not appear similar to Microfacies 5 in hand specimen. Point count data revealed that it belongs in Microfacies 5.

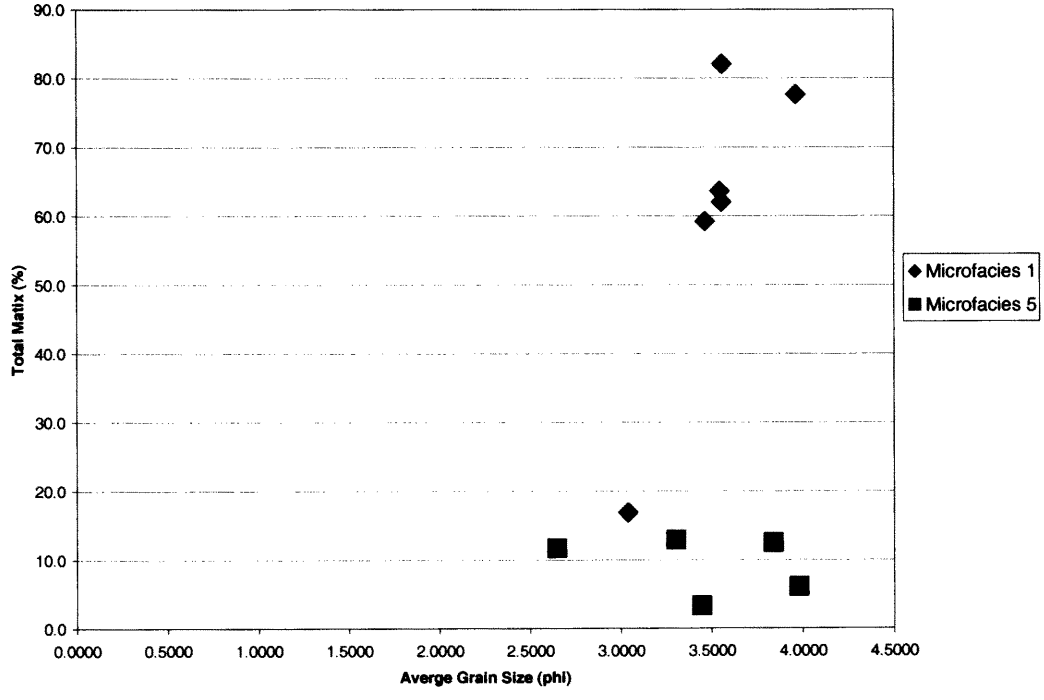

Figure 5.22 Two separate facies are distinguished by the graph of average grain size vs. total average matrix.

Another difference is seen in the amount of cement in each facies. The facies evaluated as a seal (Microfacies 1) has an average of 8.93% compared to the non-sealing

Microfacies 5 with an average of 28.08%. Based on the average matrix and cement, Microfacies 1 and Microfacies 5 were deposited in different locations relative to a paleochannel.

Microfacies 2 –Siltstone with Coarse, Silt Size Quartz Grains

The 30 samples of siltstones in this microfacies are found at most sampling locations in both the PPL and PPU with the exception of location L2, where only one sandstone sample was obtained, and location L1. This facies also includes the one sample from location L6. The samples in this facies do not appear to favor any single stratigraphic position in the sampling locations. All of the samples in this facies have quartz grains that are between 4 and 5 phi units with an average of 4.5 phi, and have an average roundness of 3, which is subangular using the qualitative scale for estimating roundness.

This facies exhibits the poorest sealing capacity of the microfacies, with a range of 467 psia to 7578 psia, an average of 2905 psia, and standard deviation is 1855 psia. Figures 5.23 and 5.24 contain photomicrographs and MICP curves for a low sealing capacity sample and a high sealing capacity sample from this microfacies. Both ends of the sealing capacity range have three classes of pore throat diameters, but the better seal has overall smaller pore throats (Figures 5.23d and 5.24d).

Microfacies 2 shows a wide range of compositions, but averages 18% quartz, 7% feldspar, 2% organics, and 57% matrix (Table 5.11). Cement makes up another 15% of the composition. On average, over 70% of the composition of the rocks in this lithofacies are composed of matrix and cement.

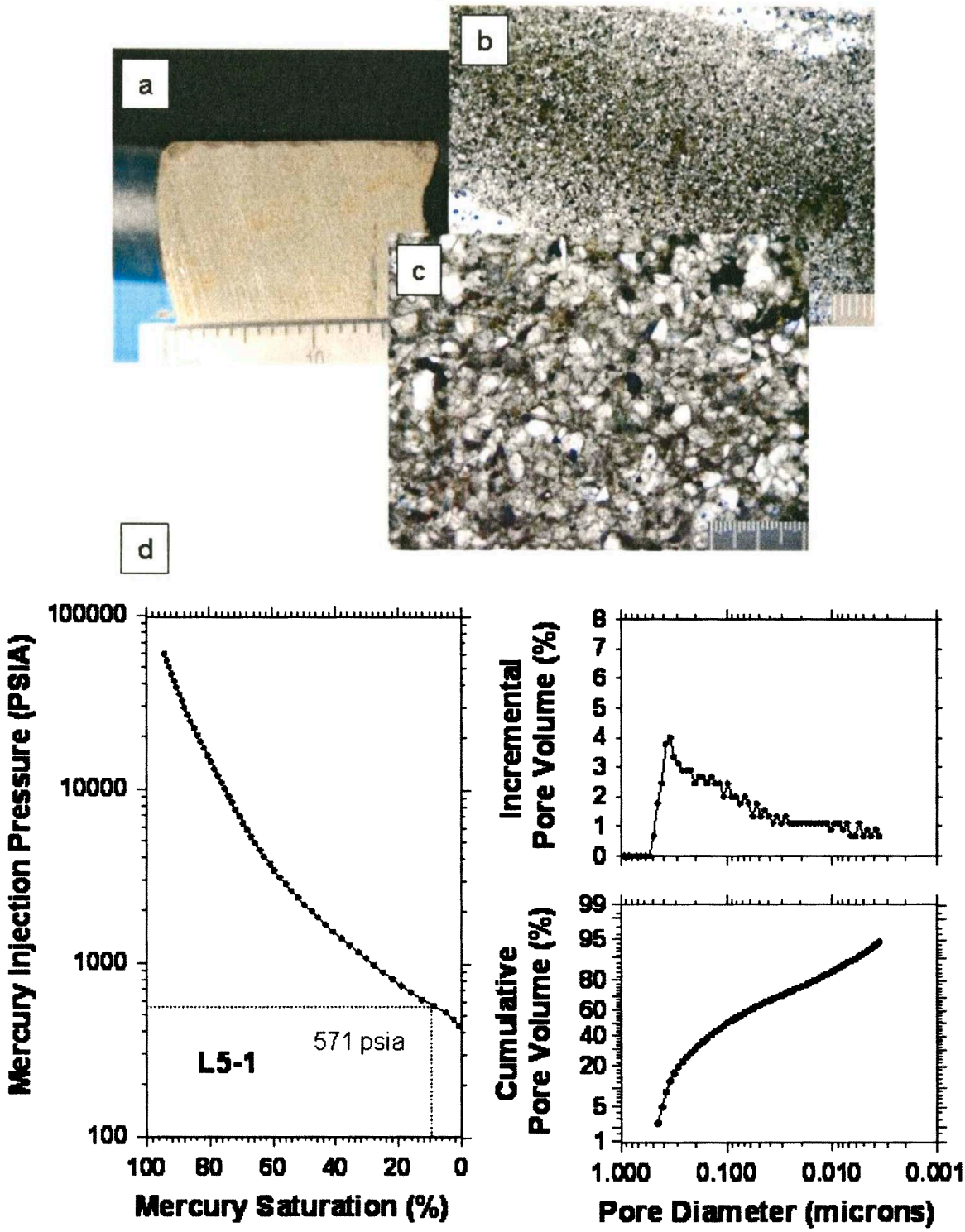

Figure 5.23 Hand sample photograph (a), 1.6X magnification photomicrograph (b), 10X magnification photomicrograph (c), and MICP curves (d) for a low sealing capacity sample for Microfacies 2. Scale for 1.6X figure is 0.5 mm and 0.2 mm for 10X figure. 10% saturation is 579 psia and there are two modal classes of pore throat diameters. (a) courtesy of Poro-Technology.

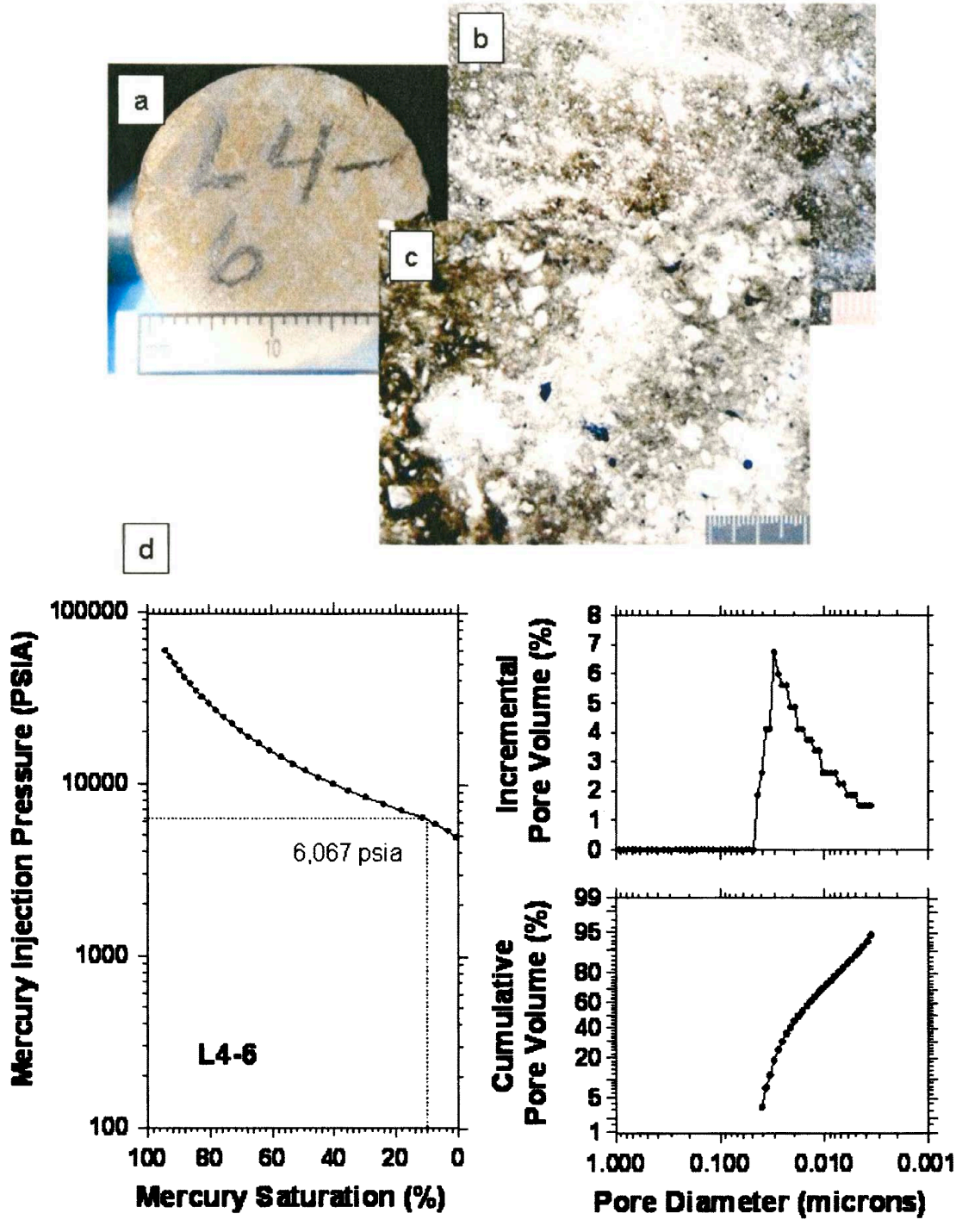

Figure 5.24 Hand sample photograph (a), 1.6X magnification photomicrograph (b), 10X magnification photomicrograph (c), and MICP curves (d) for a high sealing capacity sample for Microfacies 2. Scale for 1.6X figure is 0.5 mm and 0.2 mm for 10X figure. 10% saturation is 6,067 psia and there are two modal classes of pore throat diameters. (a) courtesy of Poro-Technology.

Bioturbation ranges from 2 to 5 on the qualitative scale, with an average of 4. This value indicates that 60-90% of the original bedding has been disturbed (Pemberton et al, 1992). Total organic carbon ranges from 0.02 – 0.54 %, with an average of 0.23%. This average is the second lowest amount of TOC of the five microfacies for this project (0.22% is the lowest).

Microfacies 3 –Siltstone with Medium, Silt Size Quartz Grains

The 35 samples of siltstones that compose this microfacies occur at sampling locations B2, L1, L3, L4, L5, and L7. The samples in this facies do not appear to favor any particular stratigraphic position at the sampling locations. All of the samples in this facies have quartz grains that are between 5 and 6 phi units with an average of 5.6 phi, and have an average roundness of 3, which is subrounded using the qualitative scale for estimating roundness.

Microfacies 3 makes the second best seal, with an average 10% saturation of 3720 psia. The range of sealing capacities for the microfacies is 837 psia to 6722 psia, and a standard deviation of 1509 psia. Figures 5.25 and 5.26 contain photomicrographs and MICP curves for a low sealing capacity sample and a high sealing capacity sample from this microfacies. Both low and high sealing capacity samples have three classes of pore throat diameters, but the better seal has overall smaller pore throats (Figures 5.25d and 5.26d).

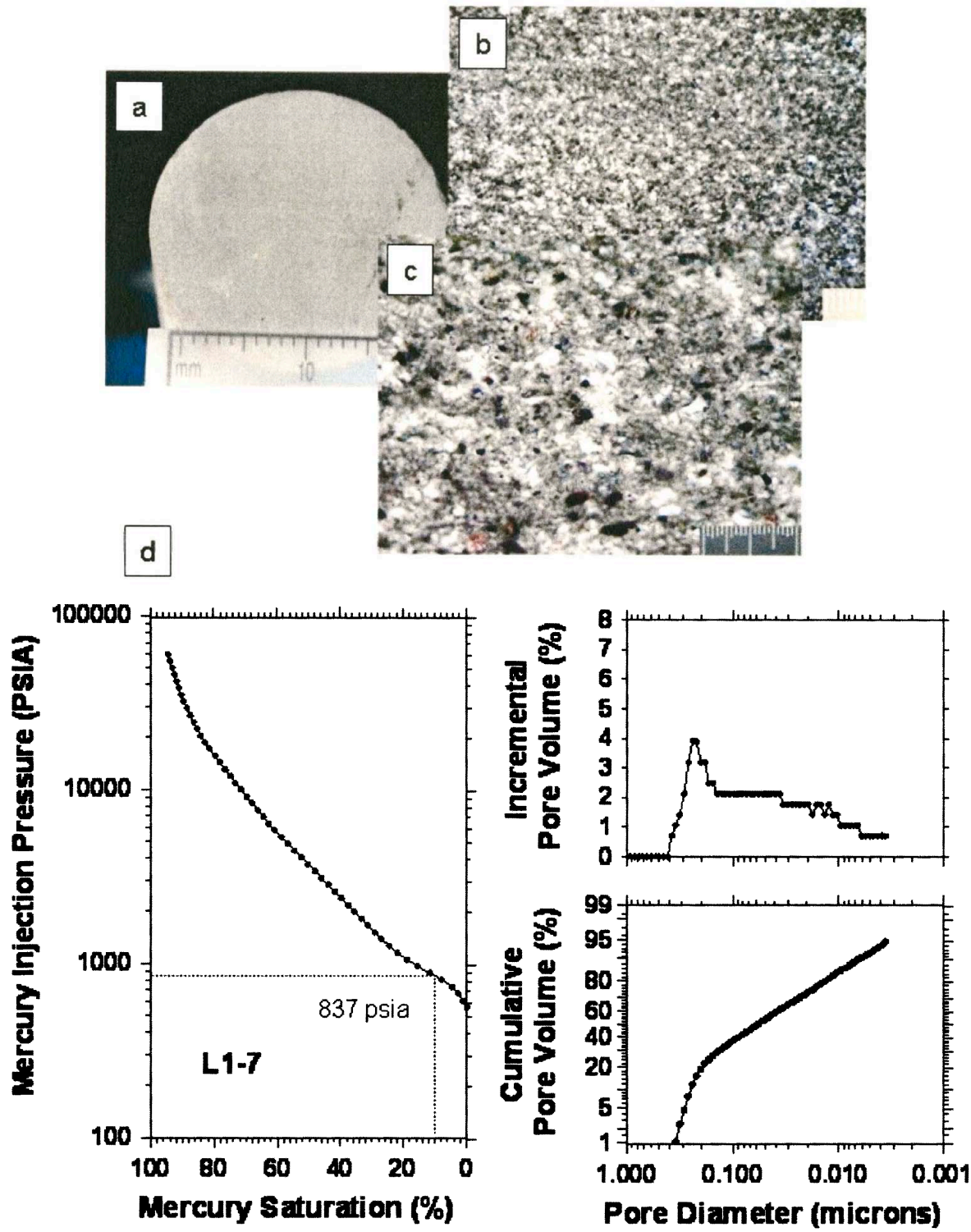

Figure 5.25 Hand sample photograph (a), 1.6X magnification photomicrograph (b), 10X magnification photomicrograph (c), and MICP curves (d) for a low sealing capacity sample for Microfacies 3. Scale for 1.6X figure is 0.5 mm and 0.2 mm for 10X figure. 10% saturation is 837 psia and there are two modal classes of pore throat diameters. (a) courtesy of Poro-Technology.

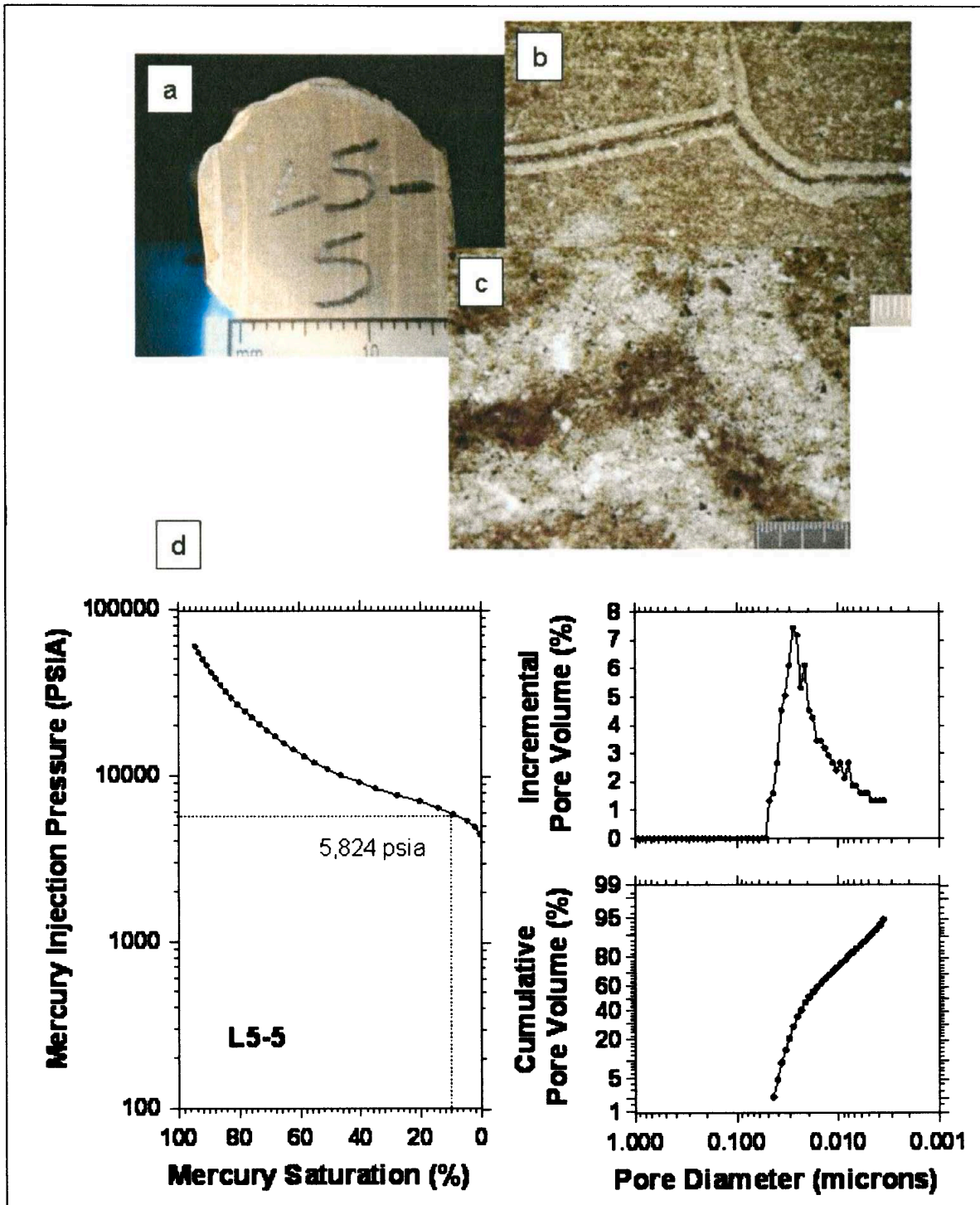

Figure 5.26 Hand sample photograph (a), 1.6X magnification photomicrograph (b), 10X magnification photomicrograph (c), and MICP curves (d) for a high sealing capacity sample for Microfacies 3. Scale for 1.6X figure is 0.5 mm and 0.2 mm for 10X figure. 10% saturation is 5,824 psia and there are two modal classes of pore throat diameters. (a) courtesy of Poro-Technology.

Microfacies 3 shows a wide range of compositions, but averages 8% quartz, 4% feldspar, 3% organics, and 71% matrix (Table 5.11). Cement makes up another 13% of the composition. On average, over 80% of the composition of the samples in Microfacies 3 is composed of matrix and cement. Bioturbation ranges from 1 to 6 on the qualitative scale, with an average of 4. This value indicates that 60-90% of the original bedding has been disturbed (Pemberton et al, 1992). Total organic carbon ranges from 0.11 – 0.74 %, with an average of 0.37%, which is the highest amount of TOC from the samples of Microfacies 3.

A clear mineral was noticed in the field on some of the larger samples collected at this location. The mineral is believed to be anhydrite, as it is harder than gypsum but softer than calcite using Moh's Scale for Hardness, and does not react to HCl acid.

Microfacies 4 –Siltstone with Fine, Silt Size Quartz Grains

The 9 siltstone samples in this microfacies occur at locations B2, L1, L5, and L7. The samples collected for this facies cover the whole range of stratigraphic positions at the sampling locations. Of the microfacies described here, Microfacies 4 makes the best seal, with a range of 10% saturation of 2332 psia to 7667 psia, an average of 4492 psia, and a standard deviation of 1540 psia. Figures 5.27 and 5.28 contain photomicrographs and MICP curves for a low sealing capacity sample and a high sealing capacity sample from this microfacies. Both high and low seals exhibit three classes of pore throat diameters, with the higher capacity seals having slightly smaller pore throat diameters.

Microfacies 4 shows a relatively narrow range of compositions, but averages 5% quartz, 3% feldspar, and 3% organics (Table 5.11). Matrix is a significant component of

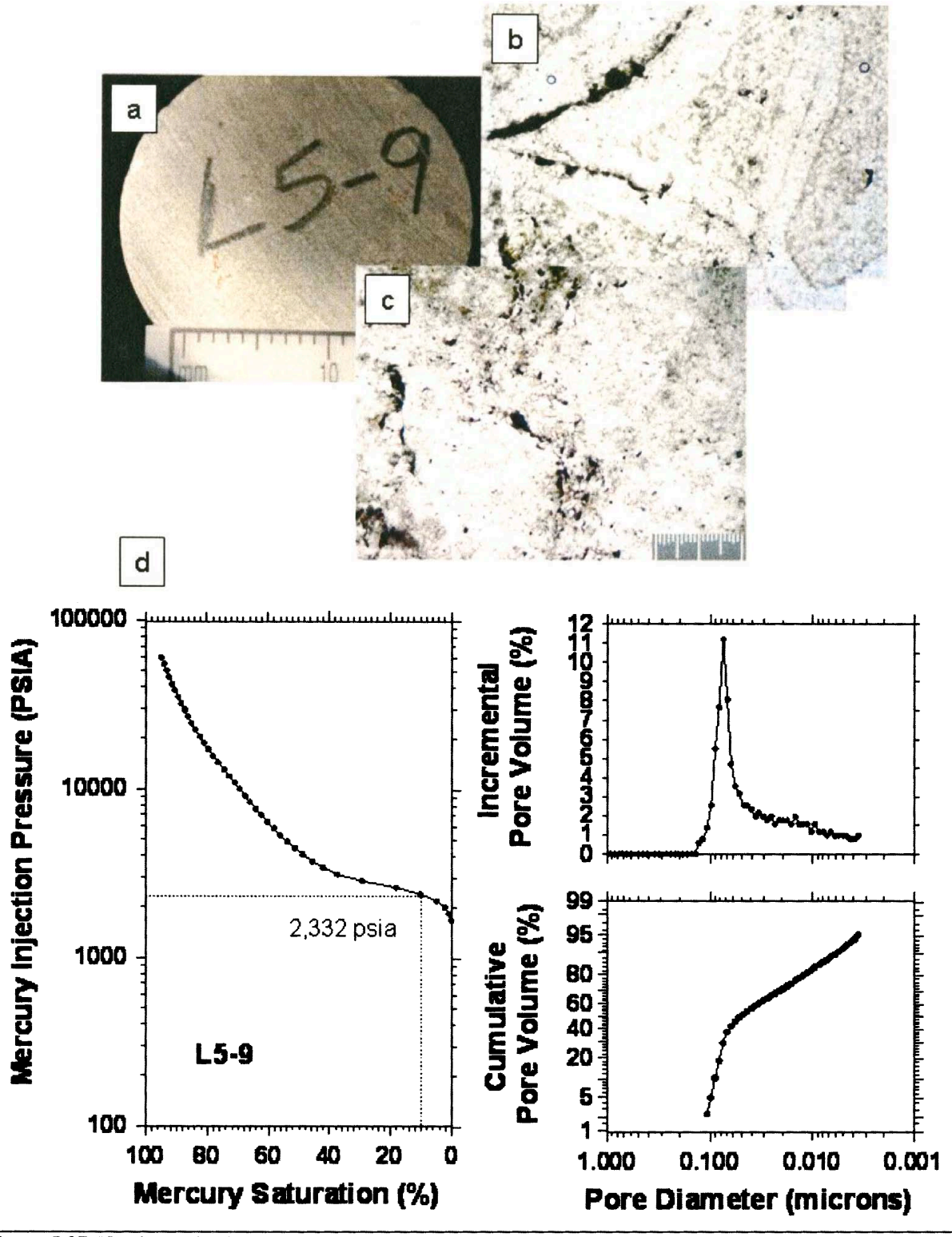

Figure 5.27 Hand sample photograph (a), 1.6X magnification photomicrograph (b), 10X magnification photomicrograph (c), and MICP curves (d) for a low sealing capacity sample for Microfacies 4. Scale for 1.6X figure is 0.5 mm and 0.2 mm for 10X figure. 10% saturation is 2,332 psia and there are two modal classes of pore throat diameters. (a) courtesy of Poro-Technology.

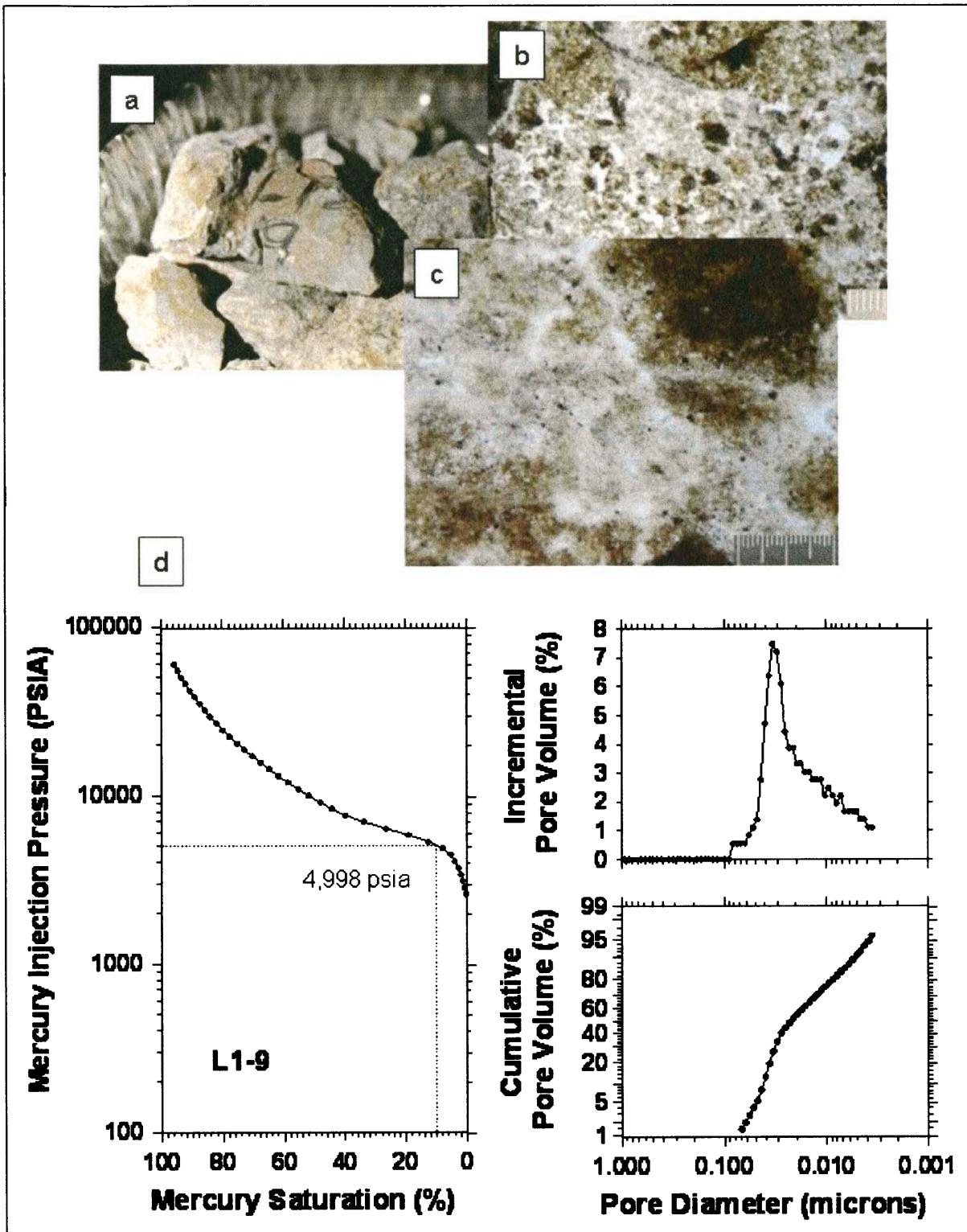

Figure 5.28 Hand sample photograph (a), 1.6X magnification photomicrograph (b), 10X magnification photomicrograph (c), and MICP curves (d) for a high sealing capacity sample for Microfacies 4. Scale for 1.6X figure is 0.5 mm and 0.2 mm for 10X figure. 10% saturation is 4,998 psia and there are two modal classes of pore throat diameters. (a) courtesy of Poro-Technology.

these rocks, making up more than three quarters of their total percentage, cement makes up another 13% of the composition. On average, over 88% of the composition of the rocks in this lithofacies is composed of matrix and cement. Bioturbation ranges from 3 to 5 on the qualitative scale, with an average of 4. This value indicates that 60-90% of the original bedding has been disturbed (Pemberton et al, 1992). Total organic carbon ranges from 0.19 – 0.74 %, with an average of 0.32% which is the second highest average values of TOC from this data set.

Microfacies 5 –Arkosic Wackes with Fine to Very Fine, Sand Size Quartz Grains

A total of 5 samples were collected as sandstones from the field area and have been classified into their own facies, although not analyzed as a seal. The only data collected on these samples was petrographic data, which includes point count data, average grain size, and roundness values. These samples came from 4 different sampling locations, all from the PPU (L1, L2, L3, and L7. The samples in this facies do not appear to favor any certain single stratigraphic position at the sampling locations. All of the samples in this facies are between 2 and 4 phi units with an average of 3.4 phi, and have an average roundness of 3, which is subrounded using the qualitative scale for estimating roundness.

Microfacies 5 shows a wide range of compositions, but averages 34% quartz, 8% feldspar, 1% organics, and 26% matrix (Table 5.11). Cement makes up another 28% of the composition. Of the microfacies listed here, this one has the highest average percentage of cement and the lowest average percentage of matrix. This was expected, as these were collected as sandstones, which generally have more cement and less matrix

than siltstones. Bioturbation ranges from 0 to 3 on the qualitative scale, with an average of 2. This value indicates that only 1 to 5% of the original bedding has been disturbed (Pemberton et al, 1992). This too, was also to be expected as the sandstones in the area were part of channel systems in a fluvial environment.

Comparison of Individual Paleosols

A total of 11 samples were collected from two distinct paleosols at location L5, five from a stratigraphically lower paleosol (Paleosol A), and 6 from a stratigraphically higher paleosol (Paleosol B). These paleosols were bounded by changes in topography and color changes (see Figure 4.9). The samples were collected to determine how sealing capacity varies between two distinct paleosols. Table 5.12 contains average MICP and compositional data obtained from these samples. According to MICP data, Paleosol B makes a slightly better seal, with an average 10% saturation value of 2533 psia compared to 2462 psia for Paleosol A. The range for Paleosol B is 970 psia to 3769 psia, with a standard deviation of 1084 psia. Paleosol A has a much smaller range, 2205 psia to 2847 psia, and a standard deviation of 245 psia. Compositionally, the two paleosols are very similar, with the exception of quartz. Paleosol B has an average percentage of 15% compared to Paleosol A quartz content of 7%. Paleosol B has lower porosity, permeability, and grain size values when compared to Paleosol A. This follows the general trend of all of the data over the whole study area. Average bioturbation is very similar between the two paleosols, with 30 to 60% of the original bedding being disturbed (Pemberton et al, 1992).

Table 5.12 Individual paleosols sampled at location L5. Porosity, 10%saturation, and all compositional data are in percentages. Permeability is in md, pore diameter is in microns, grain size is in phi units and bioturbation is qualitative.

Paleosol		Porosity	Permeability	Pore Diameter	10% Sat	Grain Size	Std Dev	TOC	Quartz	Feldspar	Muscovite	Organics	Matrix	Cement	Pores	Bioturbation
Paleosol A (n=5)	Min	10.80	0.029	0.042	2205	5.0	0.5	0.22	4	1	0	2	65	14	0	3
	Max	11.80	0.145	0.055	2847	6.3	0.6	0.74	11	4	0	4	74	22	0	4
	Average	11.36	0.071	0.051	2462	5.5	0.5	0.59	7	3	0	3	70	17	0	3
	Std. Dev	0.52	0.064	0.005	245	0.5	0.1	0.23	3	1	0	1	4	3	0	1
Paleosol B (n=6)	Min	9.47	0.052	0.031	970	3.0	0.4	0.51	4	0	0	1	17	7	0	3
	Max	11.80	0.188	0.078	3769	6.2	0.8	0.72	50	6	0	3	85	26	1	5
	Average	10.41	0.142	0.047	2533	5.2	0.5	0.61	15	3	0	2	64	15	0	4
	Std. Dev	0.80	0.078	0.018	1084	1.1	0.2	0.09	18	2	0	1	24	7	0	1

5.6 Relationships of Variables

Correlation has been used to determine if statistically significant relationships exist between sealing capacity and various measured paleosol properties. Correlations were preformed by a statistical computer program called SPSS. Significance of the correlation coefficients was determined using Pearson Correlation at the 0.05 (*) and .01 (**) levels, two tailed. Correlation has been performed on all the samples as one data set (Table 5.13).

Table 5.13 Correlations for all samples.

All Samples (n=80)			
Positive		Negative	
Var.	R	Var.	R
Grain Size	0.390**	Pore Diameter	-0.729**
Grain Density (MICP)	0.335**	Permeability (MICP)	-0.586**
Total Matrix	0.562**	Total Grains	-0.512**
		TOC	-0.328**

** significant to 0.01 level

Correlation was also used to determine if any relationships existed between the elemental percentages measured from XRF data and 10% saturation. Only 57 of 80 samples were analyzed with XRF. Table 5.14 shows the positive and negative correlations that exist between the XRF data and 10% saturation.

Table 5.14 XRF Correlations for all samples

All Samples (n=57)			
Positive		Negative	
Var.	R	Var.	R
Rb	0.694**	Na_2O	-0.448**
Al_2O_3	0.612**	CaO	-0.387**
K_2O	0.579**	Y	-0.345**
Nb	0.518**		
Fe_2O_3	0.481**		
TiO_2	0.409**		

** significant to 0.01 level

Figure 5.29 shows the positive relationship between 10% saturation and Al_2O_3. The graph shows that as the amount of Al_2O_3 increases, the sealing capacity increases. An increase in Al_2O_3 is likely associated with an increase in clay content. The graph also shows that there is generally less variation of Al_2O_3 in the samples with higher sealing capacity.

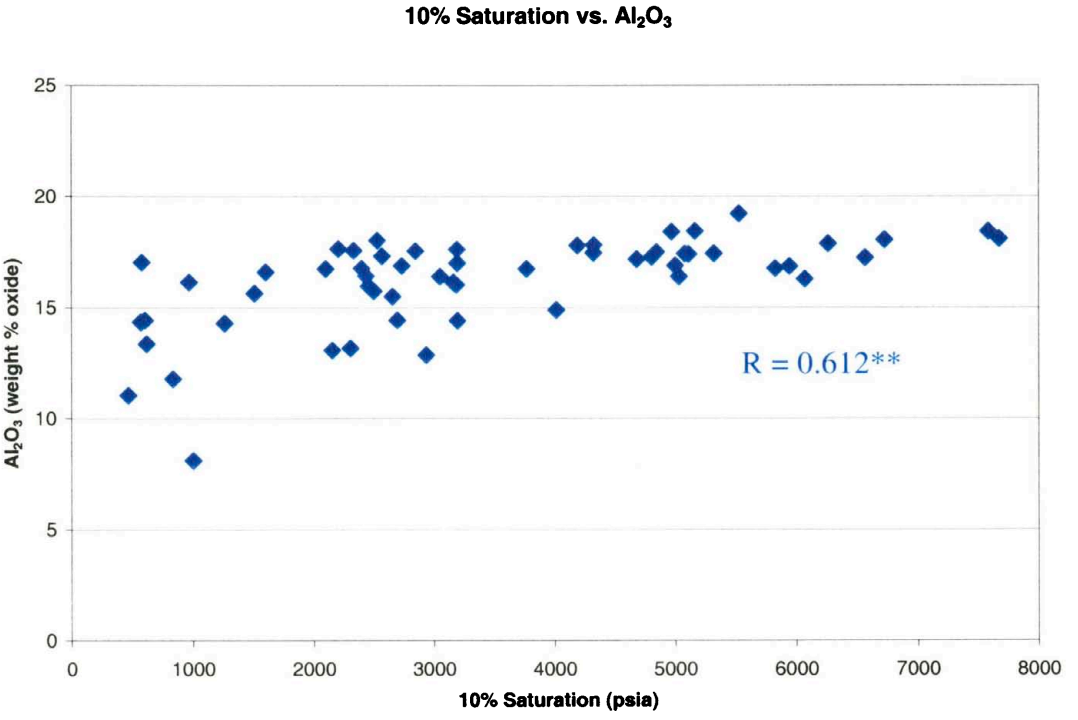

Figure 5.29 Graph of 10% saturation versus Al_2O_3. Al_2O_3 increases as 10% saturation increases.

Figure 5.30 shows the positive relationship between 10% saturation and TiO_2 for the paleosol samples collected. This graph shows that there is less variability in the lower sealing capacity samples compared to higher sealing capacity samples. The lower variability of TiO_2 in the higher seals may be an indication that there is a mineral structure that is holding onto the TiO_2, possibly a clay-mineral.

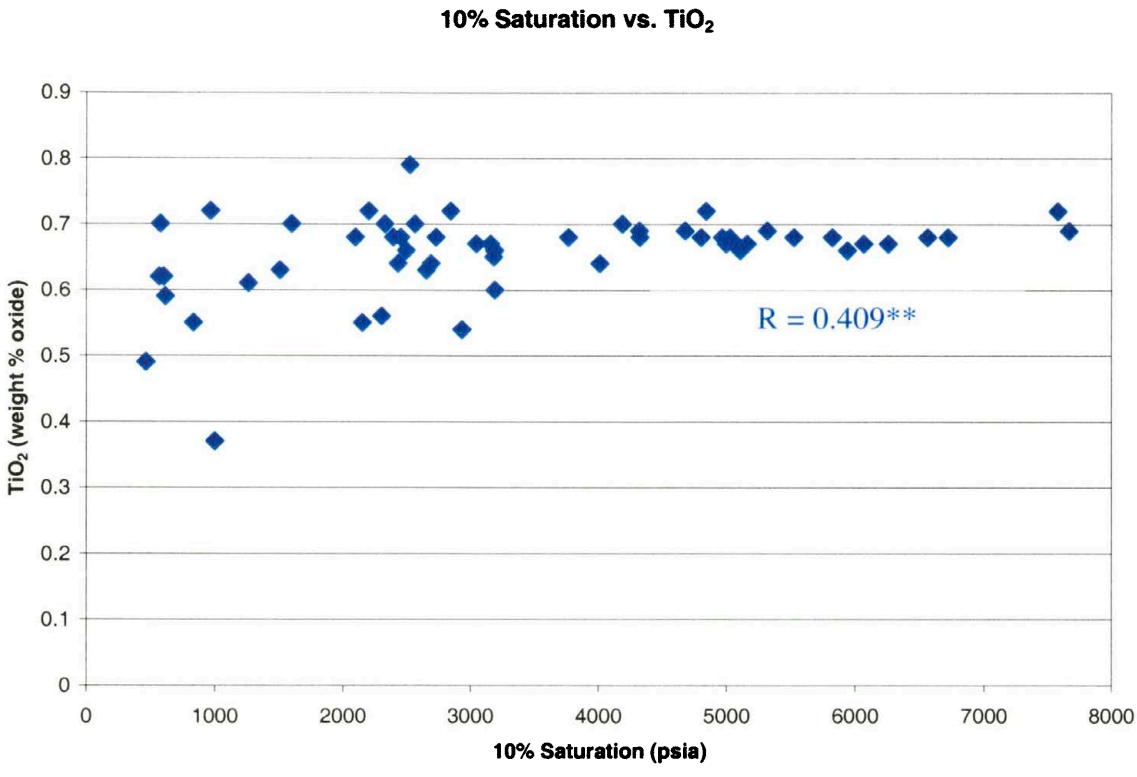

Figure 5.30 Graph of 10% saturation versus TiO_2. As TiO_2 increases 10% saturation increases. ** significant to 0.01 level.

Figure 5.31 shows the positive relationship between 10% saturation and K_20 for the paleosol samples collected. This graph shows that there is less variability in the lower sealing capacity samples compared to higher sealing capacity samples. K_2O fits into the mineral structure of clays, so the presence of K_2O in the higher seals may be an indication of the better seals having higher clay amounts.

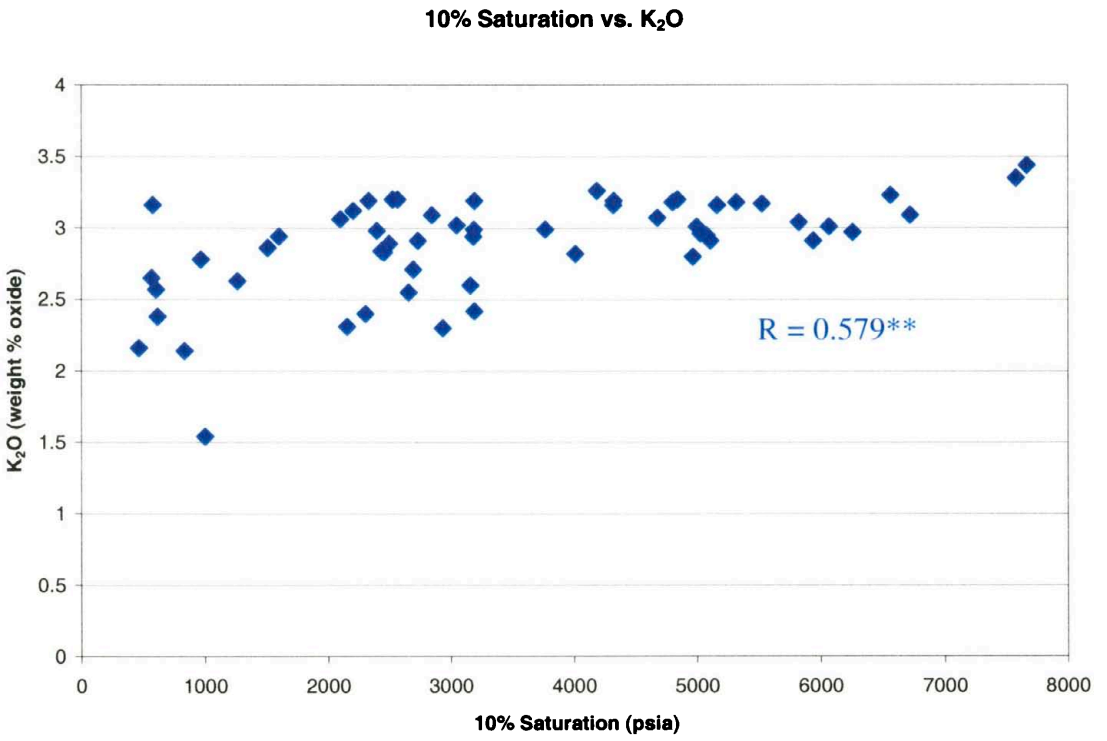

Figure 5.31 Graph of 10% saturation versus K_2O. As K_2O increases 10% saturation increases. ** significant to 0.01 level.

All of the data were analyzed together, ignoring the distinction between the PPL and PPU. The upper 10% of the samples in this distribution were classified as good seals and the lower 15% of the distribution of the samples were classified as poor seals. Graphs were made for all of the variables versus 10% saturation to help determine which variable or variables are controlling the sealing capacity of the paleosols from the Wasatch Formation.

Figure 5.32 shows the relationship between 10% saturation and quartz grain size for all of the samples. In general, samples that have higher sealing capacities have smaller quartz grain sizes. There is also slightly less variation of grain size in the good seals compared to the poor seals.

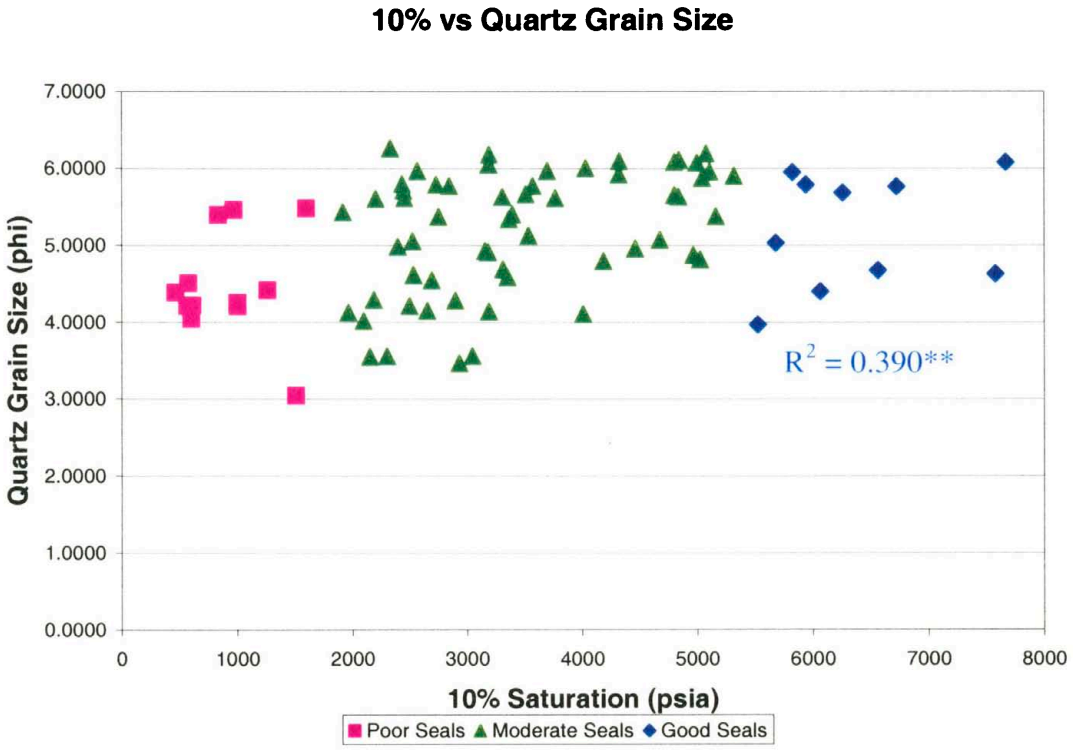

Figure 5.32 Graph of 10% saturation versus quartz grain size. As quartz grain size decreases, the sealing capacity increases. ** significant to 0.01 level.

Figure 5.33 shows the relationship between 10% saturation and total grains, which included: quartz, feldspar, muscovite, rock fragments, organics, and other grains not identifiable in thin section. This figure indicates that in general, there is less variability and a smaller percentage of total grains in the samples that make good seals.

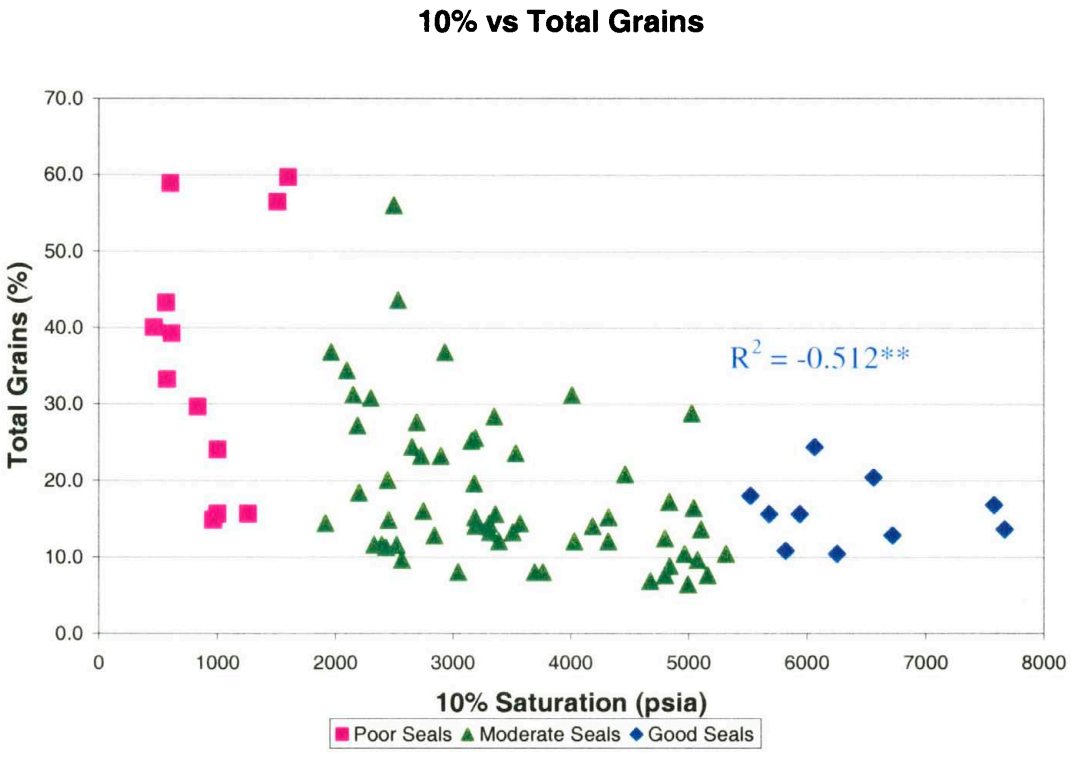

Figure 5.33 Graph of 10% saturation versus total grain percentage, which include: quartz, feldspar, muscovite, rock fragments, organics, and other grains not identifiable in thin section. Generally, better seals have less variability and smaller percentages of total grains. ** significant to 0.01 level.

Figure 5.34 demonstrates the relationship that exists between 10% saturation and the percentage of total matrix that was counted in the thin sections from all of the samples that were evaluated as seal. The figure indicates that the better seals have higher percentages of total matrix. This relationship helps to support the relationship that was noticed in the previous graph, which indicated that better seals have smaller percentages of total grains.

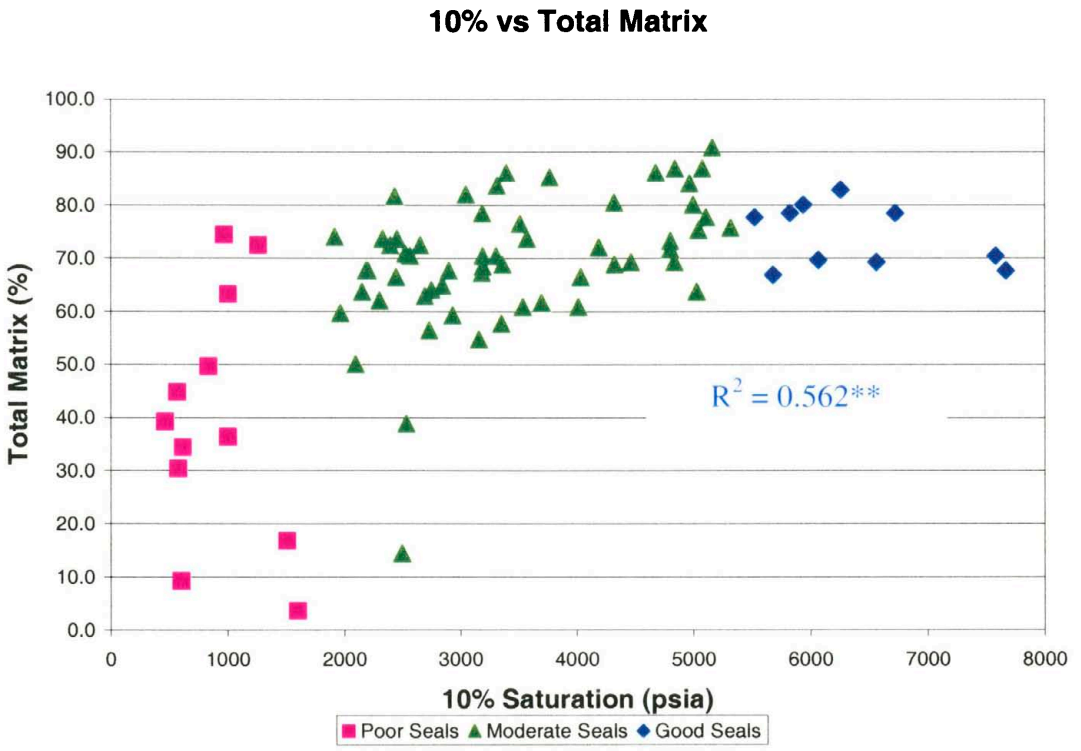

Figure 5.34 Graph of 10% saturation versus total matrix percentage. Generally, better seals have greater percentages of total matrix. ** significant to 0.01 level.

Figure 5.35 shows the relationship between 10% saturation and mean pore throat diameter. The figure indicates that there is a strong correlation that samples with better sealing capacities have smaller pore throat diameters.

The MICP curves for the poor seals were compared with the curves for the good seals to determine how the two groups differ. When the curves were plotted on top of one another, the two distinct sealing groups were visible (Figure 5.41).

Graph A in Figure 5.36 shows what percentage of the rock's pore space is saturated with mercury at a given pressure. Graph B gives a distribution of the pore throat classes and indicates that the poor seals have pore throats that are less sorted than the good seals. Graph C shows that the seal groups have very different classes of pore

throats. The good seals indicate that there is one distinct class of pore throats, while the poor seals have two distinct groups of pore throats. The graph also shows that there is less variation in the size of pore throats in the better seals.

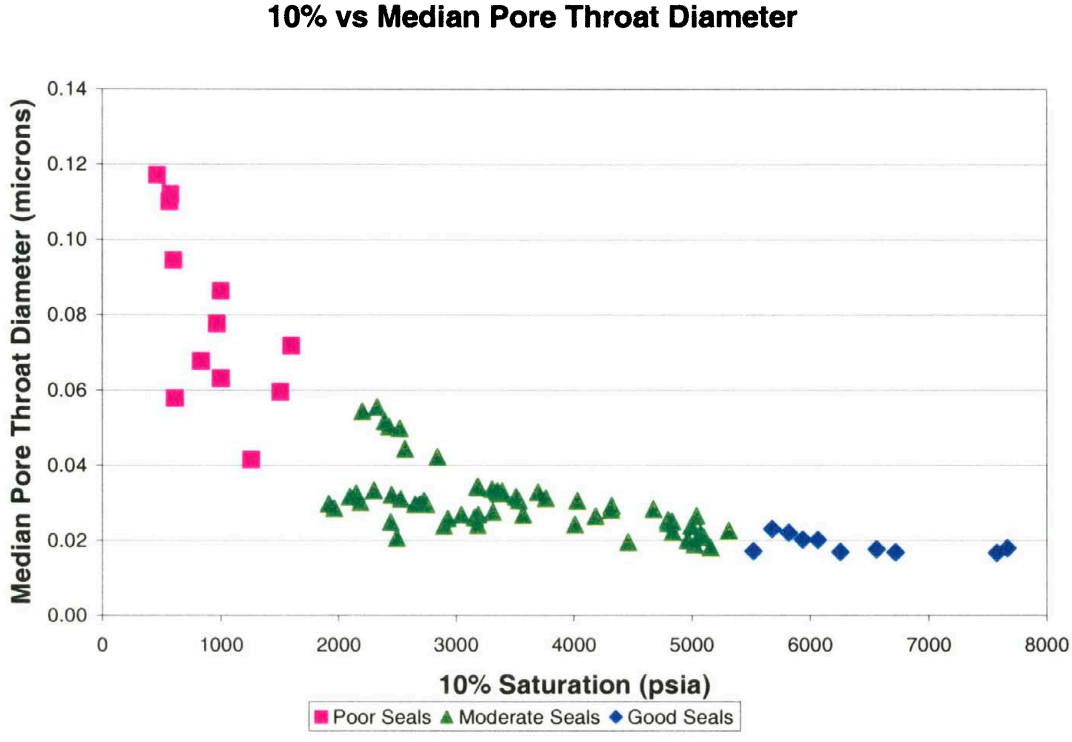

Figure 5.35 Graph of 10% saturation versus mean pore throat diameter. Relationship indicates that better seals have smaller pore throats.

Samples with lesser percentages of grains, larger percentages of total matrix, and smaller pore throat diameters make better seals. The question that needs answered is "What is controlling the sealing capacity of the paleosol samples that were collected from the Shire Member of the Wasatch Formation?" This question will be discussed in the following chapter.

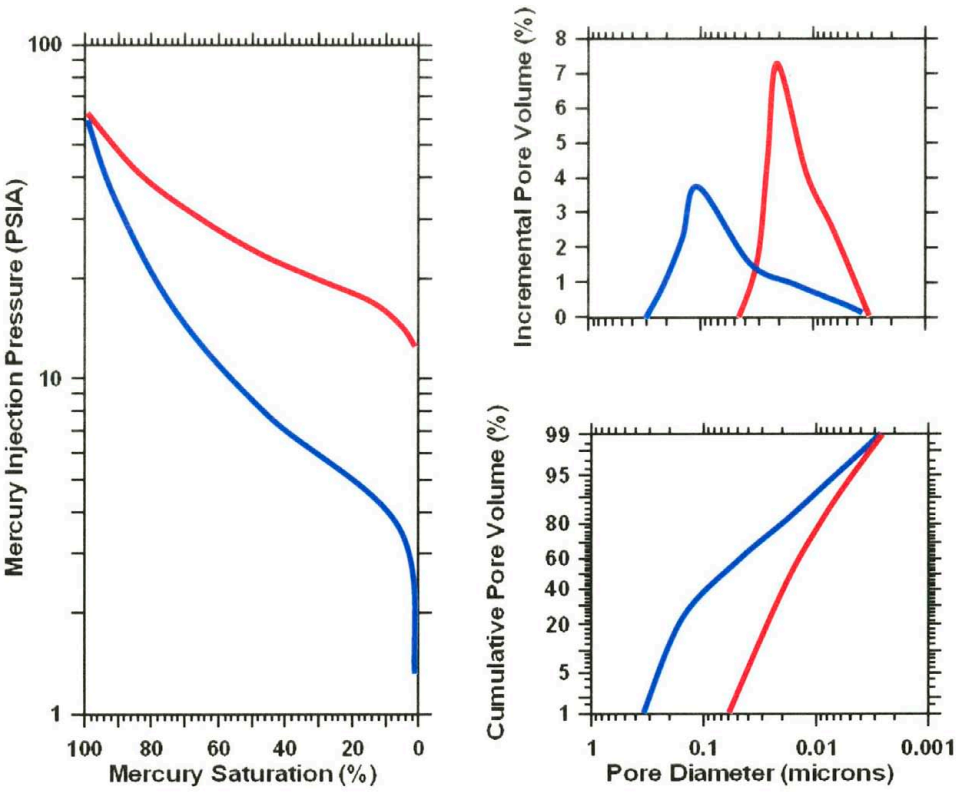

Figure 5.36 MICP curves for the low and high sealing samples. The red curves are the good sealing capacity samples and the blue curves represent the poor sealing capacity samples.

Figure 6.2 Sample L7-1, which exhibits the best sealing capacity of 7,667 psia. Inset picture is a photo of the thin section with no magnification. Scale in hand sample photo is in inches and centimeters. Inset photo is 36mm across

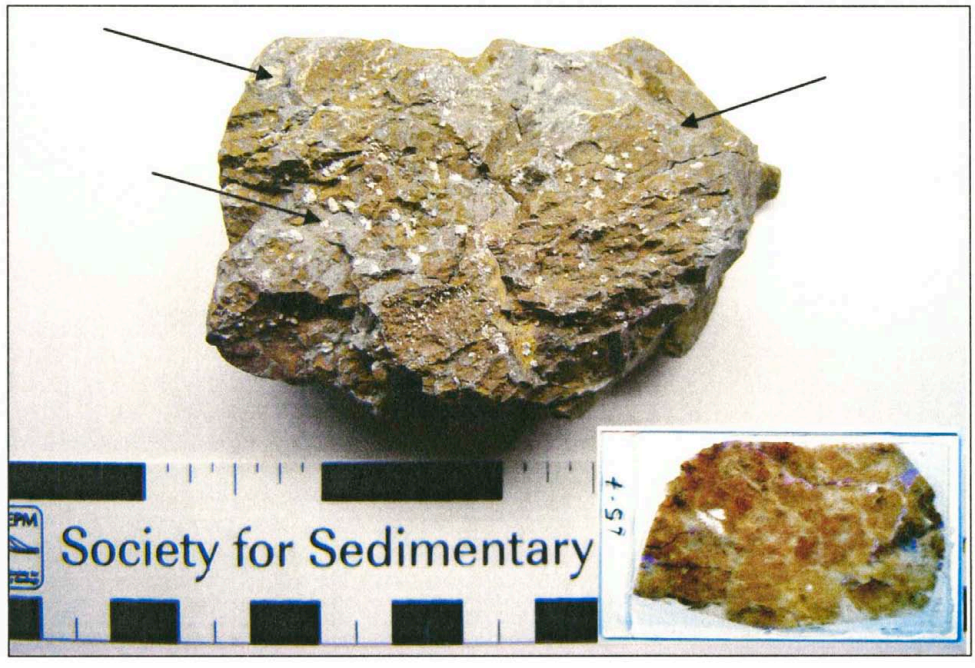

Figure 6.3 Sample L5-7, which exhibits the second best sealing capacity of 7,578 psia. Inset picture is a photo of the thin section with no magnification. Scale in hand sample photo is in inches and centimeters. Inset photo is 36mm across. Arrows indicate possible paleo-root structures.

Figure 6.4 Sample L4-4, which exhibits the poorest sealing capacity of 467 psia. Inset picture is a photo of the thin section with no magnification. Scale in hand sample photo is in inches and centimeters. Inset photo is 36mm across

Figure 6.5 Sample L5-13, which exhibits poor sealing capacity of 970 psia. Inset picture is a photo of the thin section with no magnification. Scale in hand sample photo is in inches and centimeters. Inset photo is 36mm across.

Retallack (1984) provides criteria (Table 6.1) that can be used to help determine the degree of development for paleosols.

Table 6.1 Stages of Paleosol Development

Stages	Features
Very Weakly Developed	Little evidence of soil development apart from root traces; abundant sedimentary, metamorphic, or igneous textures remaining from parent material.
Weakly Developed	With a surface rooted zone (A horizon), as well as incipient subsurface clayey, calcareous, sesquioxidic, or humic, or surface organic horizons, but not developed to the extent that they would qualify as USDA argillic, spodic, or calcic horizons or histic epipedon.
Moderately Developed	With surface rooted zone and obvious subsurface clayey, sesquioxidic, humic, or calcareous or surface organic horizons; qualifying as USDA argillic, spodic or calcic horizons or histic epipedon, and developed to an extent at least equivalent to stage II of calcic horizons.
Strongly Developed	With especially thick, red, clayey, or humic subsurface (B) horizons, or surface organic horizons (coals or lignites), or especially well-developed soil structure, or calcic horizons at stages III to IV.
Very Strongly Developed	Unusually thick subsurface (B) horizons, or surface organic horizons (coals or lignites), or calcic horizons of stage VI; such a degree of development is mostly found at major geologic unconformities.

From: Brewer, 1976

By using the above criteria, the twelve samples from the upper 15% of the distribution would be placed into the "strongly developed" stage as there are slickensides present and well developed soil structure. The samples from the bottom 15% of the distribution would be placed into the "very weakly developed" stage, as they have limited soil structure development, presence of roots, and no slickensides to indicate high amounts of clay.

Samples that are good seals exhibit angular blocky to subangular blocky soil structures or pedons (Figure 6.2 and Figure 6.3, respectively), which are good indicators of paleosol development. The good seals also have multi-colored mottling, while the poor seals are fairly homogeneous in color. Mottling is another good indication of paleosol development. Possible paleo-root structures, indicating paleosol development, are visible in Figure 6.3. Also present in the good seals, are slickensides (Figure 6.6),

which are caused by the shrinking and swelling of the clay minerals that are located in the samples. These slickensides are common in vertisols that typically contain large amounts of clay. Al Al-Anboori (2003) and Lorenz and Nadon (2002) noted fossil vertisols near the study area, which supports the findings of this project.

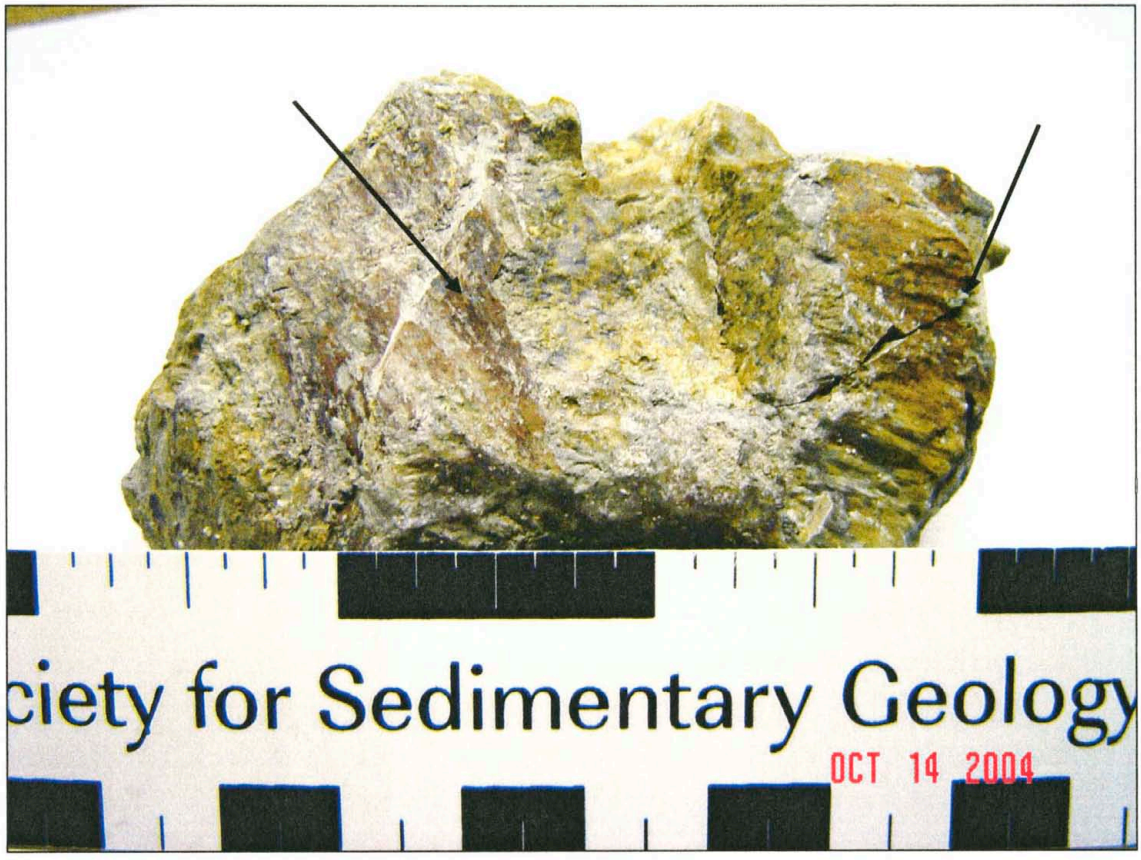

Figure 6.6 Slickensides are present in may of the samples have good sealing capacity. Slickensides are an indicator of clay minerals, which shrink and swell during wet and dry times. Arrows indicate slickensides. Scale is in inches and centimeters.

Figure 6.7 shows a distribution of sealing capacity versus stratigraphic position for location L4 from the PPU. Good seals have been indicated with a blue dot and poor seals are indicated with a red dot. The graph indicates that there are poor seals, 606, 467, and 1005 psia, directly below a sample with good sealing capacity. Multi-colored mottling is present near the top of the photograph, as well as possible paleo-root

structures (gray features). This sampling location shows how the texture of the samples varies with sealing capacity.

The relationship that was seen at location L4 is not visible at all sample locations. It is believed that modern weathering effects are masking the ability to see paleosol development at all locations. Figure 6.8 shows three of the best seals and three of the poorest seals in thin section.

The striking differences between the good and poor seals in thin section are the quantity and size of the quartz grains that are present. The poor seals have higher quantities of larger size quartz grains than the good seals (Figure 6.8). The reason for the differences seen in the quartz grain sizes and amounts is not readily apparent. Less developed paleosols retain more characteristics of their parent material (Almon, 2004, personal communication). Data collected during this project is insufficient to indicate if paleosol development affected the quartz grain sizes and quantities. It is possible that difference in grain size of the samples may be caused by primary deposition rather than paleosol development.

The Wasatch paleosols developed on flood plain deposits, which could have contained large amounts of sand sized quartz grains left behind during floods. Paleosols with poor sealing capacities might have formed in areas of the floodplain that received inputs of coarser detritus more frequently. Consequently, these paleosols have characteristics that are more representative of the parent material.

The samples at the top of the distribution have lesser amounts of sand sized quartz grains, which may be a function of deposition location. These samples may have been

located on areas of the floodplain where energy was low and infrequent, and the quartz grains were unable to be transported to these locations.

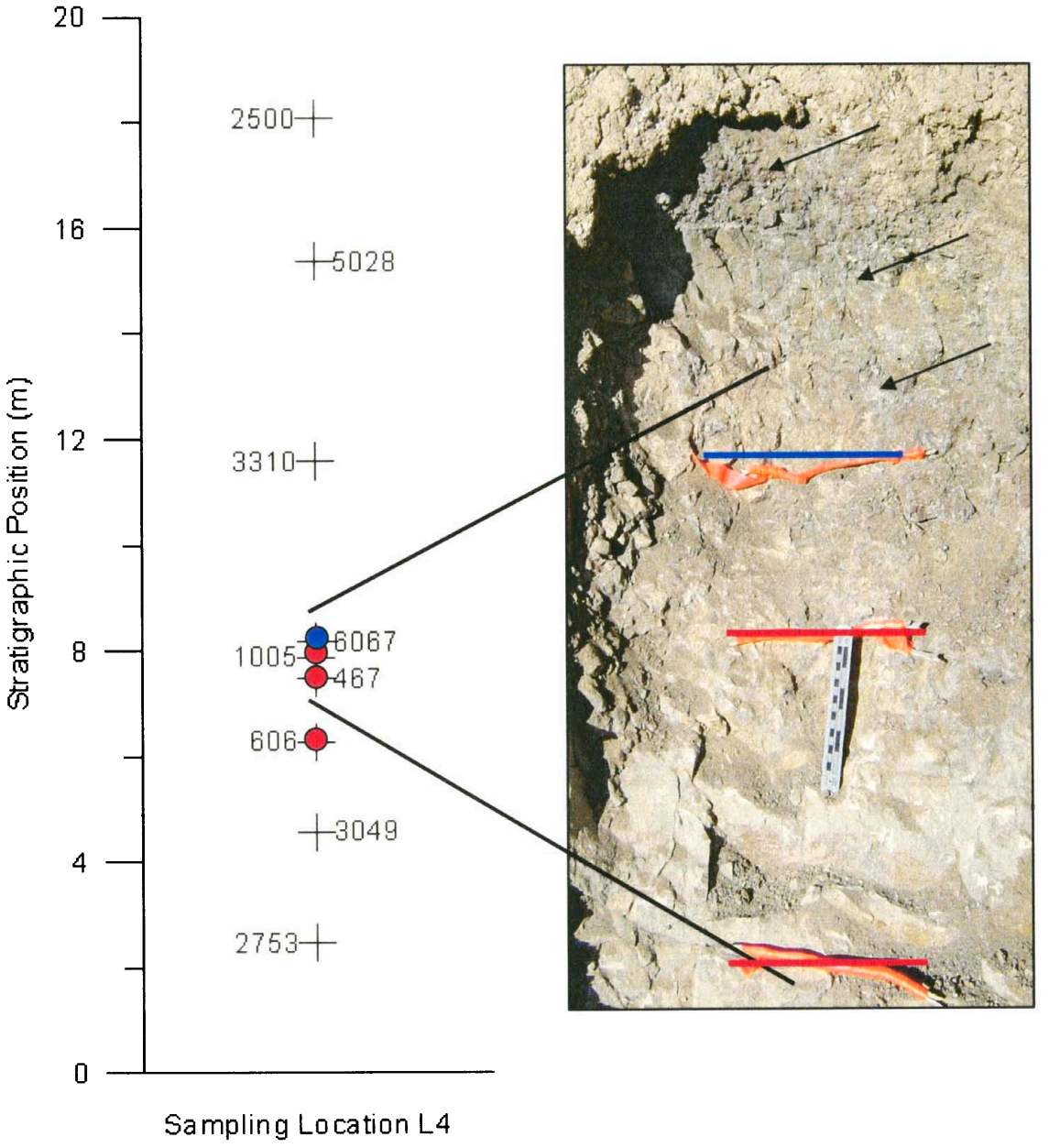

Figure 6.7 10% saturation values versus stratigraphic position for location L4, with good seals identified with a blue dot and poor seals indicated with a red dot. Photograph shows that better developed paleosols have higher sealing capacities. Possible paleo-roots indicated with arrows.

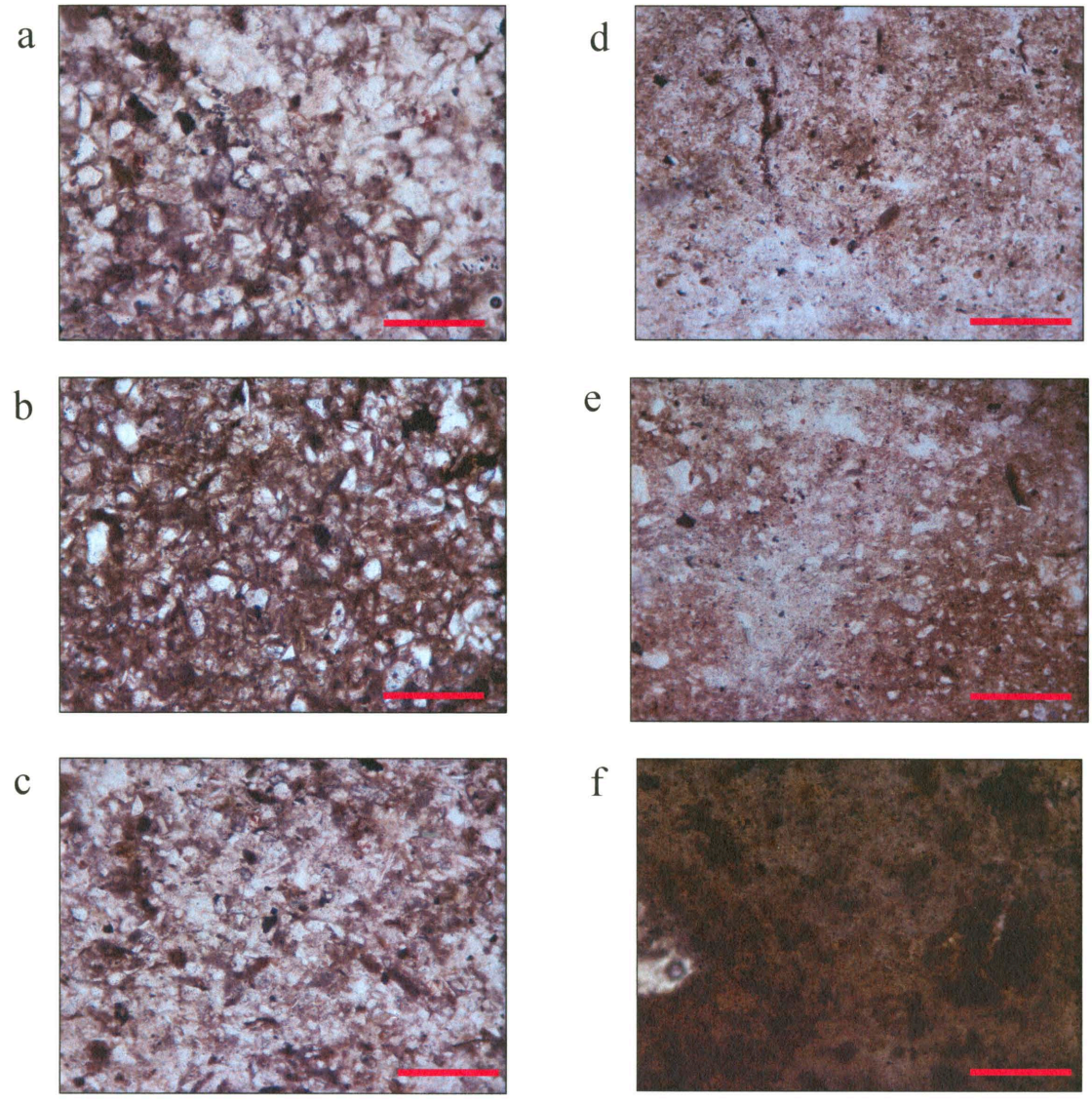

Figure 6.8 Poor sealing capacity samples (a-c) and good sealing capacity samples (d-f) in thin section, magnified 10X with uncrossed polars. Red Scale is 0.2mm.

Using the data collected during this project it is impossible to determine if paleosol development had an effect on the sealing capacity of paleosols.

6.3 Paleosol Position and Sealing Capacity

The location of the paleosol horizons within the soil profile could not be accurately determined in this study. Modern weathering effects have masked individual

paleosol horizons and so comparison of sealing capacity and soil horizons could not be made. A mass-balance model was used to determine if gains and losses of elements as reflected in XRF data could be tied to soil horizon development in the paleosols. The model works by determining open-chemical-system gains and losses in soil profiles in relation to parent material. It uses a relatively immobile element, such as titanium or zircon to measure the gains and losses. The bulk density of each sample and the thickness of each horizon sampled are necessary inputs to the mass-balance model. The model works well on igneous rocks, which have a homogenous parent material. The model may not perform well on sedimentary rocks due to the heterogeneity of the parent material.

XRF titanium data were used for this project as the immobile element to compare data losses and gains. The parent material was assumed to be the least developed paleosol that was visible in the outcrop. Samples collected above the assumed parent material were used to determine if any losses or gains of elements could help determine horizon boundaries that were not visible in outcrop.

Model results were inconclusive, as the model is derived from inputs of parent material. The parent material was derived from flood deposits, which were sorted during deposition. This sorting of the grains is what caused the model to work incorrectly.

Paleosol position relative to paleo-channels was analyzed to determine if any relationship exists. Brown and Kraus (1987) designed a model that attempts to relate soil development to sedimentation rate across the floodplain. It predicts that soil development increases laterally, away from active channels, because of the decrease in sedimentation rate and the frequency of flooding. This indicates that poorly developed soils generally

form near the channel where sediment accumulation rate is rapid. Well developed soils form on the distal floodplain where accumulation rates are extremely slow. Vertical variations in soil development within stacked paleosol packages reflect the progression of channel migration and avulsion across the floodplain. This shows that the vertical increase in soil development depends on the channel moving or avulsing. Thus, allowing soil formation to occur in the floodplain without disturbance from the channel (Ali Al-Anboori, 2003).

Data are not available to determine if a relationship exists between distance from paleo-channels and sealing capacity. Although the samples that have good sealing capacity do not appear to be close to paleo-channels, there might be a channel deposit in the subsurface that is not visible at the level of the outcrop. Good seals in the study area are located in well developed paleosols either above or below visible channels.

The question, "What is controlling the texture of the paleosol samples that were collected from the Shire Member of the Wasatch Formation?" is not easily answered. The texture visible in the samples may be a result of deposition or a function of paleosol development. Good sealing capacity rocks for this project came from areas where the paleosols were visibly better developed. The cause of this development cannot be determined from the data collected for this project. Development may be related to soil forming processes or simply to location and lack of coarse-grained sediment input. Well developed paleosols from the Wasatch Formation have higher amounts of clay, lower percentages of quartz grains, and smaller quartz grains. All other variables being equal, time exposed to the elements and sediment input is controlling the sealing capacity of the paleosols.

Chapter 7. Conclusions

Paleosol samples from an outcrop of the Eocene Wasatch Formation northwest of Rifle, Colorado have been studied to evaluate the hypothesis that paleosols with higher sealing capacities as determined from MICP analyses will have lower percentages of quartz grains and a smaller average quartz grain size. These paleosols will also have higher clay contents as determined by thin sections and XRF analysis. The hypothesis was used to evaluate the lateral variability in the sealing capacity of the paleosols relative to themselves.

Samples were collected from two paleosol packages (PPL and PPU) at eight different locations of cumulate paleosols that were developed in flood plain deposits in a fluvial environment. Paleosol properties have been characterized by using mercury injection capillary pressure tests, thin-section petrography, total organic and inorganic carbon analyses, and X-ray fluorescence bulk geochemistry. Correlation statistics were used to compare sealing capacity to various other variables to evaluate which variables, if any, have a relationship with the sealing capacity of the paleosols.

Samples with high sealing capacity are characterized by small silt grain size, high clay and low grain content, small and well sorted pore-throat diameters and visible paleosol structures, low TOC and higher grain density. No significant relations were found between adjacent paleosol packages or among lithofacies. Microfacies, determined on the basis of quartz grain size in thin-section do show a relationship with sealing capacity, with finer-grained microfacies having higher sealing capacities.

The question, "What is controlling the texture of the paleosol samples that were collected from the Shire Member of the Wasatch Formation?" is not easily answered. The texture visible in the samples may be a result of deposition, diagenesis, paleosol development or some combination of these processes. However, high sealing capacity is associated with samples that have multicolored mottling, angular to subangular peds, slickensides, and paleo-root structures

Lateral variability in the sealing capacity of paleosols is common in the samples that were collected. A clear relationship between sealing capacity and distance from a paleo-channel could not be determined from available data. Samples with good sealing capacity were not located directly above or below a visible paleo-channel in the outcrop.

Further studies could shed light on some of the other questions that were highlighted by this project. Seismic data may provide detail to the location and direction of channel deposits that are not visible in outcrop. Detailed outcrop work may help determine location of the paleosols relative to the channels that are visible. Further laboratory work may include micro-fabric studies of the thin-sections to help quantify paleosol development, and X-Ray diffraction could be used to identify any relationships that may exist between clay types present and sealing capacity.

References Cited

Ali Al-Anboori, S. 2003. Low Net-to Gross Fluvial Reservoirs: Sedimentary Architecture and Geochemical Correlation. PhD Thesis, University of Aberdeen, p. 146.

Almon, W.R., Dawson, W.C., Sutton, S.J., Ethridge, F.G., Castelblanco, B., 2001. Sequence Stratigraphy, Petrophysical Variation, and Sealing Capacity in Deepwater Shales, Upper Cretaceous Lewis Shale, South-Central Wyoming. Wyoming Geological Association Guidebook-Fifty Second Field Conference-2001, p. 163-182.

Almon, W.R., Dawson, W.C., 2000. Paleosols as Top Seals for Nonmarine Petroleum Systems; central Sumatra Basin, Indonesia. AAPGBulletin, v. 84, no. 9, p.1397

Almon, W.R., Thomas, J.B., 1991. Pore System Aspects of Hydrocarbon Trapping, in Gluskoter, H.J., Rice, D.D., and Taylor, R.B., eds., Economic Geology, U.S. Boulder, Colorado, Geological Society of America, The Geology of North America, v. P-2, p. 241-254.

Bates, R.L., Jackson, J.A., eds., 1984. Dictionary of Geological Terms, Third Edition. Prepared by The American Geological Institute, Doubleday, New York, p. 571.

Birkeland, P.W., 1999. Soils and Geomorphology, Third Edition. New York, Oxford University Press, p. 432.

Boult, P.J., Theologou, P.N., Foden, J., 1997. Capillary Seals Within the Eromanga Basin, Australia: Implications for Exploration and Production. In: Seals, Traps, and the Petroleum System (ed. by Surdam, Ronald C.) AAPG Memoir, vol. 67, p. 143-167.

Brewer, R., 1976. Fabric and Mineral Analysis of Soils, 2nd edn., New York, Krieger, p. 482.

Brown, T.M., Kraus, M.J.1987. Integration of Channel and Floodplain Suites, I. Developmental Sequence and Lateral Relations of Alluvial Paleosols. Journal of Sedimentary Petrology, v. 57, p. 587-601.

Cole, R., Cumella, S., 2003. Stratigraphic Architecture and Reservoir Characteristics of the Mesaverde Group, Southern Picenace Basin, Colorado, in Peterson, K.M., Olson, T.M., Anderson, D.S., eds. Piceance Basin Guidebook 2003. The Rocky Mountain Association of Geologists, Denver, Colorado, p. 460.

Donnell, J.R, 1969. Paleocene and Lower Eocene Units in the Southern Part of the Piceance Creek Basin, Colorado. Bulletin Report: B1274-M, U. S. Geological Survey, Reston, VA, p. 18.

Downey, M.W., 1984. Evaluating Seals for Hydrocarbon Accumulations. AAPG Bulletin, v. 68, No. 11, p. 1752-1763.

Dragomirescu, R., Kaldi, J., Lemon, N., Alexander, E., 2001. Triassic Seals in the Cooper Basin. Eastern Australasian Basins Symposium, v. 1, p. 311-320.

Holliday, V.T., 2004. Soils, Paleosols, and Geosols: A Commentary. Department of Geography, University of Wisconsin, Madison, http://fadr.msu.ru/inqua/nl-15/discussion2.htm.

Jennings, J.B., 1987. Capillary Pressure Techniques: Applications to Exploration and Development Geology. AAPG Bulletin, v. 71, No. 10, p.1196-1209.

Jiao, Z.S., Surdam, R.C., 1997. Characteristics of Anomalously Pressured Cretaceous Shales in the Laramide Basins of Wyoming. In: Seals, Traps, and the Petroleum System (ed. by Surdam, R.C.) AAPG Memoir, vol. 67, p. 243-253.

Jiao, Z.S., Surdam, R.C., 1994. Paleosols, Capillary Seals, and Pressure Compartment Boundaries in the Muddy Sandstone of the Powder River Basin, Wyoming. 1994 Abstracts with Programs, vol. 26, no. 6 p. 21.

Johnson, R.C., Flores, R.M., 2003. History of the Piceance Basin from Latest Cretaceous Through Early Eocene and the Characterization of Lower Tertiary Sandstone Reservoirs, in Peterson, K.M., Olson, T. M., Anderson, D.S., eds. Piceance Basin Guidebook 2003. The Rocky Mountain Association of Geologists, Denver, Colorado, p. 460.

Johnson, R.C., 1989. Geologic History and Hydrocarbon Potential of Late Cretaceous-Age, Low-Permeability Reservoirs, Piceance Basin, Western Colorado. USGS Survey Bulletin 1787-E, U.S. Government Printing Office, Denver, Colorado, p. 51.

Kaldi, J.G. and Atkinson, C.D., 1997. Evaluating seal potential; example from the Talang Akar Formation, offshore northwest Java, Indonesia. In: Seals, Traps, and the Petroleum System (ed. by Surdam, Ronald C.) AAPG Memoir, vol. 67, p. 85-101.

Lorenz, J.C., Nadon, G.C., 2002. Braided-River Deposits in a Muddy Depositional Setting: The Molina Member of the Wasatch Formation (Paleogene), West-Central Colorado, U.S.A. Journal of Sedimentary Research, v. 72, no. 3, p. 376-385.

Lyons, W.J. III, 2000. Interpreting Avulsion Processes from Ancient Fluvial Deposits: Wasatach Formation, West-Central Colorado, Master's Thesis, University of Wyoming, p. 48.

Obligado, A., 2002. Sealing Capacity, Shale Characteristics, and Sequence Stratigraphy of the Juncal Formation, Ventura Basin, Southern California, Master's Thesis, Colorado State University, p. 146.

Pemberton, S.G., Frey, R.W., Ranger, M.J., and MacEachern, J., 1992. The Conceptual Framework of Ichnology. In: Applications of Ichnology to Petroleum Exploration (ed. by S.G. Pemberton). SEPM (Society for Sedimentary Geology) Core Workshop, no. 17, p.1-32.

Pittman, E.D., 1992. Relationship of Porosity and Permeability to Various Parameters Derived from Mercury Injection Capillary Pressure Curves for Sandstone. AAPG Bulletin, vol. 76, no. 2, p. 191-198.

Retallack, G.J., 1997. A Colour Guide to Paleosols. West Sussex, John Wiley and Sons, p. 188.

Retallack, G.J., 2001. Soils of the Past, An Introduction to Paleopedology, Second Edition. Blackwell Science, Oxford, p. 404.

Retallack, G.J., 1997, A Colour Guide to Paleosols: West Sussex, John Wiley and Sons, p. 188.

Schieber, J., 1999. Distribution and Deposition of Mudstone Facies in the Upper Devonian Sonyea Group of New York. Journal of Sedimentary Research, vol. 69, no. 4, p. 909-925.

Schowalter, T.T., 1979. Mechanics of Secondary Hydrocarbon Migration and Entrapment. AAPG Bulletin, v. 63, p. 723-760.

Sherrod, L.A., Dunn, G., Peterson, G.A., Kolberg, R.L., 2002. Inorganic Carbon Analysis by Modified Pressure-Calcimeter Method. Soil Science of America Journal, vol. 66 p. 299-305.

Shroba, R.R., Scott, R.B., 1997. Revised Preliminary Geologic Map of the Rifle Quadrangle, Garfield County, Colorado. Open-File Report 97-852, United States Geological Survey, Denver Colorado, p. 20.

Sutton, S.J., Ethridge, F.G., Almon, W.R., Dawson, W.C., Edwards, K.K., 2004. Textural and Sequence-Stratigraphic Controls on Sealing Capacity of Lower and Upper Cretaceous Shales, Denver Basin, Colorado. AAPG Bulletin, v. 88 no. 8 p. 1185-1206.

Vavra, C.L., Kaldi, J.G., Sneider, R.M., 1992. Geological Applications of Capillary Pressure: A Review. AAPG Bulletin, v. 76, No. 6, p. 840-850.

APPENDIX A

MICP DATA

Wasatch Outcrop Sample #s:	Sample Location	Porotech. Spl No.	Stratigraphic Position	Median Pore Aperature Dia. (microns)	MICP Closure (psia) Porotech data	Pororтech's Closure	Author's Closure (psia)	Author's Closure	10% Saturation (psia)
Wast-B1-1	1	1	0.35	0.026	2157	0.0039	1442	0.0035	3161
Wast-B1-2	1	2	0.8	0.019	2589	0.0043	3194	0.0043	4465
Wast-B1-3	1	3	1	0.030	1258	0.0065	1258	0.0065	2190
Wast-B1-4	1	4	1.1	0.028	1258	0.0043	1203	0.0043	1967
Wast-B1-5	1	5	1.3	0.030	1381	0.0072	1648	0.0080	2656
Wast-B1-6	1	6	1.7	0.024	1508	0.0086	1810	0.0090	2901
Wast-B1-7	1	7	2.2	0.027	1509	0.0065	1147	0.0063	3194
Wast-B1-8	1	8	2.4	0.033	1049	0.0033	1261	0.0030	2305
Wast-B1-9	1	9	2.6	0.026	1510	0.0033	2159	0.0031	2935
Wast-B1-10	1	10	3.1	0.032	1149	0.0035	1379	0.0036	2154
Group Average				0.028	1537	0.0051	1650	0.0052	2793
Group Median				0.028	1445	0.0043	1410	0.0043	2779
Group Std. Dev.				0.004	479	0.0019	627	0.0022	733
Wast-B2-1	2	1	0.2	0.020	2368	0.0051	2834	0.0051	4968
Wast-B2-2	2	2	0.6	0.017	2588	0.0078	1977	0.0077	5525
Wast-B2-3	2	3	1.1	0.018	2827	0.0059	275	0.0050	5163
Wast-B2-4	2	4	1.5	0.017	3098	0.0048	2368	0.0048	6722
Wast-B2-5	2	5	2	0.020	2591	0.0030	3496	0.0022	5941
Wast-B2-6	2	6	2.3	0.025	1050	0.0047	734	0.0046	2447
Wast-B2-7	2	7	2.8	0.022	2587	0.0045	1979	0.0044	5078
Wast-B2-8	2	8	3.4	0.024	1380	0.0038	1205	0.0037	3190
Wast-B2-9	2	9	4.1	0.017	3387	0.0046	4184	0.0042	6257
Wast-B2-10	2	10	4.5	0.021	2827	0.0034	3988	0.0027	5108
Group Average				0.020	2470	0.0048	2304	0.0044	5040
Group Median				0.020	2590	0.0047	2174	0.0045	5136
Group Std. Dev.				0.003	726	0.0014	1337	0.0015	1314
Wast-L1-2	3	2	0.85	0.022	2826	0.0022	4436	0.0028	5318
Wast-L1-3	3	3	1.7	0.022	2367	0.0039	3494	0.0048	4843
Wast-L1-4	3	4	3.9	0.028	1807	0.0030	3762	0.0044	4322
Wast-L1-5	3	5	4	0.029	1977	0.0030	3710	0.0041	4325
Wast-L1-6	3	6	4.1	0.030	1649	0.0030	3316	0.0038	4035
Wast-L1-7	3	7	7	0.068	515	0.0026	595	0.0028	837
Wast-L1-8	3	8	1	0.025	2828	0.0028	3884	0.0030	4839
Wast-L1-9	3	9	2.7	0.024	2369	0.0042	3495	0.0050	4998
Wast-L1-10	3	10	6.4	0.032	1508	0.0034	2868	0.0045	3513
Wast-L1-11	3	11	10.2	0.030	1258	0.0138	1977	0.0152	1919
Group Average				0.031	1910	0.0042	3154	0.0050	3895
Group Median				0.029	1892	0.0030	3494	0.0043	4324
Group Std. Dev.				0.013	724	0.0034	1112	0.0037	1446

Wasatch Outcrop Sample #s:	Sample Location	Porotech. Spl No.	Stratigraphic Position	Median Pore Aperature Dia. (microns)	MICP Closure (psia) Porotech data	Porortech's Closure	Author's Closure (psia)	Author's Closure	10% Saturation (psia)
Wast-L3-1	4	1	6.5	0.025	2370	0.0035	4185	0.0047	4803
Wast-L3-2	4	2	9.5	0.072	965	0.0026	1334	0.0030	1601
Wast-L3-4	4	4	17.9	0.058	299	0.0027	391	0.0031	618
Wast-L3-5	4	5	20.3	0.024	1978	0.0041	3156	0.0050	4014
Wast-L3-6	4	6	24.6	0.031	1258	0.0030	1808	0.0030	2733
Wast-L3-7	4	7	2.4	0.032	1648	0.0020	2854	0.0029	3365
Wast-L3-8	4	8	4.3	0.003	1809	0.0027	2829	0.0032	3355
Wast-L3-9	4	9	5.6	0.031	1978	0.0036	2862	0.0040	3538
Wast-L3-10	4	10	7.7	0.026	2367	0.0048	3011	0.0048	4189
Wast-L3-11	4	11	8..5	0.028	2158	0.0029	3788	0.0035	4679
Wast-L3-12	4	12	12.7	0.041	564	0.0077	612	0.0081	1263
Group Average				0.034	1581	0.0036	2439	0.0041	3105
Group Median				0.031	1809	0.0030	2854	0.0035	3365
Group Std. Dev.				0.018	715	0.0016	1239	0.0015	1402
Wast-L4-1	5	1	2.4	0.030	1257	0.0041	1150	0.0043	2753
Wast-L4-2	5	2	4.5	0.027	1046	0.0031	2220	0.0039	3049
Wast-L4-3	5	3	6.2	0.094	390	0.0032	443	0.0034	606
Wast-L4-4	5	4	7.4	0.117	209	0.0028	241	0.0030	467
Wast-L4-5	5	5	7.8	0.063	562	0.0025	746	0.0023	1005
Wast-L4-6	5	6	8.1	0.020	2828	0.0030	4683	0.0030	6067
Wast-L4-7	5	7	11.5	0.034	1648	0.0036	2230	0.0038	3310
Wast-L4-8	5	8	15.3	0.019	2588	0.0035	3602	0.0035	5028
Wast-L4-9	5	9	18	0.021	1049	0.0049	1148	0.0054	2500
Group Average				0.047	1286	0.0034	1829	0.0036	2754
Group Median				0.030	1049	0.0032	1150	0.0035	2753
Group Std. Dev.				0.036	922	0.0007	1506	0.0009	1921
Wast-L5-1	6	1	2.1	0.110	391	0.0032	391	0.0032	571
Wast-L5-2	6	2	5	0.050	1376	0.0023	1702	0.0023	2436
Wast-L5-3	6	3	7.5	0.112	393	0.0038	393	0.0038	579
Wast-L5-4	6	4	8.25	0.033	1509	0.0033	2298	0.0033	3700
Wast-L5-5	6	5	10.1	0.022	2581	0.0028	4286	0.0028	5824
Wast-L5-6	6	6	12.5	0.024	2160	0.0032	3549	0.0032	4803
Wast-L5-7	6	7	14.5	0.017	3387	0.0035	5432	0.0035	7578

Wasatch Outcrop Sample #s:	Sample Location	Porotech. Spl No.	Stratigraphic Position	Median Pore Aperature Dia. (microns)	MICP Closure (psia) Porotech data	Porortech's Closure	Author's Closure (psia)	Author's Closure	10% Saturation (psia)
Wast-L5-8-A	6	8	4.6	0.050	1258	0.0037	1579	0.0039	2527
Wast-L5-9-A	6	9	5.1	0.055	1259	0.0028	1688	0.0030	2332
Wast-L5-10-A	6	10	5.3	0.054	965	0.0021	1697	0.0029	2205
Wast-L5-11-A	6	11	5.6	0.042	1379	0.0034	2023	0.0040	2847
Wast-L5-12-A	6	12	5.8	0.052	1511	0.0022	1950	0.0022	2398
Wast-L5-13-B	6	13	6.5	0.078	560	0.0038	343	0.0042	970
Wast-L5-14-B	6	14	6.8	0.044	1376	0.0038	1753	0.0040	2569
Wast-L5-15-B	6	1	7.1	0.059	881	0.0028	1163	0.0028	1510
Wast-L5-16-B	6	2	7.3	0.031	1978	0.0031	2708	0.0031	3769
Wast-L5-17-B	6	3	7.6	0.034	1649	0.0024	2098	0.0024	3186
Wast-L5-18-B	6	4	7.9	0.034	1378	0.0031	2113	0.0031	3193
Group Average				0.050	1444	0.0031	2065	0.0032	2944
Group Median				0.047	1377	0.0032	1851	0.0032	2548
Group Std. Dev.				0.027	749	0.0006	1308	0.0006	1775
Wast-L6-11	7	5	4	0.086	468	0.0024	777	0.0024	1003
Wast-L7-1	8	1	0.5	0.018	3099	0.0032	6650	0.0040	7667
Wast-L7-2	8	2	1	0.018	2375	0.0025	3390	0.0025	6563
Wast-L7-3	8	3	1.7	0.033	1646	0.0031	2426	0.0033	3397
Wast-L7-4	8	4	2.5	0.023	2829	0.0033	4914	0.0033	5682
Wast-L7-5	8	5	3	0.026	2158	0.0029	3780	0.0031	5045
Wast-L7-6	8		3.7	0.032	1149	0.0040	805	0.0042	2100
Wast-L7-7	8	7	4.3	0.027	1808	0.0042	1083	0.0042	3574
Wast-L7-9	8	9	7	0.027	1258	0.0037	1808	0.0039	3317
Wast-L7-10	8	10	7.4	0.029	1050	0.0071	1101	0.0073	2695
Wast-L7-11	8	11	9.4	0.031	1047	0.0048	1047	0.0050	2536
Wast-L7-12	8	12	9.9	0.032	1151	0.0041	734	0.0043	2456
Group Average				0.027	1779	0.0039	2522	0.0041	4094
Group Median				0.027	1646	0.0037	1808	0.0040	3397
Group Std. Dev.				0.005	741	0.0013	1950	0.0013	1863

NOTE: All samples were dried at ~110C prior to MICP testing. Additionally, selected samples may have been subsampled and\or examined under a binocular microscope for proper MICP analysis. (from Porotech)

APPENDIX B

MICP CURVES

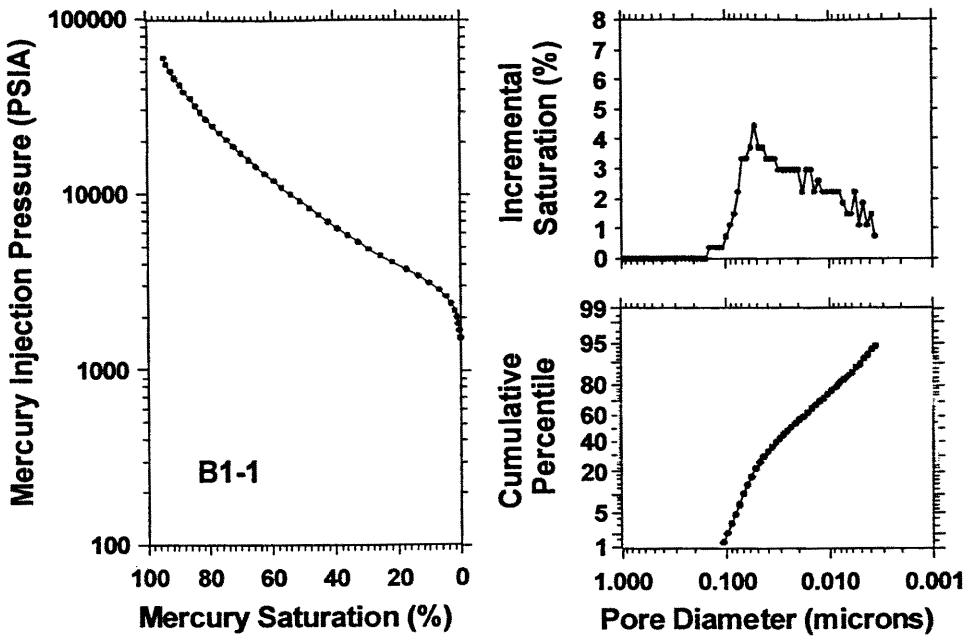
Mercury Injection Pressure (PSIA)
100000
10000
1000
100
B1-1
100 80 60 40 20 0
Mercury Saturation (%)
Incremental Saturation (%)
8 7 6 5 4 3 2 1 0
Cumulative Percentile
99 95 80 60 40 20 5 1
1.000 0.100 0.010 0.001
Pore Diameter (microns)

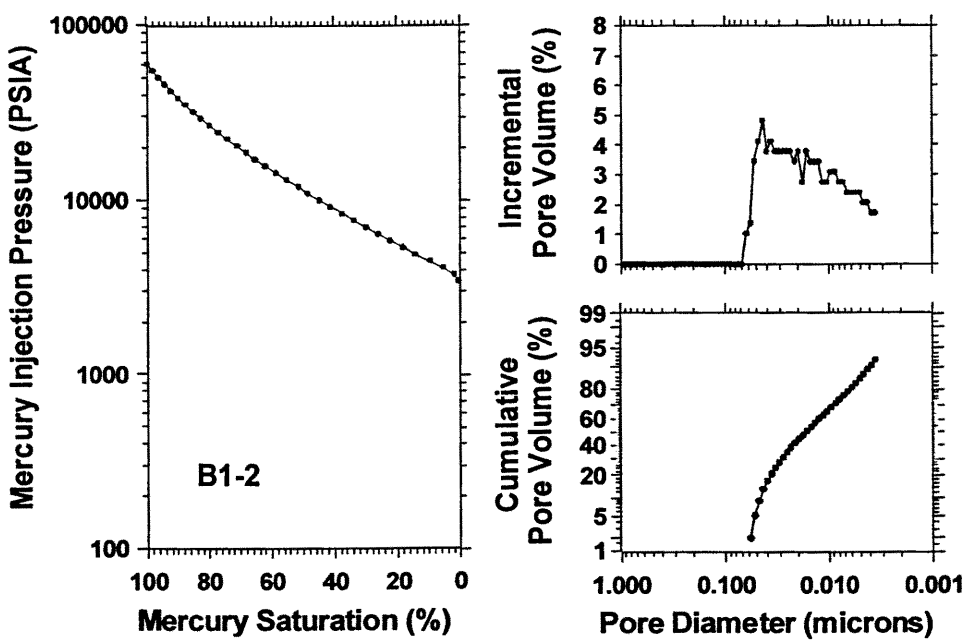
Mercury Injection Pressure (PSIA)
100000
10000
1000
100
B1-2
100 80 60 40 20 0
Mercury Saturation (%)
Incremental Pore Volume (%)
8 7 6 5 4 3 2 1 0
Cumulative Pore Volume (%)
99 95 80 60 40 20 5 1
1.000 0.100 0.010 0.001
Pore Diameter (microns)

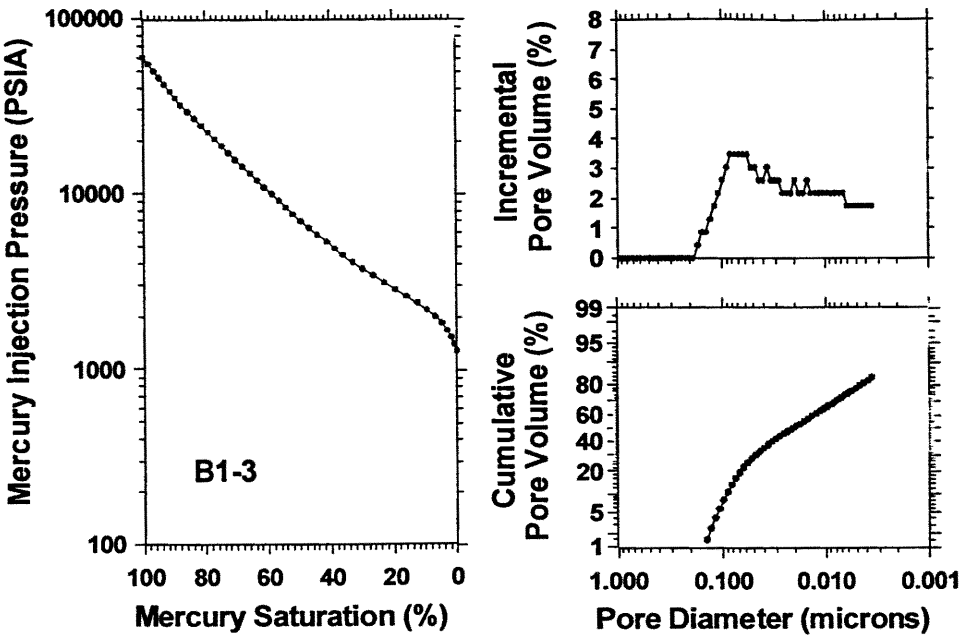
Mercury Injection Pressure (PSIA)
100000
10000
1000
100
B1-3
100 80 60 40 20 0
Mercury Saturation (%)
Incremental Pore Volume (%)
8 7 6 5 4 3 2 1 0
Cumulative Pore Volume (%)
99 95 80 60 40 20 5 1
1.000 0.100 0.010 0.001
Pore Diameter (microns)

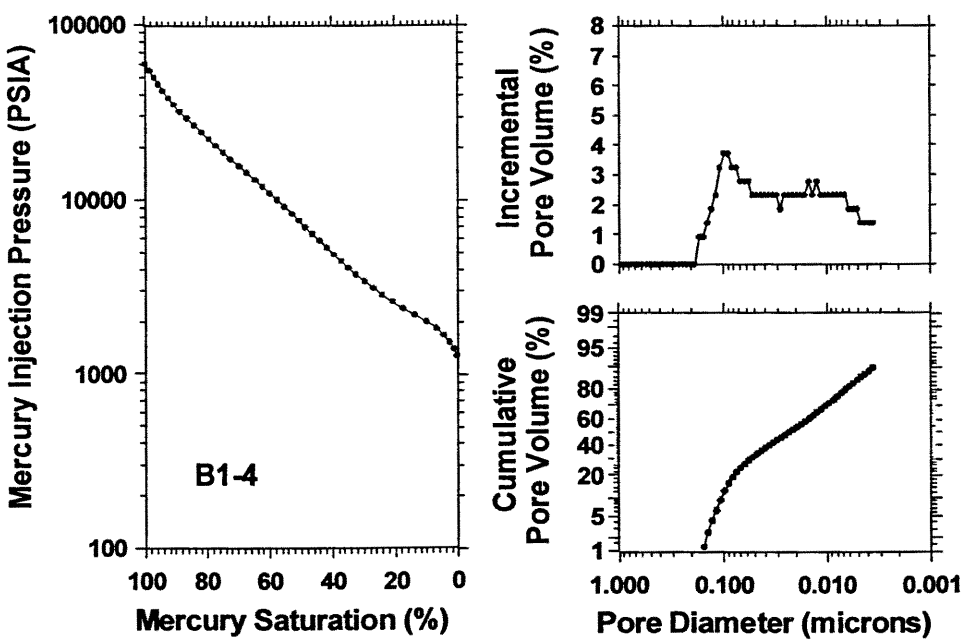
Mercury Injection Pressure (PSIA)
100000
10000
1000
100
B1-4
100 80 60 40 20 0
Mercury Saturation (%)
Incremental Pore Volume (%)
8 7 6 5 4 3 2 1 0
Cumulative Pore Volume (%)
99 95 80 60 40 20 5 1
1.000 0.100 0.010 0.001
Pore Diameter (microns)

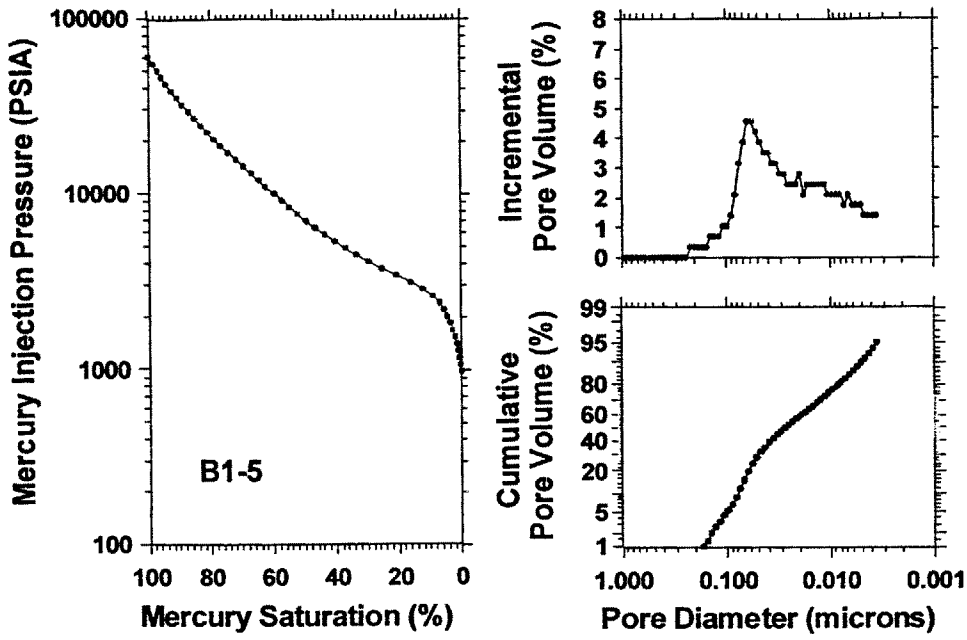
Mercury Injection Pressure (PSIA)
100000
10000
1000
100
B1-5
100 80 60 40 20 0
Mercury Saturation (%)
Incremental Pore Volume (%)
8 7 6 5 4 3 2 1 0
Cumulative Pore Volume (%)
99 95 80 60 40 20 5 1
1.000 0.100 0.010 0.001
Pore Diameter (microns)

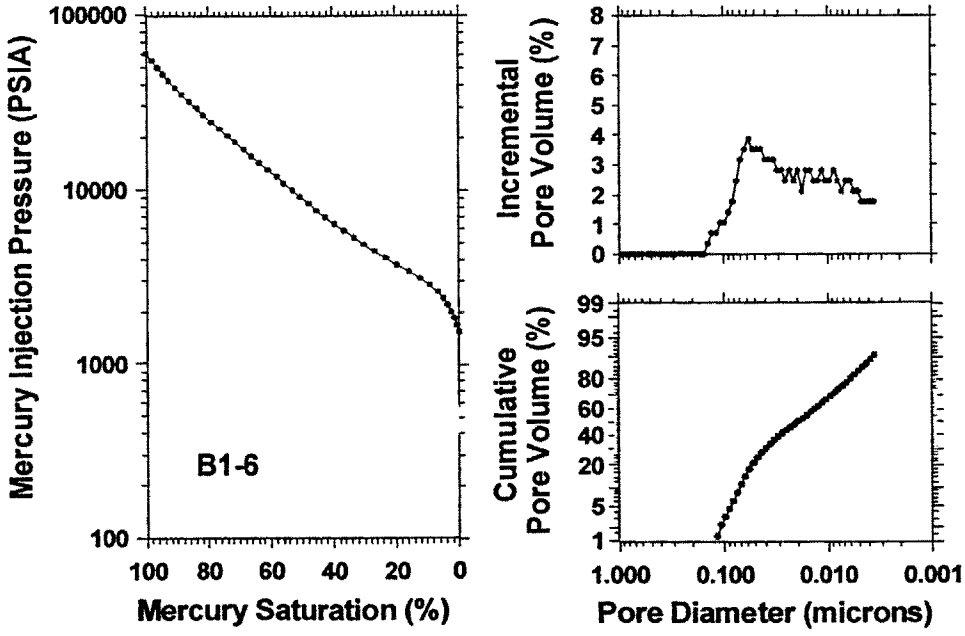
Mercury Injection Pressure (PSIA)
100000
10000
1000
100
B1-6
100 80 60 40 20 0
Mercury Saturation (%)
Incremental Pore Volume (%)
8 7 6 5 4 3 2 1 0
Cumulative Pore Volume (%)
99 95 80 60 40 20 5 1
1.000 0.100 0.010 0.001
Pore Diameter (microns)

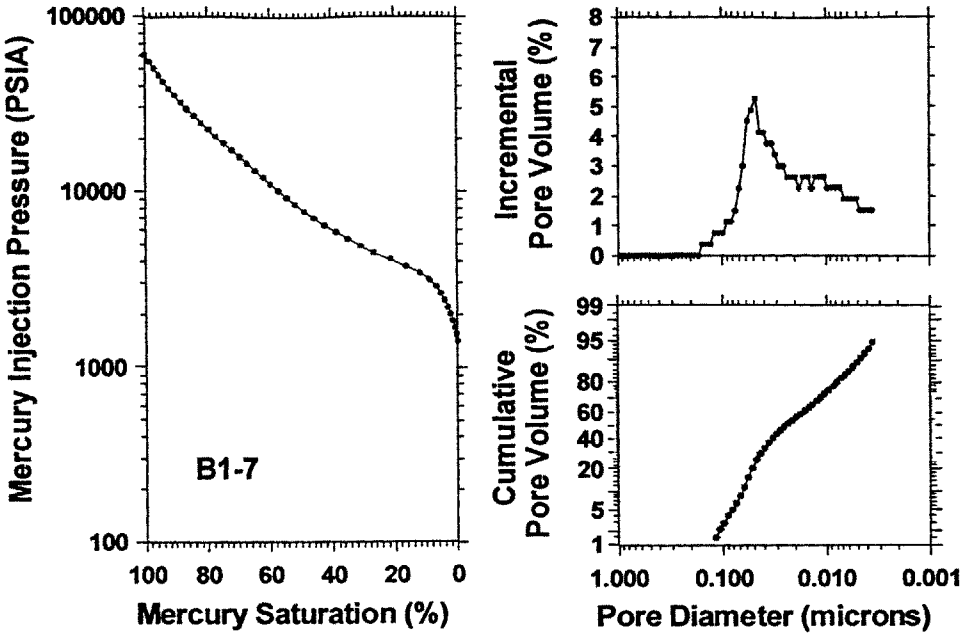
Mercury Injection Pressure (PSIA)
100000
10000
1000
100
B1-7
100 80 60 40 20 0
Mercury Saturation (%)
Incremental Pore Volume (%)
8 7 6 5 4 3 2 1 0
Cumulative Pore Volume (%)
99 95 80 60 40 20 5 1
1.000 0.100 0.010 0.001
Pore Diameter (microns)

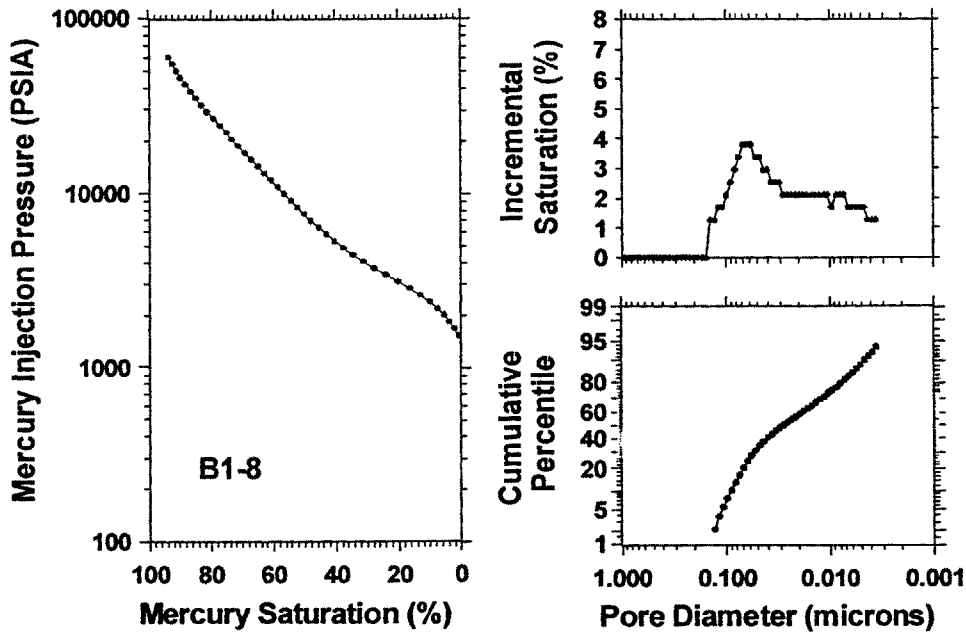
Mercury Injection Pressure (PSIA)
100000
10000
1000
100
B1-8
100 80 60 40 20 0
Mercury Saturation (%)
Incremental Saturation (%)
8 7 6 5 4 3 2 1 0
Cumulative Percentile
99 95 80 60 40 20 5 1
1.000 0.100 0.010 0.001
Pore Diameter (microns)

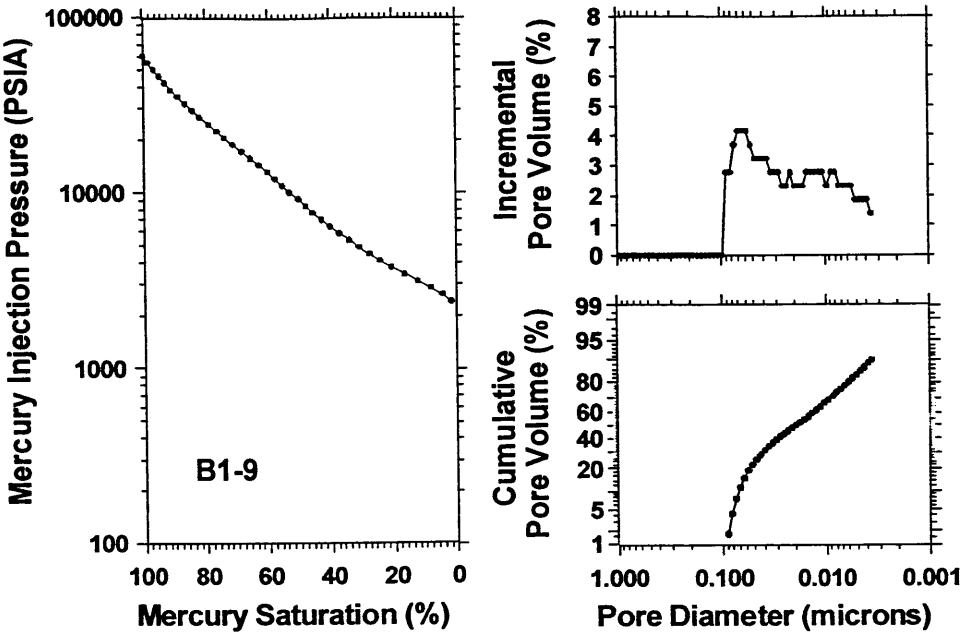
Mercury Injection Pressure (PSIA)
100000
10000
1000
100
B1-9
100 80 60 40 20 0
Mercury Saturation (%)
Incremental Pore Volume (%)
8 7 6 5 4 3 2 1 0
Cumulative Pore Volume (%)
99 95 80 60 40 20 5 1
1.000 0.100 0.010 0.001
Pore Diameter (microns)

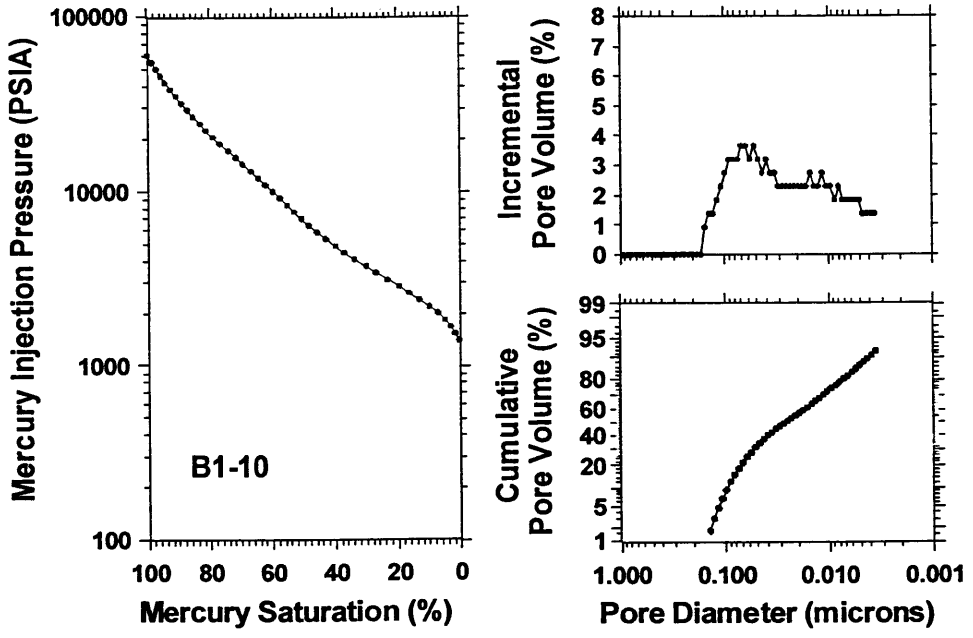
Mercury Injection Pressure (PSIA)
100000
10000
1000
100
B1-10
100 80 60 40 20 0
Mercury Saturation (%)
Incremental Pore Volume (%)
8 7 6 5 4 3 2 1 0
Cumulative Pore Volume (%)
99 95 80 60 40 20 5 1
1.000 0.100 0.010 0.001
Pore Diameter (microns)

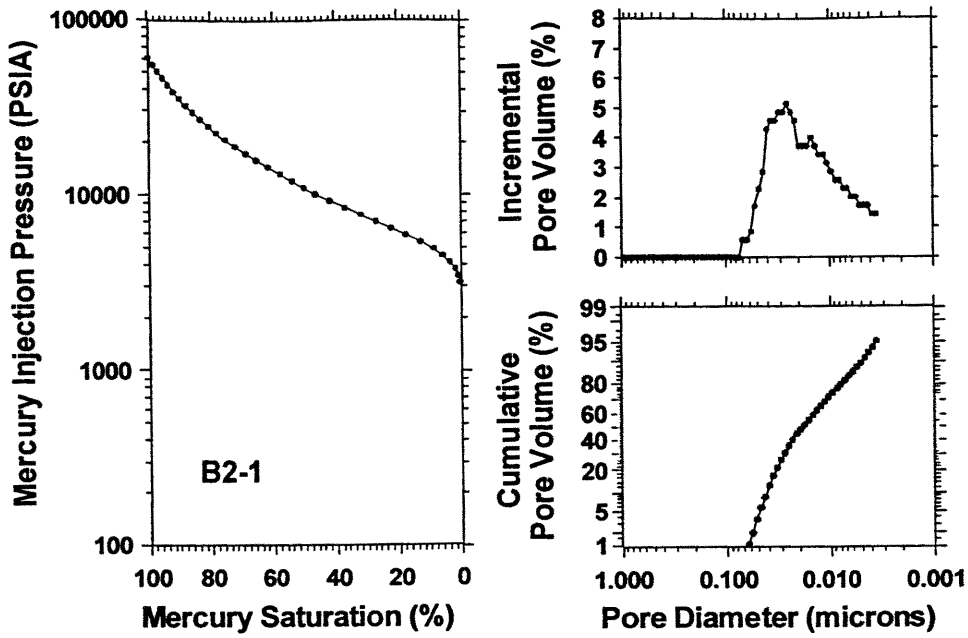
Mercury Injection Pressure (PSIA)
100000
10000
1000
100
B2-1
100 80 60 40 20 0
Mercury Saturation (%)
Incremental Pore Volume (%)
8 7 6 5 4 3 2 1 0
Cumulative Pore Volume (%)
99 95 80 60 40 20 5 1
1.000 0.100 0.010 0.001
Pore Diameter (microns)

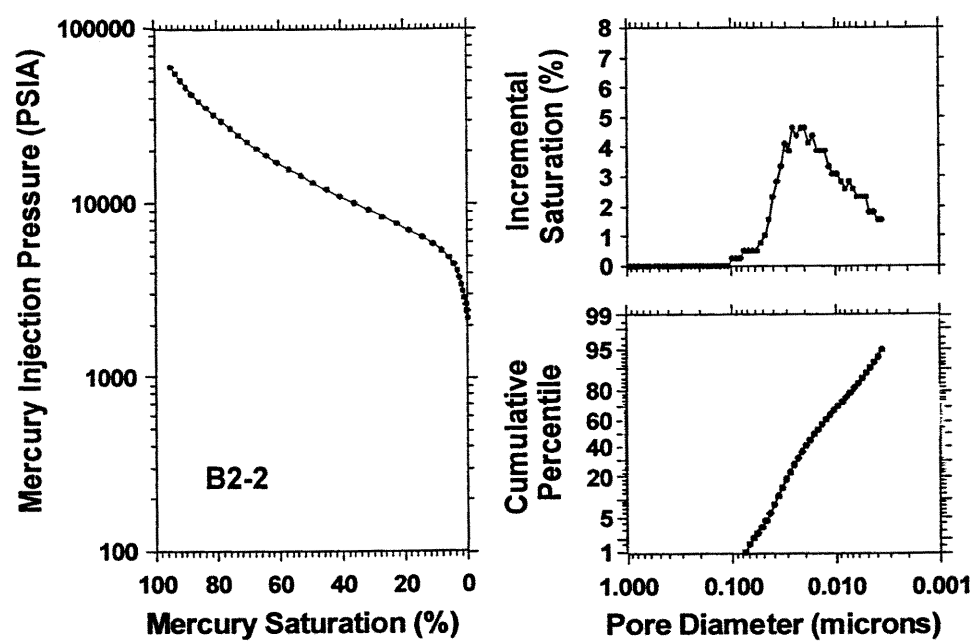
Mercury Injection Pressure (PSIA)
100000
10000
1000
100
B2-2
100 80 60 40 20 0
Mercury Saturation (%)
Incremental Saturation (%)
8 7 6 5 4 3 2 1 0
Cumulative Percentile
99 95 80 60 40 20 5 1
1.000 0.100 0.010 0.001
Pore Diameter (microns)

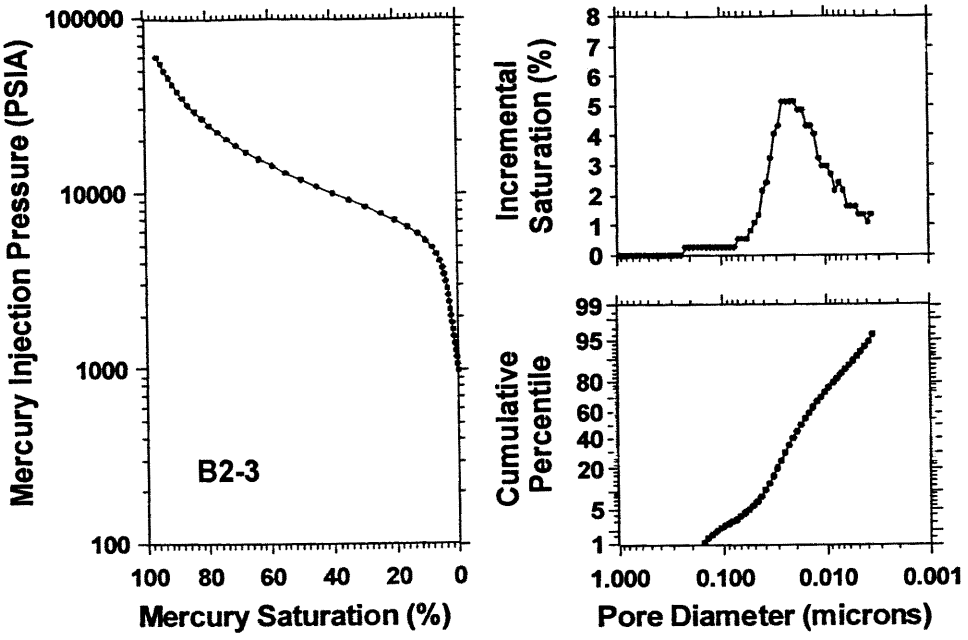
Mercury Injection Pressure (PSIA)
100000
10000
1000
100
B2-3
100 80 60 40 20 0
Mercury Saturation (%)
Incremental Saturation (%)
8 7 6 5 4 3 2 1 0
Cumulative Percentile
99 95 80 60 40 20 5 1
1.000 0.100 0.010 0.001
Pore Diameter (microns)

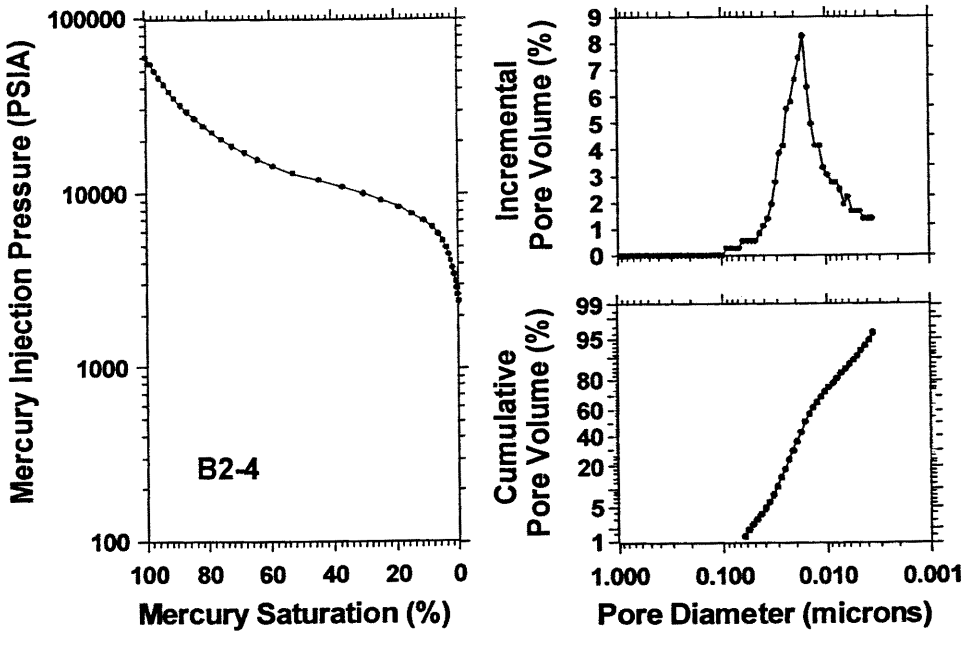
Mercury Injection Pressure (PSIA)
100000
10000
1000
100
B2-4
100 80 60 40 20 0
Mercury Saturation (%)
Incremental Pore Volume (%)
9 8 7 6 5 4 3 2 1 0
Cumulative Pore Volume (%)
99 95 80 60 40 20 5 1
1.000 0.100 0.010 0.001
Pore Diameter (microns)

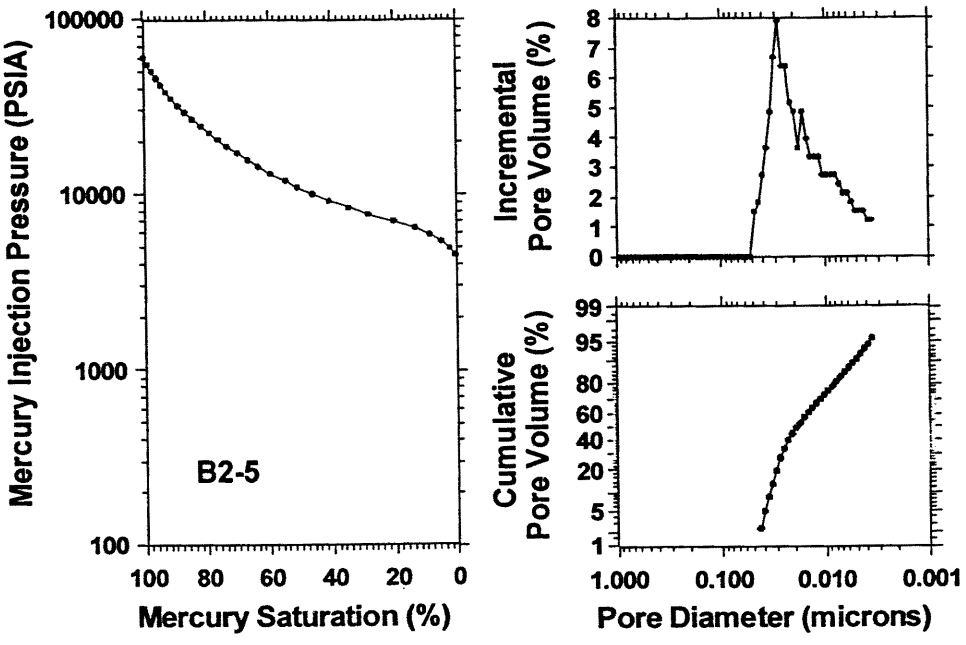
Mercury Injection Pressure (PSIA)
100000
10000
1000
100
B2-5
100 80 60 40 20 0
Mercury Saturation (%)
Incremental Pore Volume (%)
8 7 6 5 4 3 2 1 0
Cumulative Pore Volume (%)
99 95 80 60 40 20 5 1
1.000 0.100 0.010 0.001
Pore Diameter (microns)

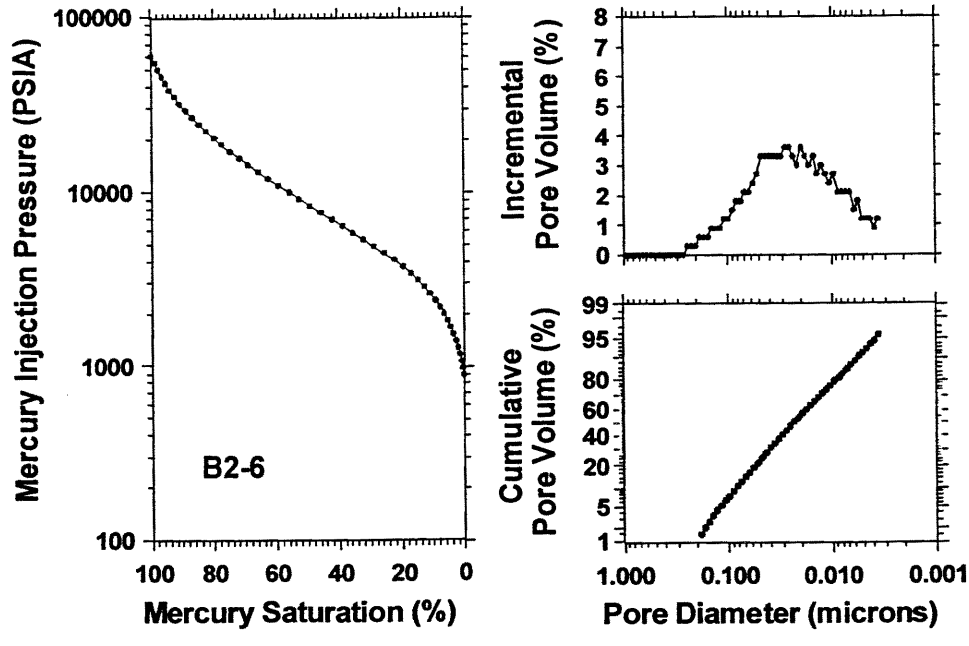
Mercury Injection Pressure (PSIA)
100000
10000
1000
100
B2-6
100 80 60 40 20 0
Mercury Saturation (%)
Incremental Pore Volume (%)
8 7 6 5 4 3 2 1 0
Cumulative Pore Volume (%)
99 95 80 60 40 20 5 1
1.000 0.100 0.010 0.001
Pore Diameter (microns)

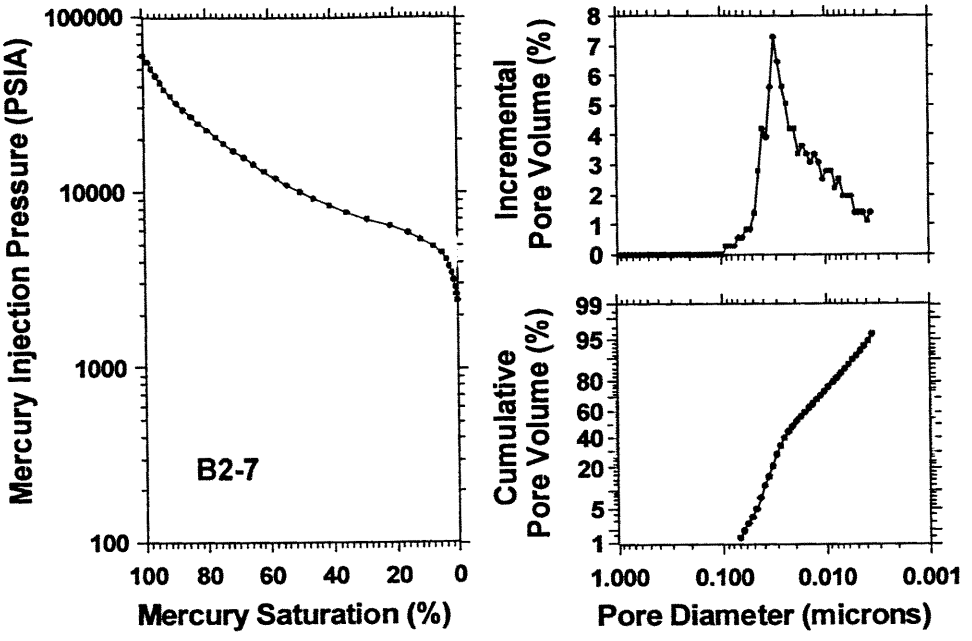
Mercury Injection Pressure (PSIA)
100000
10000
1000
100
B2-7
100 80 60 40 20 0
Mercury Saturation (%)
Incremental Pore Volume (%)
8 7 6 5 4 3 2 1 0
Cumulative Pore Volume (%)
99 95 80 60 40 20 5 1
1.000 0.100 0.010 0.001
Pore Diameter (microns)

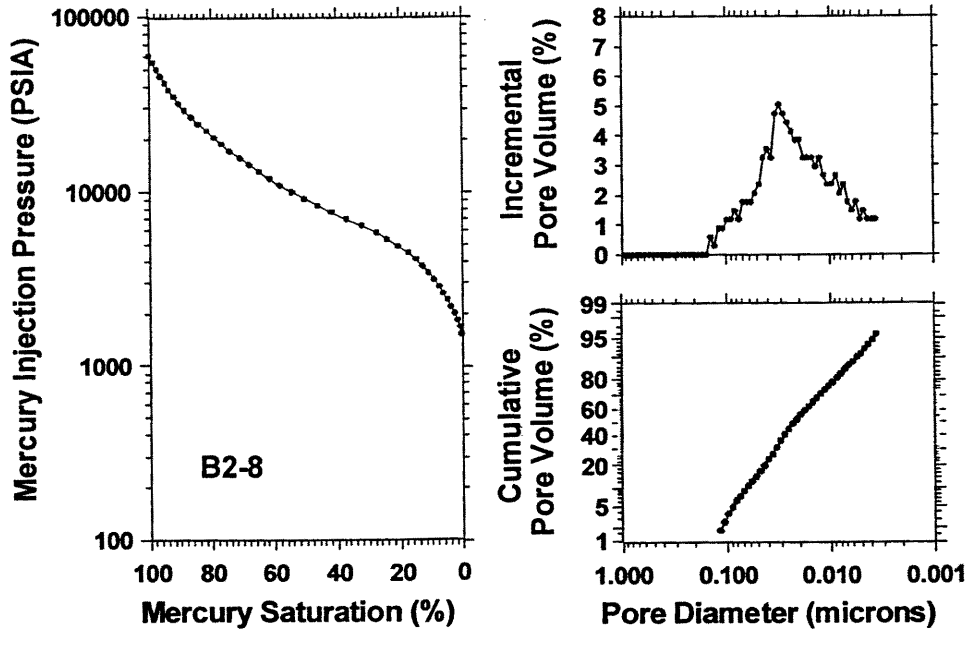
Mercury Injection Pressure (PSIA)
100000
10000
1000
100
B2-8
100 80 60 40 20 0
Mercury Saturation (%)
Incremental Pore Volume (%)
8 7 6 5 4 3 2 1 0
Cumulative Pore Volume (%)
99 95 80 60 40 20 5 1
1.000 0.100 0.010 0.001
Pore Diameter (microns)

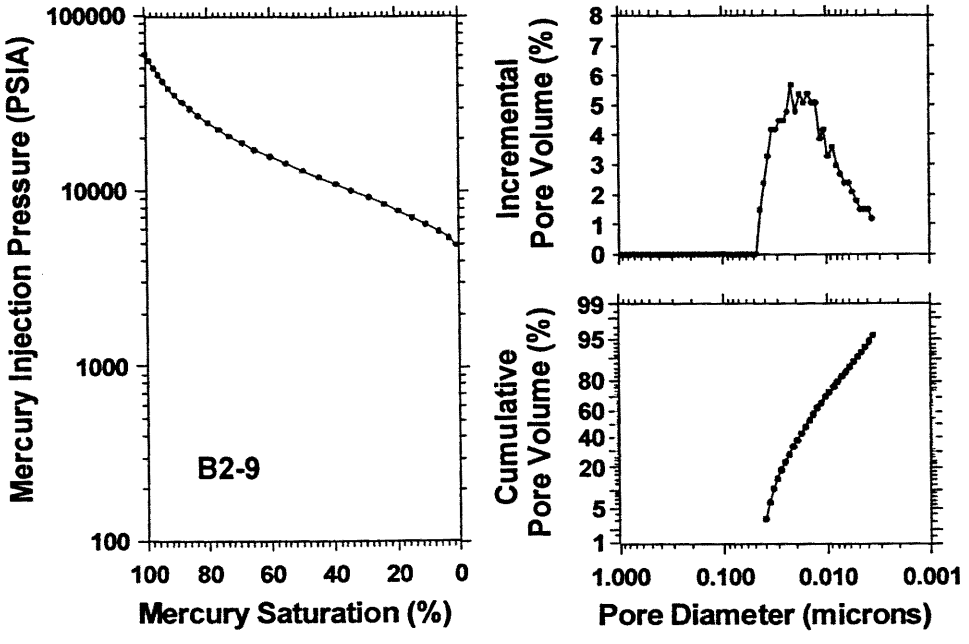
Mercury Injection Pressure (PSIA)
100000
10000
1000
100
B2-9
100 80 60 40 20 0
Mercury Saturation (%)
Incremental Pore Volume (%)
8 7 6 5 4 3 2 1 0
Cumulative Pore Volume (%)
99 95 80 60 40 20 5 1
1.000 0.100 0.010 0.001
Pore Diameter (microns)

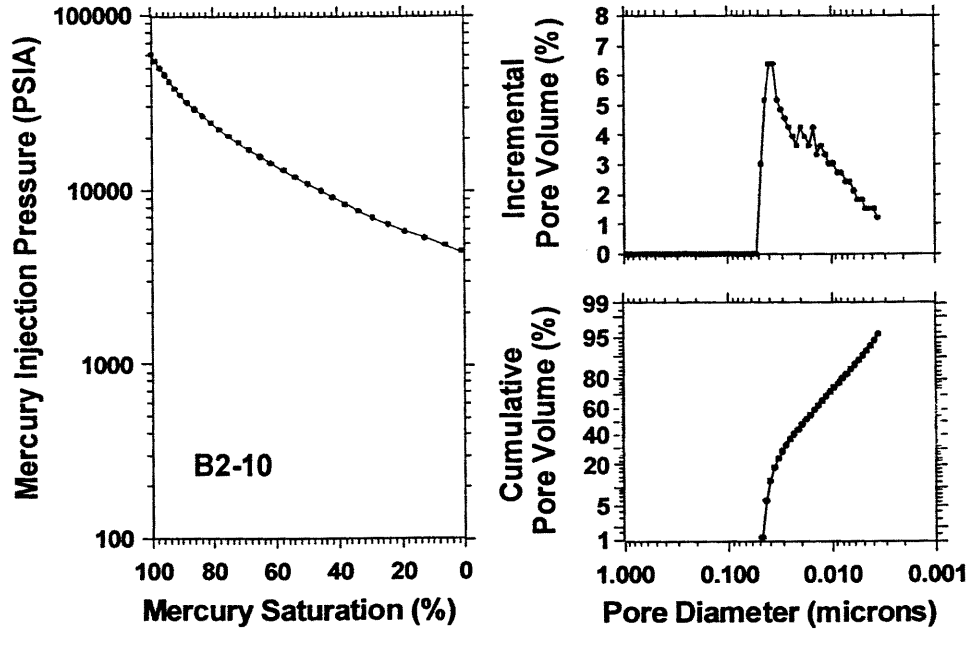
Mercury Injection Pressure (PSIA)
100000
10000
1000
100
B2-10
100 80 60 40 20 0
Mercury Saturation (%)
Incremental Pore Volume (%)
8 7 6 5 4 3 2 1 0
Cumulative Pore Volume (%)
99 95 80 60 40 20 5 1
1.000 0.100 0.010 0.001
Pore Diameter (microns)

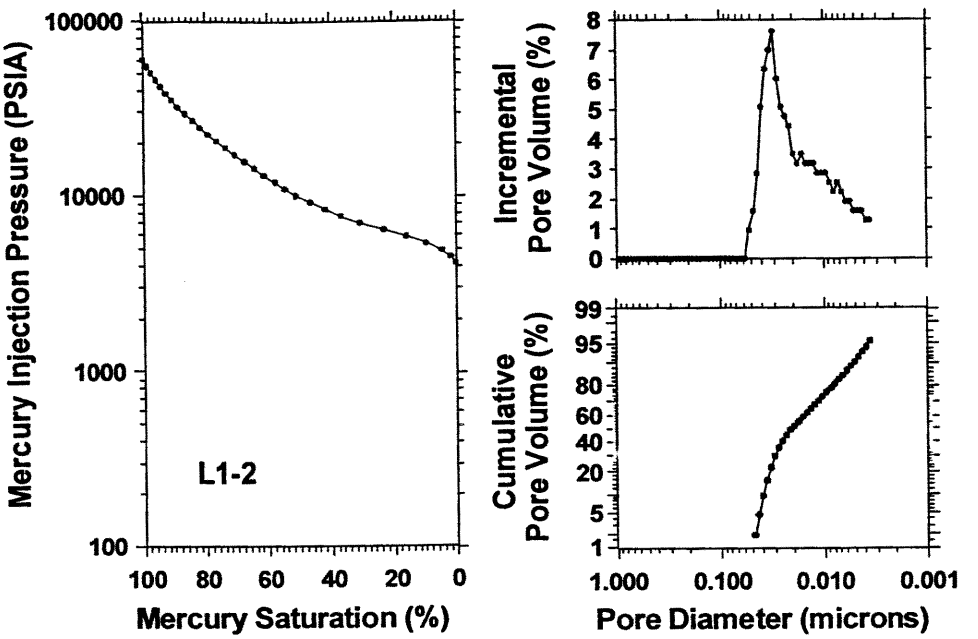
Mercury Injection Pressure (PSIA)
100000
10000
1000
100
L1-2
100 80 60 40 20 0
Mercury Saturation (%)
Incremental Pore Volume (%)
8 7 6 5 4 3 2 1 0
Cumulative Pore Volume (%)
99 95 80 60 40 20 5 1
1.000 0.100 0.010 0.001
Pore Diameter (microns)

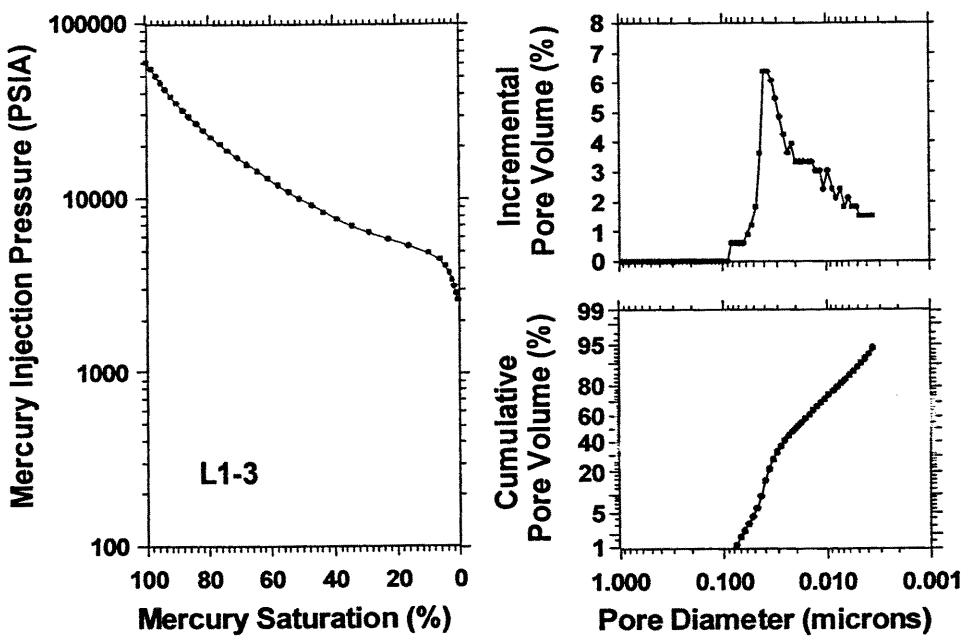
Mercury Injection Pressure (PSIA)
100000
10000
1000
100
L1-3
100 80 60 40 20 0
Mercury Saturation (%)
Incremental Pore Volume (%)
8 7 6 5 4 3 2 1 0
Cumulative Pore Volume (%)
99 95 80 60 40 20 5 1
1.000 0.100 0.010 0.001
Pore Diameter (microns)

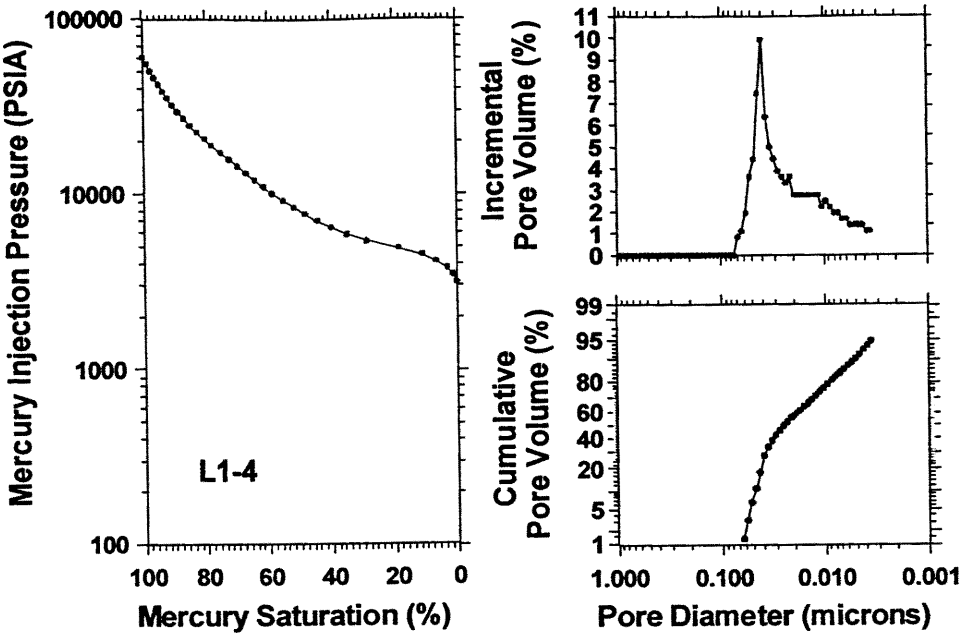
Mercury Injection Pressure (PSIA)
100000
10000
1000
100
L1-4
100 80 60 40 20 0
Mercury Saturation (%)
Incremental Pore Volume (%)
11 10 9 8 7 6 5 4 3 2 1 0
Cumulative Pore Volume (%)
99 95 80 60 40 20 5 1
1.000 0.100 0.010 0.001
Pore Diameter (microns)

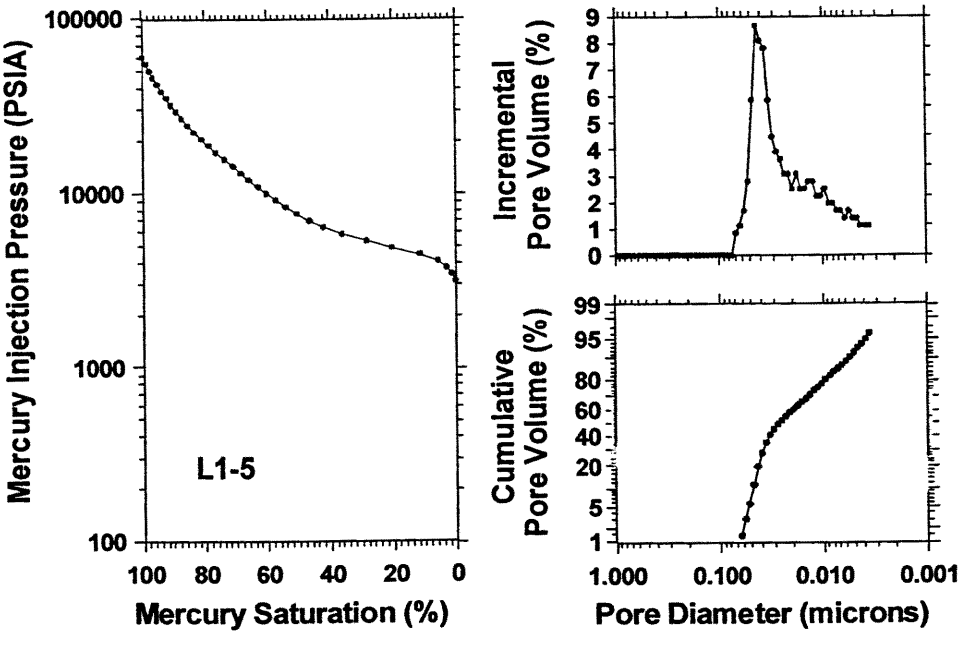
Mercury Injection Pressure (PSIA)
100000
10000
1000
100
L1-5
100 80 60 40 20 0
Mercury Saturation (%)
Incremental Pore Volume (%)
9 8 7 6 5 4 3 2 1 0
Cumulative Pore Volume (%)
99 95 80 60 40 20 5 1
1.000 0.100 0.010 0.001
Pore Diameter (microns)

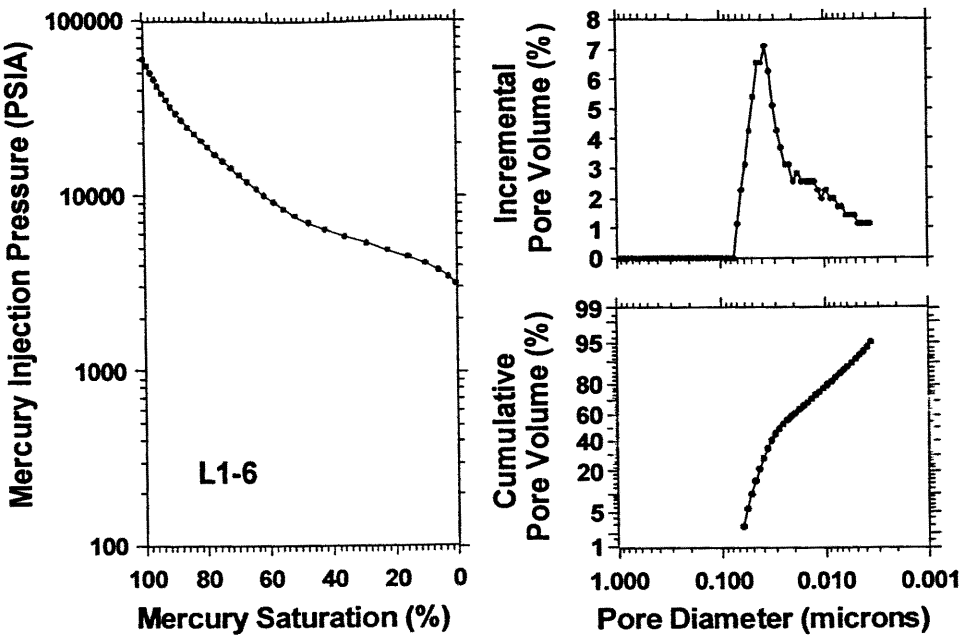
Mercury Injection Pressure (PSIA)
100000
10000
1000
100
L1-6
100 80 60 40 20 0
Mercury Saturation (%)
Incremental Pore Volume (%)
8 7 6 5 4 3 2 1 0
Cumulative Pore Volume (%)
99 95 80 60 40 20 5 1
1.000 0.100 0.010 0.001
Pore Diameter (microns)

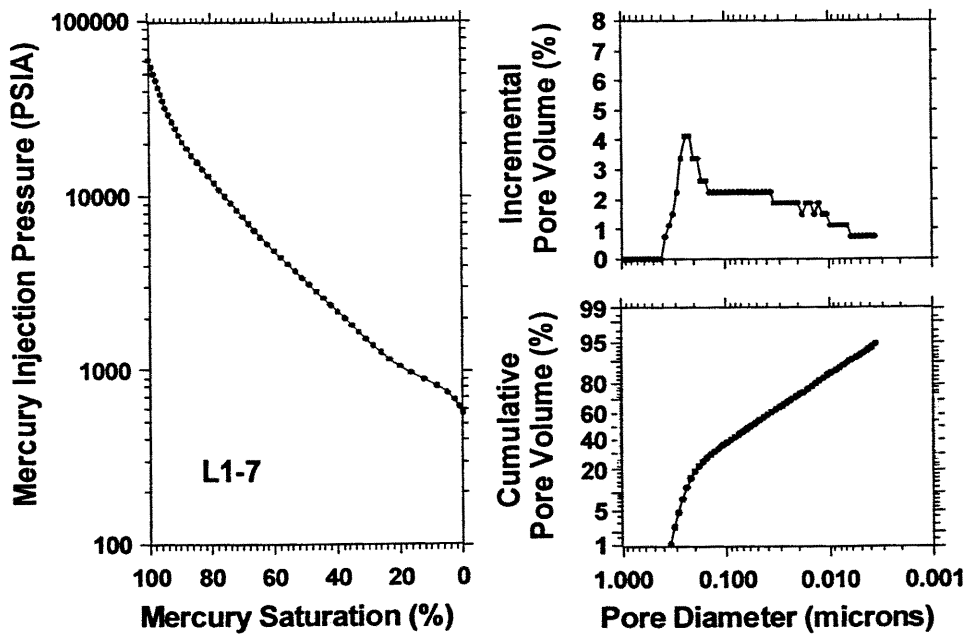
Mercury Injection Pressure (PSIA)
100000
10000
1000
100
L1-7
100 80 60 40 20 0
Mercury Saturation (%)
Incremental Pore Volume (%)
8 7 6 5 4 3 2 1 0
Cumulative Pore Volume (%)
99 95 80 60 40 20 5 1
1.000 0.100 0.010 0.001
Pore Diameter (microns)

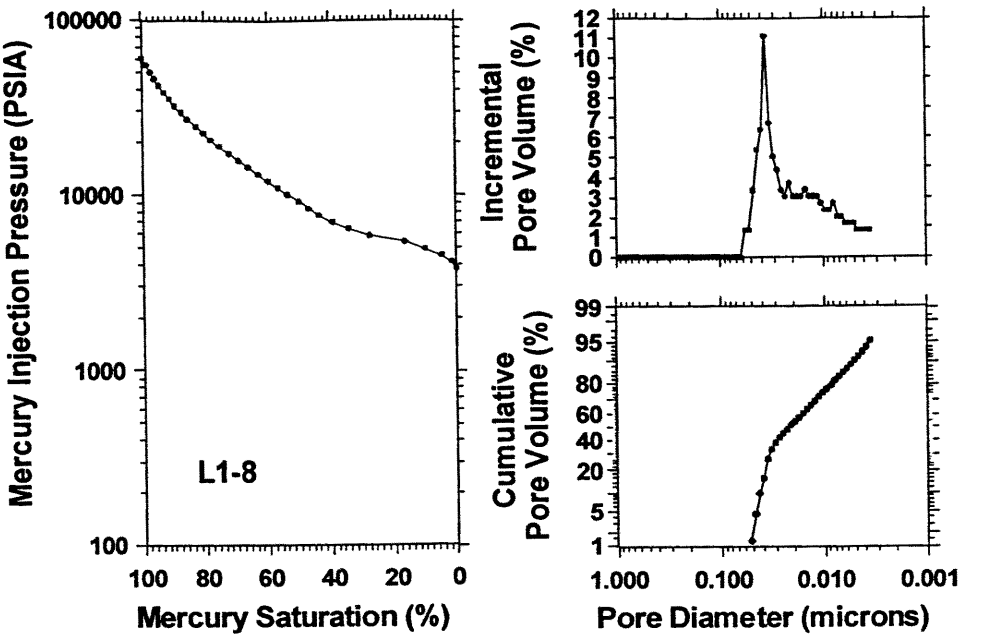
Mercury Injection Pressure (PSIA)
100000
10000
1000
100
L1-8
100 80 60 40 20 0
Mercury Saturation (%)
Incremental Pore Volume (%)
12 11 10 9 8 7 6 5 4 3 2 1 0
Cumulative Pore Volume (%)
99 95 80 60 40 20 5 1
1.000 0.100 0.010 0.001
Pore Diameter (microns)

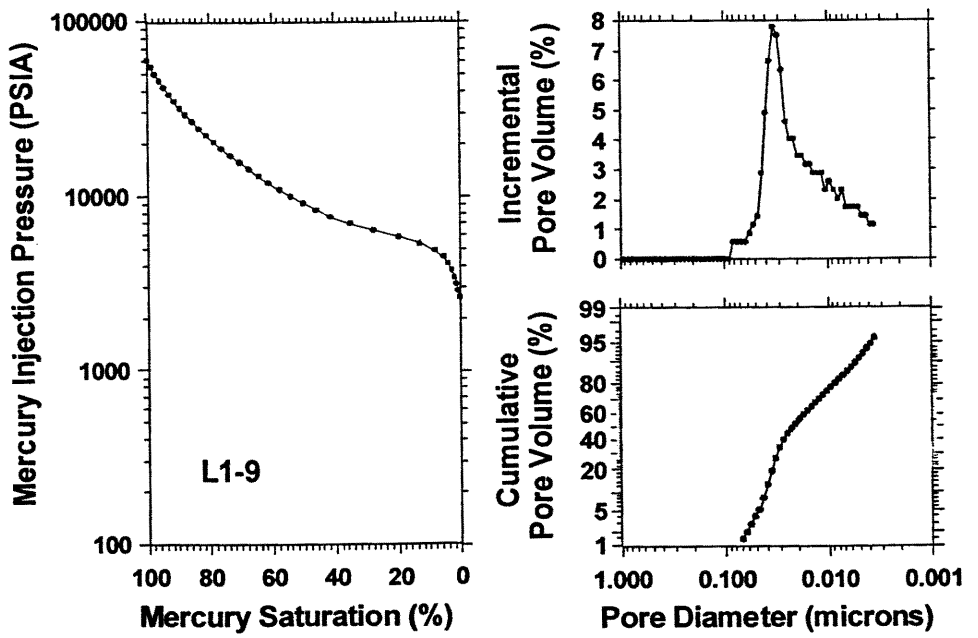
Mercury Injection Pressure (PSIA)
100000
10000
1000
100
L1-9
100 80 60 40 20 0
Mercury Saturation (%)
Incremental Pore Volume (%)
8 7 6 5 4 3 2 1 0
Cumulative Pore Volume (%)
99 95 80 60 40 20 5 1
1.000 0.100 0.010 0.001
Pore Diameter (microns)

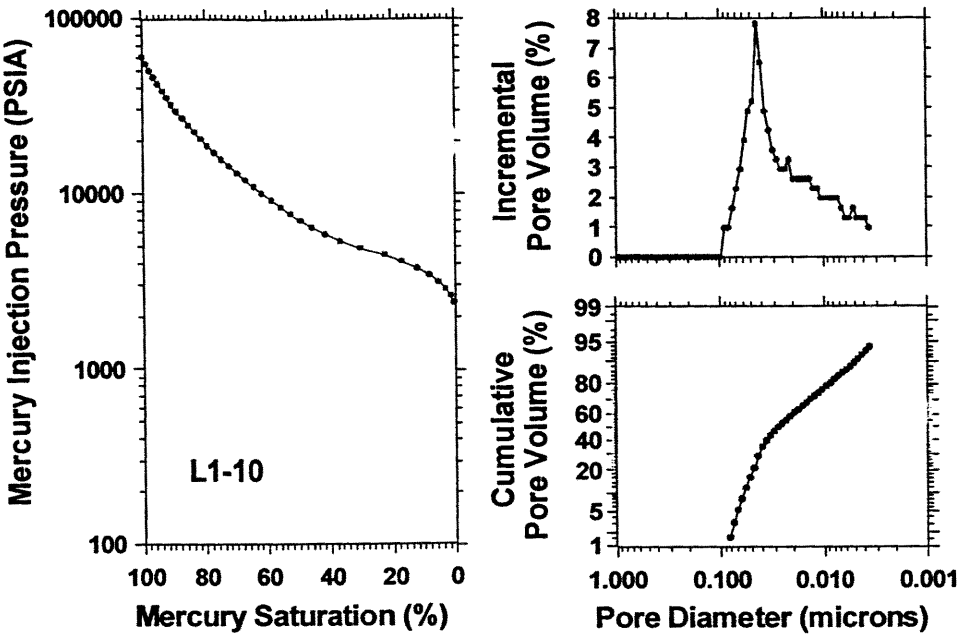
Mercury Injection Pressure (PSIA)
100000
10000
1000
100
L1-10
100 80 60 40 20 0
Mercury Saturation (%)
Incremental Pore Volume (%)
8 7 6 5 4 3 2 1 0
Cumulative Pore Volume (%)
99 95 80 60 40 20 5 1
1.000 0.100 0.010 0.001
Pore Diameter (microns)

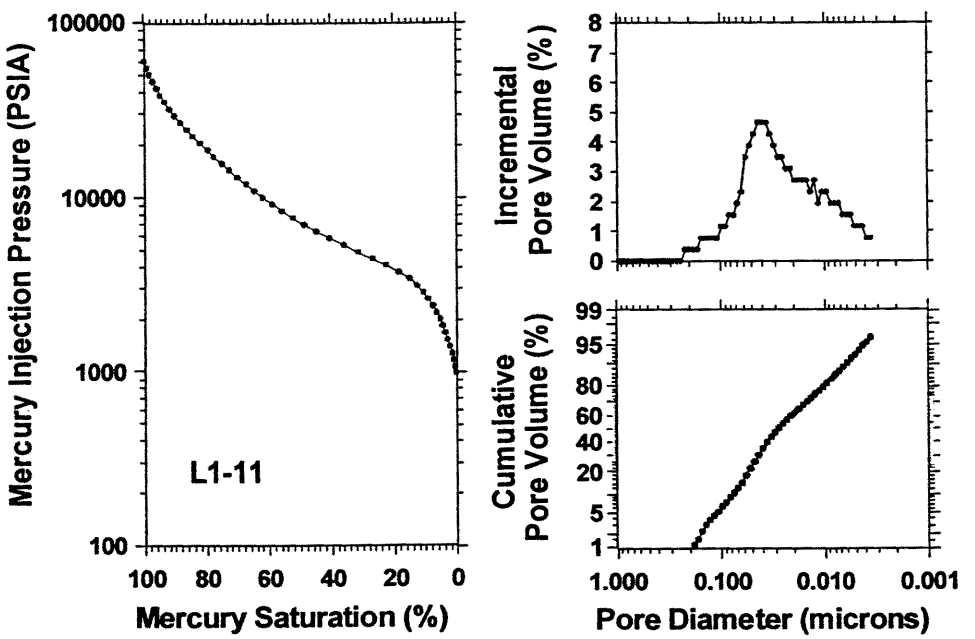
Mercury Injection Pressure (PSIA)
100000
10000
1000
100
L1-11
100 80 60 40 20 0
Mercury Saturation (%)
Incremental Pore Volume (%)
8 7 6 5 4 3 2 1 0
Cumulative Pore Volume (%)
99 95 80 60 40 20 5 1
1.000 0.100 0.010 0.001
Pore Diameter (microns)

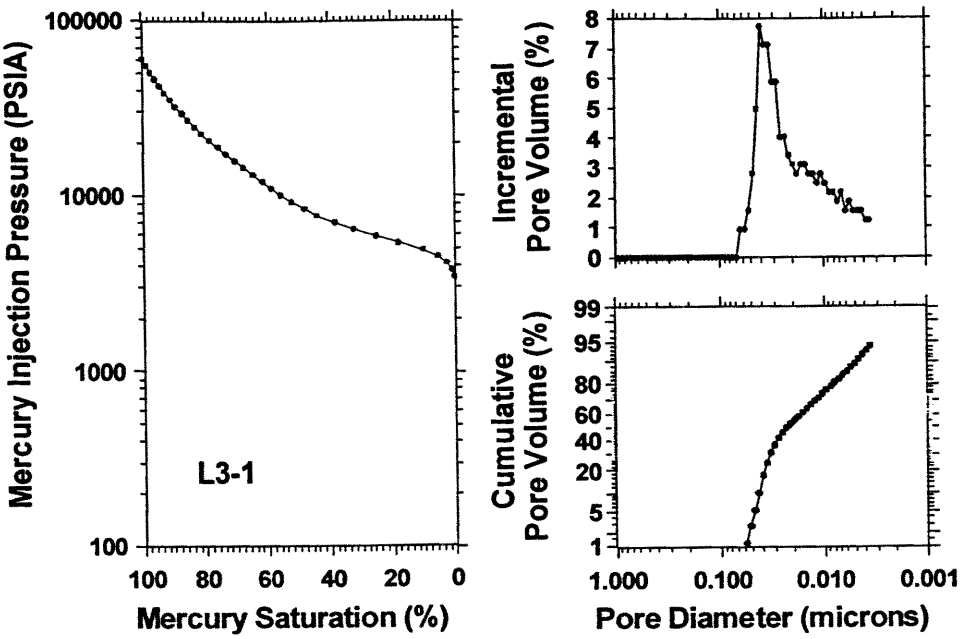
Mercury Injection Pressure (PSIA)
100000
10000
1000
100
L3-1
100 80 60 40 20 0
Mercury Saturation (%)
Incremental Pore Volume (%)
8 7 6 5 4 3 2 1 0
Cumulative Pore Volume (%)
99 95 80 60 40 20 5 1
1.000 0.100 0.010 0.001
Pore Diameter (microns)

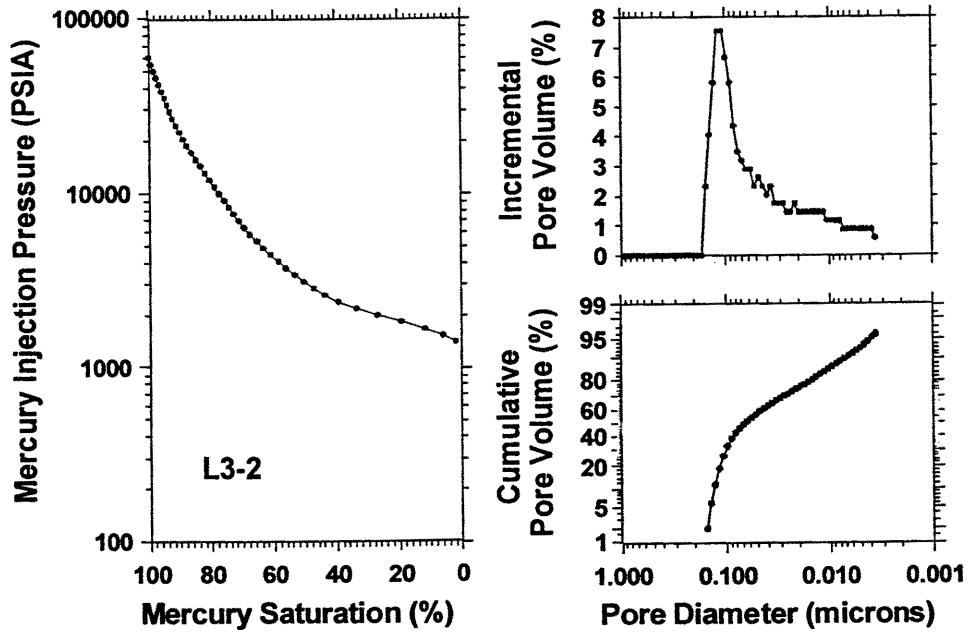
Mercury Injection Pressure (PSIA)
100000
10000
1000
100
L3-2
100 80 60 40 20 0
Mercury Saturation (%)
Incremental Pore Volume (%)
8 7 6 5 4 3 2 1 0
Cumulative Pore Volume (%)
99 95 80 60 40 20 5 1
1.000 0.100 0.010 0.001
Pore Diameter (microns)

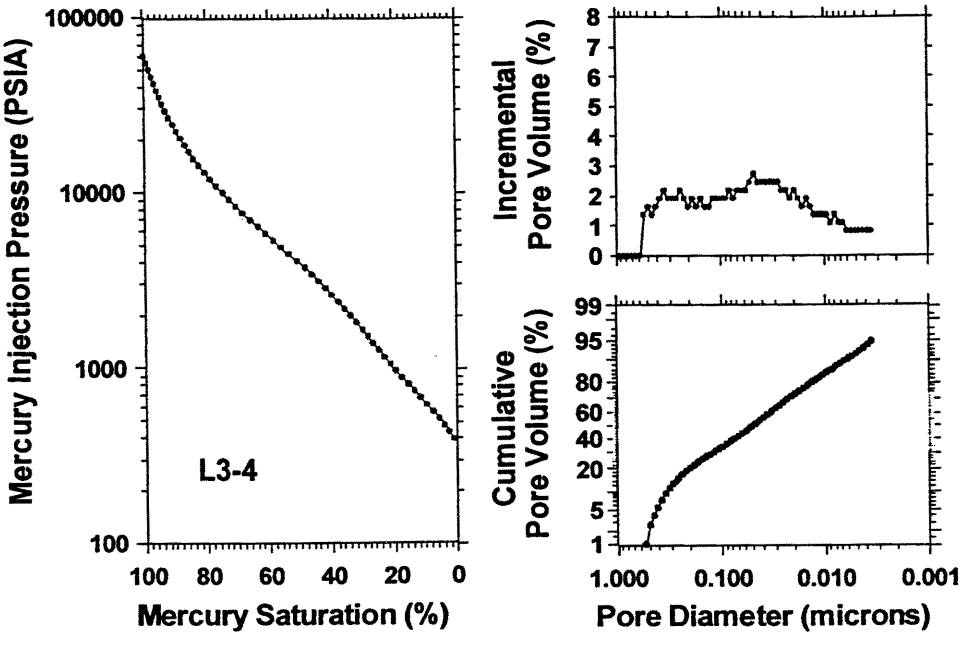
Mercury Injection Pressure (PSIA)
100000
10000
1000
100
L3-4
100 80 60 40 20 0
Mercury Saturation (%)
Incremental Pore Volume (%)
8 7 6 5 4 3 2 1 0
Cumulative Pore Volume (%)
99 95 80 60 40 20 5 1
1.000 0.100 0.010 0.001
Pore Diameter (microns)

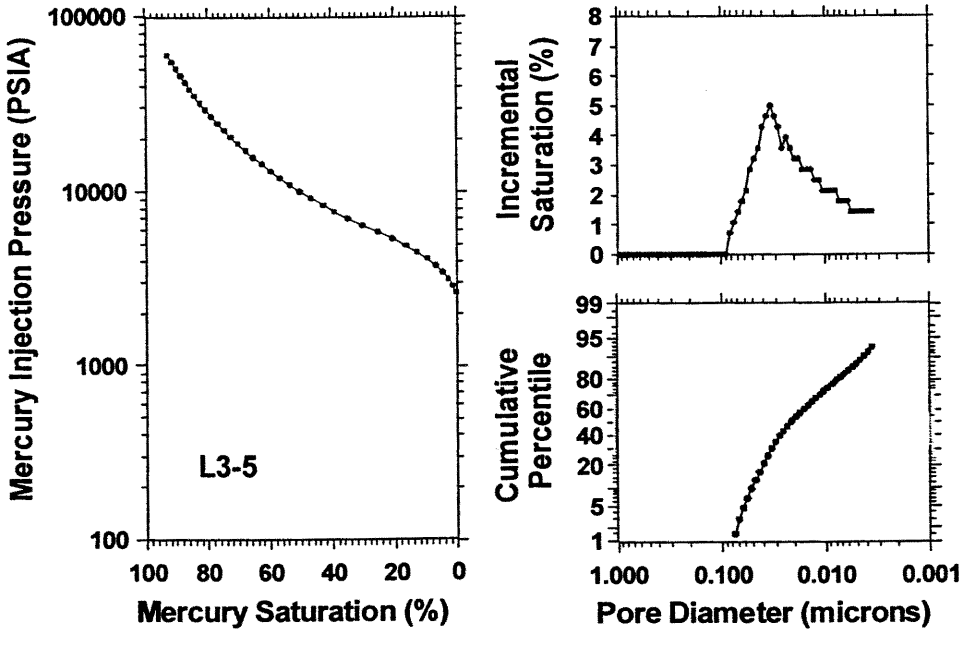
Mercury Injection Pressure (PSIA)
100000
10000
1000
100
L3-5
100 80 60 40 20 0
Mercury Saturation (%)
Incremental Saturation (%)
8 7 6 5 4 3 2 1 0
Cumulative Percentile
99 95 80 60 40 20 5 1
1.000 0.100 0.010 0.001
Pore Diameter (microns)

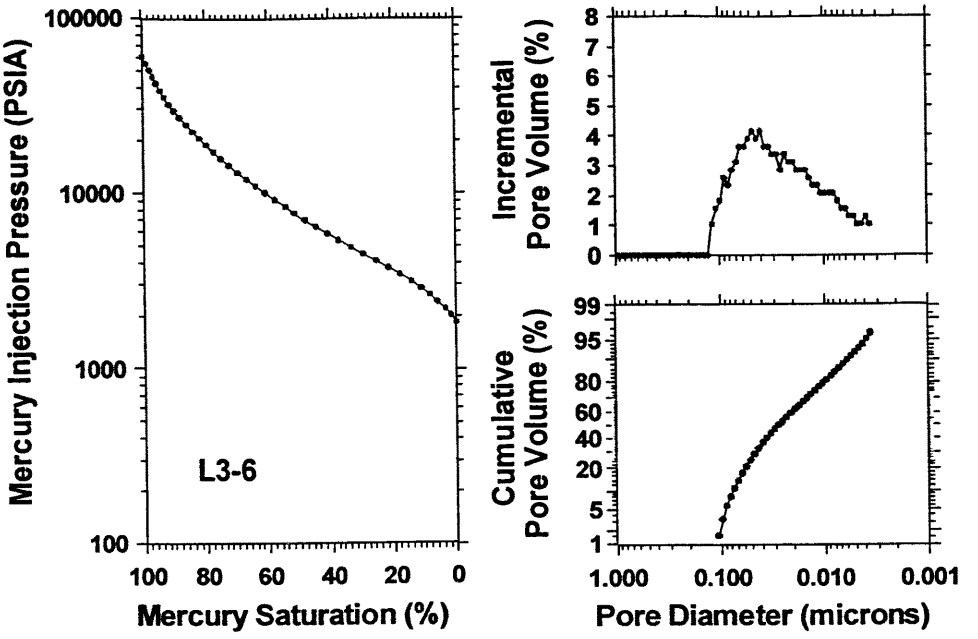
Mercury Injection Pressure (PSIA)
100000
10000
1000
100
L3-6
100 80 60 40 20 0
Mercury Saturation (%)
Incremental Pore Volume (%)
8 7 6 5 4 3 2 1 0
Cumulative Pore Volume (%)
99 95 80 60 40 20 5 1
1.000 0.100 0.010 0.001
Pore Diameter (microns)

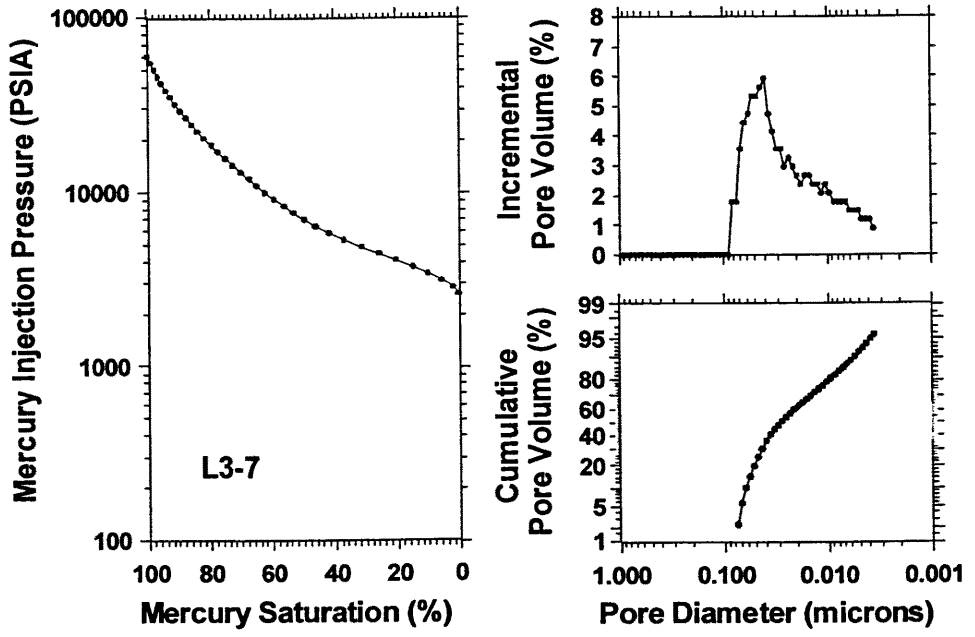
Mercury Injection Pressure (PSIA)
100000
10000
1000
100
L3-7
100 80 60 40 20 0
Mercury Saturation (%)
Incremental Pore Volume (%)
8 7 6 5 4 3 2 1 0
Cumulative Pore Volume (%)
99 95 80 60 40 20 5 1
1.000 0.100 0.010 0.001
Pore Diameter (microns)

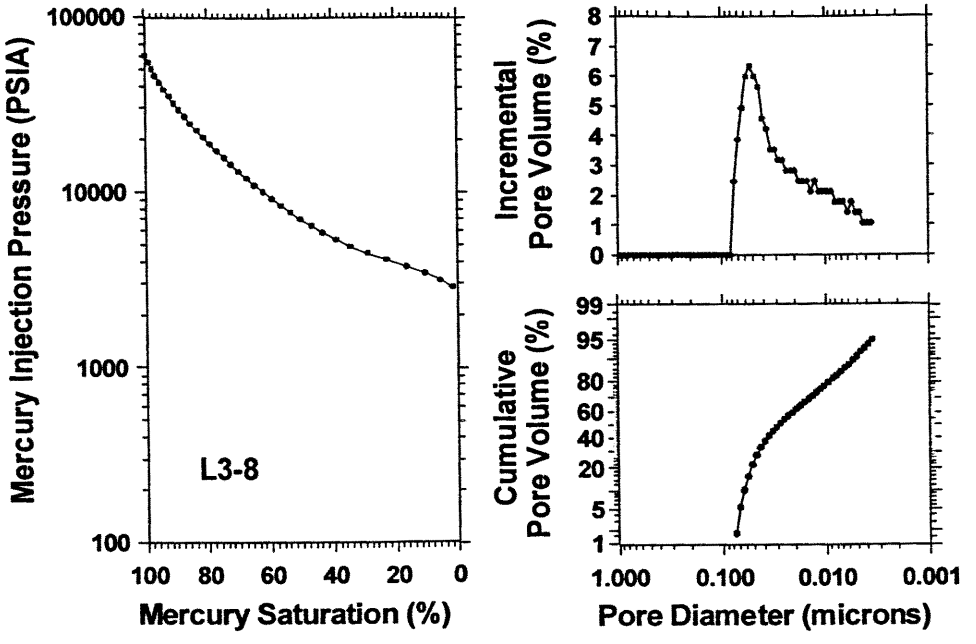
Mercury Injection Pressure (PSIA)
100000
10000
1000
100
L3-8
100 80 60 40 20 0
Mercury Saturation (%)
Incremental Pore Volume (%)
8 7 6 5 4 3 2 1 0
Cumulative Pore Volume (%)
99 95 80 60 40 20 5 1
1.000 0.100 0.010 0.001
Pore Diameter (microns)

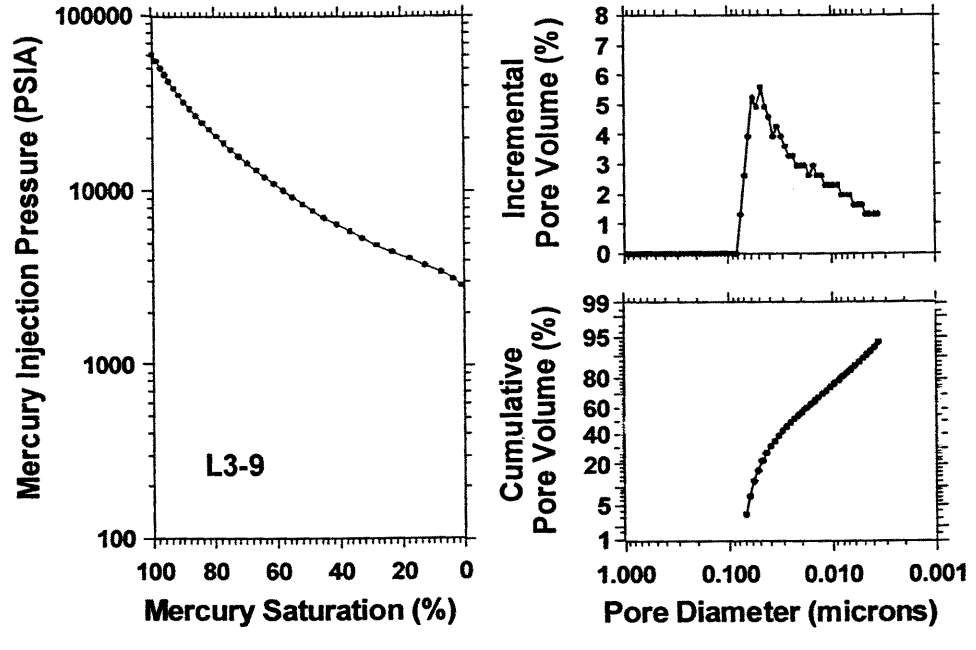
Mercury Injection Pressure (PSIA)
100000
10000
1000
100
L3-9
100 80 60 40 20 0
Mercury Saturation (%)
Incremental Pore Volume (%)
8 7 6 5 4 3 2 1 0
Cumulative Pore Volume (%)
99 95 80 60 40 20 5 1
1.000 0.100 0.010 0.001
Pore Diameter (microns)

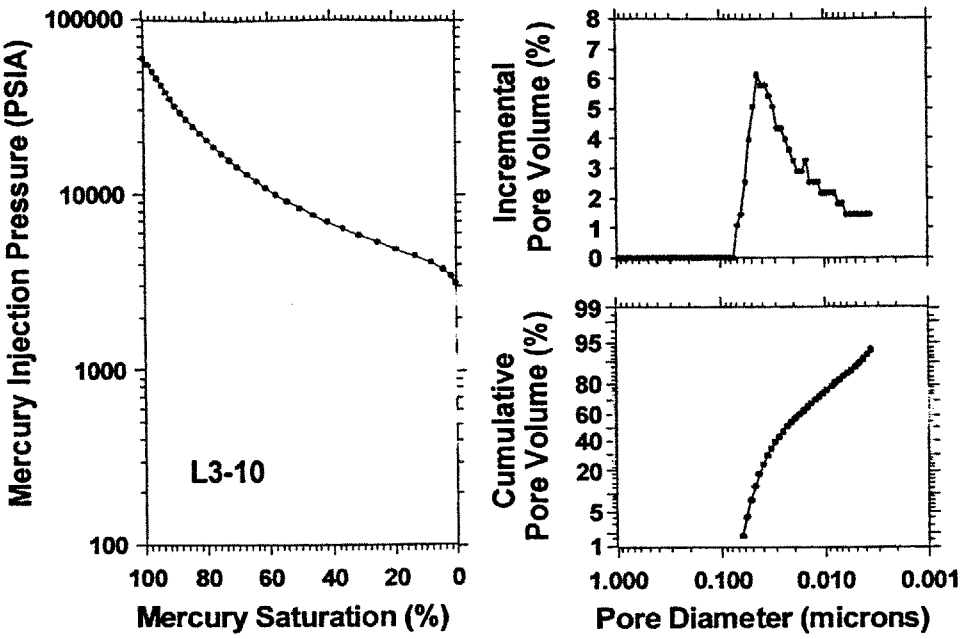
Mercury Injection Pressure (PSIA)
100000
10000
1000
100
L3-10
100 80 60 40 20 0
Mercury Saturation (%)
Incremental Pore Volume (%)
8 7 6 5 4 3 2 1 0
Cumulative Pore Volume (%)
99 95 80 60 40 20 5 1
1.000 0.100 0.010 0.001
Pore Diameter (microns)

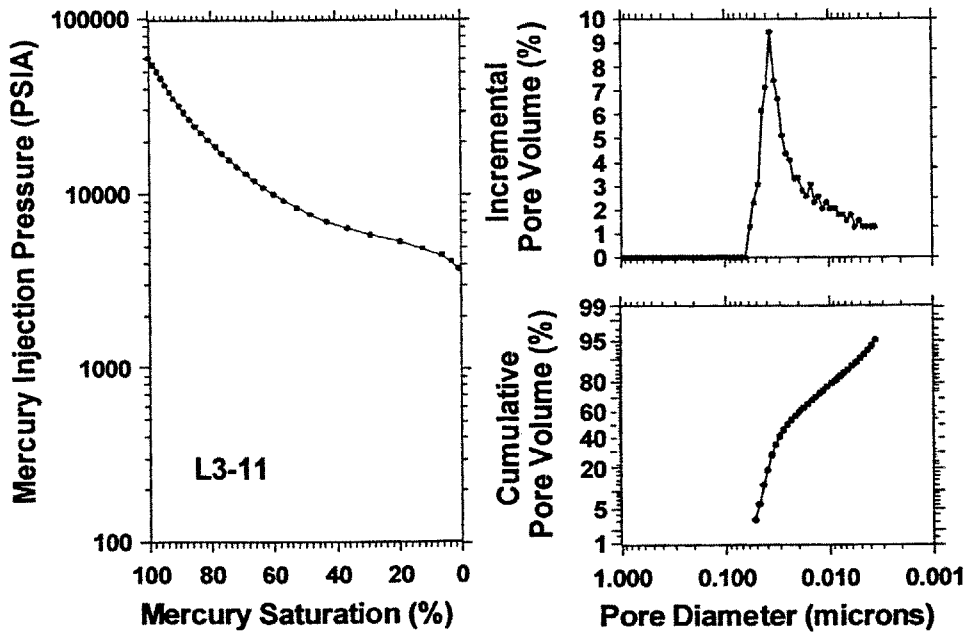
Mercury Injection Pressure (PSIA)
100000
10000
1000
100
L3-11
100 80 60 40 20 0
Mercury Saturation (%)
Incremental Pore Volume (%)
10 9 8 7 6 5 4 3 2 1 0
Cumulative Pore Volume (%)
99 95 80 60 40 20 5 1
1.000 0.100 0.010 0.001
Pore Diameter (microns)

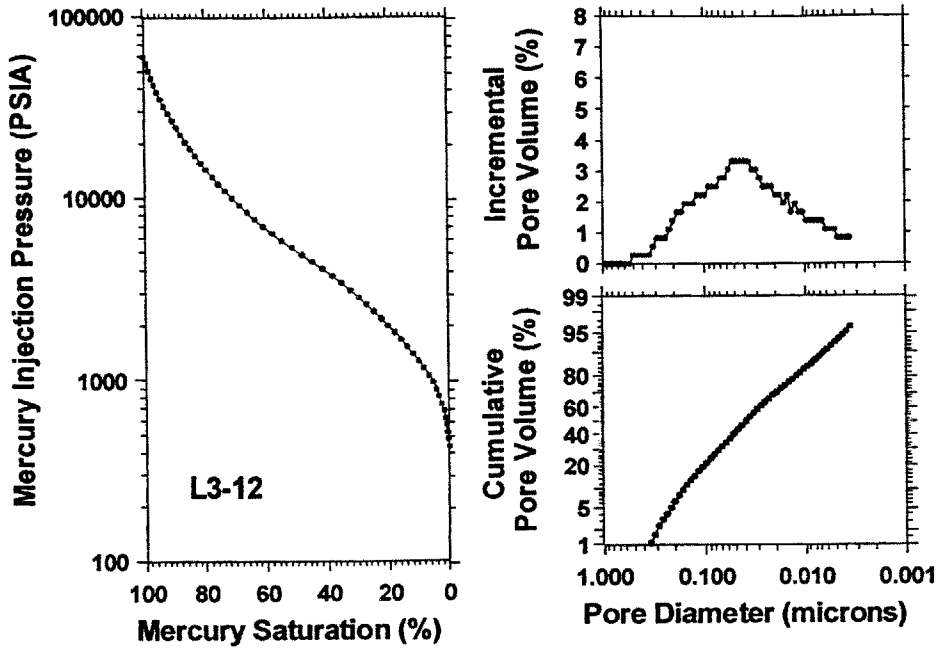
Mercury Injection Pressure (PSIA)
100000
10000
1000
100
L3-12
100 80 60 40 20 0
Mercury Saturation (%)
Incremental Pore Volume (%)
8 7 6 5 4 3 2 1 0
Cumulative Pore Volume (%)
99 95 80 60 40 20 5 1
1.000 0.100 0.010 0.001
Pore Diameter (microns)

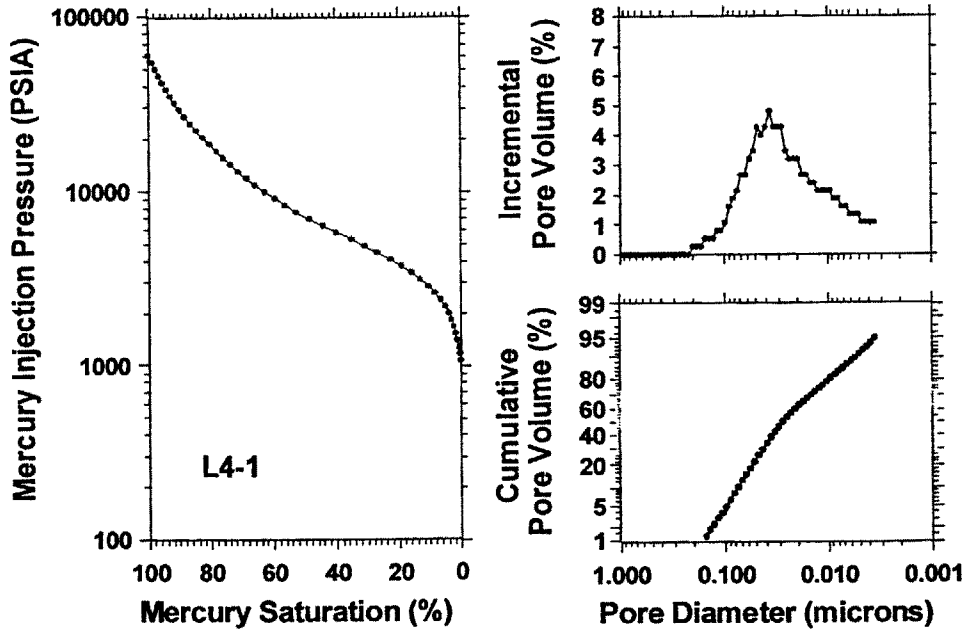
Mercury Injection Pressure (PSIA)
100000
10000
1000
100
L4-1
100 80 60 40 20 0
Mercury Saturation (%)
Incremental Pore Volume (%)
8 7 6 5 4 3 2 1 0
Cumulative Pore Volume (%)
99 95 80 60 40 20 5 1
1.000 0.100 0.010 0.001
Pore Diameter (microns)

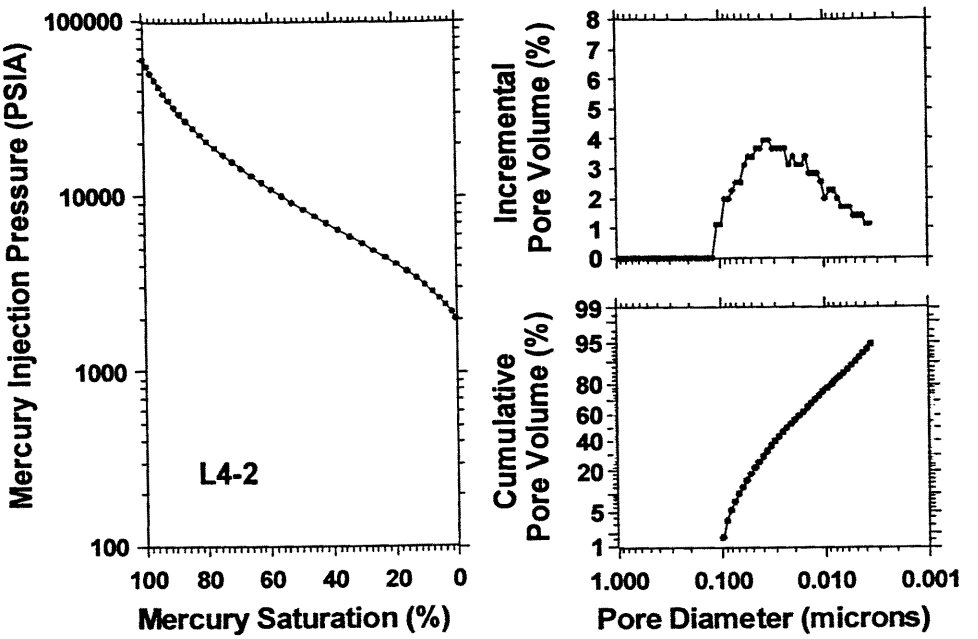
Mercury Injection Pressure (PSIA)
100000
10000
1000
100
L4-2
100 80 60 40 20 0
Mercury Saturation (%)
Incremental Pore Volume (%)
8 7 6 5 4 3 2 1 0
Cumulative Pore Volume (%)
99 95 80 60 40 20 5 1
1.000 0.100 0.010 0.001
Pore Diameter (microns)

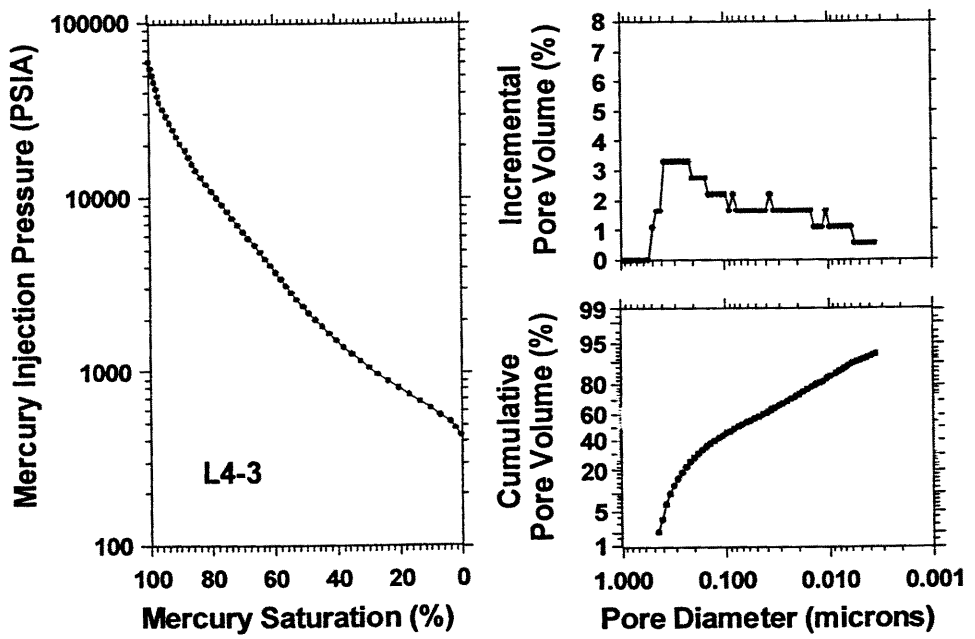
Mercury Injection Pressure (PSIA)
100000
10000
1000
100
L4-3
100 80 60 40 20 0
Mercury Saturation (%)
Incremental Pore Volume (%)
8 7 6 5 4 3 2 1 0
Cumulative Pore Volume (%)
99 95 80 60 40 20 5 1
1.000 0.100 0.010 0.001
Pore Diameter (microns)

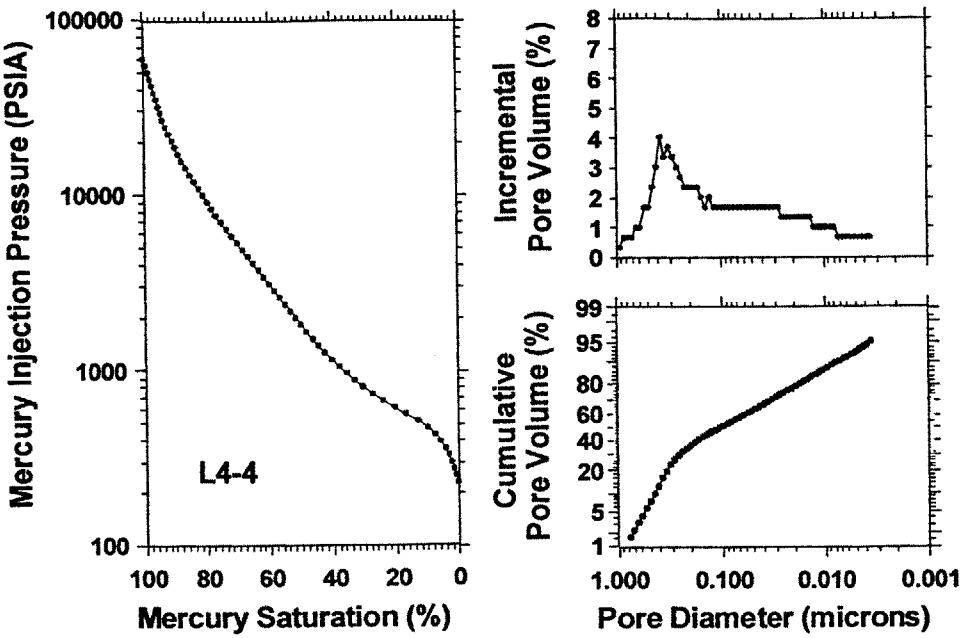
Mercury Injection Pressure (PSIA)
100000
10000
1000
100
L4-4
100 80 60 40 20 0
Mercury Saturation (%)
Incremental Pore Volume (%)
8 7 6 5 4 3 2 1 0
Cumulative Pore Volume (%)
99 95 80 60 40 20 5 1
1.000 0.100 0.010 0.001
Pore Diameter (microns)

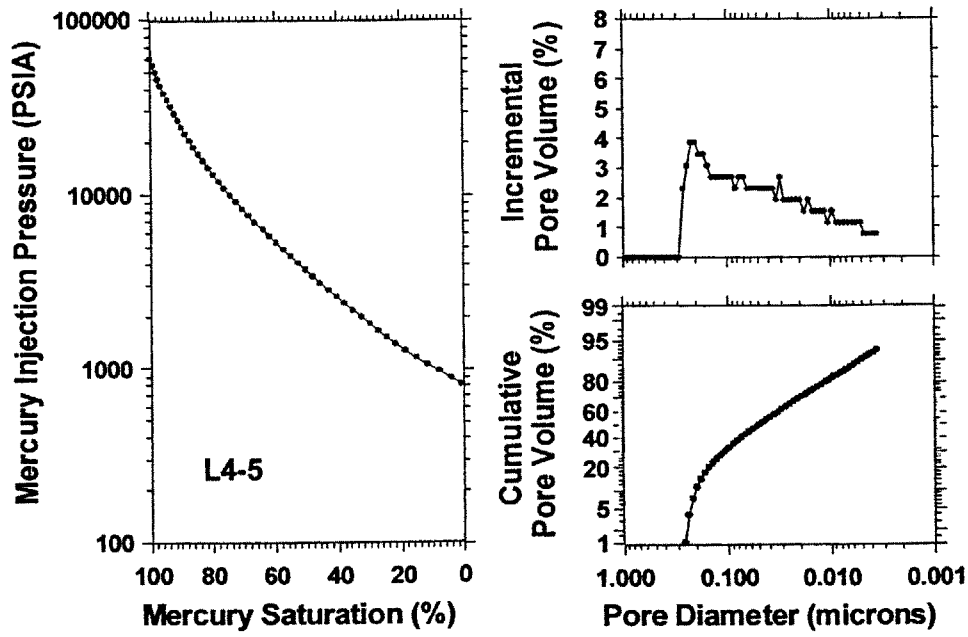
Mercury Injection Pressure (PSIA)
100000
10000
1000
100
L4-5
100 80 60 40 20 0
Mercury Saturation (%)
Incremental Pore Volume (%)
8 7 6 5 4 3 2 1 0
Cumulative Pore Volume (%)
99 95 80 60 40 20 5 1
1.000 0.100 0.010 0.001
Pore Diameter (microns)

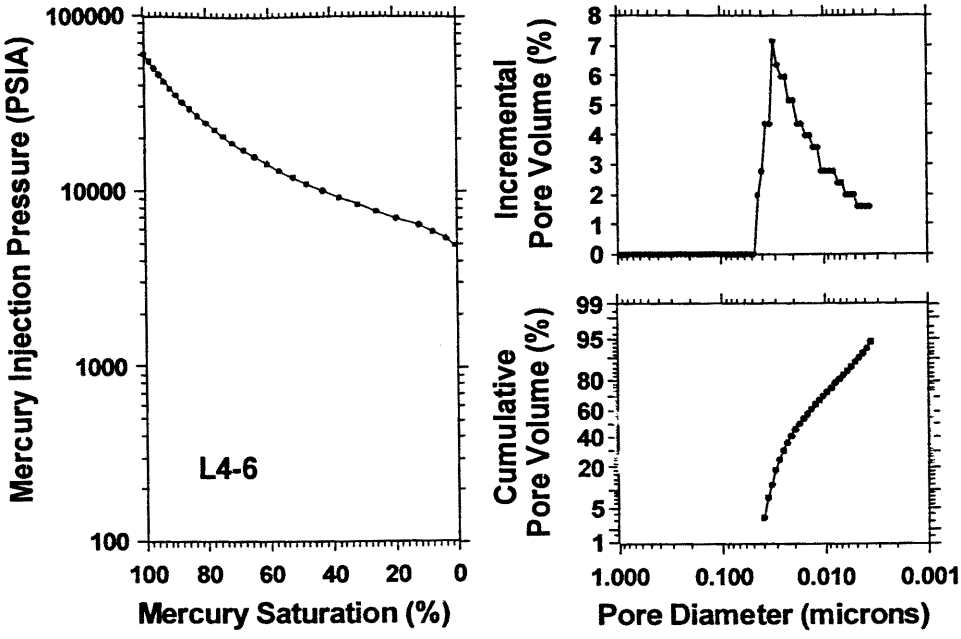
Mercury Injection Pressure (PSIA)
100000
10000
1000
100
L4-6
100 80 60 40 20 0
Mercury Saturation (%)
Incremental Pore Volume (%)
8 7 6 5 4 3 2 1 0
Cumulative Pore Volume (%)
99 95 80 60 40 20 5 1
1.000 0.100 0.010 0.001
Pore Diameter (microns)

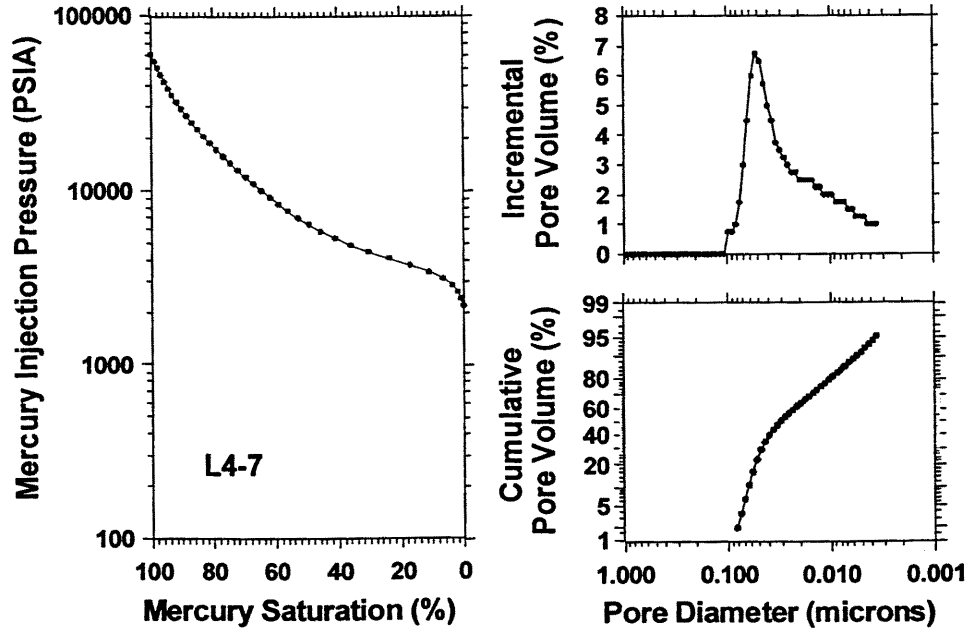
Mercury Injection Pressure (PSIA)
100000
10000
1000
100
L4-7
100 80 60 40 20 0
Mercury Saturation (%)
Incremental Pore Volume (%)
8 7 6 5 4 3 2 1 0
Cumulative Pore Volume (%)
99 95 80 60 40 20 5 1
1.000 0.100 0.010 0.001
Pore Diameter (microns)

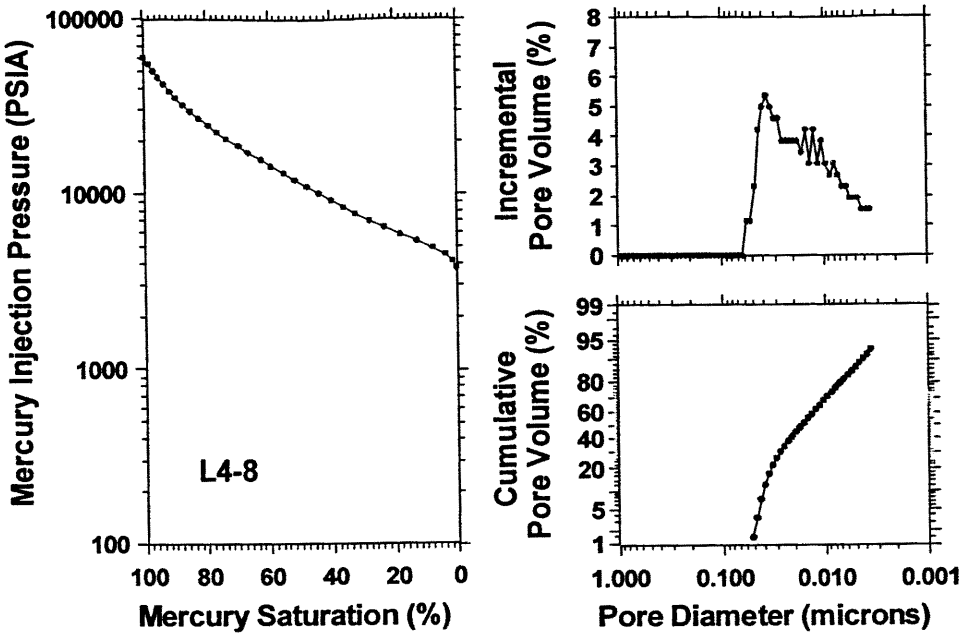
Mercury Injection Pressure (PSIA)
100000
10000
1000
100
L4-8
100 80 60 40 20 0
Mercury Saturation (%)
Incremental Pore Volume (%)
8 7 6 5 4 3 2 1 0
Cumulative Pore Volume (%)
99 95 80 60 40 20 5 1
1.000 0.100 0.010 0.001
Pore Diameter (microns)

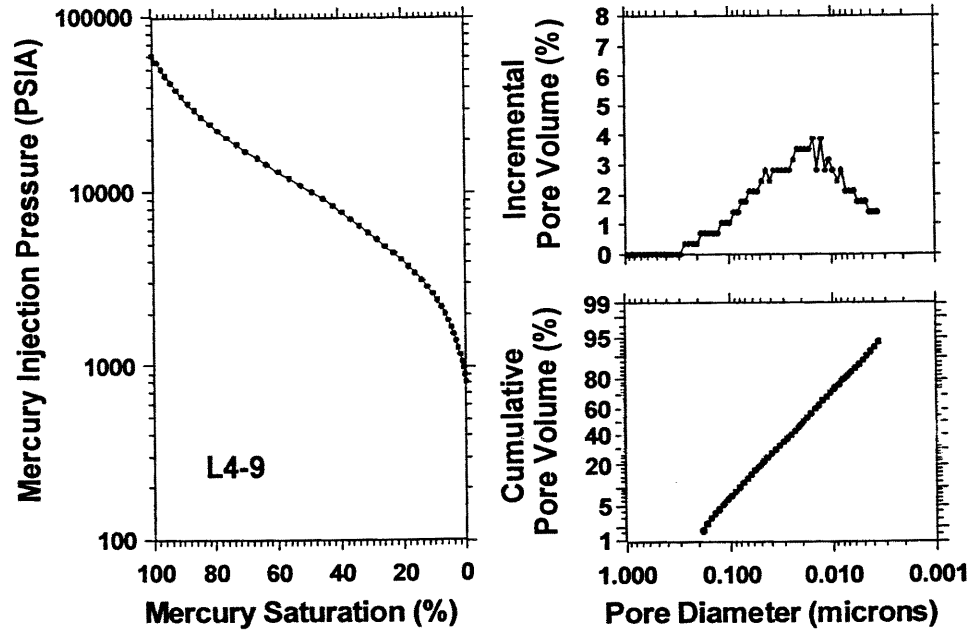
Mercury Injection Pressure (PSIA)
100000
10000
1000
100
L4-9
100 80 60 40 20 0
Mercury Saturation (%)
Incremental Pore Volume (%)
8 7 6 5 4 3 2 1 0
Cumulative Pore Volume (%)
99 95 80 60 40 20 5 1
1.000 0.100 0.010 0.001
Pore Diameter (microns)

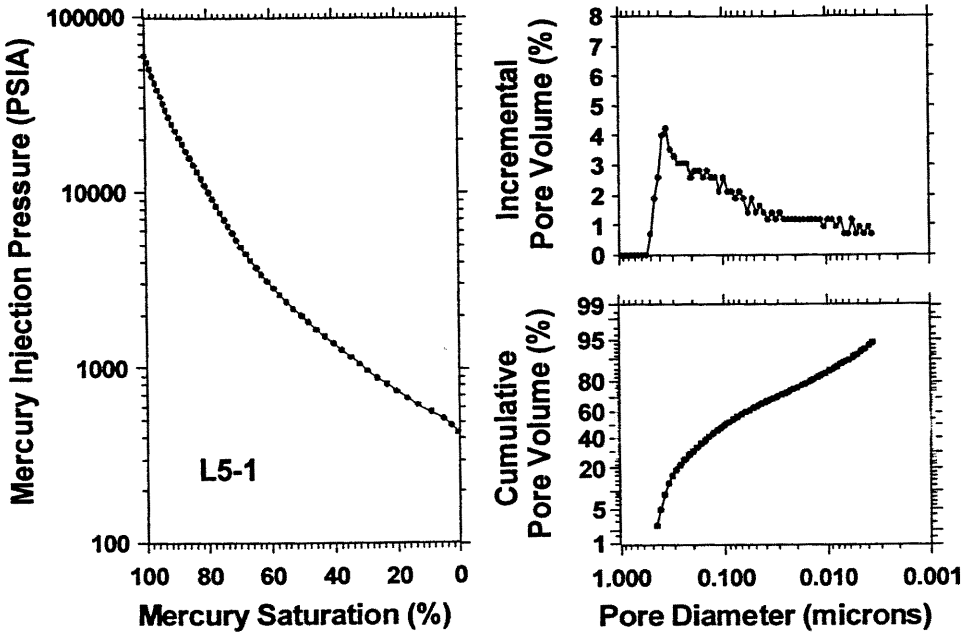
Mercury Injection Pressure (PSIA)
100000
10000
1000
100
L5-1
100 80 60 40 20 0
Mercury Saturation (%)
Incremental Pore Volume (%)
8 7 6 5 4 3 2 1 0
Cumulative Pore Volume (%)
99 95 80 60 40 20 5 1
1.000 0.100 0.010 0.001
Pore Diameter (microns)

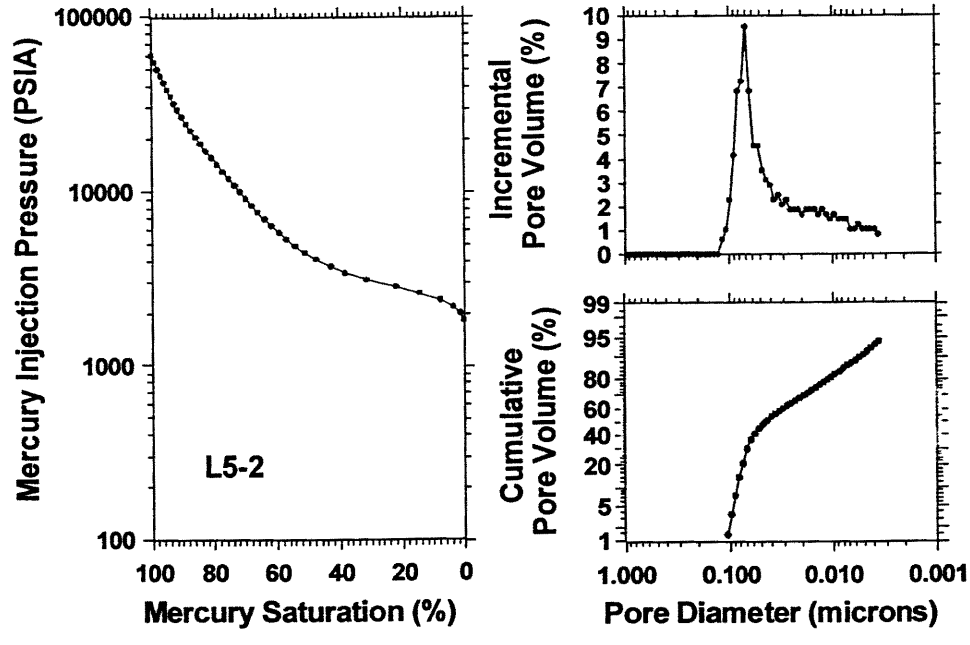
Mercury Injection Pressure (PSIA)
100000
10000
1000
100
L5-2
100 80 60 40 20 0
Mercury Saturation (%)
Incremental Pore Volume (%)
10 9 8 7 6 5 4 3 2 1 0
Cumulative Pore Volume (%)
99 95 80 60 40 20 5 1
1.000 0.100 0.010 0.001
Pore Diameter (microns)

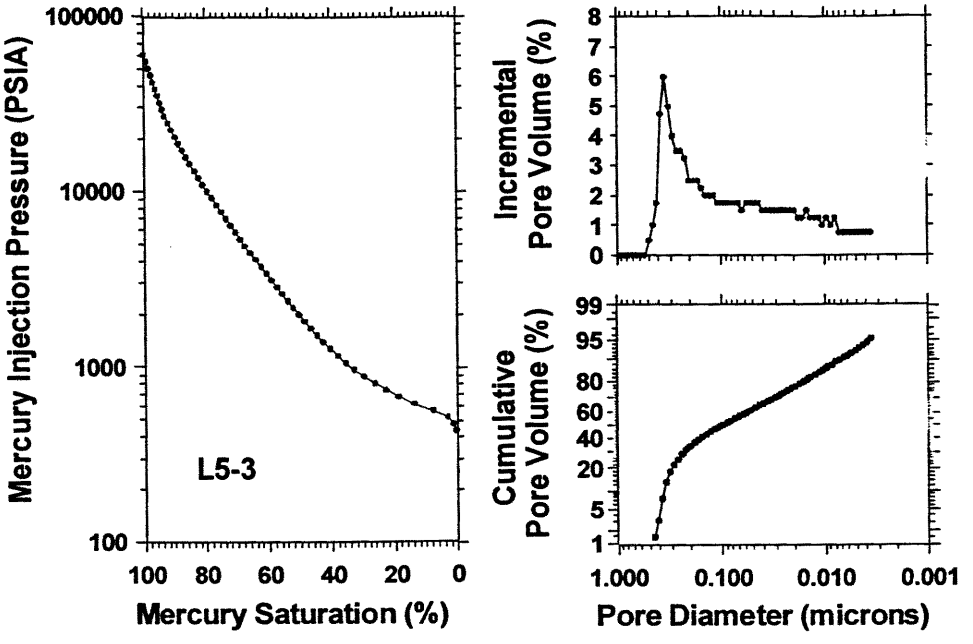
Mercury Injection Pressure (PSIA)
100000
10000
1000
100
L5-3
100 80 60 40 20 0
Mercury Saturation (%)
Incremental Pore Volume (%)
8 7 6 5 4 3 2 1 0
Cumulative Pore Volume (%)
99 95 80 60 40 20 5 1
1.000 0.100 0.010 0.001
Pore Diameter (microns)

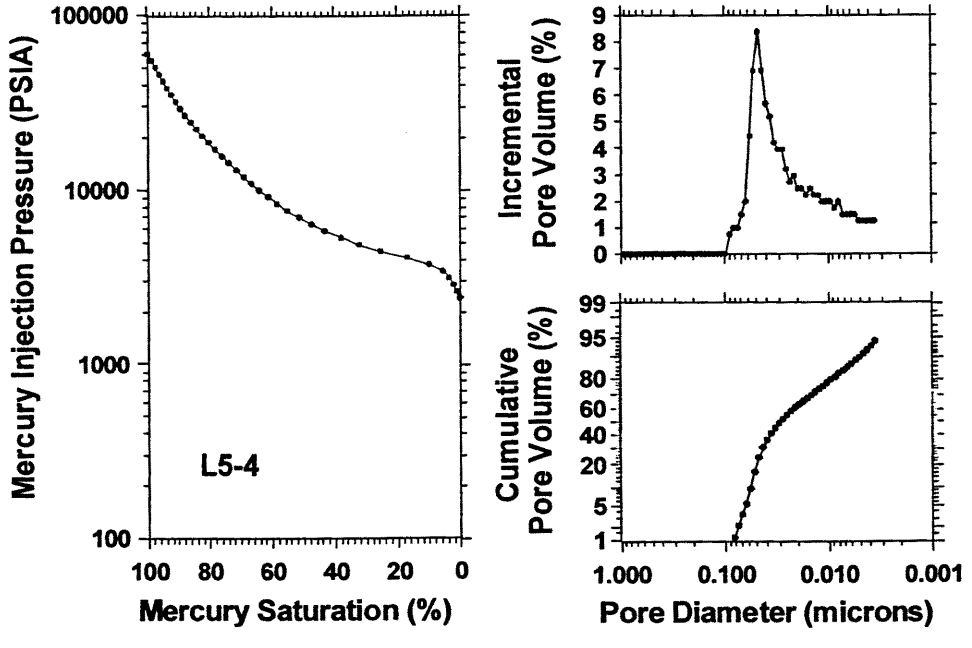
Mercury Injection Pressure (PSIA)
100000
10000
1000
100
L5-4
100 80 60 40 20 0
Mercury Saturation (%)
Incremental Pore Volume (%)
9 8 7 6 5 4 3 2 1 0
Cumulative Pore Volume (%)
99 95 80 60 40 20 5 1
1.000 0.100 0.010 0.001
Pore Diameter (microns)

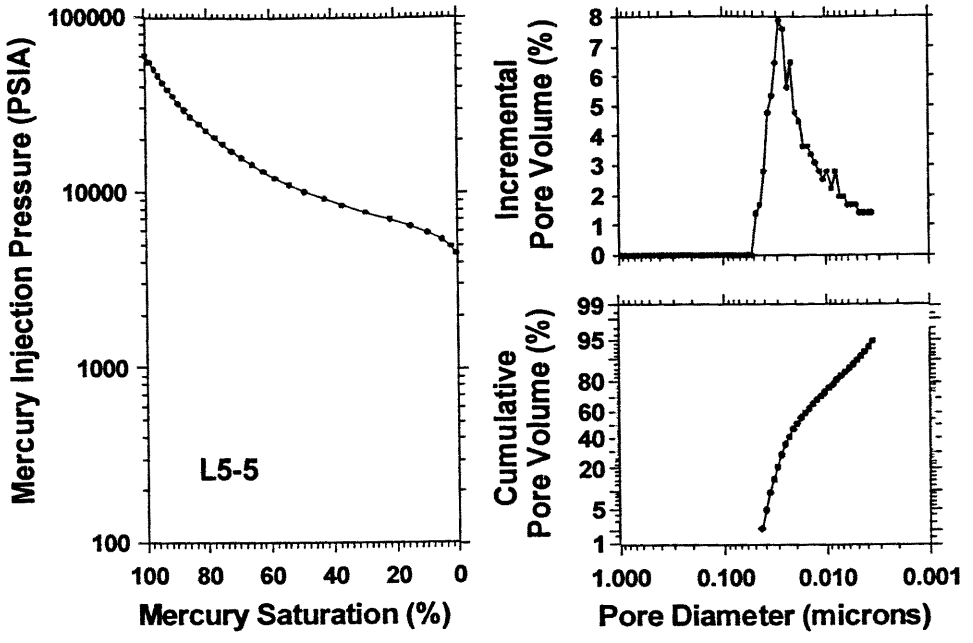
Mercury Injection Pressure (PSIA)
100000
10000
1000
100
L5-5
100 80 60 40 20 0
Mercury Saturation (%)
Incremental Pore Volume (%)
8 7 6 5 4 3 2 1 0
Cumulative Pore Volume (%)
99 95 80 60 40 20 5 1
1.000 0.100 0.010 0.001
Pore Diameter (microns)

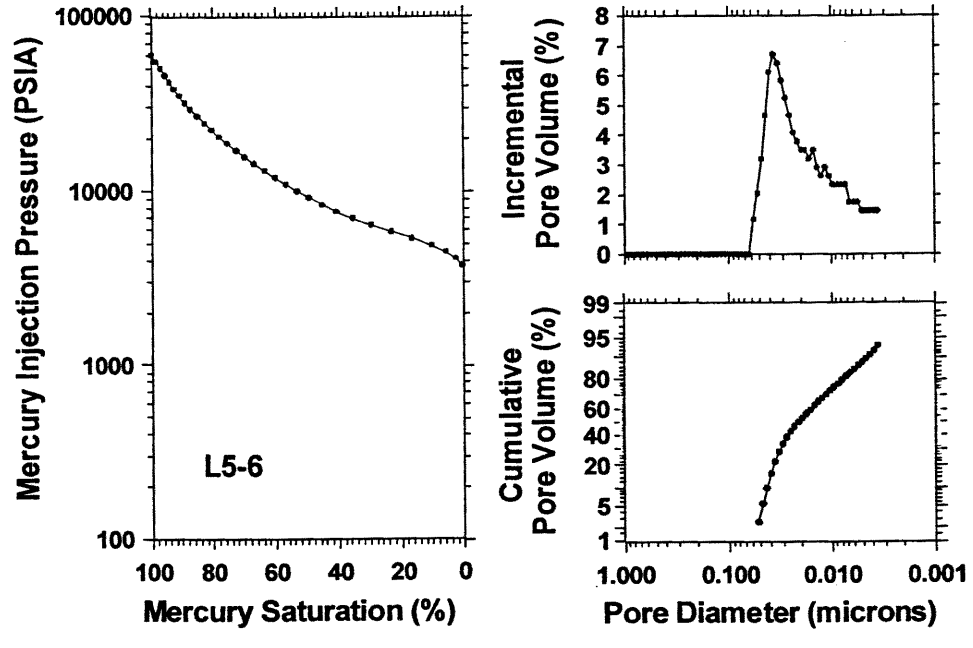
Mercury Injection Pressure (PSIA)
100000
10000
1000
100
L5-6
100 80 60 40 20 0
Mercury Saturation (%)
Incremental Pore Volume (%)
8 7 6 5 4 3 2 1 0
Cumulative Pore Volume (%)
99 95 80 60 40 20 5 1
1.000 0.100 0.010 0.001
Pore Diameter (microns)

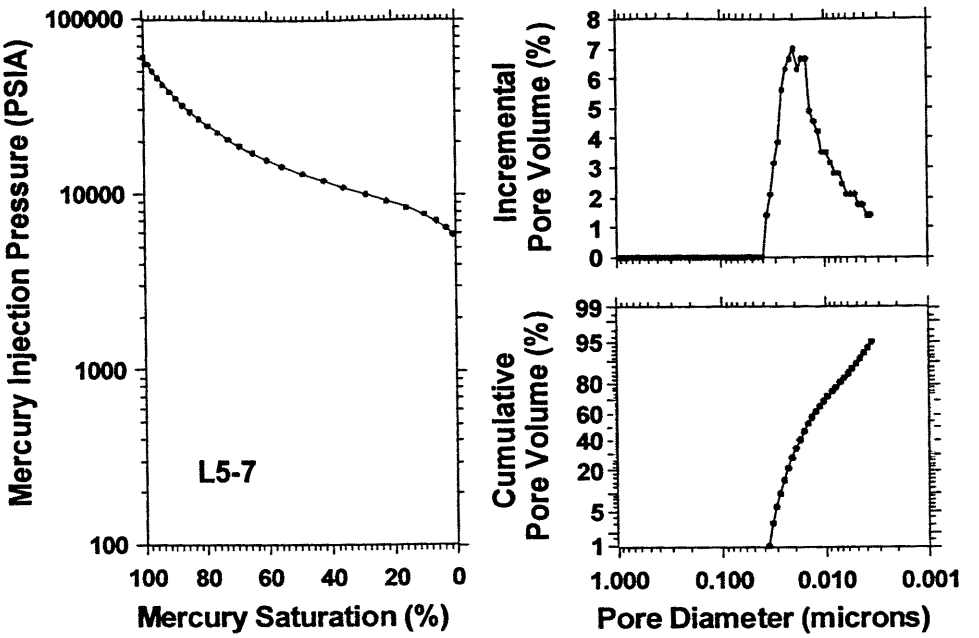
Mercury Injection Pressure (PSIA)
100000
10000
1000
100
L5-7
100 80 60 40 20 0
Mercury Saturation (%)
Incremental Pore Volume (%)
8 7 6 5 4 3 2 1 0
Cumulative Pore Volume (%)
99 95 80 60 40 20 5 1
1.000 0.100 0.010 0.001
Pore Diameter (microns)

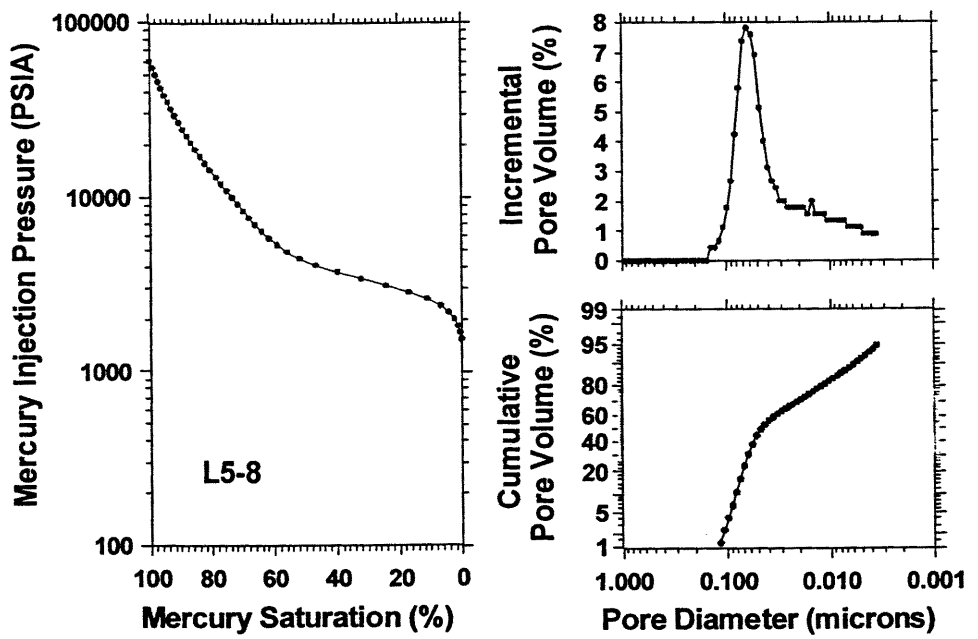
Mercury Injection Pressure (PSIA)
100000
10000
1000
100
L5-8
100 80 60 40 20 0
Mercury Saturation (%)
Incremental Pore Volume (%)
8 7 6 5 4 3 2 1 0
Cumulative Pore Volume (%)
99 95 80 60 40 20 5 1
1.000 0.100 0.010 0.001
Pore Diameter (microns)

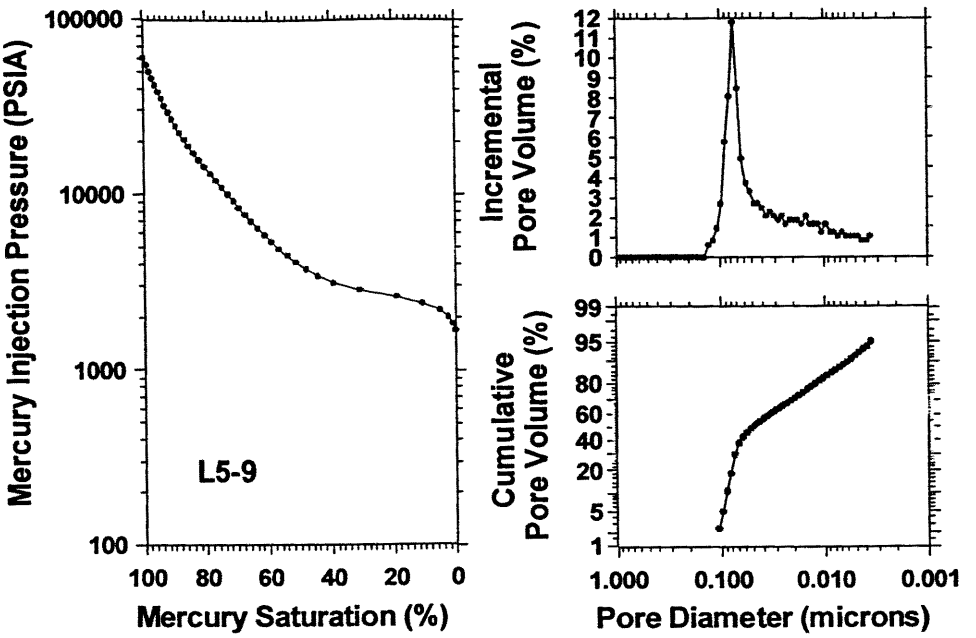
Mercury Injection Pressure (PSIA)
100000
10000
1000
100
L5-9
100 80 60 40 20 0
Mercury Saturation (%)
Incremental Pore Volume (%)
12
11
10
9
8
7
6
5
4
3
2
1
0
Cumulative Pore Volume (%)
99
95
80
60
40
20
5
1
1.000 0.100 0.010 0.001
Pore Diameter (microns)

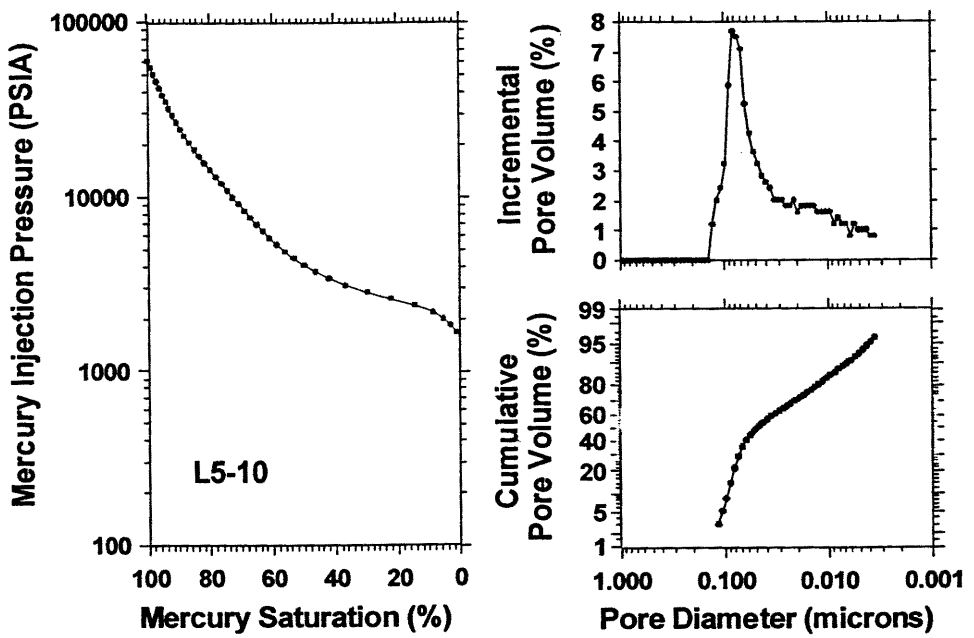
Mercury Injection Pressure (PSIA)
100000
10000
1000
100
L5-10
100 80 60 40 20 0
Mercury Saturation (%)
Incremental Pore Volume (%)
8
7
6
5
4
3
2
1
0
Cumulative Pore Volume (%)
99
95
80
60
40
20
5
1
1.000 0.100 0.010 0.001
Pore Diameter (microns)

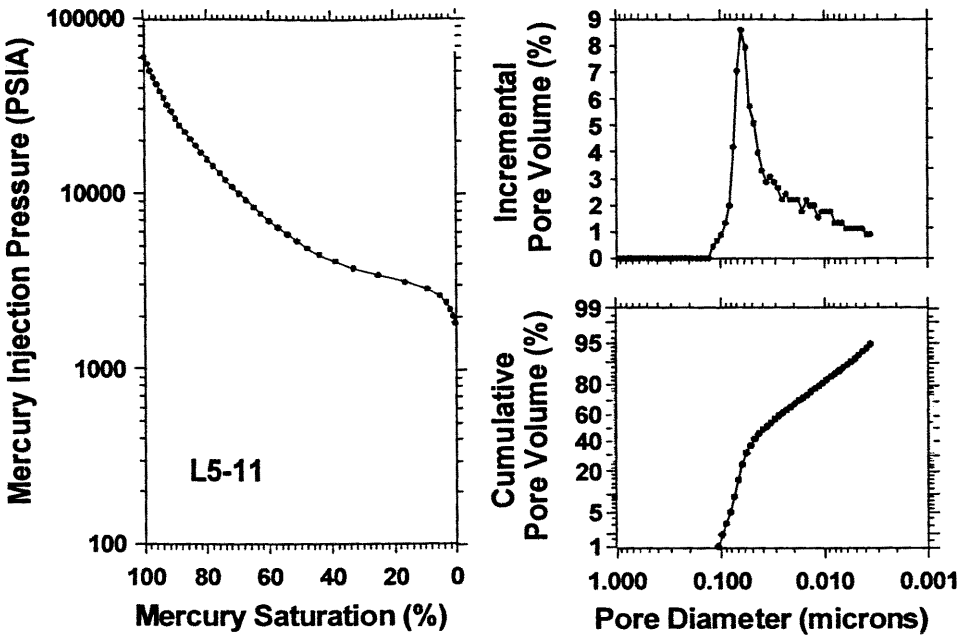
Mercury Injection Pressure (PSIA)
100000
10000
1000
100
L5-11
100 80 60 40 20 0
Mercury Saturation (%)
Incremental Pore Volume (%)
9 8 7 6 5 4 3 2 1 0
Cumulative Pore Volume (%)
99 95 80 60 40 20 5 1
1.000 0.100 0.010 0.001
Pore Diameter (microns)

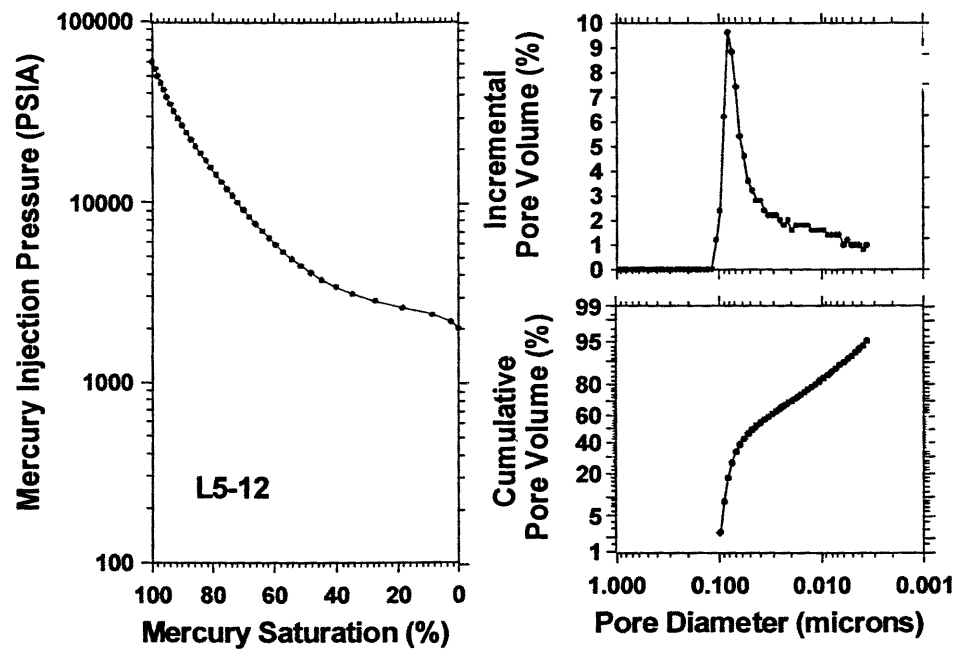
Mercury Injection Pressure (PSIA)
100000
10000
1000
100
L5-12
100 80 60 40 20 0
Mercury Saturation (%)
Incremental Pore Volume (%)
10 9 8 7 6 5 4 3 2 1 0
Cumulative Pore Volume (%)
99 95 80 60 40 20 5 1
1.000 0.100 0.010 0.001
Pore Diameter (microns)

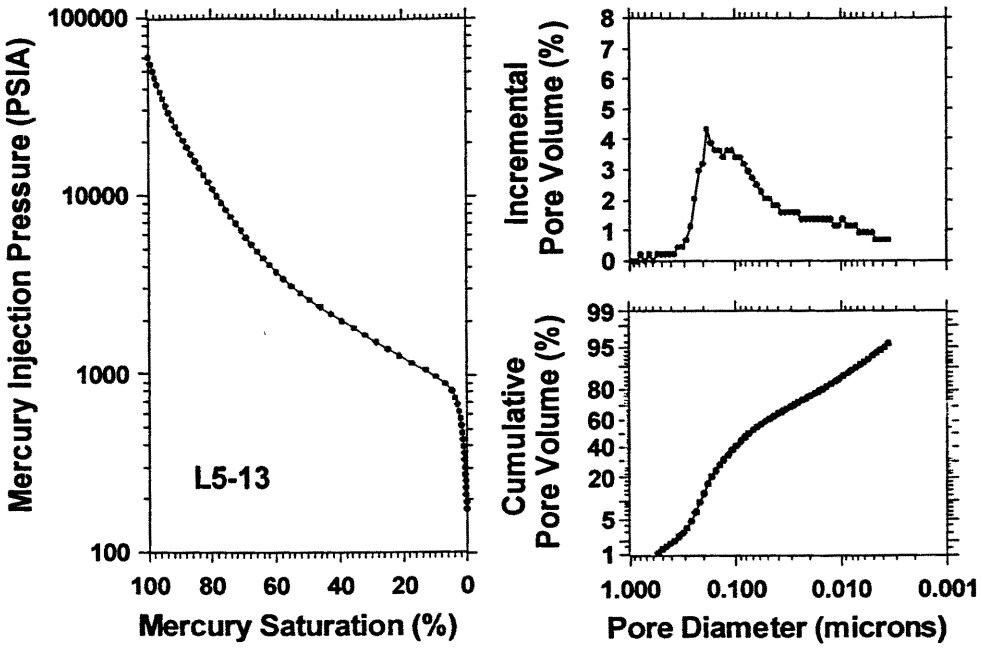
Mercury Injection Pressure (PSIA)
100000
10000
1000
100
L5-13
100 80 60 40 20 0
Mercury Saturation (%)
Incremental Pore Volume (%)
8 7 6 5 4 3 2 1 0
Cumulative Pore Volume (%)
99 95 80 60 40 20 5 1
1.000 0.100 0.010 0.001
Pore Diameter (microns)

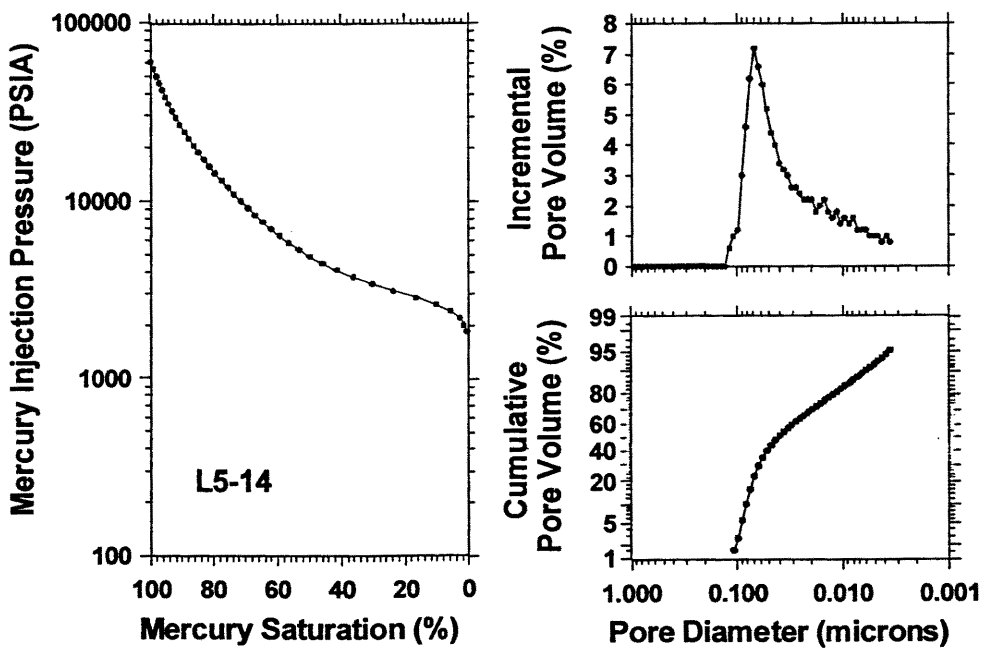
Mercury Injection Pressure (PSIA)
100000
10000
1000
100
L5-14
100 80 60 40 20 0
Mercury Saturation (%)
Incremental Pore Volume (%)
8 7 6 5 4 3 2 1 0
Cumulative Pore Volume (%)
99 95 80 60 40 20 5 1
1.000 0.100 0.010 0.001
Pore Diameter (microns)

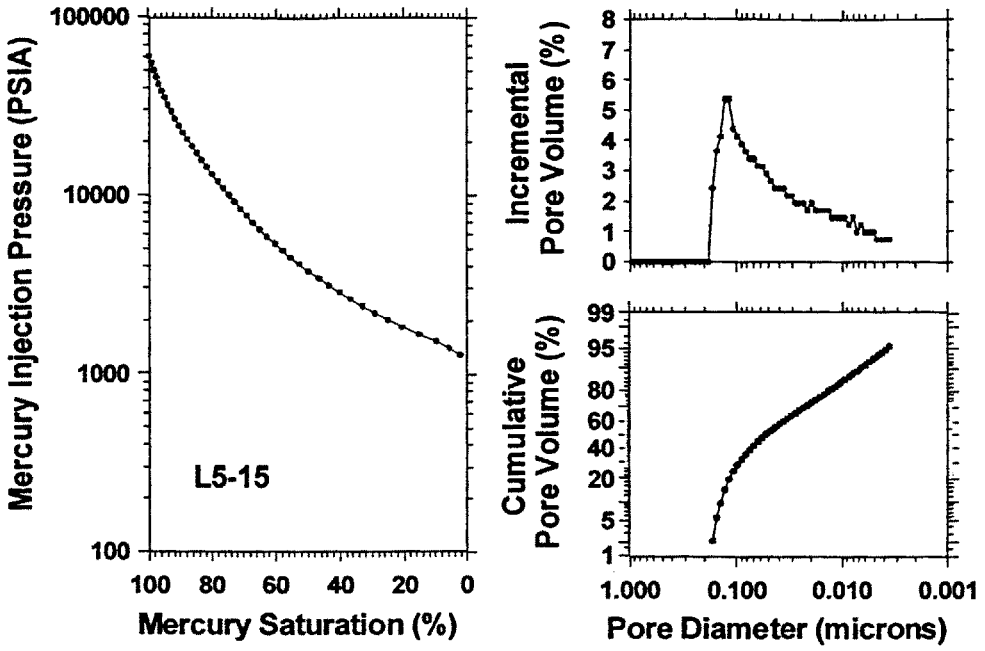
Mercury Injection Pressure (PSIA)
100000
10000
1000
100
L5-15
100 80 60 40 20 0
Mercury Saturation (%)
Incremental Pore Volume (%)
8 7 6 5 4 3 2 1 0
Cumulative Pore Volume (%)
99 95 80 60 40 20 5 1
1.000 0.100 0.010 0.001
Pore Diameter (microns)

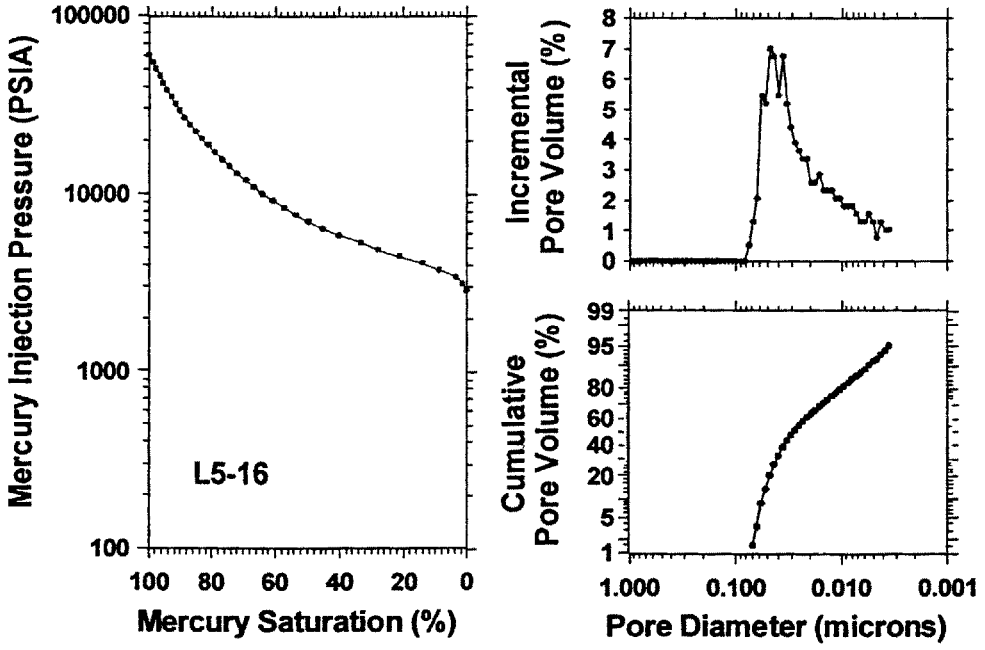
Mercury Injection Pressure (PSIA)
100000
10000
1000
100
L5-16
100 80 60 40 20 0
Mercury Saturation (%)
Incremental Pore Volume (%)
8 7 6 5 4 3 2 1 0
Cumulative Pore Volume (%)
99 95 80 60 40 20 5 1
1.000 0.100 0.010 0.001
Pore Diameter (microns)

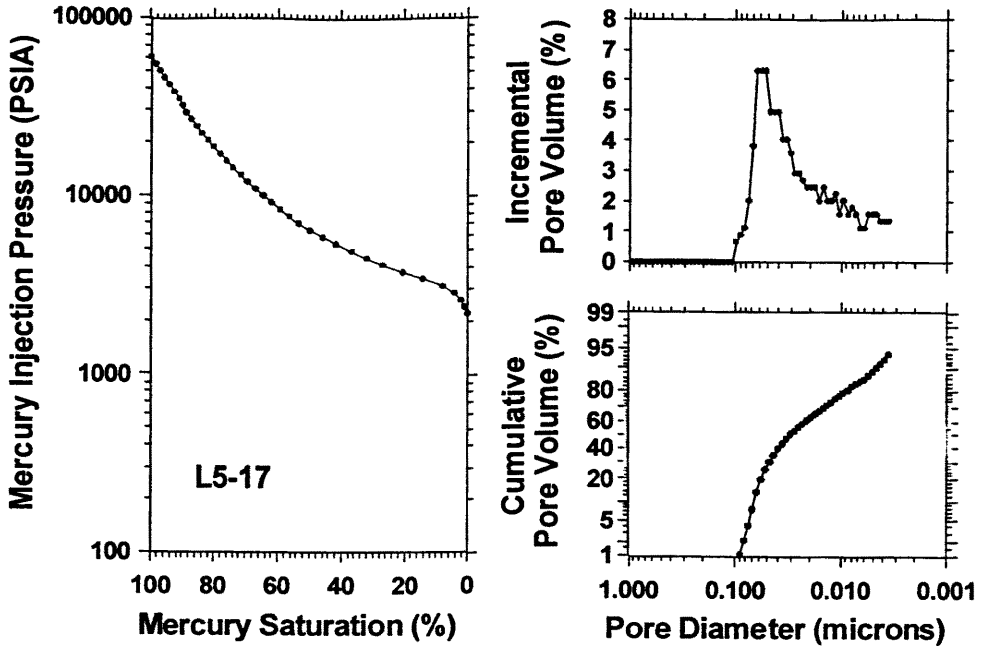
Mercury Injection Pressure (PSIA)
100000
10000
1000
100
L5-17
100 80 60 40 20 0
Mercury Saturation (%)
Incremental Pore Volume (%)
8 7 6 5 4 3 2 1 0
Cumulative Pore Volume (%)
99 95 80 60 40 20 5 1
1.000 0.100 0.010 0.001
Pore Diameter (microns)

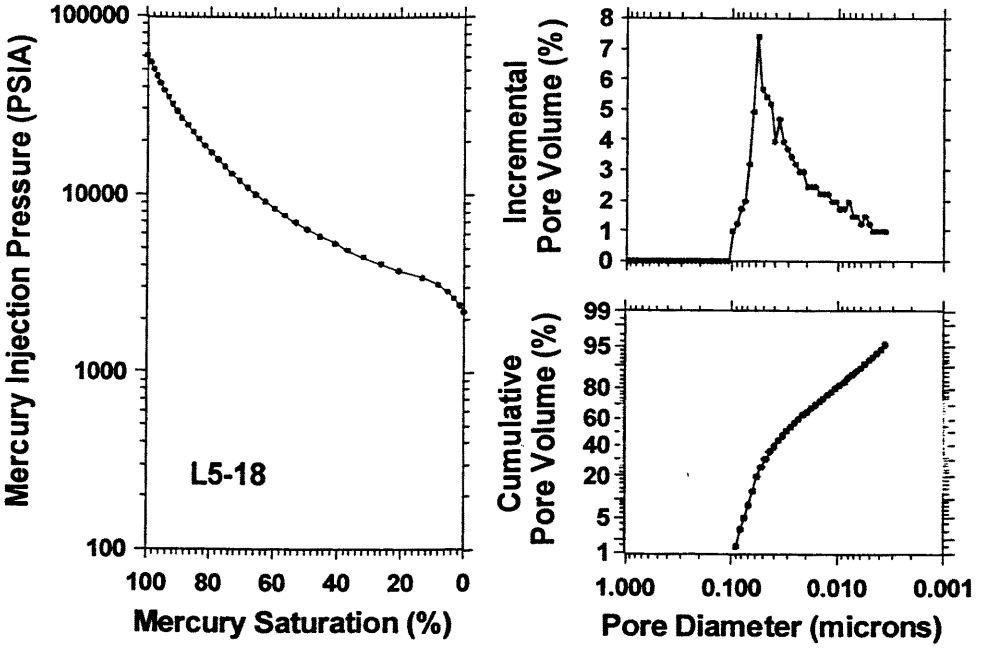
Mercury Injection Pressure (PSIA)
100000
10000
1000
100
L5-18
100 80 60 40 20 0
Mercury Saturation (%)
Incremental Pore Volume (%)
8 7 6 5 4 3 2 1 0
Cumulative Pore Volume (%)
99 95 80 60 40 20 5 1
1.000 0.100 0.010 0.001
Pore Diameter (microns)

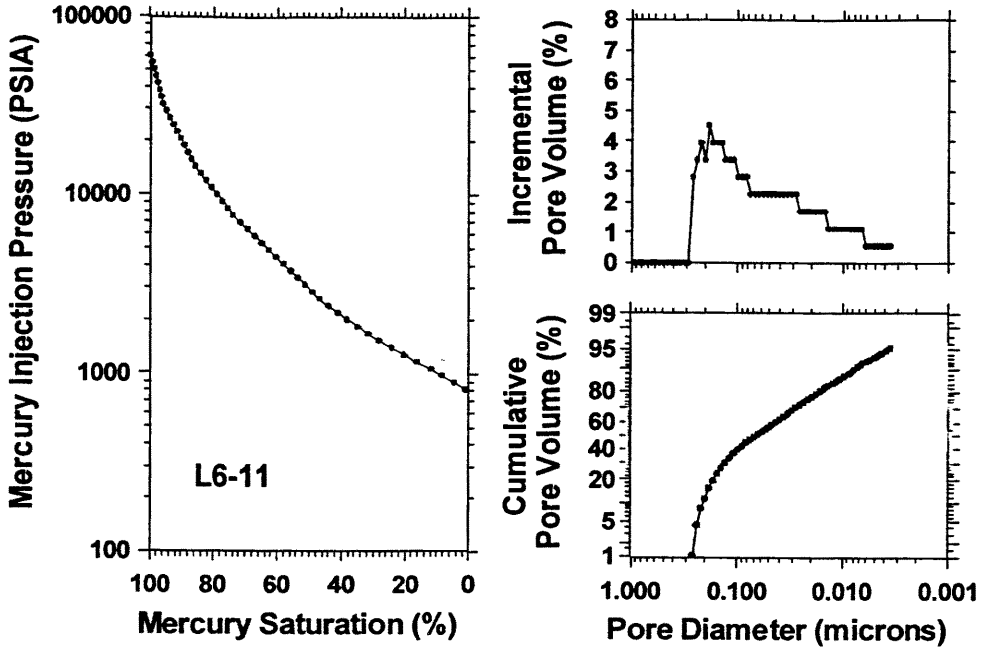
Mercury Injection Pressure (PSIA)
100000
10000
1000
100
L6-11
100 80 60 40 20 0
Mercury Saturation (%)
Incremental Pore Volume (%)
8 7 6 5 4 3 2 1 0
Cumulative Pore Volume (%)
99 95 80 60 40 20 5 1
1.000 0.100 0.010 0.001
Pore Diameter (microns)

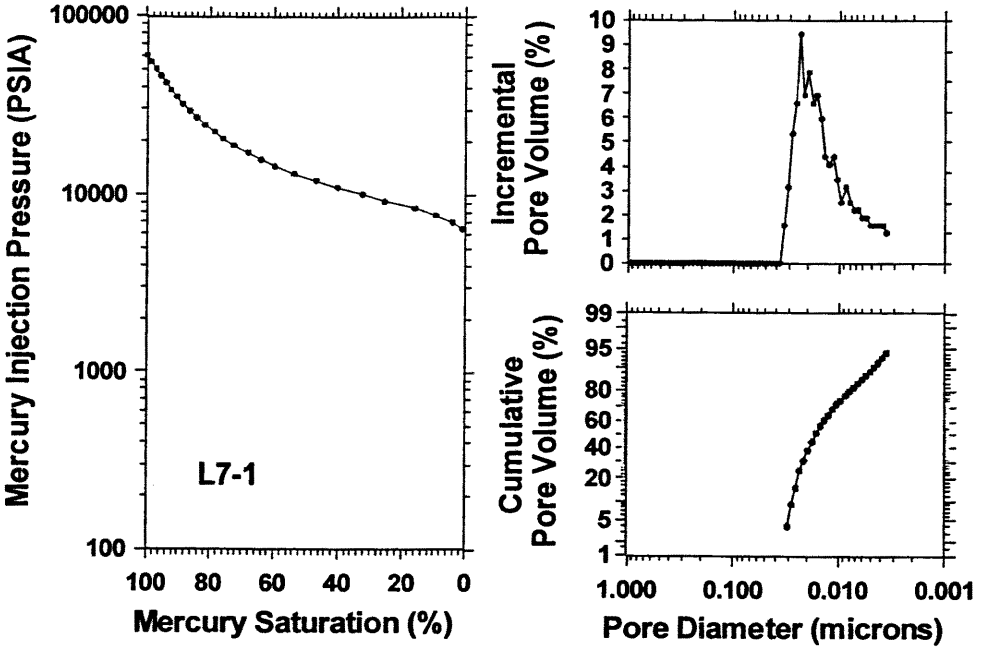
Mercury Injection Pressure (PSIA)
100000
10000
1000
100
L7-1
100 80 60 40 20 0
Mercury Saturation (%)
Incremental Pore Volume (%)
10 9 8 7 6 5 4 3 2 1 0
Cumulative Pore Volume (%)
99 95 80 60 40 20 5 1
1.000 0.100 0.010 0.001
Pore Diameter (microns)

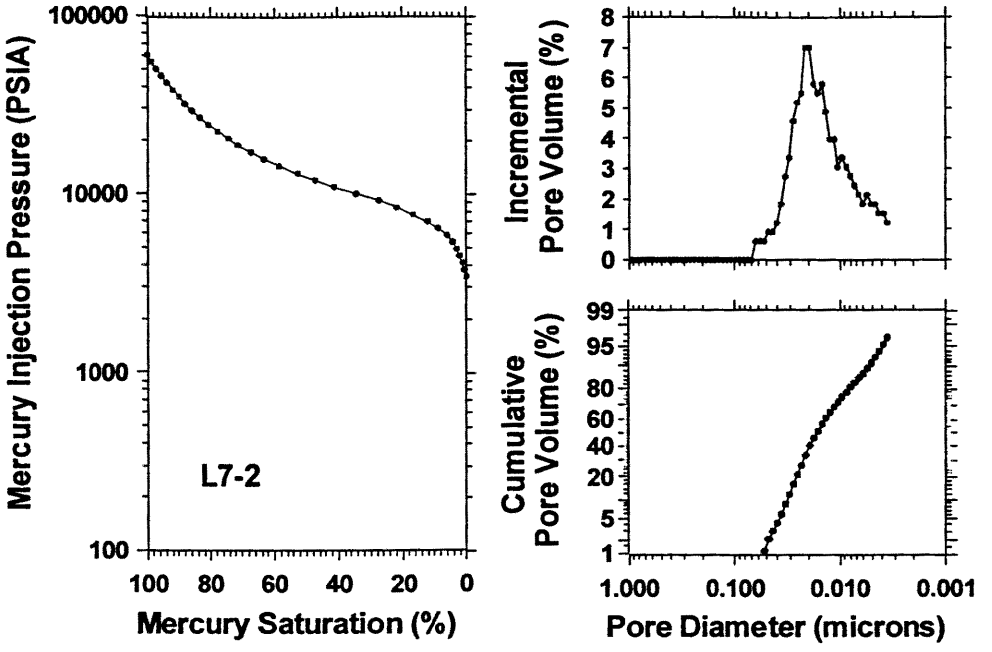
Mercury Injection Pressure (PSIA)
100000
10000
1000
100
L7-2
100 80 60 40 20 0
Mercury Saturation (%)
Incremental Pore Volume (%)
8 7 6 5 4 3 2 1 0
Cumulative Pore Volume (%)
99 95 80 60 40 20 5 1
1.000 0.100 0.010 0.001
Pore Diameter (microns)

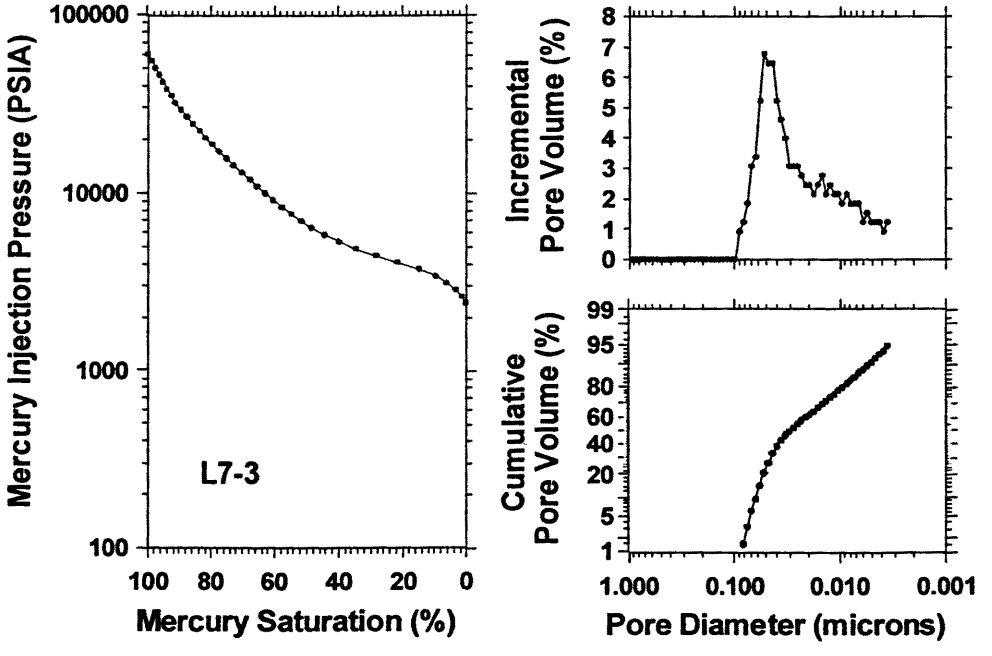
Mercury Injection Pressure (PSIA)
100000
10000
1000
100
L7-3
100 80 60 40 20 0
Mercury Saturation (%)
Incremental Pore Volume (%)
8 7 6 5 4 3 2 1 0
Cumulative Pore Volume (%)
99 95 80 60 40 20 5 1
1.000 0.100 0.010 0.001
Pore Diameter (microns)

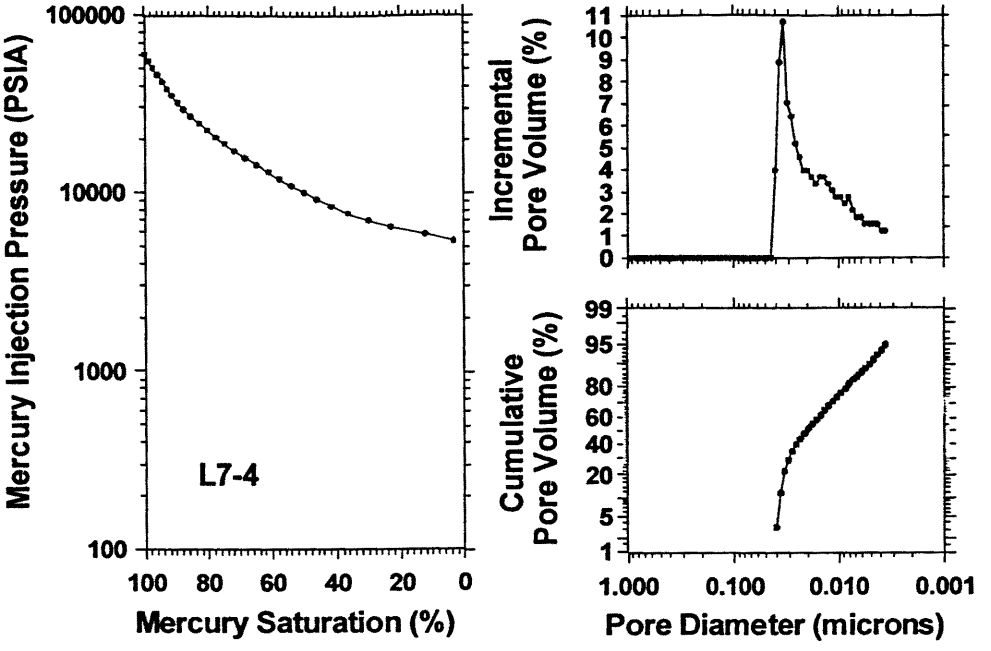
Mercury Injection Pressure (PSIA)
100000
10000
1000
100
L7-4
100 80 60 40 20 0
Mercury Saturation (%)
Incremental Pore Volume (%)
11 10 9 8 7 6 5 4 3 2 1 0
Cumulative Pore Volume (%)
99 95 80 60 40 20 5 1
1.000 0.100 0.010 0.001
Pore Diameter (microns)

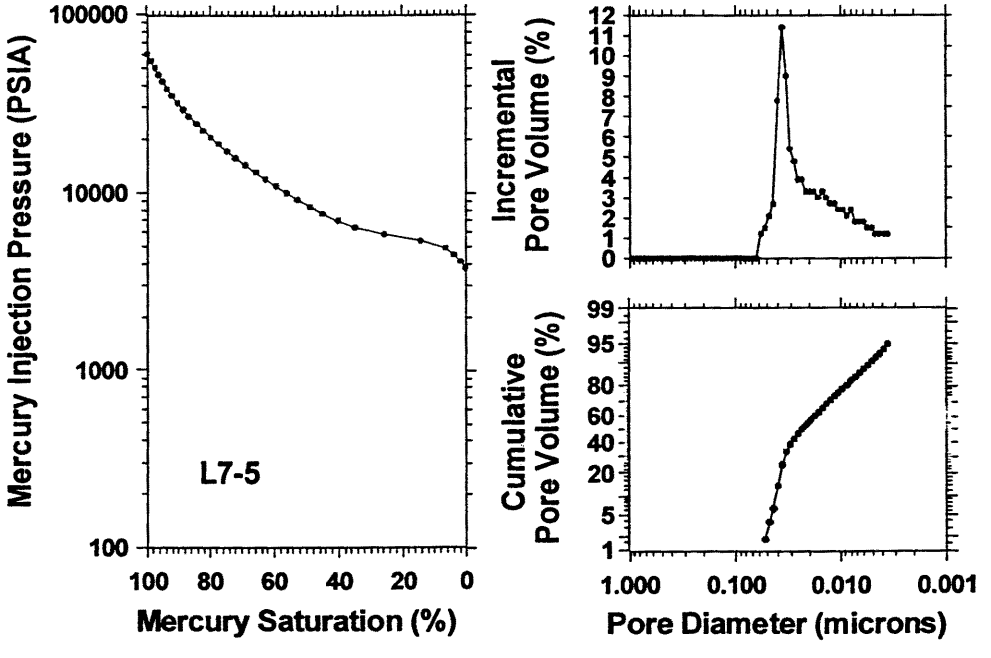
Mercury Injection Pressure (PSIA)
100000
10000
1000
100
L7-5
100 80 60 40 20 0
Mercury Saturation (%)
Incremental Pore Volume (%)
12 11 10 9 8 7 6 5 4 3 2 1 0
Cumulative Pore Volume (%)
99 95 80 60 40 20 5 1
1.000 0.100 0.010 0.001
Pore Diameter (microns)

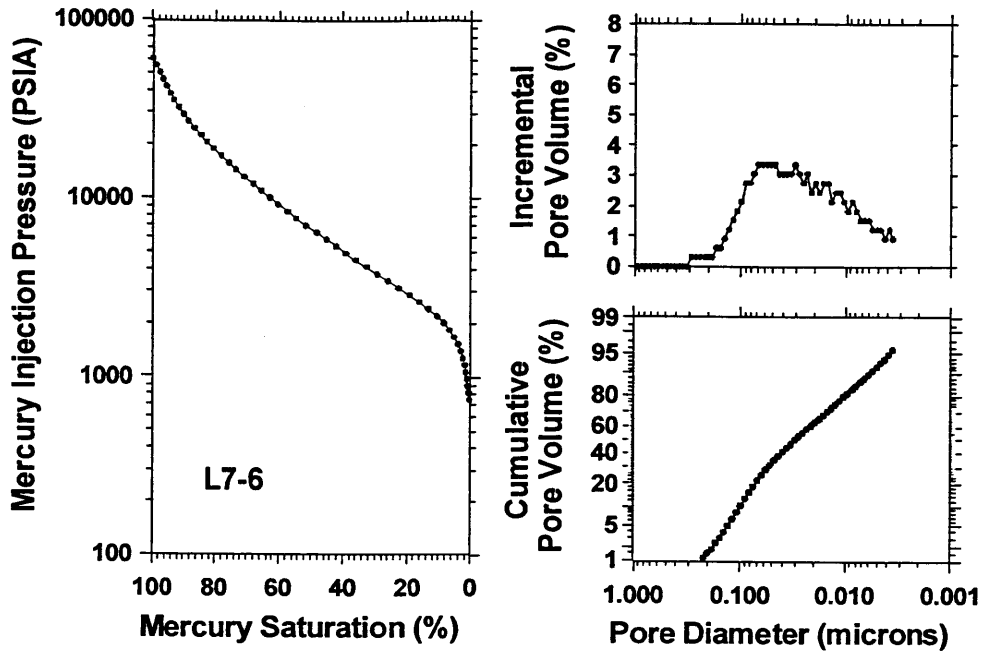
Mercury Injection Pressure (PSIA)
100000
10000
1000
100
L7-6
100 80 60 40 20 0
Mercury Saturation (%)
Incremental Pore Volume (%)
8 7 6 5 4 3 2 1 0
Cumulative Pore Volume (%)
99 95 80 60 40 20 5 1
1.000 0.100 0.010 0.001
Pore Diameter (microns)

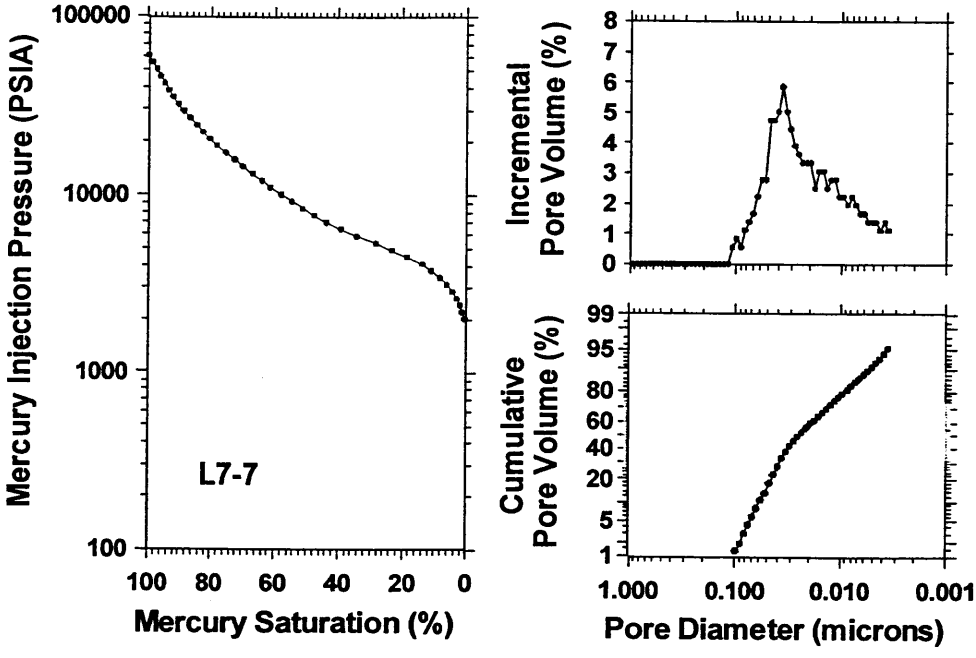
Mercury Injection Pressure (PSIA)
100000
10000
1000
100
L7-7
100 80 60 40 20 0
Mercury Saturation (%)
Incremental Pore Volume (%)
8 7 6 5 4 3 2 1 0
Cumulative Pore Volume (%)
99 95 80 60 40 20 5 1
1.000 0.100 0.010 0.001
Pore Diameter (microns)

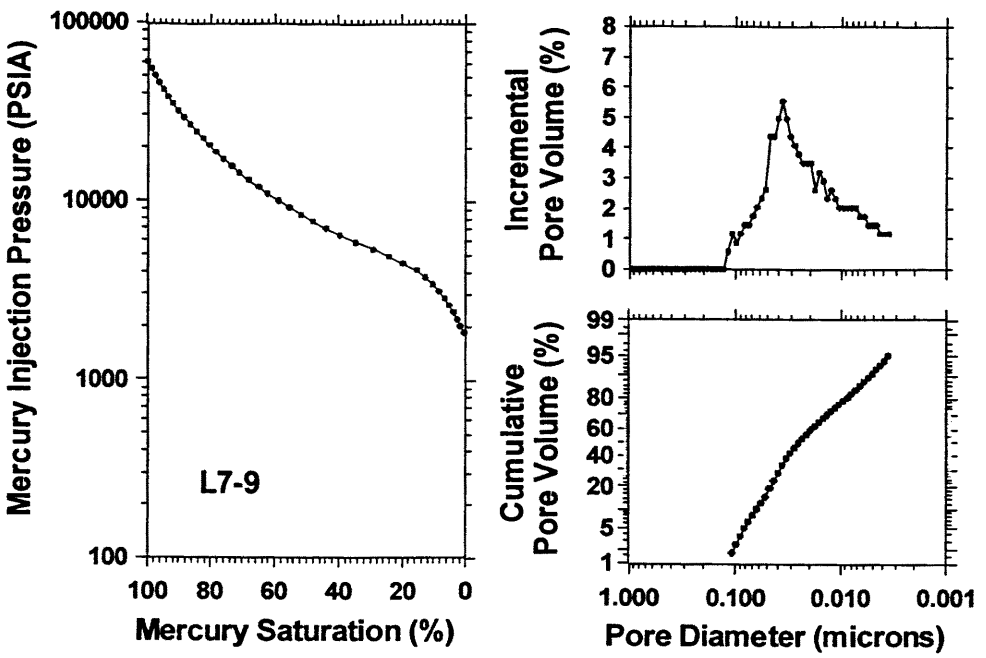
Mercury Injection Pressure (PSIA)
100000
10000
1000
100
L7-9
100 80 60 40 20 0
Mercury Saturation (%)
Incremental Pore Volume (%)
8 7 6 5 4 3 2 1 0
Cumulative Pore Volume (%)
99 95 80 60 40 20 5 1
1.000 0.100 0.010 0.001
Pore Diameter (microns)

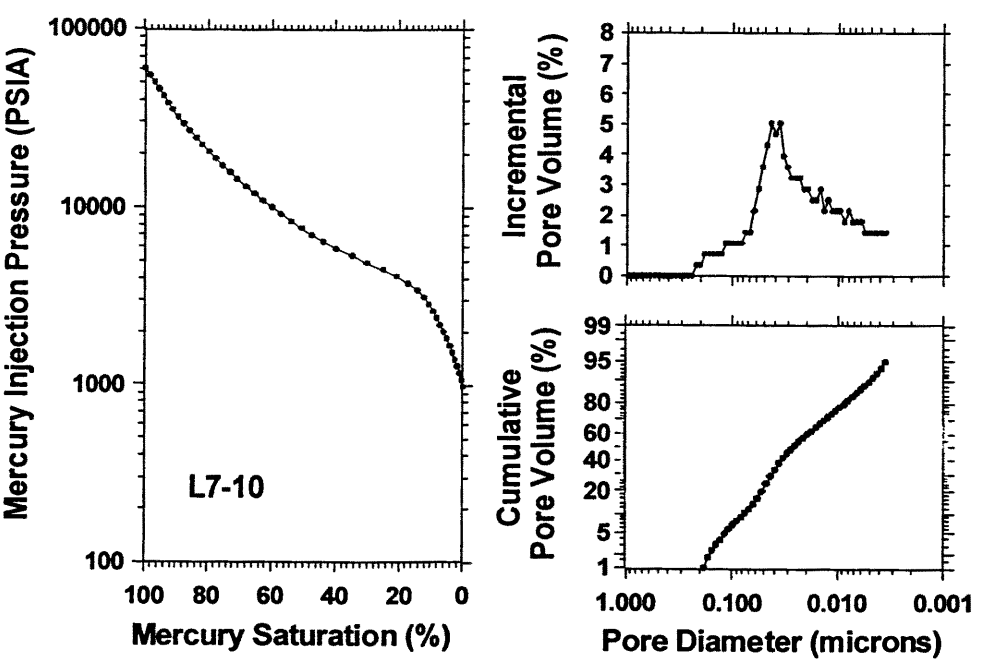
Mercury Injection Pressure (PSIA)
100000
10000
1000
100
L7-10
100 80 60 40 20 0
Mercury Saturation (%)
Incremental Pore Volume (%)
8 7 6 5 4 3 2 1 0
Cumulative Pore Volume (%)
99 95 80 60 40 20 5 1
1.000 0.100 0.010 0.001
Pore Diameter (microns)

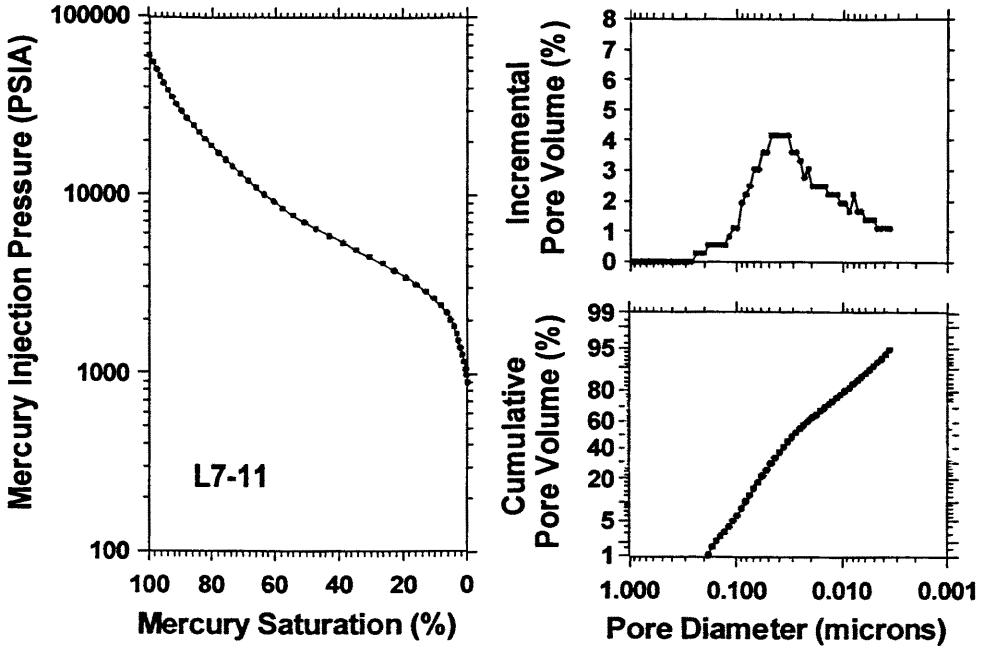
Mercury Injection Pressure (PSIA)
100000
10000
1000
100
L7-11
100 80 60 40 20 0
Mercury Saturation (%)
Incremental Pore Volume (%)
8 7 6 5 4 3 2 1 0
Cumulative Pore Volume (%)
99 95 80 60 40 20 5 1
1.000 0.100 0.010 0.001
Pore Diameter (microns)

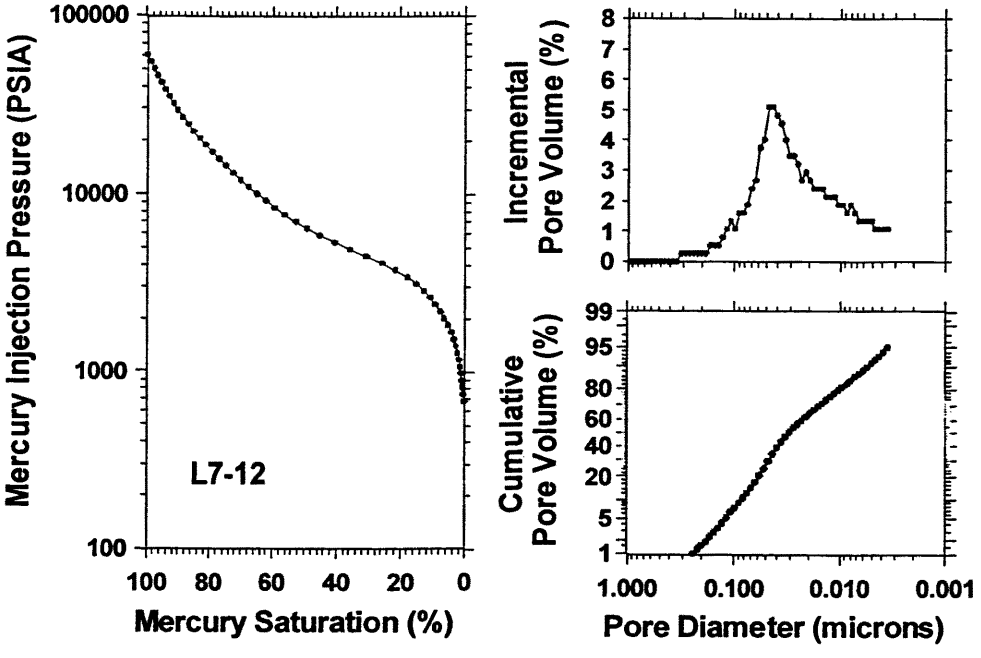
Mercury Injection Pressure (PSIA)
100000
10000
1000
100
L7-12
100 80 60 40 20 0
Mercury Saturation (%)
Incremental Pore Volume (%)
8 7 6 5 4 3 2 1 0
Cumulative Pore Volume (%)
99 95 80 60 40 20 5 1
1.000 0.100 0.010 0.001
Pore Diameter (microns)

APPENDIX C

POROSITY, PERMEABILITY, AND GRAIN DENSTITY DATA

Wasatch Outcrop Sample #s:	Porotech. Spl No.	Stratigraphic Position (m)	Sample Porosity(%)	Spl MICP Porosity(%)	Sample Air Perm(md)	Calc MICP Perm(md)	Sample Gr Den(g\cc)	Spl MICP Gr Den(g\cc)
Wast-B1-1	1	0.35	11.0	6.3	*	0.001	2.77	2.70
Wast-B1-2	2	0.8	8.6	7.3	*	0.001	2.71	2.67
Wast-B1-3	3	1	8.7	5.8	*	0.001	2.72	2.66
Wast-B1-4	4	1.1	6.1	5.4	*	0.001	2.66	2.66
Wast-B1-5	5	1.3	8.4	6.9	*	0.001	2.67	2.65
Wast-B1-6	6	1.7	8.9	7.1	*	0.001	2.69	2.68
Wast-B1-7	7	2.2	8.7	6.6	*	0.001	2.69	2.67
Wast-B1-8	8	2.4	8.0	5.8	0.1530	0.001	2.69	2.67
Wast-B1-9	9	2.6	9.1	5.8	1.0830	0.001	2.72	2.68
Wast-B1-10	10	3.1	7.9	5.6	0.0750	0.001	2.68	2.64
Wast-B2-1	1	0.2	9.7	8.7	*	0.001	2.68	2.68
Wast-B2-2	2	0.6	12.2	9.0	1.4450	0.001	2.70	2.67
Wast-B2-3	3	1.1	12.7	8.5	0.3050	0.001	2.69	2.69
Wast-B2-4	4	1.5	10.1	8.8	*	0.001	2.69	2.68
Wast-B2-5	5	2	8.1	8.4	*	0.001	2.65	2.67
Wast-B2-6	6	2.3	13.4	8.1	0.5020	0.001	2.67	2.67
Wast-B2-7	7	2.8	11.8	8.6	0.5420	0.001	2.70	2.68
Wast-B2-8	8	3.4	11.7	8.3	1.1850	0.001	2.71	2.67
Wast-B2-9	9	4.1	13.1	8.6	1.2160	0.001	2.71	2.69
Wast-B2-10	10	4.5	11.9	8.4	*	0.001	2.75	2.67
Wast-L1-2	2	6	12.0	8.0	0.1220	0.001	2.73	2.68
Wast-L1-3	3	1.7	12.1	8.2	*	0.001	2.73	2.70
Wast-L1-4	4	3.9	13.4	9.1	*	0.001	2.67	2.67
Wast-L1-5	5	4	13.3	9.0	*	0.001	2.76	2.66
Wast-L1-6	6	4.1	12.8	8.9	*	0.002	2.73	2.68
Wast-L1-7	7	7	8.7	6.7	0.0010	0.006	2.69	2.65
Wast-L1-8	8	1	9.2	7.5	*	0.001	2.69	2.64
Wast-L1-9	9	2.7	11.7	8.5	*	0.001	2.81	2.68
Wast-L1-10	10	6.4	10.3	7.9	*	0.001	2.76	2.72
Wast-L1-11	11	10.2	*	6.4	*	0.001	*	2.64
Wast-L3-1	1	6.5	12.5	8.2	*	0.001	2.72	2.68
Wast-L3-2	2	9.5	10.6	8.7	0.0010	0.007	2.72	2.68
Wast-L3-4	4	17.9	10.2	9.1	0.0010	0.011	2.71	2.68
Wast-L3-5	5	20.3	10.4	6.5	*	0.001	2.79	2.66

Wasatch Outcrop Sample #s:	Porotech. Spl No.	Stratigraphic Position (m)	Sample Porosity(%)	Spl MICP Porosity(%)	Sample Air Perm(md)	Calc MICP Perm(md)	Sample Gr Den(g\cc)	Spl MICP Gr Den(g\cc)
Wast-L3-6	6	24.6	8.7	9.7	*	0.002	2.63	2.68
Wast-L3-7	7	2.4	8.0	8.6	*	0.002	2.65	2.67
Wast-L3-8	8	4.3	11.1	7.4	*	0.001	2.74	2.67
Wast-L3-9	9	5.6	10.3	7.7	*	0.001	2.71	2.68
Wast-L3-10	10	7.7	9.6	6.9	*	0.001	2.69	2.64
Wast-L3-11	11	8..5	*	9.7	*	0.002	*	2.68
Wast-L3-12	12	12.7	*	8.9	*	0.003	*	2.68
Wast-L4-1	1	2.4	9.5	9.0	0.0880	0.002	2.71	2.68
Wast-L4-2	2	4.5	10.8	8.9	0.0610	0.001	2.73	2.68
Wast-L4-3	3	6.2	5.1	4.7	0.0730	0.006	2.67	2.66
Wast-L4-4	4	7.4	7.4	7.3	0.1090	0.019	2.66	2.65
Wast-L4-5	5	7.8	7.1	6.7	0.0290	0.005	2.67	2.64
Wast-L4-6	6	8.1	7.5	6.7	0.0410	0.000	2.71	2.67
Wast-L4-7	7	11.5	12.3	9.8	*	0.002	2.70	2.68
Wast-L4-8	8	15.3	8.9	6.6	*	0.000	2.70	2.65
Wast-L4-9	9	18	8.8	6.8	*	0.001	2.69	2.66
Wast-L5-1	1	2.1	14.4	10.1	*	0.023	2.75	2.65
Wast-L5-2	2	5	16.0	11.6	*	0.006	2.72	2.67
Wast-L5-3	3	7.5	10.4	9.6	0.1810	0.025	2.69	2.66
Wast-L5-4	4	8.25	15.1	9.9	*	0.002	2.67	2.66
Wast-L5-5	5	10.1	12.0	9.1	*	0.001	2.71	2.68
Wast-L5-6	6	12.5	11.6	8.7	*	0.001	2.71	2.67
Wast-L5-7	7	14.5	11.5	7.5	*	0.000	2.74	2.69
Wast-L5-8	8	4.6	15.7	10.8	0.0290	0.005	2.72	2.68
Wast-L5-9	9	5.1	10.9	11.6	0.0400	0.007	2.70	2.67
Wast-L5-10	10	5.3	13.9	11.8	0.1450	0.007	2.68	2.64
Wast-L5-11	11	5.6	12.4	10.8	*	0.004	2.68	2.66
Wast-L5-12	12	5.8	13.7	11.8	*	0.006	2.63	2.65
Wast-L5-13	13	6.5	11.4	10.4	0.1880	0.011	2.69	2.69
Wast-L5-14	14	6.8	14.4	11.8	*	0.005	2.70	2.63
Wast-L5-15	1	7.1	10.0	10.0	0.0520	0.007	2.68	2.65
Wast-L5-16	2	7.3	10.3	9.5	0.1850	0.002	2.68	2.65
Wast-L5-17	3	7.6	13.3	10.7	*	0.003	2.69	2.66
Wast-L5-18	4	7.9	11.8	10.1	*	0.002	2.66	2.66
Wast-L6-11	5	4	6.7	5.0	*	0.004	2.70	2.68

Wasatch Outcrop Sample #s:	Porotech. Spl No.	Stratigraphic Position (m)	Sample Porosity(%)	Spl MICP Porosity(%)	Sample Air Perm(md)	Calc MICP Perm(md)	Sample Gr Den(g\cc)	Spl MICP Gr Den(g\cc)
Wast-L7-1	1	0.5	9.3	8.2	22.7000	0.001	2.71	2.67
Wast-L7-2	2	1	10.8	8.3	*	0.001	2.69	2.70
Wast-L7-3	3	1.7	10.5	8.3	0.0250	0.002	2.73	2.69
Wast-L7-4	4	2.5	10.5	8.6	*	0.001	2.70	2.68
Wast-L7-5	5	3	10.2	8.5	*	0.001	2.69	2.67
Wast-L7-6	6	3.7	8.5	7.9	0.0320	0.002	2.71	2.66
Wast-L7-7	7	4.3	11.7	8.7	*	0.001	2.70	2.67
Wast-L7-9	9	7	12.8	8.6	*	0.001	2.76	2.69
Wast-L7-10	10	7.4	12.5	7.0	*	0.001	2.77	2.68
Wast-L7-11	11	9.4	10.4	8.7	*	0.002	2.68	2.64
Wast-L7-12	12	9.9	10.8	8.9	*	0.002	2.70	2.68

NOTE: Sample perm data designated by " * " represents samples for which a result could not be made on the plug cut from the outcrop sample. (from Porotech)

APPENDIX D

TOTAL ORGANIC CARBON DATA

Wasatch Outcrop Sample #s:	Stratigraphic Position	Total Organic Carbon (%)
Wast-B1-1	0.35	0.11
Wast-B1-2	0.8	0.09
Wast-B1-3	1	0.07
Wast-B1-4	1.1	0.05
Wast-B1-5	1.3	0.02
Wast-B1-6	1.7	0.03
Wast-B1-7	2.2	0.05
Wast-B1-8	2.4	0.04
Wast-B1-9	2.6	0.03
Wast-B1-10	3.1	0.04
Group Average		0.05
Group Median		0.04
Group Std. Dev.		0.03
Wast-B2-1	0.2	0.05
Wast-B2-2	0.6	0.08
Wast-B2-3	1.1	0.22
Wast-B2-4	1.5	0.23
Wast-B2-5	2	0.22
Wast-B2-6	2.3	0.24
Wast-B2-7	2.8	0.27
Wast-B2-8	3.4	0.19
Wast-B2-9	4.1	0.15
Wast-B2-10	4.5	0.11
Group Average		0.18
Group Median		0.21
Group Std. Dev.		0.08
Wast-L1-2	0.85	0.23
Wast-L1-3	1.7	0.20
Wast-L1-4	3.9	0.23
Wast-L1-5	4	0.21
Wast-L1-6	4.1	0.21
Wast-L1-7	7	0.35
Wast-L1-8	1	0.37
Wast-L1-9	2.7	0.19
Wast-L1-10	6.4	0.35
Wast-L1-11	10.2	NA
Group Average		0.26
Group Median		0.23
Group Std. Dev.		0.07

Wasatch Outcrop Sample #s:	Stratigraphic Position	Total Organic Carbon (%)
Wast-L3-1	6.5	0.40
Wast-L3-2	9.5	0.34
Wast-L3-4	17.9	0.34
Wast-L3-5	20.3	0.12
Wast-L3-6	24.6	0.27
Wast-L3-7	2.4	0.54
Wast-L3-8	4.3	0.37
Wast-L3-9	5.6	0.46
Wast-L3-10	7.7	0.23
Wast-L3-11	8..5	0.36
Wast-L3-12	12.7	0.51
Group Average		0.36
Group Median		0.36
Group Std. Dev.		0.12
Wast-L4-1	2.4	0.38
Wast-L4-2	4.5	0.47
Wast-L4-3	6.2	0.36
Wast-L4-4	7.4	0.31
Wast-L4-5	7.8	0.20
Wast-L4-6	8.1	0.10
Wast-L4-7	11.5	0.24
Wast-L4-8	15.3	0.09
Wast-L4-9	18	0.16
Group Average		0.26
Group Median		0.24
Group Std. Dev.		0.13
Wast-L5-1	2.1	0.54
Wast-L5-2	5	0.71
Wast-L5-3	7.5	0.53
Wast-L5-4	8.25	0.41
Wast-L5-5	10.1	0.29
Wast-L5-6	12.5	0.29
Wast-L5-7	14.5	0.16
Group Average		0.42
Group Median		0.41
Group Std. Dev.		0.19

Wasatch Outcrop Sample #s:	Stratigraphic Position	Total Organic Carbon (%)
Wast-L5-8	4.6	0.53
Wast-L5-9	5.1	0.74
Wast-L5-10	5.3	0.74
Wast-L5-11	5.6	0.74
Wast-L5-12	5.8	0.22
Wast-L5-13	6.5	0.72
Wast-L5-14	6.8	0.55
Wast-L5-15	7.1	0.68
Wast-L5-16	7.3	0.67
Wast-L5-17	7.6	0.54
Wast-L5-18	7.9	0.51
Group Average		0.60
Group Median		0.67
Group Std. Dev.		0.16
Wast-L6-11	4	0.16
Wast-L7-1	0.5	0.27
Wast-L7-2	1	0.25
Wast-L7-3	1.7	0.27
Wast-L7-4	2.5	0.23
Wast-L7-5	3	0.28
Wast-L7-6	3.7	0.38
Wast-L7-7	4.3	0.33
Wast-L7-9	7	0.37
Wast-L7-10	7.4	0.15
Wast-L7-11	9.4	0.29
Wast-L7-12	9.9	NA
Group Average		0.28
Group Median		0.28
Group Std. Dev.		0.07

APPENDIX E

XRF DATA

Sample	Strat. Position (m)	SiO2	Al2O3	CaO	MgO	Na2O	K2O	Fe2O3	MnO	TiO2	P2O5	Cr2O3	LOI	Sum
Det. Lim.		0.01	0.01	0.01	0.01	0.01	0.01	0.01	0.01	0.01	0.01	0.01	0.01	0.01
B1-1	0.35	66.27	16.12	1.1	1.65	0.93	2.6	5.33	0.03	0.67	0.21	0.01	5.3	100.3
B1-5	1.3	65.43	15.48	1.82	1.36	0.79	2.55	5.39	0.06	0.63	0.13	0.01	5.85	99.61
B1-7	2.2	70.85	14.4	0.16	1.28	0.77	2.42	4.71	0.02	0.6	0.11	0.02	4.75	100.2
B1-8	2.4	73.06	13.16	0.14	1.05	0.69	2.4	5.16	0.02	0.56	0.08	0.02	3.8	100.3
B1-9	2.6	74.59	12.85	0.19	1	0.71	2.3	4.2	0.01	0.54	0.06	0.02	3.85	100.4
B1-10	3.1	73.74	13.06	0.54	1	0.68	2.31	4.22	0.01	0.55	0.05	0.02	3.8	100.1
B2-1	0.2	64.31	18.4	0.21	1.45	0.64	2.8	6.82	0.01	0.68	0.07	0.02	5.05	100.5
B2-2	0.6	62.13	19.22	0.26	1.68	0.66	3.17	6.48	0.02	0.68	0.12	0.01	5.75	100.3
B2-3	1.1	62.58	18.43	1.62	1.83	0.63	3.16	4.91	0.02	0.67	0.19	0.01	6.3	100.5
B2-4	1.5	62.7	18.05	1.37	1.83	0.62	3.09	5.47	0.02	0.68	0.19	0.01	6.15	100.3
B2-5	2	63.01	16.85	2.42	1.88	0.66	2.91	4.94	0.03	0.66	0.21	0.02	6.5	100.2
B2-7	2.8	61.67	17.42	2.15	1.94	0.73	2.95	5	0.03	0.67	0.18	0.01	7.5	100.4
B2-8	3.4	61.14	17.6	2.21	1.93	0.72	2.99	5.39	0.02	0.66	0.21	0.01	6.85	99.84
B2-9	4.1	62.89	17.87	0.75	1.95	0.71	2.97	6.32	0.02	0.67	0.23	0.01	5.85	100.3
B2-10	4.5	65.06	17.39	0.37	1.61	0.78	2.91	6.18	0.02	0.66	0.26	0.01	4.8	100.2
L1-2	1.5	58.45	17.43	3.93	2.32	0.72	3.18	5.3	0.04	0.69	0.19	0.01	7.95	100.3
L1-3	1.7	56.74	17.49	3.73	2.67	0.65	3.2	6.78	0.05	0.72	0.2	0.01	7.95	100.3
L1-4	3.9	59.43	17.45	3.26	2.16	0.67	3.16	5.58	0.03	0.69	0.19	0.01	7.55	100.3
L1-5	4	59.29	17.81	2.92	2.33	0.72	3.19	5.72	0.03	0.68	0.18	0.01	7.3	100.3
L1-7	7	69.14	11.78	4.13	1.95	0.95	2.14	2.79	0.03	0.55	0.15	0.01	6.5	100.2
L1-9	2.7	57.81	16.88	4.56	2.13	0.68	3.01	5.91	0.04	0.67	0.19	0.01	8.35	100.4
L3-2	9.5	60.04	16.58	3.1	2.72	1.03	2.94	5.17	0.03	0.7	0.18	0.01	7.45	100.1
L3-4	17.9	61.2	13.36	5.31	2.54	1.08	2.38	5.32	0.07	0.59	0.2	0.01	8.1	100.3
L3-5	20.3	68.95	14.88	0.41	1.61	0.98	2.82	5.38	0.02	0.64	0.12	0.01	4.3	100.2
L3-6	24.6	59.18	16.87	2.65	2.29	0.84	2.91	7.11	0.04	0.68	0.24	0.01	7.4	100.3
L3-10	7.7	62.34	17.78	1.5	2.2	0.97	3.26	5.11	0.03	0.7	0.17	0.01	6	100.2
L3-11	8.5	58.9	17.16	3.19	2.32	1.02	3.07	5.84	0.03	0.69	0.2	0.01	7.65	100.2
L3-12	12.7	62.33	14.29	4.35	2.11	1.01	2.63	5.03	0.04	0.61	0.2	0.01	7.45	100.2
L4-2	4.5	61.55	16.39	2.71	2.24	0.78	3.02	5.43	0.03	0.67	0.2	0.01	7.15	100.3
L4-3	6.2	64.2	14.42	4.46	2.06	0.92	2.57	3.08	0.04	0.62	0.14	0.01	7.55	100.2
L4-4	7.4	70.91	11.04	4.23	1.72	1.06	2.16	2.15	0.03	0.49	0.13	0.01	6.2	100.3
L4-6	8.1	66.44	16.27	0.69	1.87	0.83	3.01	5.28	0.02	0.67	0.19	0.01	4.8	100.2
L4-8	15.3	66.95	16.38	0.19	1.77	0.65	2.96	5.67	0.02	0.68	0.07	0.01	4.7	100.1
L4-9	18	61.04	15.73	3.71	2.25	0.46	2.89	5.57	0.05	0.66	0.27	0.01	7.45	100.2
L5-1	2.1	65.25	14.34	3.13	2.11	0.99	2.65	4.25	0.02	0.62	0.16	0.01	6.55	100.2
L5-2	5	58.73	16.41	4.57	2.25	0.71	2.84	4.98	0.03	0.64	0.41	0.01	8.45	100.2
L5-3	7.5	59.65	17.03	3.41	2.53	0.75	3.16	4.95	0.03	0.7	0.17	0.01	7.85	100.3

Sample	Strat. Position (m)	SiO2	Al2O3	CaO	MgO	Na2O	K2O	Fe2O3	MnO	TiO2	P2O5	Cr2O3	LOI	Sum
Det. Lim.		0.01	0.01	0.01	0.01	0.01	0.01	0.01	0.01	0.01	0.01	0.01	0.01	0.01
L5-5	11.1	60	16.75	3.25	2.33	0.73	3.04	5.66	0.03	0.68	0.22	0.01	7.45	100.2
L5-6	12.5	58.4	17.27	3.43	2.28	0.77	3.18	5.69	0.03	0.68	0.19	0.01	8	100
L5-7	14.5	59.25	18.42	1.21	2.62	0.83	3.35	6.63	0.03	0.72	0.26	0.01	6.25	99.69
L5-8	4.6	53.67	18.01	3.27	3.89	0.94	3.2	7.79	0.05	0.79	0.17	0.01	8.35	100.3
L5-9	5.1	60.71	17.56	2.61	2.46	0.71	3.19	4.57	0.02	0.7	0.18	0.01	7.35	100.2
L5-10	5.3	58.58	17.63	3.08	2.76	0.78	3.12	5.19	0.03	0.72	0.16	0.01	8.1	100.3
L5-11	5.6	59.21	17.53	3.1	2.69	0.72	3.09	4.88	0.02	0.72	0.16	0.01	8.05	100.3
L5-12	5.8	61.04	16.75	3.74	2.24	0.68	2.98	4.07	0.03	0.68	0.18	0.02	8	100.5
L5-13	6.5	57.01	16.13	4.32	3.39	1.14	2.78	6.21	0.06	0.72	0.17	0.01	8.2	100.2
L5-14	6.8	58.93	17.3	3.63	2.58	0.76	3.2	5.04	0.03	0.7	0.36	0.01	7.85	100.5
L5-15	7.1	60.13	15.63	4.31	2.39	0.74	2.86	4.93	0.04	0.63	0.45	0.01	7.95	100.2
L5-16	7.3	59.91	16.73	3.56	2.39	0.75	2.99	4.95	0.03	0.68	0.18	0.01	7.95	100.3
L5-17	7.6	60.21	16.02	4.19	2.14	0.68	2.94	4.88	0.03	0.65	0.18	0.01	8.15	100.2
L5-18	7.9	59.71	16.99	4.25	2.1	0.64	3.19	4.2	0.03	0.66	0.19	0.01	8.15	100.2
L6-11	3	48.21	8.11	18.85	1.24	0.72	1.54	1.68	1.47	0.37	0.45	0.01	16.9	99.63
L7-1	0.5	59.87	18.09	2.6	2.36	0.66	3.44	4.96	0.02	0.69	0.18	0.01	7.25	100.3
L7-2	1	60.61	17.23	2.72	2.32	0.67	3.23	5.72	0.03	0.68	0.17	0.01	6.8	100.3
L7-6	3.7	59.35	16.73	3.53	2.35	0.69	3.06	5.93	0.04	0.68	0.2	0.01	7.55	100.2
L7-10	7.4	68.91	14.42	0.74	1.7	1.02	2.71	4.86	0.02	0.64	0.18	0.01	4.3	99.62
L7-12	9.9	60.95	15.95	3.69	2.29	0.87	2.83	5.15	0.04	0.68	0.2	0.01	7.45	100.2

Sample	Strat. Position (m)	Rb	Sr	Y	Zr	Nb	Ba
Det. Lim.		2	2	2	2	2	20
B1-1	0.35	123	90	47	203	17	389
B1-5	1.3	140	92	49	209	16	377
B1-7	2.2	123	81	55	261	16	391
B1-8	2.4	119	95	54	243	15	412
B1-9	2.6	114	78	43	264	15	354
B1-10	3.1	123	82	34	277	15	356
B2-1	0.2	159	102	30	182	17	388
B2-2	0.6	177	103	40	166	17	409
B2-3	1.1	166	106	45	165	19	395
B2-4	1.5	157	109	49	169	19	428
B2-5	2	145	120	51	169	17	399
B2-7	2.8	144	118	44	165	18	388
B2-8	3.4	150	110	55	162	18	395
B2-9	4.1	150	101	54	173	18	382
B2-10	4.5	148	106	130	187	17	387
L1-2	1.5	146	131	52	153	17	399
L1-3	1.7	146	130	54	156	17	410
L1-4	3.9	149	160	48	159	16	414
L1-5	4	152	141	47	152	15	400
L1-7	7	88	123	41	262	14	366
L1-9	2.7	140	154	51	145	14	369
L3-2	9.5	132	109	48	187	17	410
L3-4	17.9	105	136	46	229	14	668
L3-5	20.3	127	96	44	267	15	452
L3-6	24.6	140	106	50	163	16	555
L3-10	7.7	146	99	43	201	17	422
L3-11	8.5	144	129	51	156	17	387
L3-12	12.7	118	135	46	193	15	406
L4-2	4.5	140	118	51	174	17	393
L4-3	6.2	119	139	49	221	14	451
L4-4	7.4	92	120	46	286	11	438
L4-6	8.1	138	99	52	229	16	421
L4-8	15.3	138	95	34	225	18	389
L4-9	18	138	116	56	181	16	358
L5-1	2.1	119	132	50	240	15	381
L5-2	5	135	166	72	155	16	381
L5-3	7.5	143	137	50	176	17	396
L5-5	11.1	140	130	55	168	15	388
L5-6	12.5	151	129	53	157	17	419
L5-7	14.5	161	95	55	172	18	423
L5-8	4.6	127	158	42	165	16	465
L5-9	5.1	150	129	49	170	16	427

Sample	Strat. Position (m)	Rb	Sr	Y	Zr	Nb	Ba
Det. Lim.		2	2	2	2	2	20
L5-10	5.3	144	125	48	171	18	385
L5-11	5.6	145	132	49	171	17	387
L5-12	5.8	141	150	52	175	16	402
L5-13	6.5	115	120	45	212	16	398
L5-14	6.8	149	144	75	162	17	440
L5-15	7.1	129	153	87	170	14	422
L5-16	7.3	141	158	51	176	17	428
L5-17	7.6	135	147	53	173	16	409
L5-18	7.9	147	156	55	152	16	379
L6-11	3	67	111	73	111	8	251
L7-1	0.5	161	142	49	154	17	409
L7-2	1	155	124	49	168	15	387
L7-6	3.7	146	138	52	159	16	381
L7-10	7.4	117	87	46	253	16	387
L7-12	9.9	134	119	52	178	15	363

Major and Trace Elements for Location B1

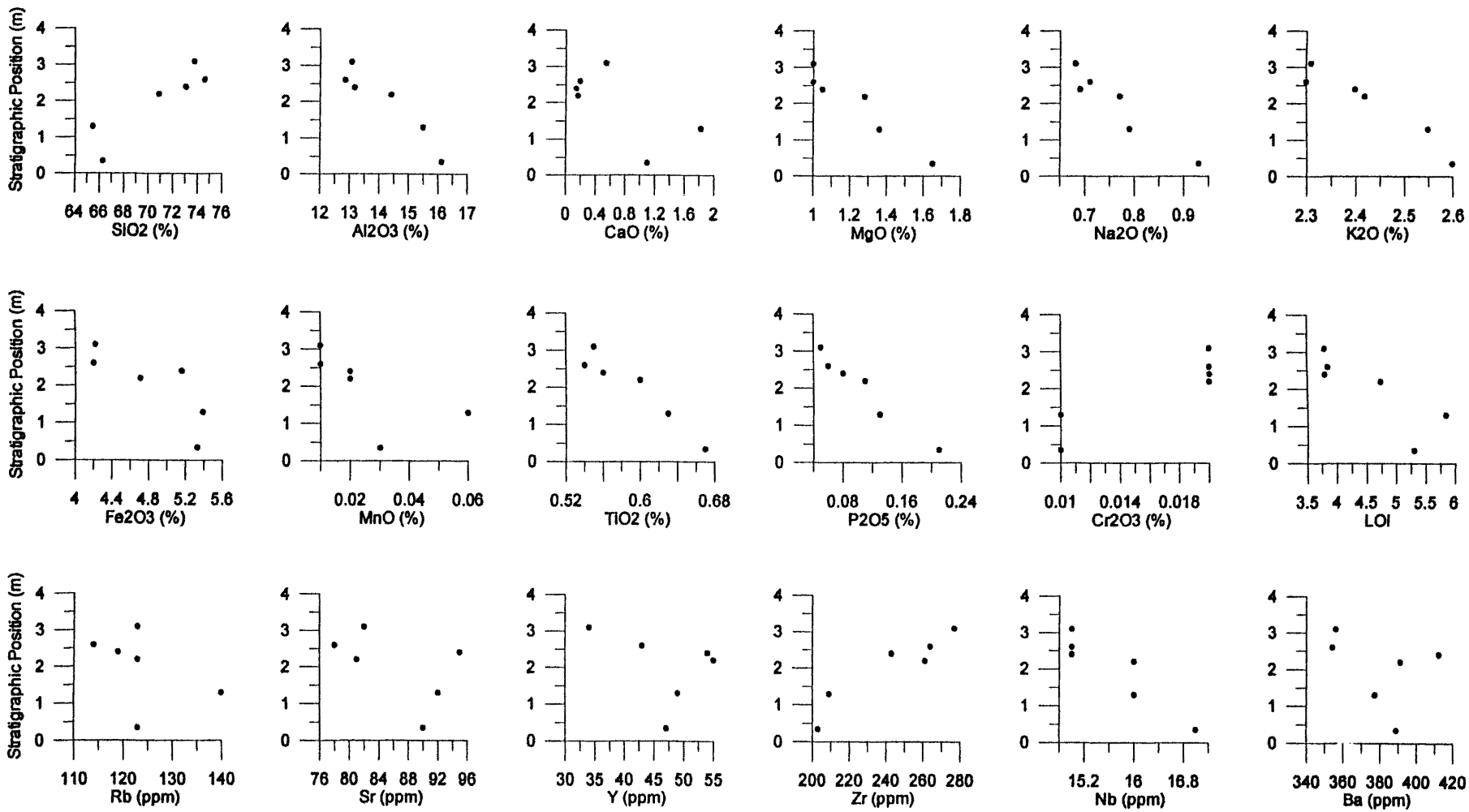

Major and Trace Elements for Location B2

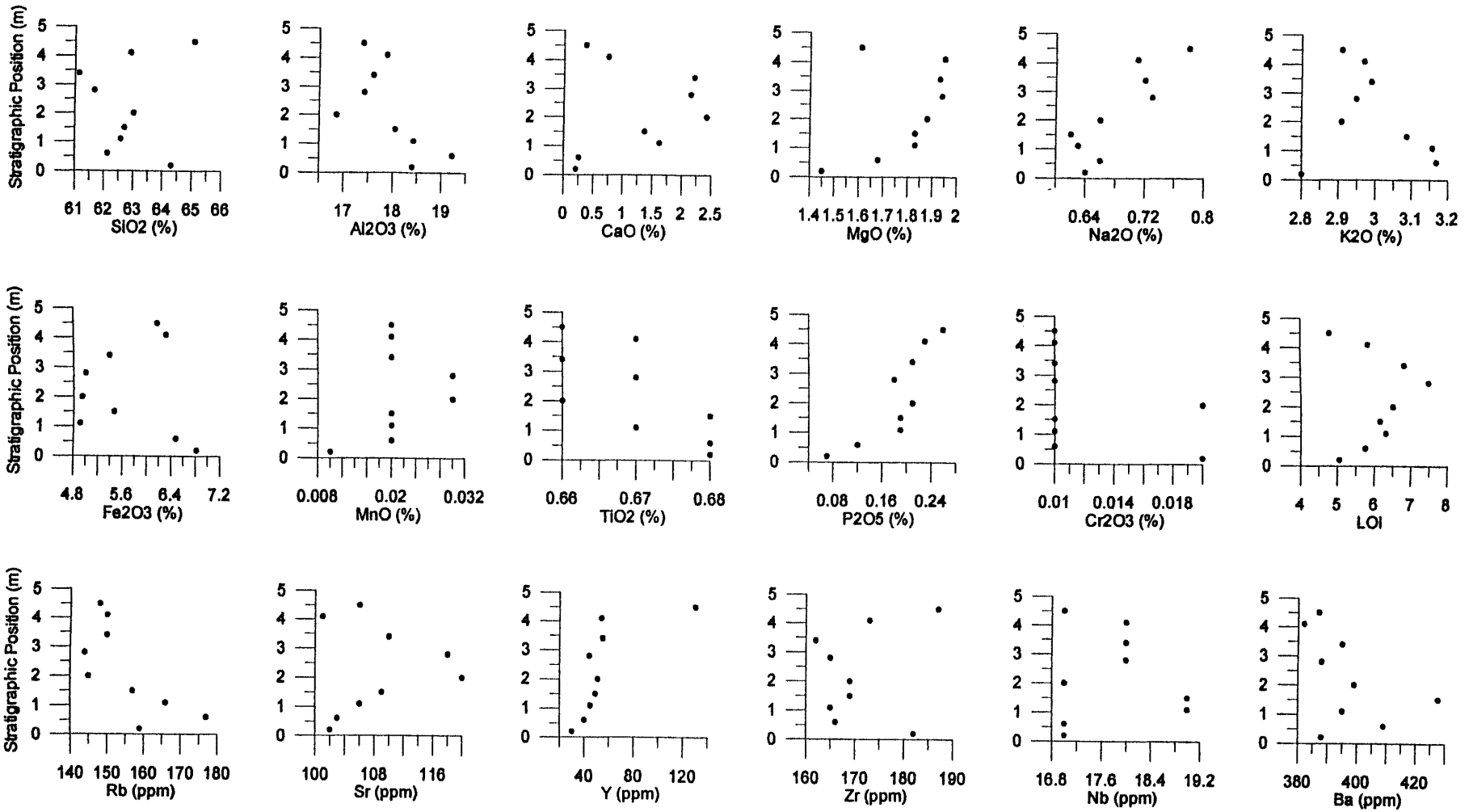

Major and Trace Elements for Location L1

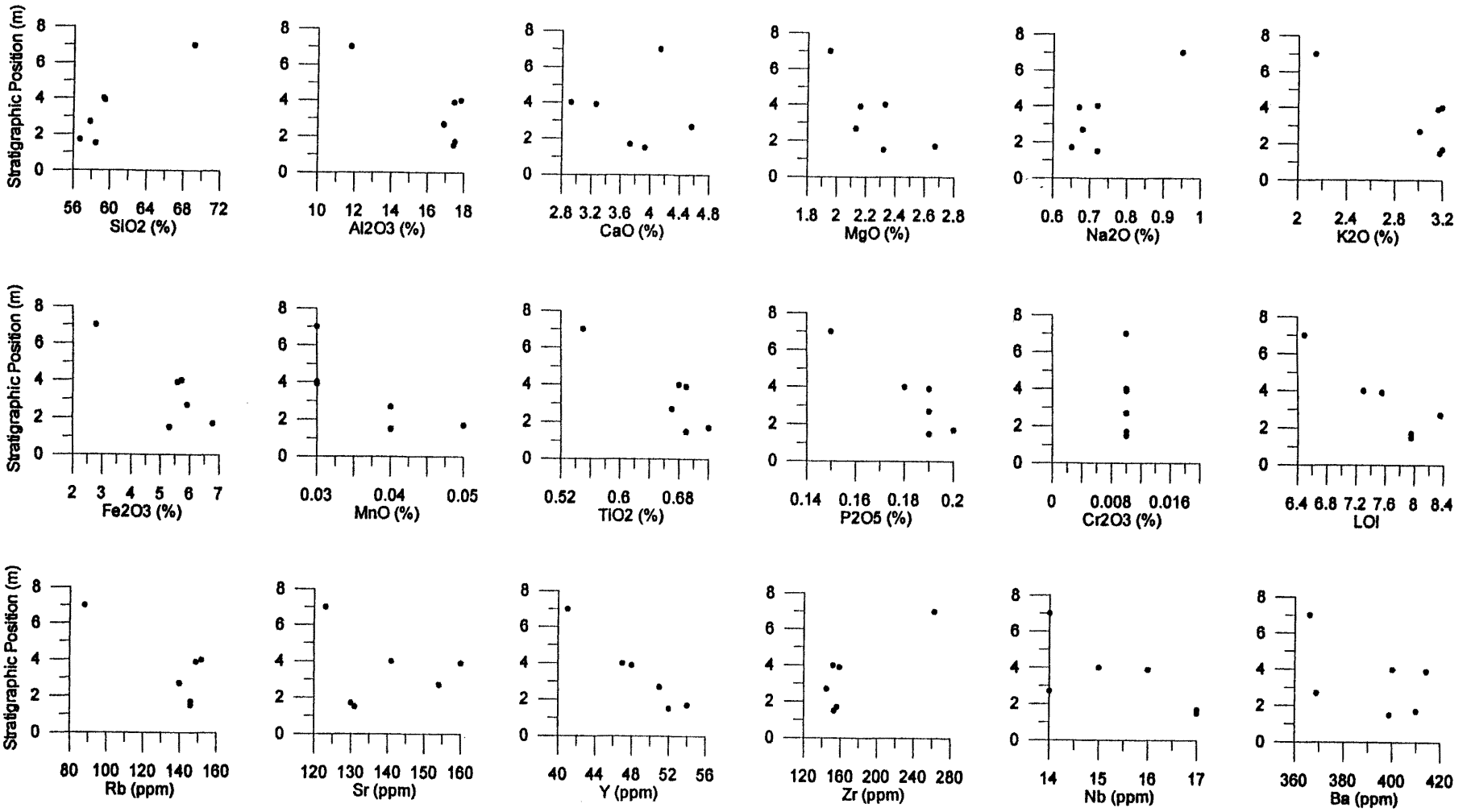

Major and Trace Elements for Location L3

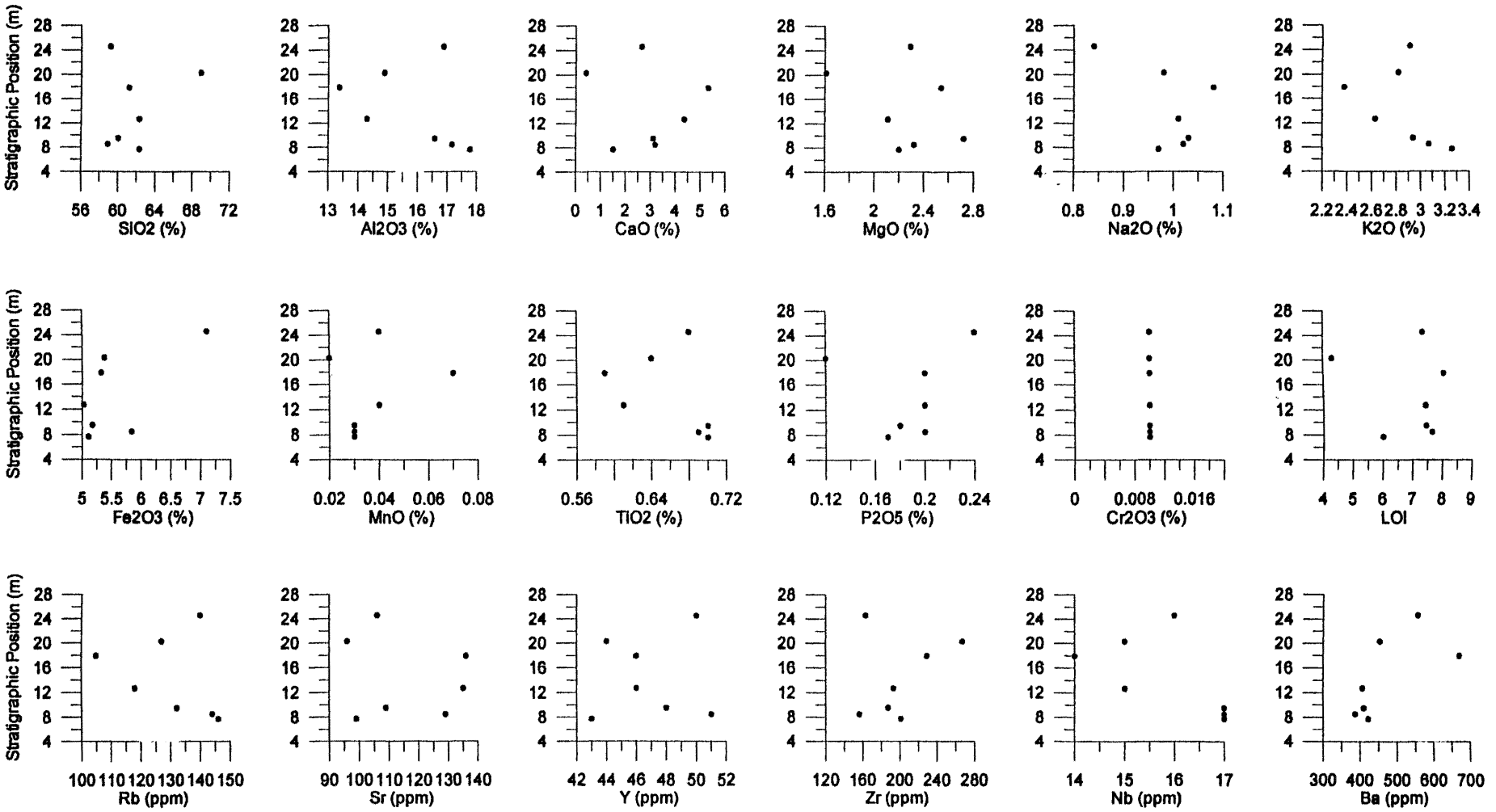

Major and Trace Elements for Location L4

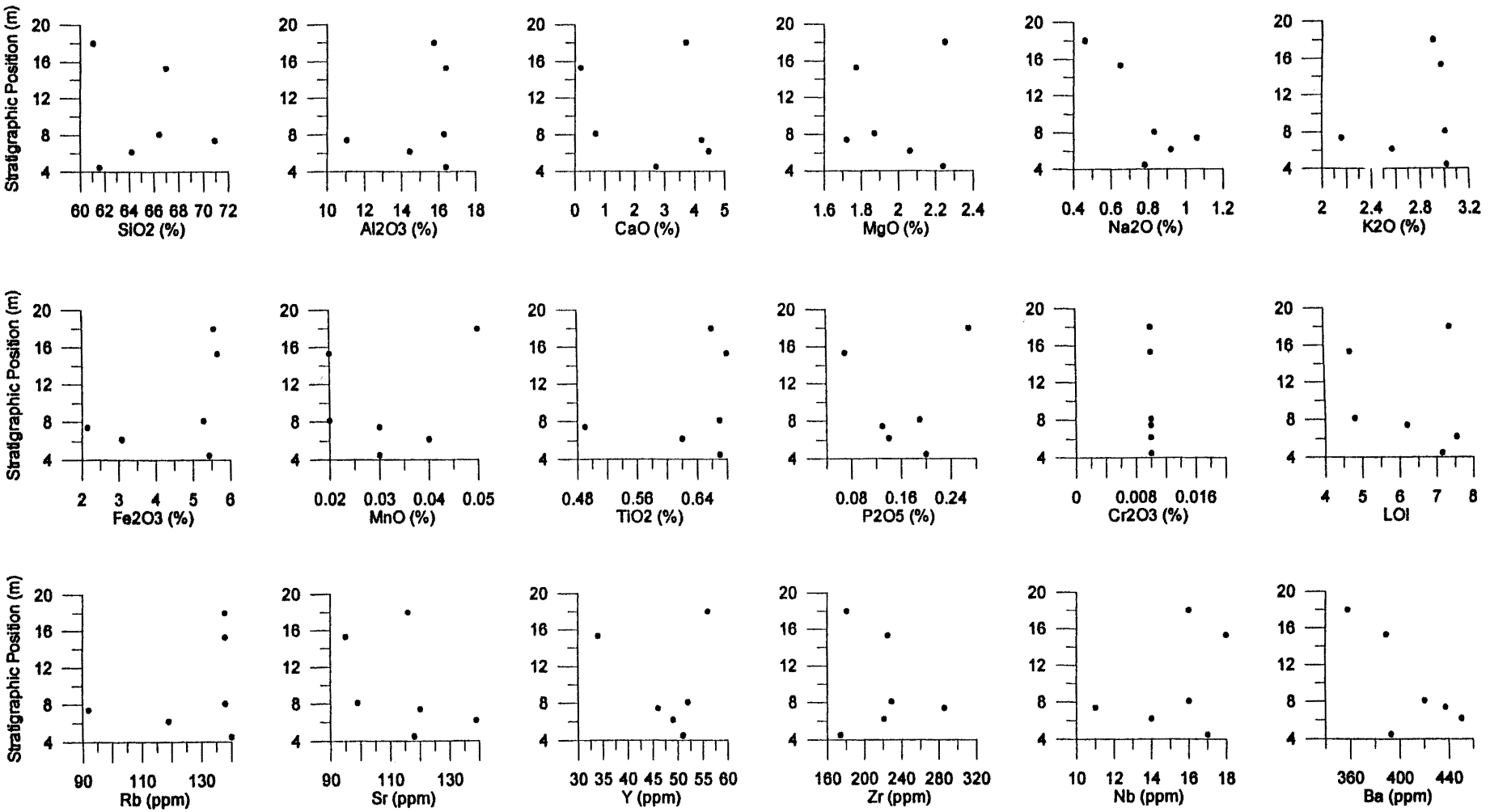

Major and Trace Elements for Location L5 (Whole Outcrop, samples 1-7)

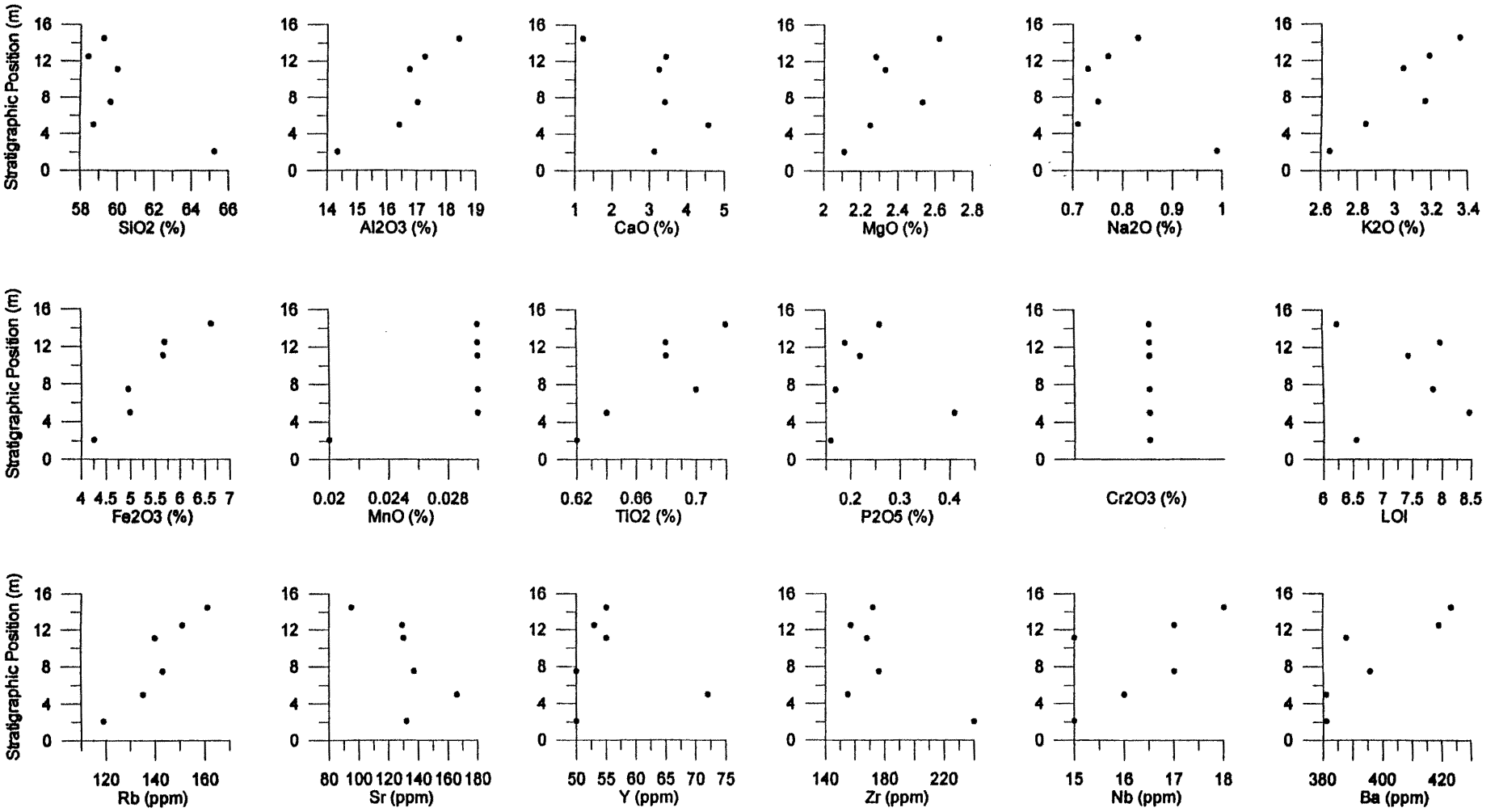

Major and Trace Elements for Location L5 (Two Paleosols, samples 8-18)

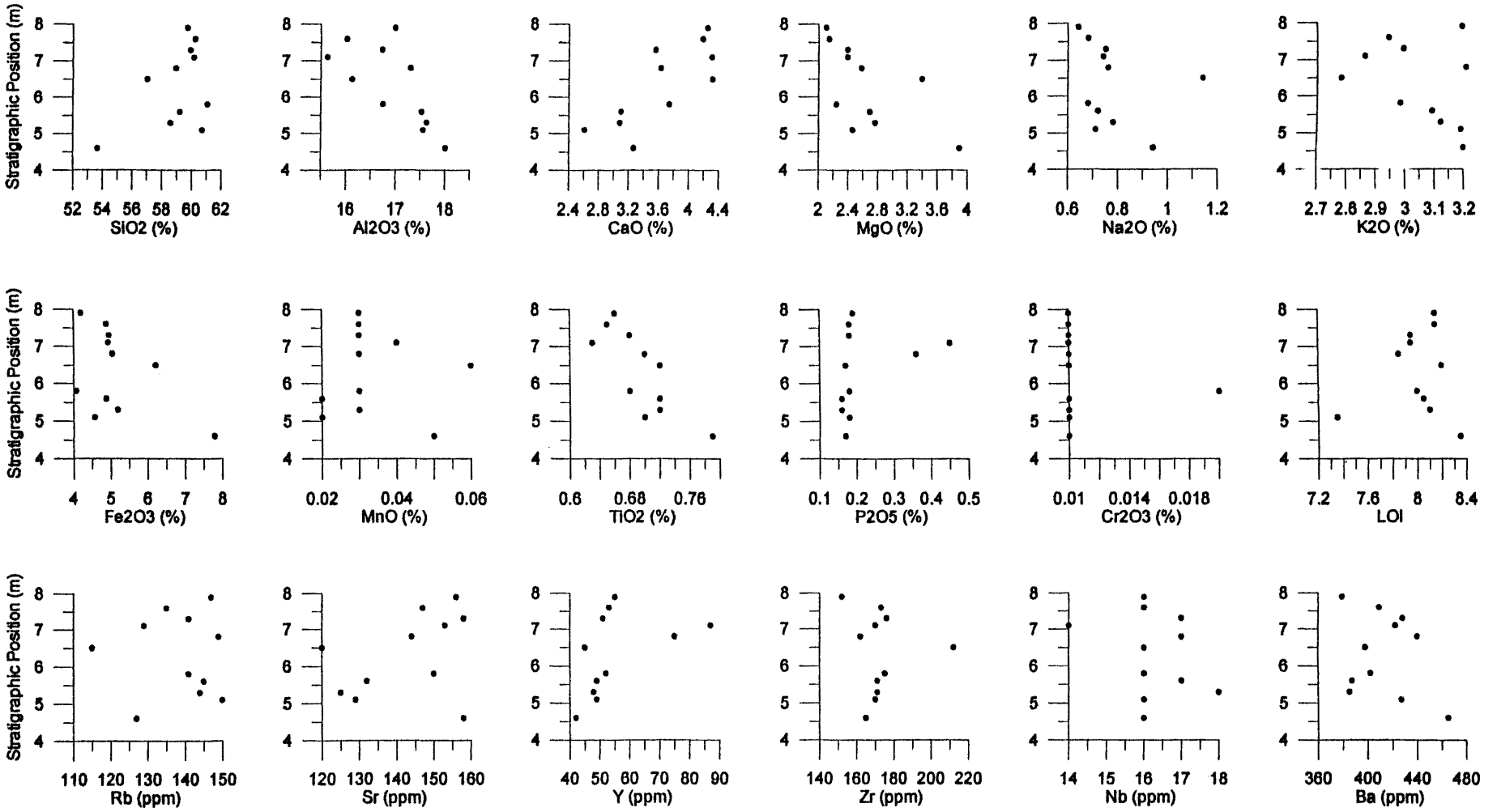

Major and Trace Elements for Location L6

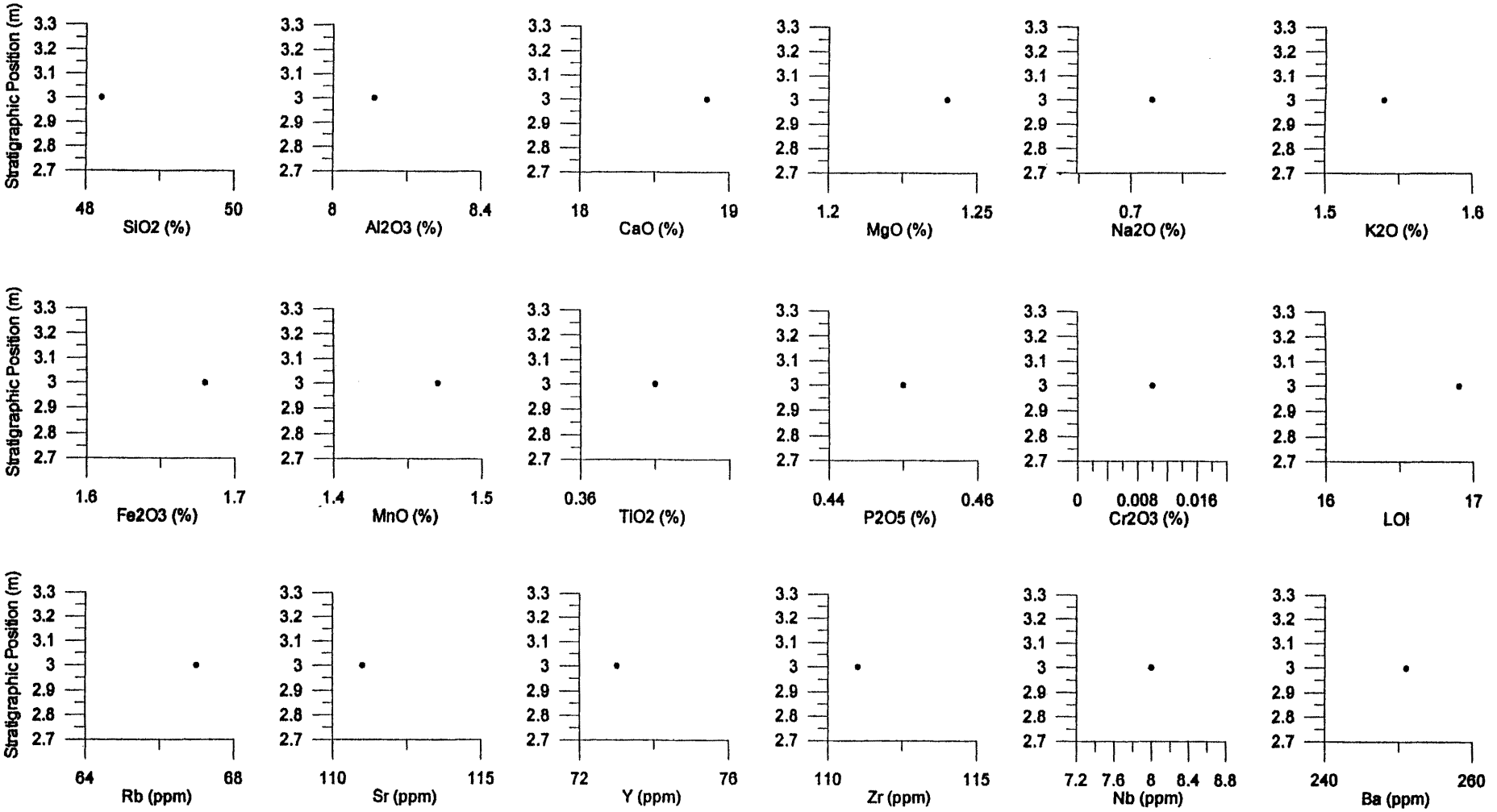

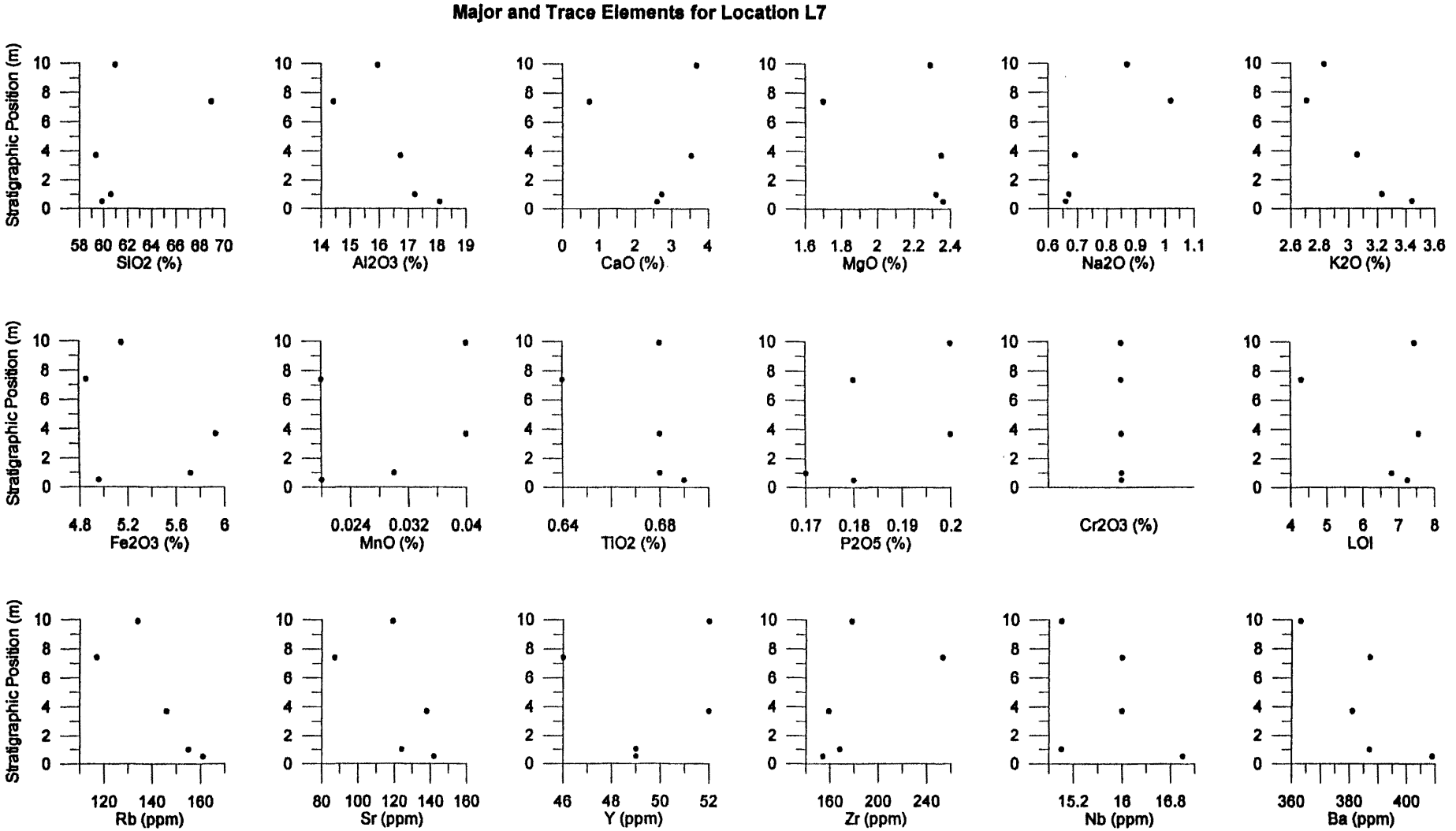
Major and Trace Elements for Location L7
Stratigraphic Position (m)
SiO2 (%)
Al2O3 (%)
CaO (%)
MgO (%)
Na2O (%)
K2O (%)
Fe2O3 (%)
MnO (%)
TiO2 (%)
P2O5 (%)
Cr2O3 (%)
LOI
Rb (ppm)
Sr (ppm)
Y (ppm)
Zr (ppm)
Nb (ppm)
Ba (ppm)

APPENDIX F

PETROGRAPHIC DATA

Wasatch Outcrop Sample #s:	Average quartz grain size (in Phi units)	Standard Deviation of quartz grain size (in Phi units)	Average Roundness of quartz grains (Qualitative)	Standard Deviation of quartz grain roundness
Wast-B1-1	4.9	0.6	3	0.6
Wast-B1-2	5.0	0.6	3	0.9
Wast-B1-3	4.3	0.6	2	0.9
Wast-B1-4	4.1	0.5	2	0.7
Wast-B1-5	4.1	0.7	3	0.8
Wast-B1-6	4.3	0.9	3	1.1
Wast-B1-7	4.1	1.0	2	1.0
Wast-B1-8	3.6	0.6	3	0.9
Wast-B1-9	3.5	0.5	3	0.9
Wast-B1-10	3.6	0.9	3	0.9
Group Average	4.1	0.7	3	0.9
Group Median	4.1	0.6	3	0.9
Group Std. Dev.	0.5	0.2	0	0.1
Wast-B2-1	4.9	0.8	3	0.9
Wast-B2-2	4.0	0.7	3	0.9
Wast-B2-3	5.4	0.6	3	0.6
Wast-B2-4	5.8	0.6	3	0.6
Wast-B2-5	5.8	0.7	3	0.7
Wast-B2-6	5.7	0.6	3	0.6
Wast-B2-7	6.2	0.6	3	0.9
Wast-B2-8	6.0	0.6	3	0.7
Wast-B2-9	5.7	0.6	3	0.6
Wast-B2-10	6.0	0.5	3	0.7
Group Average	5.5	0.6	3	0.7
Group Median	5.7	0.6	3	0.7
Group Std. Dev.	0.7	0.1	0	0.1
Wast-L1-2	5.9	0.7	3	0.6
Wast-L1-3	6.1	0.5	3	0.7
Wast-L1-4	5.9	0.5	3	0.5
Wast-L1-5	6.1	0.7	3	0.7
Wast-L1-6	6.0	0.5	3	0.6
Wast-L1-7	5.4	0.7	3	0.7
Wast-L1-8	5.6	0.5	3	0.9
Wast-L1-9	6.1	0.6	3	0.8
Wast-L1-10	5.7	0.5	3	0.7
Wast-L1-11	5.4	0.7	3	1.2
Group Average	5.8	0.6	3	0.7
Group Median	5.9	0.5	3	0.7
Group Std. Dev.	0.3	0.1	0	0.2
Wast-L3-1	5.7	0.6	3	0.9
Wast-L3-2	5.5	0.6	3	0.7
Wast-L3-4	4.2	0.6	2	1.4
Wast-L3-5	4.1	0.9	3	0.8
Wast-L3-6	5.8	0.6	3	0.8
Wast-L3-7	5.3	0.6	3	0.8
Wast-L3-8	4.6	0.6	3	0.7
Wast-L3-9	5.1	0.4	3	0.9
Wast-L3-10	4.8	0.5	3	0.9
Wast-L3-11	5.1	0.7	3	0.7
Wast-L3-12	4.4	0.5	3	0.8
Group Average	5.0	0.6	3	0.8
Group Median	5.1	0.6	3	0.8
Group Std. Dev.	0.6	0.1	0	0.2

Wasatch Outcrop Sample #s:	Average quartz grain size (in Phi units)	Standard Deviation of quartz grain size (in Phi units)	Average Roundness of quartz grains (Qualitative)	Standard Deviation of quartz grain roundness
Wast-L4-1	5.4	0.8	3	0.8
Wast-L4-2	3.6	0.6	3	0.9
Wast-L4-3	4.0	0.3	3	0.8
Wast-L4-4	4.4	0.5	3	0.8
Wast-L4-5	4.2	0.7	3	0.7
Wast-L4-6	4.4	0.6	3	0.8
Wast-L4-7	5.6	0.6	3	0.6
Wast-L4-8	4.8	0.6	3	0.8
Wast-L4-9	4.2	0.5	2	1.2
Group Average	4.5	0.6	3	0.8
Group Median	4.4	0.6	3	0.8
Group Std. Dev.	0.7	0.1	0	0.2
Wast-L5-1	4.2	0.3	3	0.7
Wast-L5-2	5.8	0.6	3	0.7
Wast-L5-3	4.5	0.4	3	0.4
Wast-L5-4	6.0	0.6	3	0.9
Wast-L5-5	5.9	0.8	3	0.7
Wast-L5-6	6.1	0.5	3	0.7
Wast-L5-7	4.6	0.5	3	0.6
Group Average	5.3	0.5	3	0.7
Group Median	5.8	0.5	3	0.7
Group Std. Dev.	0.8	0.2	0	0.1
Wast-L5-8	5.1	0.6	3	0.8
Wast-L5-9	6.3	0.5	3	0.6
Wast-L5-10	5.6	0.5	3	0.9
Wast-L5-11	5.8	0.5	3	0.8
Wast-L5-12	5.0	0.6	3	0.7
Wast-L5-13	5.5	0.4	3	0.7
Wast-L5-14	6.0	0.4	3	0.7
Wast-L5-15	3.0	0.7	3	0.7
Wast-L5-16	5.6	0.4	3	0.5
Wast-L5-17	4.9	0.5	3	0.7
Wast-L5-18	6.2	0.8	3	0.6
Group Average	5.3	0.5	3	0.7
Group Median	5.6	0.5	3	0.7
Group Std. Dev.	0.9	0.1	0	0.1
Wast-L6-11	4.3	0.5	3	0.7
Wast-L7-1	6.1	0.5	3	0.5
Wast-L7-2	4.7	0.7	3	0.7
Wast-L7-3	5.4	0.7	3	0.5
Wast-L7-4	5.0	0.5	3	0.6
Wast-L7-5	5.9	0.5	3	0.5
Wast-L7-6	4.0	0.8	3	0.8
Wast-L7-7	5.8	0.9	3	0.6
Wast-L7-9	4.7	0.6	3	0.7
Wast-L7-10	4.5	0.6	3	0.5
Wast-L7-11	4.6	0.7	3	0.8
Wast-L7-12	5.6	0.7	3	0.6
Group Average	5.1	0.7	3	0.6
Group Median	5.0	0.7	3	0.6
Group Std. Dev.	0.7	0.1	0	0.1

Wasatch Outcrop Sample #s:	Stratigraphic Position (m)	PC Qz		MC Qz		Felds		Musc	
		Count	%	Count	%	Count	%	Count	%
Wast-B1-1	0.35	4	2	55	21	0	0	0	0
Wast-B1-2	0.8	3	1	22	9	23	9	1	0
Wast-B1-3	1	2	1	44	18	15	6	0	0
Wast-B1-4	1.1	9	4	50	20	26	10	3	1
Wast-B1-5	1.3	1	0	30	12	20	8	4	2
Wast-B1-6	1.7	1	0	40	16	12	5	1	0
Wast-B1-7	2.2	3	1	43	17	11	4	1	0
Wast-B1-8	2.4	4	2	57	23	8	3	1	0
Wast-B1-9	2.6	16	6	63	25	8	3	0	0
Wast-B1-10	3.1	5	2	52	21	13	5	0	0
Group Average		5	2	46	18	14	5	1	0
Group Median		4	1	47	19	13	5	1	0
Group Std. Dev.		5	2	13	5	8	3	1	1
Wast-B2-1	0.2	0	0	11	4	14	6	0	0
Wast-B2-2	0.6	0	0	26	10	14	6	0	0
Wast-B2-3	1.1	0	0	12	5	2	1	0	0
Wast-B2-4	1.5	0	0	14	6	12	5	0	0
Wast-B2-5	2	2	1	17	7	7	3	0	0
Wast-B2-6	2.3	3	1	26	10	18	7	0	0
Wast-B2-7	2.8	0	0	7	3	5	2	2	1
Wast-B2-8	3.4	0	0	19	8	14	6	0	0
Wast-B2-9	4.1	0	0	8	3	7	3	0	0
Wast-B2-10	4.5	1	0	13	5	14	6	0	0
Group Average		1	0	15	6	11	4	0	0
Group Median		0	0	14	5	13	5	0	0
Group Std. Dev.		1	0	7	3	5	2	1	0
Wast-L1-2	6	0	0	15	6	4	2	2	1
Wast-L1-3	1.7	0	0	9	4	7	3	0	0
Wast-L1-4	3.9	1	0	8	3	12	5	0	0
Wast-L1-5	4	0	0	8	3	10	4	0	0
Wast-L1-6	4.1	0	0	12	5	8	3	0	0
Wast-L1-7	7	8	3	30	12	18	7	1	0
Wast-L1-8	1	2	1	23	9	7	3	1	0
Wast-L1-9	2.7	0	0	8	3	4	2	0	0
Wast-L1-10	6.4	0	0	13	5	13	5	0	0
Wast-L1-11	10.2	3	1	15	6	8	3	1	0
Group Average		1	1	14	6	9	4	1	0
Group Median		0	0	13	5	8	3	0	0
Group Std. Dev.		3	1	7	3	4	2	1	0
Wast-L3-1	6.5	0	0	12	5	9	4	1	0
Wast-L3-2	9.5	12	5	111	44	20	8	0	0
Wast-L3-4	17.9	2	1	58	23	18	7	0	0
Wast-L3-5	20.3	8	3	40	16	18	7	0	0
Wast-L3-6	24.6	5	2	29	12	14	6	0	0
Wast-L3-7	2.4	0	0	20	8	9	4	0	0
Wast-L3-8	4.3	4	2	35	14	19	8	2	1
Wast-L3-9	5.6	2	1	27	11	17	7	1	0
Wast-L3-10	7.7	1	0	16	6	11	4	0	0
Wast-L3-11	8..5	0	0	5	2	5	2	0	0
Wast-L3-12	12.7	3	1	18	7	8	3	0	0
Group Average		3	1	34	13	13	5	0	0
Group Median		2	1	27	11	14	6	0	0
Group Std. Dev.		4	2	30	12	5	2	1	0
Wast-L4-1	2.4	6	2	21	8	6	2	0	0
Wast-L4-2	4.5	1	0	7	3	6	2	0	0
Wast-L4-3	6.2	19	8	84	34	41	16	0	0
Wast-L4-4	7.4	9	4	52	21	31	12	0	0
Wast-L4-5	7.8	4	2	32	13	18	7	0	0
Wast-L4-6	8.1	6	2	38	15	10	4	0	0
Wast-L4-7	11.5	0	0	16	6	14	6	0	0
Wast-L4-8	15.3	7	3	38	15	13	5	3	1
Wast-L4-9	18	12	5	98	39	16	6	0	0
Group Average		7	3	43	17	17	7	0	0
Group Median		6	2	38	15	14	6	0	0
Group Std. Dev.		6	2	31	12	12	5	1	0

Wasatch Outcrop Sample #s:	GRAINS									
	Rk. Frags		Black Organics		Brown Organics		Other grains		TOTAL GRAINS	
	Count	%	Count	%	Count	%	Count	%	Count	%
Wast-B1-1	0	0	3	1	2	1	1	0	65	25
Wast-B1-2	0	0	0	0	2	1	1	0	52	21
Wast-B1-3	0	0	0	0	5	2	2	1	68	27
Wast-B1-4	0	0	0	0	2	1	2	1	92	37
Wast-B1-5	0	0	0	0	5	2	1	0	61	24
Wast-B1-6	0	0	0	0	3	1	1	0	58	23
Wast-B1-7	0	0	0	0	3	1	3	1	64	26
Wast-B1-8	0	0	0	0	5	2	2	1	77	31
Wast-B1-9	0	0	0	0	3	1	2	1	92	37
Wast-B1-10	0	0	0	0	5	2	3	1	78	31
Group Average	0	0	0	0	4	1	2	1	71	28
Group Median	0	0	0	0	3	1	2	1	67	26
Group Std. Dev.	0	0	1	0	1	1	1	0	14	6
Wast-B2-1	0	0	0	0	0	0	1	0	26	10
Wast-B2-2	0	0	0	0	4	2	1	0	45	18
Wast-B2-3	0	0	0	0	5	2	0	0	19	8
Wast-B2-4	0	0	0	0	4	2	2	1	32	13
Wast-B2-5	0	0	0	0	13	5	0	0	39	16
Wast-B2-6	0	0	1	0	1	0	1	0	50	20
Wast-B2-7	0	0	0	0	10	4	0	0	24	10
Wast-B2-8	0	0	0	0	4	2	1	0	38	15
Wast-B2-9	0	0	0	0	9	4	2	1	26	10
Wast-B2-10	0	0	0	0	4	2	2	1	34	14
Group Average	0	0	0	0	5	2	1	0	33	13
Group Median	0	0	0	0	4	2	1	0	33	13
Group Std. Dev.	0	0	0	0	4	2	1	0	10	4
Wast-L1-2	0	0	2	1	3	1	0	0	26	10
Wast-L1-3	0	0	0	0	4	2	2	1	22	9
Wast-L1-4	0	0	0	0	9	4	0	0	30	12
Wast-L1-5	0	0	0	0	16	6	4	2	38	15
Wast-L1-6	0	0	0	0	10	4	0	0	30	12
Wast-L1-7	0	0	0	0	12	5	5	2	74	30
Wast-L1-8	0	0	0	0	8	3	2	1	43	17
Wast-L1-9	0	0	0	0	4	2	0	0	16	6
Wast-L1-10	0	0	0	0	7	3	0	0	33	13
Wast-L1-11	0	0	0	0	6	2	3	1	36	14
Group Average	0	0	0	0	8	3	2	1	35	14
Group Median	0	0	0	0	8	3	1	0	32	13
Group Std. Dev.	0	0	1	0	4	2	2	1	16	6
Wast-L3-1	0	0	0	0	9	4	0	0	31	12
Wast-L3-2	0	0	0	0	6	2	0	0	149	60
Wast-L3-4	0	0	0	0	18	7	2	1	98	39
Wast-L3-5	0	0	0	0	10	4	2	1	78	31
Wast-L3-6	0	0	0	0	10	4	0	0	58	23
Wast-L3-7	0	0	0	0	10	4	0	0	39	16
Wast-L3-8	0	0	0	0	8	3	3	1	71	28
Wast-L3-9	0	0	0	0	12	5	0	0	59	24
Wast-L3-10	0	0	0	0	6	2	1	0	35	14
Wast-L3-11	0	0	0	0	7	3	0	0	17	7
Wast-L3-12	0	0	0	0	8	3	2	1	39	16
Group Average	0	0	0	0	9	4	1	0	61	25
Group Median	0	0	0	0	9	4	0	0	58	23
Group Std. Dev.	0	0	0	0	3	1	1	0	37	15
Wast-L4-1	0	0	0	0	7	3	0	0	40	16
Wast-L4-2	0	0	0	0	6	2	0	0	20	8
Wast-L4-3	0	0	0	0	1	0	2	1	147	59
Wast-L4-4	0	0	0	0	7	3	1	0	100	40
Wast-L4-5	0	0	0	0	4	2	2	1	60	24
Wast-L4-6	0	0	0	0	4	2	3	1	61	24
Wast-L4-7	0	0	0	0	6	2	0	0	36	14
Wast-L4-8	2	1	0	0	7	3	2	1	72	29
Wast-L4-9	2	1	0	0	8	3	4	2	140	56
Group Average	0	0	0	0	6	2	2	1	75	30
Group Median	0	0	0	0	6	2	2	1	61	24
Group Std. Dev.	1	0	0	0	2	1	1	1	45	18

Wasatch Outcrop Sample #s:	MATRIX						CEMENT							
	Fe Stained		Gray		TOTAL MATRIX		Carbonate		Clay		Siderite		TOTAL CEMENT	
	Count	%	Count	%	Count	%	Count	%	Count	%	Count	%	Count	%
Wast-B1-1	77	30	64	25	141	55	35	14	17	7	0	0	52	20
Wast-B1-2	104	42	69	28	173	69	4	2	19	8	0	0	23	9
Wast-B1-3	73	29	96	38	169	68	0	0	9	4	0	0	9	4
Wast-B1-4	61	24	88	35	149	60	0	0	9	4	0	0	9	4
Wast-B1-5	48	19	133	53	181	72	0	0	2	1	6	2	8	3
Wast-B1-6	34	14	135	54	169	68	0	0	18	7	5	2	23	9
Wast-B1-7	57	23	114	46	171	68	0	0	15	6	0	0	15	6
Wast-B1-8	88	35	67	27	155	62	0	0	17	7	0	0	17	7
Wast-B1-9	63	25	85	34	148	59	0	0	9	4	0	0	9	4
Wast-B1-10	82	33	77	31	159	64	1	0	6	2	0	0	7	3
Group Average	69	27	93	37	162	64	4	2	12	5	1	0	17	7
Group Median	68	27	87	35	164	66	0	0	12	5	0	0	12	5
Group Std. Dev.	20	8	26	11	13	6	11	4	6	2	2	1	14	5
Wast-B2-1	100	40	110	44	210	84	0	0	11	4	0	0	11	4
Wast-B2-2	68	27	126	50	194	78	0	0	11	4	0	0	11	4
Wast-B2-3	160	64	67	27	227	91	0	0	2	1	0	0	2	1
Wast-B2-4	113	45	83	33	196	78	1	0	19	8	1	0	21	8
Wast-B2-5	121	48	79	32	200	80	3	1	7	3	1	0	11	4
Wast-B2-6	85	34	81	32	166	66	14	6	19	8	1	0	34	14
Wast-B2-7	138	55	79	32	217	87	4	2	5	2	0	0	9	4
Wast-B2-8	68	27	128	51	196	78	0	0	15	6	1	0	16	6
Wast-B2-9	104	42	103	41	207	83	0	0	17	7	0	0	17	7
Wast-B2-10	116	46	78	31	194	78	1	0	20	8	0	0	21	8
Group Average	107	43	93	37	201	80	2	1	13	5	0	0	15	6
Group Median	109	43	82	33	198	79	1	0	13	5	0	0	14	5
Group Std. Dev.	29	12	22	9	16	7	4	2	6	3	1	0	9	4
Wast-L1-2	94	38	95	38	189	76	17	7	0	0	15	6	32	13
Wast-L1-3	142	57	75	30	217	87	4	2	6	2	1	0	11	4
Wast-L1-4	104	42	97	39	201	80	10	4	9	4	0	0	19	8
Wast-L1-5	38	15	134	54	172	69	2	1	36	14	0	0	38	15
Wast-L1-6	110	44	56	22	166	66	14	6	38	15	0	0	52	21
Wast-L1-7	61	24	63	25	124	50	25	10	22	9	0	0	47	19
Wast-L1-8	63	25	110	44	173	69	11	4	23	9	0	0	34	14
Wast-L1-9	142	57	58	23	200	80	0	0	34	14	0	0	34	14
Wast-L1-10	173	69	18	7	191	76	8	3	18	7	0	0	26	10
Wast-L1-11	157	63	28	11	185	74	3	1	10	4	0	0	13	5
Group Average	108	43	73	29	182	73	9	4	20	8	2	1	31	12
Group Median	107	43	69	28	187	75	9	4	20	8	0	0	33	13
Group Std. Dev.	45	18	36	14	25	10	8	3	13	5	5	2	14	5
Wast-L3-1	151	60	32	13	183	73	3	1	26	10	1	0	30	12
Wast-L3-2	0	0	9	4	9	4	38	15	8	3	46	18	92	37
Wast-L3-4	64	26	22	9	86	34	34	14	26	10	6	2	66	26
Wast-L3-5	110	44	42	17	152	61	0	0	20	8	0	0	20	8
Wast-L3-6	63	25	78	31	141	56	23	9	28	11	0	0	51	20
Wast-L3-7	82	33	90	36	172	69	16	6	21	8	2	1	39	16
Wast-L3-8	51	20	93	37	144	58	16	6	19	8	0	0	35	14
Wast-L3-9	106	42	46	18	152	61	16	6	22	9	1	0	39	16
Wast-L3-10	23	9	157	63	180	72	1	0	34	14	0	0	35	14
Wast-L3-11	71	28	144	58	215	86	2	1	13	5	3	1	18	7
Wast-L3-12	63	25	118	47	181	72	9	4	21	8	0	0	30	12
Group Average	71	29	76	30	147	59	14	6	22	9	5	2	41	17
Group Median	64	26	78	31	152	61	16	6	21	8	1	0	35	14
Group Std. Dev.	41	17	50	20	56	23	13	5	7	3	14	5	21	9
Wast-L4-1	54	22	106	42	160	64	22	9	28	11	0	0	50	20
Wast-L4-2	115	46	90	36	205	82	2	1	23	9	0	0	25	10
Wast-L4-3	7	3	16	6	23	9	49	20	11	4	20	8	80	32
Wast-L4-4	18	7	80	32	98	39	18	7	16	6	18	7	52	21
Wast-L4-5	56	22	102	41	158	63	0	0	32	13	0	0	32	13
Wast-L4-6	47	19	127	51	174	70	1	0	14	6	0	0	15	6
Wast-L4-7	41	16	135	54	176	70	12	5	26	10	0	0	38	15
Wast-L4-8	111	44	48	19	159	64	1	0	18	7	0	0	19	8
Wast-L4-9	4	2	32	13	36	14	46	18	0	0	28	11	74	30
Group Average	50	20	82	33	132	53	17	7	19	7	7	3	43	17
Group Median	47	19	90	36	159	64	12	5	18	7	0	0	38	15
Group Std. Dev.	40	16	42	17	65	26	19	8	10	4	11	5	23	9

Wasatch Outcrop Sample #s:	PORES		TOTAL COUNTS	Biotur	Notes
	Count	%			
Wast-B1-1	0	0	258	4	60X
Wast-B1-2	2	1	250	5	60X, bioturbated, qtz grains oriented
Wast-B1-3	4	2	250	5	60X, bioturbated, yellowish matriz
Wast-B1-4	0	0	250	5	60X, bioturbated
Wast-B1-5	0	0	250	4	60X, bioturbated, alignment of qtz in roots or burrows?
Wast-B1-6	0	0	250	5	60X, bioturbated, siderite clustered in patches, qtz in roots/burrows
Wast-B1-7	0	0	250	4	60X, qtz all towards the top of the slide, lines from thin section making
Wast-B1-8	1	0	250	5	60X, qtz oriented in areas
Wast-B1-9	1	0	250	4	60X, poorly sorted qtz grains
Wast-B1-10	6	2	250	5	60X, poorly sorted qtz grains
Group Average	1	1			
Group Median	1	0			
Group Std. Dev.	2	1			
Wast-B2-1	3	1	250	3	60X, bad slide, ground too much?
Wast-B2-2	0	0	250	4	60X, some darker organic matter
Wast-B2-3	2	1	250	5	60X, lots of Fe stained matrix
Wast-B2-4	1	0	250	4	60X, few qtz grains
Wast-B2-5	0	0	250	5	60X, pieces, lots of organic matter
Wast-B2-6	0	0	250	3	60X
Wast-B2-7	0	0	250	5	60X, very few grains
Wast-B2-8	0	0	250	4	60X
Wast-B2-9	0	0	250	5	60X, few grains
Wast-B2-10	1	0	250	5	60X, few grains
Group Average	1	0		4	
Group Median	0	0		5	
Group Std. Dev.	1	0		1	
Wast-L1-2	3	1	250	3	60X, very fine grained, possible roots, om present,
Wast-L1-3	0	0	250	3	60X, pieces, few grains, lines from thin section construction
Wast-L1-4	0	0	250	4	60X, pieces, few grains
Wast-L1-5	2	1	250	3	60X, pieces, few grains, bad slide
Wast-L1-6	2	1	250	5	60X, pieces, few grains, lots of iron staining
Wast-L1-7	5	2	250	5	60X
Wast-L1-8	0	0	250	5	60X, few large grains
Wast-L1-9	0	0	250	5	60X, few large grains, lots of iron staining
Wast-L1-10	0	0	250	4	60X, few large grains, lots of iron staining
Wast-L1-11	16	6	250	6	60X, poorly sorted sorted
Group Average	3	1		4	
Group Median	1	0		5	
Group Std. Dev.	5	2		1	
Wast-L3-1	6	2	250	5	60X, fractures
Wast-L3-2	0	0	250	1	20X, sandstone, lines from construction
Wast-L3-4	0	0	250	2	60X
Wast-L3-5	0	0	250	4	60X
Wast-L3-6	0	0	250	4	60X
Wast-L3-7	0	0	250	4	60X, pieces
Wast-L3-8	0	0	250	3	60X, fractures
Wast-L3-9	0	0	250	5	60X, lots of Fe stained matrix, possible roots
Wast-L3-10	0	0	250	6	60X, quartz concentrated in areas
Wast-L3-11	0	0	250	6	60X
Wast-L3-12	0	0	250	6	60X
Group Average	1	0		4	
Group Median	0	0		4	
Group Std. Dev.	2	1		2	
Wast-L4-1	0	0	250	4	60X
Wast-L4-2	0	0	250	5	60X
Wast-L4-3	0	0	250	4	60X
Wast-L4-4	0	0	250	4	60X
Wast-L4-5	0	0	250	3	60X
Wast-L4-6	0	0	250	5	60X
Wast-L4-7	0	0	250	4	60X
Wast-L4-8	0	0	250	5	60X
Wast-L4-9	0	0	250	4	60X
Group Average	0	0		4	
Group Median	0	0		4	
Group Std. Dev.	0	0		1	

Wasatch Outcrop Sample #s:	Stratigraphic Position (m)	PC Qz		MC Qz		Felds		Musc	
		Count	%	Count	%	Count	%	Count	%
Wast-L5-1	2.1	9	4	64	26	21	8	2	1
Wast-L5-2	5	0	0	16	6	4	2	0	0
Wast-L5-3	7.5	5	2	54	22	15	6	1	0
Wast-L5-4	8.25	0	0	5	2	6	2	0	0
Wast-L5-5	10.1	0	0	9	4	8	3	0	0
Wast-L5-6	12.5	0	0	10	4	5	2	0	0
Wast-L5-7	14.5	1	0	28	11	13	5	0	0
Group Average		2	1	27	11	10	4	0	0
Group Median		0	0	16	6	8	3	0	0
Group Std. Dev.		4	1	24	9	6	3	1	0
Wast-L5-8	4.6	0	0	20	8	2	1	0	0
Wast-L5-9	5.1	1	0	15	6	7	3	0	0
Wast-L5-10	5.3	2	1	25	10	11	4	0	0
Wast-L5-11	5.6	0	0	16	6	10	4	0	0
Wast-L5-12	5.8	0	0	10	4	10	4	0	0
Wast-L5-13	6.5	0	0	15	6	15	6	0	0
Wast-L5-14	6.8	2	1	13	5	7	3	0	0
Wast-L5-15	7.1	9	4	116	46	5	2	1	0
Wast-L5-16	7.3	0	0	10	4	1	0	1	0
Wast-L5-17	7.6	1	0	33	13	10	4	1	0
Wast-L5-18	7.9	3	1	18	7	6	2	0	0
Group Average		2	1	26	11	8	3	0	0
Group Median		1	0	16	6	7	3	0	0
Group Std. Dev.		3	1	30	12	4	2	0	0
Wast-L6-11	4	1	0	18	7	17	7	0	0
Wast-L7-1	0.5	1	0	16	6	12	5	0	0
Wast-L7-2	1	3	1	28	11	17	7	0	0
Wast-L7-3	1.7	0	0	6	2	15	6	0	0
Wast-L7-4	2.5	5	2	19	8	8	3	0	0
Wast-L7-5	3	5	2	14	6	15	6	0	0
Wast-L7-6	3.7	9	4	44	18	26	10	1	0
Wast-L7-7	4.3	5	2	15	6	8	3	0	0
Wast-L7-9	7	1	0	15	6	10	4	0	0
Wast-L7-10	7.4	6	2	39	16	15	6	0	0
Wast-L7-11	9.4	3	1	91	36	11	4	2	1
Wast-L7-12	9.9	1	0	22	9	9	4	1	0
Group Average		4	1	28	11	13	5	0	0
Group Median		3	1	19	8	12	5	0	0
Group Std. Dev.		3	1	24	9	5	2	1	0
Wast-L1-1		19	8	124	50	5	2	0	0
Wast-L2-1		14	6	76	30	34	14	0	0
Wast-L3-3		4	2	20	8	24	10	2	1
Wast-L7-8		9	4	81	32	29	12	1	0
Wast-L7-13		6	2	78	31	14	6	0	0

Key to bioturbation numbers:

1 - Very slightly bioturbated
2 - Slightly bioturbated
3 - Moderatly bioturbated
4 - Highly bioturbated
5 - Intensely bioturbated
6 - Completely bioturbated

Wasatch Outcrop Sample #s:	GRAINS									
	Rk. Frags		Black Organics		Brown Organics		Other grains		TOTAL GRAINS	
	Count	%	Count	%	Count	%	Count	%	Count	%
Wast-L5-1	2	1	0	0	9	4	1	0	108	43
Wast-L5-2	0	0	0	0	6	2	2	1	28	11
Wast-L5-3	1	0	0	0	3	1	4	2	83	33
Wast-L5-4	0	0	0	0	7	3	2	1	20	8
Wast-L5-5	1	0	0	0	6	2	3	1	27	11
Wast-L5-6	0	0	0	0	3	1	1	0	19	8
Wast-L5-7	0	0	0	0	0	0	0	0	42	17
Group Average	1	0	0	0	5	2	2	1	47	19
Group Median	0	0	0	0	6	2	2	1	28	11
Group Std. Dev.	1	0	0	0	3	1	1	1	35	14
Wast-L5-8	0	0	1	0	6	2	0	0	29	12
Wast-L5-9	0	0	0	0	6	2	0	0	29	12
Wast-L5-10	0	0	0	0	7	3	1	0	46	18
Wast-L5-11	0	0	0	0	5	2	1	0	32	13
Wast-L5-12	0	0	0	0	8	3	1	0	29	12
Wast-L5-13	0	0	0	0	6	2	1	0	37	15
Wast-L5-14	0	0	0	0	2	1	0	0	24	10
Wast-L5-15	2	1	0	0	3	1	5	2	141	56
Wast-L5-16	0	0	0	0	5	2	3	1	20	8
Wast-L5-17	0	0	0	0	3	1	1	0	49	20
Wast-L5-18	0	0	0	0	8	3	0	0	35	14
Group Average	0	0	0	0	5	2	1	0	43	17
Group Median	0	0	0	0	6	2	1	0	32	13
Group Std. Dev.	1	0	0	0	2	1	2	1	34	13
Wast-L6-11	0	0	0	0	2	1	1	0	39	16
Wast-L7-1	0	0	0	0	5	2	0	0	34	14
Wast-L7-2	0	0	0	0	1	0	2	1	51	20
Wast-L7-3	0	0	0	0	7	3	2	1	30	12
Wast-L7-4	0	0	0	0	3	1	4	2	39	16
Wast-L7-5	0	0	0	0	7	3	0	0	41	16
Wast-L7-6	0	0	0	0	4	2	2	1	86	34
Wast-L7-7	0	0	0	0	5	2	3	1	36	14
Wast-L7-9	0	0	0	0	6	2	1	0	33	13
Wast-L7-10	1	0	0	0	4	2	3	1	69	28
Wast-L7-11	0	0	0	0	2	1	0	0	109	44
Wast-L7-12	0	0	0	0	4	2	0	0	37	15
Group Average	0	0	0	0	4	2	2	1	51	21
Group Median	0	0	0	0	4	2	2	1	39	16
Group Std. Dev.	0	0	0	0	2	1	1	1	26	10
Wast-L1-1	4	2	0	0	2	1	3	1	157	63
Wast-L2-1	2	1	0	0	6	2	2	1	134	54
Wast-L3-3	0	0	0	0	6	2	0	0	56	22
Wast-L7-8	2	1	0	0	3	1	1	0	126	50
Wast-L7-13	3	1	0	0	1	0	2	1	104	42

Wasatch Outcrop Sample #s:	MATRIX						CEMENT							
	Fe Stained		Gray		TOTAL MATRIX		Carbonate		Clay		Siderite		TOTAL CEMENT	
	Count	%	Count	%	Count	%	Count	%	Count	%	Count	%	Count	%
Wast-L5-1	90	36	22	9	112	45	24	10	0	0	6	2	30	12
Wast-L5-2	102	41	102	41	204	82	18	7	0	0	0	0	18	7
Wast-L5-3	33	13	43	17	76	30	25	10	22	9	44	18	91	36
Wast-L5-4	78	31	76	30	154	62	25	10	37	15	14	6	76	30
Wast-L5-5	139	56	57	23	196	78	13	5	9	4	5	2	27	11
Wast-L5-6	96	38	83	33	179	72	20	8	21	8	11	4	52	21
Wast-L5-7	138	55	38	15	176	70	2	1	23	9	3	1	28	11
Group Average	97	39	60	24	157	63	18	7	16	6	12	5	46	18
Group Median	96	38	57	23	176	70	20	8	21	8	6	2	30	12
Group Std. Dev.	36	15	28	11	47	19	8	3	14	5	15	6	28	11
Wast-L5-8	71	28	106	42	177	71	12	5	18	7	14	6	44	18
Wast-L5-9	41	16	143	57	184	74	16	6	21	8	0	0	37	15
Wast-L5-10	89	36	80	32	169	68	19	8	16	6	0	0	35	14
Wast-L5-11	76	30	86	34	162	65	16	6	40	16	0	0	56	22
Wast-L5-12	66	26	115	46	181	72	22	9	18	7	0	0	40	16
Wast-L5-13	127	51	59	24	186	74	9	4	18	7	0	0	27	11
Wast-L5-14	79	32	97	39	176	70	22	9	28	11	0	0	50	20
Wast-L5-15	23	9	19	8	42	17	57	23	0	0	8	3	65	26
Wast-L5-16	178	71	35	14	213	85	10	4	7	3	0	0	17	7
Wast-L5-17	120	48	48	19	168	67	15	6	14	6	4	2	33	13
Wast-L5-18	47	19	129	52	176	70	13	5	18	7	8	3	39	16
Group Average	83	33	83	33	167	67	19	8	18	7	3	1	40	16
Group Median	76	30	86	34	176	70	16	6	18	7	0	0	39	16
Group Std. Dev.	44	18	40	16	43	17	13	5	10	4	5	2	13	5
Wast-L6-11	84	34	7	3	91	36	72	29	3	1	45	18	120	48
Wast-L7-1	20	8	149	60	169	68	10	4	32	13	5	2	47	19
Wast-L7-2	122	49	51	20	173	69	6	2	10	4	10	4	26	10
Wast-L7-3	214	86	1	0	215	86	5	2	0	0	0	0	5	2
Wast-L7-4	50	20	117	47	167	67	12	5	22	9	10	4	44	18
Wast-L7-5	47	19	141	56	188	75	7	3	13	5	1	0	21	8
Wast-L7-6	106	42	19	8	125	50	11	4	12	5	16	6	39	16
Wast-L7-7	59	24	125	50	184	74	12	5	15	6	3	1	30	12
Wast-L7-9	196	78	13	5	209	84	1	0	5	2	2	1	8	3
Wast-L7-10	81	32	76	30	157	63	7	3	15	6	2	1	24	10
Wast-L7-11	42	17	55	22	97	39	23	9	13	5	8	3	44	18
Wast-L7-12	82	33	102	41	184	74	9	4	10	4	10	4	29	12
Group Average	93	37	77	31	170	68	9	4	13	5	6	2	29	12
Group Median	81	32	76	30	173	69	9	4	13	5	5	2	29	12
Group Std. Dev.	63	25	53	21	34	14	6	2	8	3	5	2	14	6
Wast-L1-1	0	0	29	12	29	12	30	12	0	0	34	14	64	26
Wast-L2-1	12	5	32	13	44	18	38	15	2	1	32	13	72	29
Wast-L3-3	126	50	8	3	134	54	28	11	32	13	0	0	60	24
Wast-L7-8	25	10	15	6	40	16	41	16	5	2	38	15	84	34
Wast-L7-13	44	18	31	12	75	30	37	15	7	3	27	11	71	28

Wasatch Outcrop Sample #s:	PORES		TOTAL COUNTS	Biotur	Notes
	Count	%			
Wast-L5-1	0	0	250	2	60X, bad slide
Wast-L5-2	0	0	250	2	60X, pieces, dark Fe stains on edges of peds
Wast-L5-3	0	0	250	2	60X
Wast-L5-4	0	0	250	4	60X, pieces, dark Fe stains on edges of peds
Wast-L5-5	0	0	250	3	60X
Wast-L5-6	0	0	250	4	60X
Wast-L5-7	4	2	250	5	60X
Group Average	1	0		3	
Group Median	0	0		3	
Group Std. Dev.	2	1		1	
Wast-L5-8	0	0	250	4	60X
Wast-L5-9	0	0	250	4	60X
Wast-L5-10	0	0	250	3	60X
Wast-L5-11	0	0	250	3	60X
Wast-L5-12	0	0	250	3	60X
Wast-L5-13	0	0	250	5	60X
Wast-L5-14	0	0	250	3	60X
Wast-L5-15	2	1	250	3	60X
Wast-L5-16	0	0	250	3	60X
Wast-L5-17	0	0	250	4	60X
Wast-L5-18	0	0	250	5	60X
Group Average	0	0		4	
Group Median	0	0		3	
Group Std. Dev.	1	0		1	
Wast-L6-11	0	0	250	4	60X
Wast-L7-1	0	0	250	4	60X
Wast-L7-2	0	0	250	5	60X
Wast-L7-3	0	0	250	3	60X, lots of Fe stained matrix
Wast-L7-4	0	0	250	4	60X
Wast-L7-5	0	0	250	4	60X
Wast-L7-6	0	0	250	4	60X
Wast-L7-7	0	0	250	4	60X
Wast-L7-9	0	0	250	4	60X
Wast-L7-10	0	0	250	3	60X
Wast-L7-11	0	0	250	3	60X
Wast-L7-12	0	0	250	5	60X
Group Average	0	0		4	
Group Median	0	0		4	
Group Std. Dev.	0	0		1	
Wast-L1-1	0	0		0	20X, sandstone
Wast-L2-1	0	0		0	60X, sandstone
Wast-L3-3	0	0		3	60X
Wast-L7-8	0	0		2	60X, sandstone
Wast-L7-13	0	0		3	60X, sandstone